Relaxation dynamics in molecular glass-formers with systematic structure modifications

Daniel Lindley Baker

School of Physics and Astronomy

University of Leeds

Submitted in accordance with the requirements for the degree of

Doctor of Philosophy

September 2014

The candidate confirms that the work submitted is his own and that appropriate credit has been given where reference has been made to the work of others.

To Mum, Andrew, Jim and Kat

Acknowledgements

Throughout my PhD there have been a great many people who have made the experience both enjoyable and worthwhile.

First and foremost, I would like to thank my supervisor Johan Mattsson. If I were to try and list all the things that Johan has done for me over the last 4 years, I would likely need another thesis-worth of paper. He has provided (amongst many other things) guidance, inspiration and meticulous editing skills whilst maintaining an almost super-human level of patience. For this, I cannot thank him enough.

Thanks to Peter Olmsted for all the help he gave me during my undergraduate degree and for pushing me in the right direction and thanks to Mike Evans, Mike Ries and Oscar Cespedes for useful discussions along the way. Thanks also to Olivier Cayre and Soyeb Manga for their advice and conversations on all things colloidal. Thanks to everyone in the Condensed Matter Group at Chalmers for making my intense measurement sessions over there more bearable and especially to Johan Sjöström for helping out with the initial experiments and for introducing the 'quirks' of dielectric spectroscopy.

I would also like to thank all my friends and colleagues for making the good times better and the bad times manageable, be they in the lab or in the pub. Thanks especially to Robin Richardson and May Wheeler for providing excellent company for the rapid descent into insanity that accompanies the writing of a thesis. Also thanks to my office mates: Winke, Ben, Outi, James, Steve, Agnes and Guanghui for making the return to the office to do work a less arduous task. Thanks also to Glenys Bowles for being a port of calm in a sea of madness and thanks to Faith Bonner for the support in the daunting world of administrative procedure.

Thanks to Mum, Andrew and Jim for being there when I needed them and for never failing to put a smile on my face.

Last but certainly not least, thanks to Kat for looking after me, especially in the closing weeks of crazed thesis panic, and for a million other things.

Abstract

Glasses are amorphous materials which do not exhibit the long-range order or periodicity found in crystalline solids. A glass is formed by cooling a liquid at a sufficient rate such that crystallisation can be avoided. The structural disorder of glasses give them unique properties which make them suitable for a wide range of industrial, pharmaceutical or biological applications. Glass-forming materials generally exhibit several characteristic mechanisms of molecular motion. The physical origins and interrelation between these mechanisms are not well understood. In order to address this, detailed investigations of how glass-transition related dynamics are affected by systematic modification of the molecular structure are needed.

This thesis concerns the measurement of the glass-forming properties of three series of molecular glass-formers. These series are comprised of samples which vary systematically in their structure: an alkylbenzene series involving the systematic variation of the length of an alkyl-tail attached to a phenyl-ring and two series involving the successive oligomerisation of styrene and α-methylstyrene. The glass forming properties of these series were analysed using Broadband Dielectric Spectroscopy (BDS) and Differential Scanning Calorimetry (DSC). Thermogravimetric Analysis was also employed in order to optimise the sample preparation procedure.

The work in this thesis identifies and characterises the detailed molecular weight dependent behaviour of several key relaxation mechanisms in the glassy and supercooled state of three different glass-forming systems. Strong similarities between the relaxation behaviour of the two polymeric and the alkyl chain modified benzene series were found. This demonstrates that much of the observed phenomenology is remarkably general and the work forms a basis for developments of models to address the glass-transition and glassy behaviour. Moreover, it is demonstrated that the glass transition in the three different series of samples behave in a highly similar manner with regards to the system molecular weight and strong support is found for a link between the primary structural relaxation that exists in the supercooled state and the secondary relaxation mechanisms that persist within the glassy state.

Abbreviations

k_B	Boltzmann's constant
T	Temperature
R	Universal gas constant
T_g	Glass transition temperature
τ	Relaxation timescale
T_m	Melting point
T_g	Boiling point
ΔH_{fus}	Enthalpy of fusion
ΔS_{fus}	Entropy of fusion
E_A	Activation energy
C_p	Specific heat capacity at constant pressure
M_w	Weight averaged molecular weight
M_n	Number averaged molecular weight
PDI	Polydispersity index
$\Delta\varepsilon$	Dielectric strength
ε'	Real part of the dielectric permittivity
ε''	Imaginary part of the dielectric permittivity
RB	Rikard Bergman
HN	Havriliak-Negami
CD	Cole-Davidson
CC	Cole-Cole
a	Low frequency flank exponent (Rikard Bergman function)
b	High frequency flank exponent (Rikard Bergman function)
C	Bluntness parameter (Rikard Bergman function)
ε''_p	Amplitude of the dielectric loss
α	Symmetric stretching parameter (Havriliak-Negami function)
β	Anti-symmetric stretching parameter (Havriliak-Negami function)
PAMS	Poly($\alpha-$methylstyrene)
PS	Polystyrene

Contents

List of Figures

Chapter 1

Phenomenology of glass

1.1 Introduction: What is a glass?

There are three well-defined thermodynamic states of matter: gas, liquid and solid. One way in which materials can traverse these different states is as a result of a change in temperature. If a gas is cooled below its boiling point, T_b, a first order thermodynamic phase transition is encountered, characterised by a significant release of energy and a large discontinuous change in the density; the gas becomes a liquid. As a result of the change in density, the constituent particles of the liquid are far more closely packed than they were in the gaseous state. This means that, although they still have enough energy to move, the characteristic timescales of their motion increase. As a liquid is cooled, these timescales continue to increase. If the rate of cooling is slower than the timescales of motion for the particles then another thermodynamic phase transition is found at the melting temperature, T_m. At this phase transition the material again releases a significant amount of energy and the constituent particles become fixed in regular positions relating to a minimum in the free energy and the liquid becomes a crystalline solid, characterised by long range order and periodicity. If, however, a liquid is cooled at a sufficiently fast rate past T_m then crystallisation might be avoided. The now *supercooled* liquid exhibits a dramatic increase in the viscosity upon further cooling. At some point, the constituent molecules of the supercooled liquid rearrange on such slow timescales that they cannot find their equilibrium positions with further reduction of the temperature. Eventually the supercooled

liquid falls out of equilibrium on experimental timescales [1]. Dynamic arrest is observed and the liquid becomes an amorphous solid-like material: a glass. The temperature at which dynamic arrest is observed is termed the glass transition temperature, T_g.

Glasses are ubiquitous in industrial and artistic production and the methods required to form a glass have been known for thousands of years. The earliest recorded example of a pure glass is an ancient Egyptian moulded amulet which dates back as far as 7000 B.C. [2, 3]. Glass production in ancient Egypt varied from the accidental to the controlled. In 1500 B.C. it is thought that the ancient Egyptians had a regularised production routine for the creation of glass vessels. Such production required in-depth knowledge of the high temperature properties of the glass forming materials used [4].

We find a wide variety of amorphous materials or glasses in modern day society. If you were to pose the question "what is a glass?" to someone, they would likely list a number of *examples* of glasses such as windows, containers, spectacle lenses and television screens. These examples are typically made by supercooling a molten mixture of, amongst other things, silica, limestone and sodium carbonate [5]. However, there are many other examples of manufactured products made of amorphous materials and new applications are still being discovered [2]. For example the glass transition is thought to be a key issue in the preservation of food [6] and has far reaching implications for the pharmaceutical industry [7, 8].

The humble STYROFOAM^{TM} cup for example is an amorphous extruded polystyrene foam. Atactic polystyrene is particularly interesting since, due to its lack of steric order almost always forms a glass upon cooling rather than a crystalline solid. Metals, which are highly likely to form crystals upon cooling, can also form glasses if supercooled at a sufficient rate [9]. In fact it can be stated that *any* liquid would be able to form a glass, if cooled fast enough to avoid crystallisation [2, 10].

Although the method of *how* to create a glass is well known, this knowledge is based purely on the empirical observation of the behaviour of supercooled liquids. The question of what properties in a material control the dynamic arrest behaviour does not presently have a definitive answer and remains an important area of study in modern physics [1, 2, 11–13].

Glass formers generally exhibit several molecular relaxation mechanisms (usually designated using Greek letters: $\alpha, \beta, \gamma, \delta$ et.c.) which characterise their behaviour. The slowest relaxation mode, the structural α relaxation process, involves long range collective motions of the constituent molecules and the rapid increase of the timescale on which this process acts is used to characterise the transition to an amorphous glassy state. Glass formers also exhibit secondary relaxations which occur on faster timescales than that of the α relaxation. At the glass transition, a supercooled liquid falls out of equilibrium and the α relaxation is effectively frozen on experimental timescales. In this regime, the secondary modes of molecular motion become more important. Although there is no consensus on the physical nature of the molecular motions involved in these secondary modes, they have been shown to be important in many different systems and applications [9].

Sugar-based glassy matrices can be used to stabilise proteins or preserve proteins for instance in biotechnology or medical applications. It has been shown that the stability of these proteins is directly linked to the timescale of the secondary β relaxation in such systems [14]. Furthermore the β relaxation may prove to be important in controlling glassy ion transport properties used in polymer electrolytes for battery applications. On a more fundamental level, the temperature dependence of the timescale of the β relaxation has been directly related to T_g for a number of different molecular glasses and also metallic glasses and has been suggested as a precursor to the α relaxation [9, 15]. Therefore the understanding of the nature of secondary relaxation processes is of paramount importance and may be the key to understanding the underlying physics of the glass transition.

The following sections serve as a brief introduction to the typical nomenclature encountered when discussing the dynamics of supercooled liquids and the characteristics of glass formation.

1.2 The experimental glass transition

A diagram depicting the behaviour of various thermodynamic quantities such as the enthalpy, H, the entropy, S, and the specific volume V with decreasing temperature at constant pressure is given in Figure 1.1. These properties are

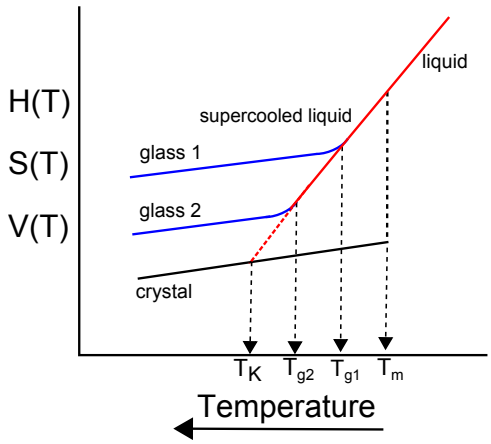

Figure 1.1: Diagram showing the variation of several thermodynamic properties (enthalpy, H; entropy, S; and the specific volume, V) with decreasing temperature at constant pressure. The red line indicates the behaviour of the liquid/supercooled liquid. The black line indicates the behaviour of the crystalline state, with the dashed black line indicating the discontinuity of H, S and V at the melting point, T_m. The two blue lines indicated the behaviour of two glassy states. Glass 1 is formed with a higher cooling rate than glass 2 and thus has a higher glass transition temperature, T_g. The Kauzmann temperature [16],T_K, indicates the point at which the supercooled liquid entropy would become lower than that of the corresponding crystal. This so-called entropy crisis is explained in the text.

all 'first order' in the sense that they are obtained as first order derivatives of the free energy and their temperature dependent behaviour in the liquid state is denoted by the red line. Cooling a liquid thus sometimes results in a first-order thermodynamic transition at the melting temperature, T_m. This results in a discontinuous decrease in the thermodynamic parameters shown in the figure. The material is now in the crystalline state, indicated by the black line in Figure 1.1. If the cooling rate is sufficiently fast, then crystallisation at T_m can be avoided and the thermodynamic properties of the now supercooled liquid decrease at the same rate below T_m as they did above T_m [1, 17].

Upon further cooling, the supercooled liquid exhibits a change in the temperature dependence of H, S and V at a temperature where the material falls out of thermodynamic equilibrium and becomes a glass at the glass transition temperature, T_g. As these 'first order' thermodynamic quantities show continuity (as opposed to discontinuity at the liquid to crystal transition, T_m) at T_g, the glass transition can be said to resemble a second-order thermodynamic phase transition [2, 18]. However, a second-order transition of this type would also exhibit a discontinuous change in the temperature derivative of H, S and V and this is not the case. This is quantified by the specific heat capacity at constant pressure, C_p, as will be described in Chapter 3. Moreover, T_g is not unique and is sensitive to the cooling rate. The blue lines in Figure 1.1 denote the behaviour of two different glasses where 'glass 1' has been formed with a faster cooling rate than 'glass 2' at glass transition temperatures T_{g1} and T_{g2} respectively. This suggests that the observed glass transition is not a genuine thermodynamic phase transition and is also coupled to the kinetics of the supercooled liquid.

The entropy of a material in the supercooled liquid state is significantly higher that the entropy of the corresponding crystal state just below the melting point [2]. However, as temperature is decreased the entropy of the supercooled liquid decreases at a faster rate than that of the corresponding crystal. It follows that at a certain temperature, the entropy of the supercooled liquid would become lower than the entropy of the corresponding crystal, which is unphysical and was termed an 'entropy crisis' by Kauzmann [16, 17, 19]. The temperature at which this crisis occurs is known as the Kauzmann temperature, T_K. In reality, supercooled liquids exhibit a glass transition above T_K and therefore the entropy

crisis is never realised. The idea has however motivated the idea of the possible existence of an underlying true thermodynamic second-order phase transition that would occur at T_K [17] if experiments could be performed at slow enough rates without interference from crystallization.

1.3 Dynamics of supercooled liquids

Supercooled liquids exhibit a significant increase in their shear viscosity, η with decreasing temperature. In order to characterise this increase, we can consider the relaxation mechanisms present in a supercooled molecular liquid. The α, relaxation is the time-scale on which a particular disordered structure relaxes and thus flow can take place. The temperature dependence of this structural relaxation timescale, τ_α can be used in order to define the glass transition.

1.3.1 The structural relaxation

As a glass-forming system is cooled, the α relaxation involves an increasing number of collective molecular motions and thus the timescale on which this relaxation take place, τ_α, increases. The increasingly cooperative nature of the α relaxation as temperature is decreased also leads to an increase in the shear viscosity, η. At a certain viscosity, the supercooled liquid will act 'solid-like' on experimental timescales [20]. The glass transition temperature, T_g, is often defined at the temperature at which the shear viscosity, η, reaches values above 10^{13} Poise [21]. Maxwell's theory of viscoelasticity provides a relationship between η and τ_α [2, 18, 22],

$$\eta = G_\infty \tau_\alpha, \tag{1.1}$$

where, G_∞ is the instantaneous shear modulus. If the glass transition is defined at the point at which $\eta = 10^{13}$ Poise, then this corresponds to a structural relaxation timescale of around 100s. Although this definition of the glass transition is somewhat arbitrary, T_g values defined in this manner correspond well to those defined from the variation of thermodynamic properties such as the heat capacity.

Molecular motions within a material can often be described as thermally activated or Arrhenius processes with a fixed activation energy, E_A [23]. The timescale on which these molecular motions is thus simply related to the ratio of the activation energy and thermal energy, as E_A/k_BT:

$$\tau = \tau_0 e^{\frac{E_A}{k_B T}}, \tag{1.2}$$

where τ_0 is the limiting timescale at infinite temperature and k_B is the Boltzmann constant. Values of τ_0 are usually comparable to typical microscopic timescales of liquids at high temperature, between 10^{-12} and 10^{-14}s [2, 24–26].

However, the timescale of the structural α relaxation often increases at a much faster rate with decreasing temperature than that predicted by the Arrhenius equation. This suggests that the mechanism of the structural relaxation process in this case is not governed by a temperature independent energy barrier but rather one which increases with decreasing temperature. The rapid change of τ_α as the glass transition is approached is well described by the empirically derived Vogel-Fulcher-Tammann equation [27–29],

$$\tau_\alpha = \tau_0 e^{\frac{DT_0}{T-T_0}}. \tag{1.3}$$

Here, T_0 is the temperature at which τ_α tends to infinity. D is the so-called strength parameter and is a measure of the temperature dependence of τ_α.

The behaviour of the timescales of the α, β and γ relaxations in a so-called Arrhenius plot ($\log_{10}(\tau)$ versus $1/T$) are shown in Figure 1.2a. The dashed line indicates $\tau_\alpha = 100$s, the point at which T_g is often defined. The timescales for the secondary relaxation processes generally follow an Arrhenius temperature dependence in the glassy state, or in other words have a fixed gradient in an Arrhenius plot. For some glass formers, the τ_β data appear to cross the τ_α data implying a relaxation bifurcation scenario [30], where a separation of the two relaxation processes occurs. This occurs at a temperature, $T^{\alpha\beta}$ (with a corresponding timescale, $\tau_{\alpha\beta}$) as marked in the figure.

It should be noted that although the VFT expression provides good description of the temperature dependence of τ_α at $T < T_g$, there are several examples of experiments in which this description of τ_α breaks down in the highly viscous

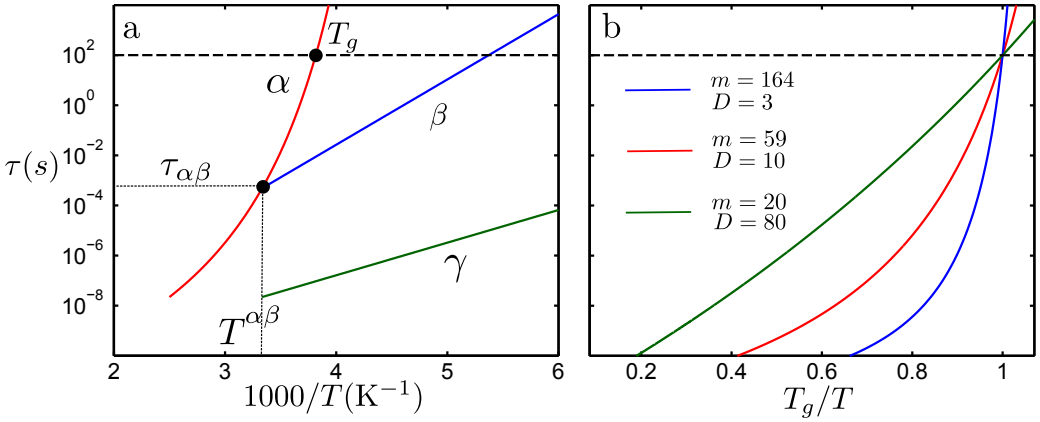

Figure 1.2: a) Typical timescale behaviour of the α, β and γ relaxations. The timescale at which the τ_β data cross the τ_α data occurs at the so-called crossover temperature, T^*. b) VFT behaviour of τ with differing values of the strength parameter, D.

regime above the empirically defined glass transition [2, 25, 31, 32]. However, for the purposes of this research, in which values of τ_α will be considered at timescales less than 100s, it provides a means through which the τ_α data can be accurately described.

Dynamic Fragility

Different glass-formers vary in the behaviour of τ_α in the region close to T_g. The departure from the fixed energy barrier behaviour suggested by the Arrhenius equation is quantified by the D parameter in the VFT equation (Equation 1.3) and this is most clearly observed in a T_g rescaled Arrhenius plot as shown in Figure 1.2b. The τ_α behaviour predicted by the VFT equation with differing values of D as T_g is approached is shown in Figure 1.2b. It is clear from the figure that glass-formers with smaller values of D have a stronger temperature dependence of τ_α. This allows for the classification of glass-formers based on this temperature dependence. Supercooled liquids with weaker temperature dependence of τ_α (high D) are termed 'strong', whereas liquids with the greatest departure from this behaviour are termed 'fragile'.

Another metric for describing this behaviour is the fragility parameter, m,

which is defined as the rate of change of $log_{10}\tau_\alpha$ at T_g, proposed by Angell [32].

$$m = \left.\frac{d(log_{10}\tau_\alpha)}{d(\frac{T_g}{T})}\right|_{T=T_g} \tag{1.4}$$

Values of m are also shown in Figure 1.2b. If it is assumed that τ_0 is 10^{-14} (a typical microscopic timescale [2, 24–26]) then a value of $m = 16$ represents Arrhenius behaviour of τ_α [2]. Strong glasses generally have low values of m, whereas fragile glasses have much higher values of m. For example, the m value of toluene, a typically fragile glass-former, is over 100 [33]. However it should be noted that this definition of m does not necessarily imply a departure from Arrhenius behaviour. Indeed, one could imagine a situation in which the structural relaxation timescale behaves in an Arrhenius manner (fixed gradient in an Arrhenius plot) but is characterised by a large energy barrier. In this situation, the derivative of the data at $\tau = 100$s would be large, corresponding to a large m parameter but also a low D parameter. In this sense it is perhaps more logical to describe the temperature dependence of τ_α over the entire temperature range, rather than considering the gradient of the VFT description at a fixed temperature.

Another method used in order to analyse the temperature dependence of τ_α is to investigate whether $\tau_\alpha(T)$ behaves in a VFT-manner by linearizing the relaxation time data using a derivative or so called Stickel [31] analysis of τ_α. We introduce the quantity, Z, as follows:

$$Z = \left(\frac{dlog\tau_\alpha}{d(\frac{1}{T})}\right)^{-\frac{1}{2}} = \left(\frac{loge^1 DT_0}{(\frac{T_0}{T}-1)^2}\right)^{-\frac{1}{2}}. \tag{1.5}$$

An example of such an analysis is shown for a molecular glass former, butylbenzene, in Figure 1.3a. The dashed horizontal line indicates Arrhenius behaviour of τ_α and thus we can see that such a plot leads to yet another definition of the departure from such behaviour. This is quantified by the gradient of the linearised values, $-S$. The line interpolating the data is a result of the temperature derivative of the VFT fit to the τ_α data for butylbenzene, calculated using Equation 1.5. Furthermore, the gradient $-S$ is related simply to the strength parameter

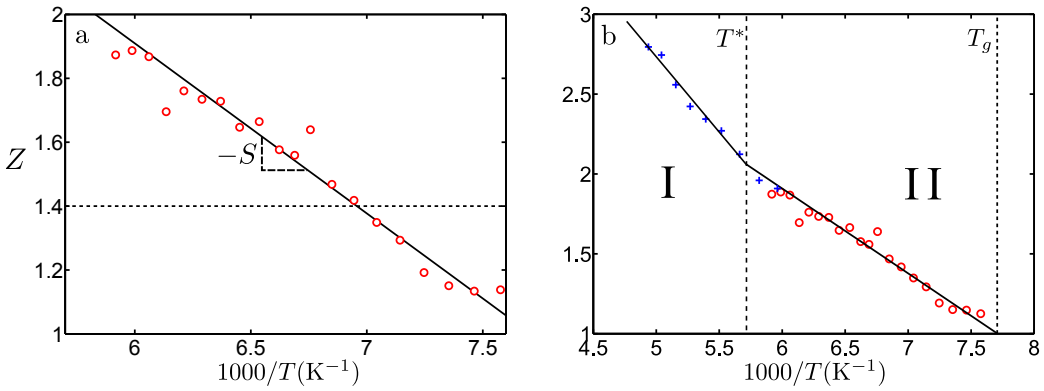

Figure 1.3: a) Linearised τ_α data determined for butylbenzene. The dashed horizontal line represents Arrhenius behaviour. (b) Stickel parameters for determined for butylbenzene with data from the literature (+)[34]. There is a marked change in the VFT behaviour of τ_α at a specific temperature, T^*, leading two regions (I and II) to be defined.

D and T_0 obtained through VFT fits of the τ_α data:

$$S = \left(\frac{T_0}{loge^1 D}\right)^{-\frac{1}{2}}. \tag{1.6}$$

In some instances, the linearisation of the timescale data can yield a change in the temperature dependence of τ_α which can not be easily resolved in an Arrhenius plot. An example of this is shown for butylbenzene in Figure 1.3b, where the data in Figure 1.3 have been combined with data measured by Hansen *et. al.* [34]. From this figure, we see a 'kink' in the data indicating a change in the temperature dependence of τ_α. This allows us to define two dynamic regimes, I and II, as indicated in the figure. Close to T_g (region II), the τ_α data follow one VFT behaviour but as the temperature is increased past a certain point, the VFT behaviour changes. This occurs at a temperature defined as the dynamic crossover temperature, T^* [30, 35, 36].

A number of dynamic properties have been observed to change at T^* [37]. The decoupling or bifurcation of the α and β relaxations has often been observed at this temperature, indicating that $T^{\alpha\beta} = T^*$ [30]. One can also observe the decoupling of rotational and translation diffusion [38] and changes in the temperature dependence of the dielectric strength [37, 39].

Non-exponential relaxation

The relaxation function, $\Phi_\alpha(t)$ characterises the evolution in time of the α relaxation process. It is observed, that this relaxation function generally decays in a non-exponential fashion [2, 40] and is often described using the Kohlrausch-Williams-Watts stretched exponential function [41, 42]:

$$\phi(t) = e^{-\left(\frac{t}{\tau}\right)^{\beta}}. \tag{1.7}$$

Here, the stretching parameter, β, takes values between 0 and 1 and parametrises the degree of non-exponentiality. In this research, measurements of a range of molecular glass formers were studied in the frequency domain using Broadband Dielectric Spectroscopy (BDS). Relaxation mechanisms are manifested as peaks in the dielectric loss, ε''. The stretched nature of $\phi_\alpha(t)$ is evident in the frequency response and results in the anti-symmetric stretching of the peak found for the α relaxation. This will be fully explained in Chapter 2.

The origins of the non-exponential nature of $\Phi_\alpha(t)$ are much debated. On the one hand one could say that the relaxation function is inherently non-exponential and each region in a glass former contributes equally to the decay of the relaxation function. This is an attractive scenario as it implies that the relaxation of each region is representative of the macroscopic variation of the glass [43]. On the other hand, one could consider the possibility of so-called dynamic heterogeneity, suggesting that a supercooled liquid contains many dynamic regions each of which relaxes with an exponential nature and with its own relaxation time [44]. Although experimental evidence for either case depends on the time scale of the probe used to analyse a supercooled liquid, the majority of measurements suggest a dynamically heterogeneous scenario is more likely [45–47]. This does not, however, mean the issue has been fully resolved [44].

1.3.2 Secondary relaxation mechanisms

In some molecular glass formers, relaxation mechanisms which occur on faster timescales than the structural α relaxation are observed as the supercooled liquid is cooled. Unlike the α relaxation, the timescales of these secondary mechanisms

are usually well described by the Arrhenius equation (Equation 1.2). The typical temperature dependence of the timescales of two secondary mechanisms (β and γ) are shown in Figure 1.2a.

The first observed secondary relaxation mechanism is generally termed the β relaxation process. This relaxation process has been the subject of many studies into the the dynamics of glass formation. Below T_g, the α relaxation is completely arrested on typical experimental timescales and thus much of the motion in the glassy state can be attributed to the β relaxation process [9].

The secondary β relaxation was first observed in polymeric glass formers [48–50]. For many polymeric systems, this relaxation mechanism was attributed to the small, trivial rotation of a methyl-group or motion involving the side chains of a polymer [49]. Thus, β relaxation processes were thought to be of intramolecular origin and were often thought not to play an important role in the glass transition [51]. However, Johari and Goldstein observed β relaxations in a number of 'rigid' molecular glass formers [52–54]. An example of the dielectric loss, ε'', spectrum for such a molecular glass-former, toluene, is shown in Figure 1.4a (a full description of Broadband Dielectric Spectroscopy and the obtained spectra is available in Chapter 2). Here we see two peaks in the spectrum relating to the α and β relaxation mechanisms as indicated in the figure. The fact that such secondary relaxations can be observed in 'simple' molecular glass formers comprised of rigid molecules with no intramolecular degrees of freedom suggests that the observed β relaxations could involve certain motions of the entire molecule [51]. Furthermore, it could be said that the β relaxation is of intermolecular origin.

There is no general consensus on the microscopic origins of the β relaxation but there have been several suggestions. Johari proposed that a supercooled liquid could be thought of as a solid matrix with so-called islands of mobility which arise due to the redistribution of the free volume [52, 54, 56, 57]. The β relaxation was thought to be a consequence of the relaxation of these liquid-like regions within the solid matrix. Goldstein attributed the β relaxation to 'connecting tissue' between amorphous clusters [18]. Tanaka introduced the idea of 'metastable islands' of particles, the creation and destruction of which are controlled by the α relaxation [58]. The β relaxation was suggested to be local restricted reorientational, vibrational or hopping motion within an island. Contrary to the idea that

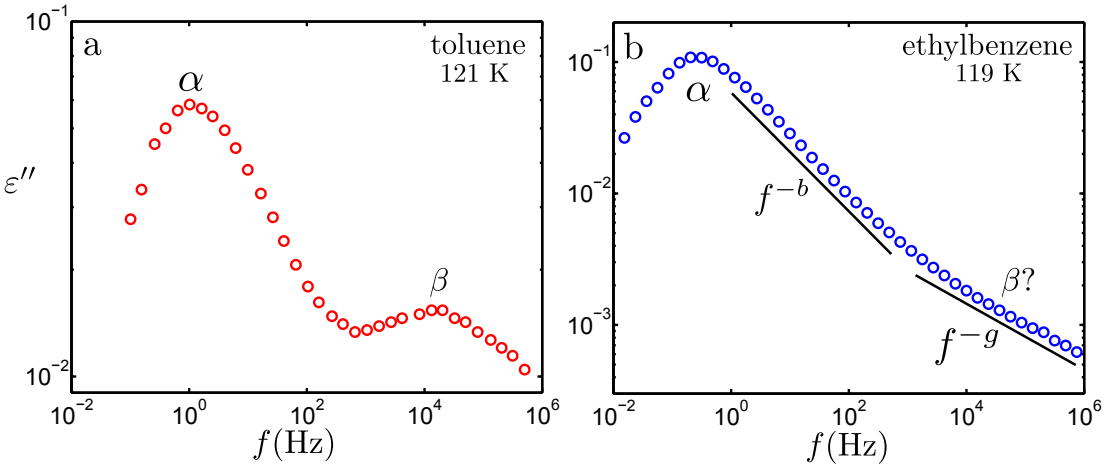

Figure 1.4: a) Dielectric loss, ε'', spectrum for toluene at 121 K, showing both α and β relaxation loss peaks. Data obtained from Ref.[55]. b) Dielectric loss spectrum for ethylbenzene at 119 K showing so-called 'excess-wing' behaviour.

the β and α relaxations relate to small areas of motion within the supercooled liquid, Williams and Watts stated that the β relaxation is due to the relaxation of *all* molecules of a system where the microscopic motion involves small angular fluctuations and is thought to be related to the so-called 'primitive' α behaviour [59, 60]. Thus, we do not know what the β relaxation is; what molecular motions it involves or what length scale it acts on. This enhances the need for further study, particularly of systems in which the structure is varied systematically, in order to determine the physical origins of the β relaxation.

Several interesting connections between the α relaxation and the β relaxation have been observed and the relationship between the two relaxation processes will be a key feature in the research presented in this thesis. Firstly, Kudlik *et. al.* [55, 61] noticed that for several glass formers, T_g, is proportional to the activation energy of the observed β relaxation and suggested the following relationship,

$$E_A = KRT_g, \tag{1.8}$$

where R is the universal gas constant. They found that the proportionality constant, K, was similar for the systems analysed and yielded a value of $K = 24 \pm 3$. This was confirmed by Ngai through the analysis of a wide selection of glass formers [15]. This observation also appears to hold also for metallic

glasses for which K was found to be 26 ± 2 [9]. As T_g is defined through analysis of the timescales of the α relaxation, this implies a direct connection between the β relaxation and the α relaxation. Furthermore correlations between the timescale of the β relaxation at the glass transition temperature, $\tau_\beta(T_g)$, the fragility parameter, m, and the stretching exponent of the KWW function have been observed for more than 50 molecular glass formers [56]. In some situations it has been observed that $\tau_\beta \approx \tau_0$, where τ_0 is the high temperature limiting timescale of the α relaxation [62]. These observations all imply a connection between the α and β relaxations and enforces the need for more comprehensive analyses of secondary processes within glass forming materials.

1.3.3 The excess-wing

A different scenario is shown in Figure 1.4b. In this figure, the dielectric spectrum for ethylbenzene at 119 K is shown. Toluene and ethylbenzene both contain benzene rings with an attached alkyl-tail. Although they only differ by a methylene group (CH_2) the nature of their spectra are clearly different. The spectrum for ethylbenzene does not have a resolvable loss peak relating to the β relaxation. Instead, we observe a change of the exponent of the high frequency power law of the α relaxation (from b to g as indicated in the figure). This so-called 'excess-wing' has been observed for a number of molecular glass formers (for example: glycerol [63] propylene carbonate [64] and salol [65]) and in the past this has led to the classification of glass-formers based on whether they exhibit an excess-wing (Type A) or a separately resolved β process (Type B) [55, 66].

Nagel and co-workers showed that the dielectric loss for a number of glass-formers which exhibit excess-wing behaviour can be scaled onto one master-curve [67]. This led them to suggest that the excess-wing is an intrinsic property of all glass-formers [68]. However, more recently it has been shown that the excess-wing is likely of a similar physical origin to the β relaxation in studies of an oligomeric chain series of propylene glycol based dimethyl ethers in research published by Mattsson *et. al.* [69]. In this research it was shown that for the longest chain length the α and β processes were separately resolvable in dielectric loss spectra. It was observed, for the shorter chain-length samples, that the peak frequencies of

the observed β relaxation moved closer to that of the α relaxation: the timescales of the β relaxation became increasingly slower with decreasing chain-length. For the lowest molecular weight samples, this meant that the β loss peak was no longer discernible as a separate process, and an excess wing was observed on the high frequency flank of the α loss peak. This is evidence to suggest that the excess-wing could be due to a 'submerged' β relaxation process. Several other studies involving variation of pressure [70], ageing [71] and confinement [72] yield similar conclusions. Evidence for similar behaviour in the systems studied in this research will be presented in Chapters 4, 6 and 7.

Thus, in conclusion it appears that at least one secondary relaxation is generally present in molecular glass-formers and this relaxation is coupled to the structural α relaxation and thus glass-formation. Thus, the importance of secondary relaxation modes together with their relatively 'local' nature makes them ideal channels for controlling material behaviour if we can learn how to systematically control them and properly understand the link to the structural relaxation. As described above, a lot of research has gone into trying to understand the exact mechanisms of motion involved in β relaxations. However, we note that the detailed motions are almost by necessity chemistry and system dependent and this might not be the most interesting question to ask in order to reach a general understanding of the glass-transition phenomenology. Recent work both on molecular [15], metallic [9] and colloidal systems [73] indicate that the glass transition phenomenology might be largely emergent. Thus any secondary relaxation mode that is efficient at 'locally' relaxing the material might serve to 'nucleate' the α relaxation and thus control the glass-transition.

1.4 Models to explain the dynamics of supercooled liquids.

Many models have been suggested in order to explain the rapid increase of the structural relaxation timescale at temperatures close to T_g. Given the wide array of approaches, it is beyond the scope of this thesis to provide a detailed analysis of these models (the following references provide more detailed discussions: [1, 2, 11,

13, 32, 44, 74, 75]). However, the following sections serve as a brief introduction to those theories most commonly discussed in the literature and, more specifically, those mentioned in latter chapters in this thesis.

1.4.1 Entropy models

Some models attribute the observed increase of the structural relaxation timescale with decreasing temperature to a reduction in the number of molecular configurations and therefore a decrease in the configurational entropy, S_c. Such models consider the observed glass transition to be an indication of an underlying thermodynamic glass transition at which $S_c = 0$, equivalent to that of the ideal crystalline state. The most commonly discussed example of an entropy based model is that presented by Adam and Gibbs [76]. They introduced the concept of cooperatively rearranging regions (CRRs) which are defined as a subsystem of molecules whose relaxations between different configurational states are independent of the surrounding media [2, 13, 75]. The minimum size of a CRR is assumed to be temperature dependent, including more molecules as the temperature decreases. In this manner, the structural relaxation timescale can be expressed in terms of S_c under the assumption that the activation energy of the structural relaxation is proportional to the volume of a CRR [2]:

$$\tau_\alpha = \tau_0 e^{\frac{A}{TS_c(T)}}. \tag{1.9}$$

The constant, A, relates to the size of a CRR. The exponent in Equation 1.9 suggests that the increase in the structural relaxation time is related to the increasing size of a CRR with decreasing temperature. If it is assumed that an ideal thermodynamic glassy state exists at the Kauzmann temperature, T_K (see Section 1.2) and that the configurational entropy, S_c would be zero at T_K, one can define the temperature dependence of S_c as:

$$S_c = B\frac{(T - T_K)}{T}, \tag{1.10}$$

where B is a constant. Substitution of this into Equation 1.9 yields the VFT equation with the identification that $T_0 = T_K$ and that $1/B = DT_K$. The fact that

experimentally determined values of T_0 are sometimes close to those of T_K yields a level of validation for the Adam-Gibbs model [1] although this has also been shown not to apply in general [77]. Furthermore, experimental determination of the variation of configurational entropy is difficult for glass formers and even if this is achieved (to a certain approximation), determination of the 'size' of a CRR typically yields regions which consist of a very small number of molecules [78] which makes it unlikely that the relaxations within CRRs act independently of their surroundings [2].

1.4.2 Free volume models

Another approach used to explain the dynamics of the glass transition has been to consider the 'free volume' of a glass former as originally suggested by Cohen and Turnbull [79]. The fundamental principle of this approach is based on the assumption that the constituent molecules within a glass former require a certain free volume, V_f, in order for structural reorientation to take place [2]. The free volume is simply defined as the volume in the system which is unoccupied, and the free volume of the system is shared between the constituent molecules [1, 18]. As the temperature of a glass forming material decreases, V_f decreases. At a certain critical temperature, the system no longer has enough free-volume in order for structural relaxation of the system to occur, resulting in dynamic arrest. The prediction of the models is that the structural relaxation timescale is related to the temperature dependent free volume per molecule, v_f [2]:

$$\tau = \tau_0 e^{\frac{A}{v_f}}. \tag{1.11}$$

Under some assumptions, this equation can be shown to be related to the VFT equation [2]. An extension to the simple free volume model was proposed by Cohen and Grest [80] who suggested that a supercooled liquid could be described as having solid-like and liquid like regions. Relaxation within the liquid was then thought to be due to the exchange of the free volume between molecules in the liquid regions. As the temperature of a system decreases the solid-like regions become larger due to the lack of free volume. The glass transition is then defined

at the point at which the solid-like regions span the entire system, at the so-called percolation limit [1].

One obvious problem with models of this type is that the free volume of a molecule can not be defined rigorously. Furthermore the structural relaxation time is not only a function of the density of a glass former [2] and supercooled liquids measured at constant volume (isochoric) conditions can still exhibit a glass transition [81]. These problems suggest that one needs to consider more than just the redistribution of free volume in order to explain dynamic arrest.

1.4.3 The coupling model

The 'coupling model' introduced by Ngai [18, 82–84] is a generalised approach to the relaxation in complex systems which suggests the motions of molecules are inhibited by interactions between them. The model predicts a temperature insensitive crossover time, t_c, and for times shorter than t_c the relaxation of constituent molecules occurs non-cooperatively. The correlation function is thus described as a single exponential: $\Phi(t) = \Phi_0 e^{-t/\tau_0}$, where τ_0 is the primitive relaxation timescale of the molecules. At $t > t_c$, a stretching of the correlation function is predicted, leading to non-exponential decay:

$$\Phi(t) = e^{-\left(\frac{t}{\tau}\right)^{1-n}} \tag{1.12}$$

This is characterised by the coupling parameter, n, which is dependent on the interaction between the molecules. The coupling parameter can take values between 0 and 1 and is related to the KWW stretching parameter: $n = 1 - \beta$. In this regime, the decay of the correlation function is characterised by a timescale, τ^*. The crossover between exponential and non-exponential decay of the correlation function occurs smoothly over a small region surrounding t_c. The continuity between these two relaxation regimes leads to the following expression:

$$\tau^* = \left[t_c^{-n}\right]^{\frac{1}{1-n}} \tag{1.13}$$

Although no insight into the microscopic relaxations of molecules are provided by this model, it has been shown to apply in a wide range of different fields

dealing with complex dynamics[82]. It has also be used to predict the relationship between T_g and the activation energy, E_a of the β relaxation [62]. An important conceptual feature of the model is that it is based on the idea of a secondary relaxation acting as the precursor for the α relaxation.

1.4.4 Mode coupling theory

Mode Coupling Theory (MCT) [18, 85–88] has been highly successful in explaining the dynamics of supercooled liquids in a certain temperature regime above the experimentally observed glass transition [1]. MCT is a purely dynamic picture of the glassy state involving the idea of a molecule fluctuating within a 'cage' of its neighbouring molecules. The motion of each individual molecule will affect both the motion of the same molecule at a later time and the surrounding molecules. The 'coupling' stems from the idea that there is an energy exchange between the different dynamic modes of the system. MCT involves finding solutions to a set of equations for the density autocorrelation function, $\phi(t) = \langle \rho_q(t)\rho_q(0)\rangle \,/\, \langle |\rho_q|^2\rangle$, where the subscript, q, denotes the wave vector dependence of $\phi_q(t)$. Density fluctuations within a liquid are thought to govern the structural relaxation timescale and are thus responsible for the glass transition. The simplest example of MCT's approach to describe the time variation of $\phi_q(t)$ can be expressed by considering the density fluctuations to act as oscillators [85, 86]:

$$\partial_t^2\phi_q(t) + \nu_q\partial_t\phi_q(t) + \Omega_q^2\phi_q(t) + \Omega^2\int_0^t m_q(t-t')\partial_t\phi_q(t')\mathrm{d}t' = 0. \tag{1.14}$$

Here ν_q and Ω_q set the frequencies of liquid dynamics and thus set the timescales for microscopic motion, where ν_q is proportional to the bulk and shear viscosities and Ω_q is proportional to the the bulk and shear moduli [88]. The MCT 'kernel', m_q, is a so-called memory function which acts as a non-linear feedback mechanism for density fluctuations of a single particle [85]. In other words, a moving molecule will affect the density fluctuations of the surrounding molecules which will in turn 'feed back' to the original molecule and this effect is encompassed by m_q. In order to solve Equation 1.14, appropriate choices of m_q must be made.

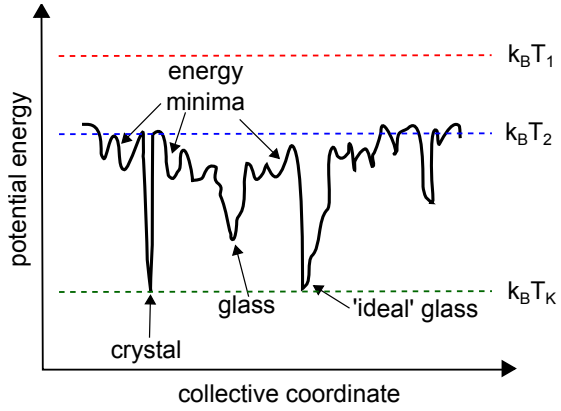

Figure 1.5: Diagram depicting the energy landscape as described in the text

The simplest choice is to describe m_q in terms of two control parameters, v_1 and v_2:

$$m_q(t) = v_1\phi_q(t) + v_2\phi^2(t) \tag{1.15}$$

Under this simple approximation of the memory function, a set of solutions to Equation 1.14 can be obtained which predict the dynamic arrest associated with the glass transition [86, 87]. The theory also predicts two separate relaxation mechanisms, related to the structural relaxation and a more local relaxation [87].

1.4.5 The energy landscape

The energy landscape model, proposed by Goldstein [89], provides a description of a viscous liquid by means of a potential energy hypersurface as a function of the coordinates of the constituent particles [13, 18, 90]. In the simplest example, in which N particles are considered to have no orientational or vibrational degrees of freedom, the landscape has 3N + 1 dimensional shape [17] as each particle coordinate can be described in three dimensions with the configurations of all particles described by a potential energy. A representative diagram of this landscape is shown in Figure 1.5 in which a generalised coordinate for all the particles in the system is shown.

The landscape is considered to be virtually independent of temperature and thus the temperature of the viscous liquid only affects the resolution at which

the liquid 'feels' the landscape [17]. For example, at $T = T_1$ in Figure 1.5, the system is unaffected by the landscape and the particles are free to diffuse. As the temperature is decreased, $T = T_2$, the topology of the landscape comes into effect but the system still has enough energy to sample the entire landscape and the energy minima appear shallow. In some cases, the system falls into the sharp minimum corresponding to the crystalline state.

Further decreases of temperature mean the system no longer has enough energy to surpass the larger energy barriers between minima and is therefore forced to sample the deeper, less common minima in the landscape. This leads to non-exponential behaviour of the structural relaxation timescale due to the increasing size of the energy barriers between different configurational minima [17]. At a certain temperature, the system will effectively become 'stuck' in a certain energy minimum, corresponding to the glass transition. If we assume the suggestion that there should be an 'ideal' thermodynamic glassy state, this will correspond to a deep minimum on the order of the size of the crystal minimum. In terms of the fragility, more fragile glasses are thought to have a greater density of states [13, 91, 92]. It is also interesting to note that computer-based investigations of the landscape properties have demonstrated that within one of the larger minima corresponding to a particular glassy state, there is a secondary structure of smaller minima [17]. Thus, a landscape approach can conceptualise the bifurcation of the relaxation dynamics into α and β relaxations as the temperature is reduced below a cross-over temperature, T^*, denoted T_2 in Figure 1.5.

1.5 Research aims

The work presented in this thesis is aimed at understanding the dynamics of glass-forming systems through the analysis of three systematic series of molecular glass formers. These series are characterised by the systematic variation of chemical structure: an alkylbenzene series involving the systematic variation of the length of an alkyl tail attached to a phenyl-ring and two series involving the successive oligomerisation of styrene and α-methylstyrene, respectively. All three series are structurally related which facilitates a consistent investigation of how structural modification affects relaxation behaviour in supercooled liquids and polymers.

The aims of the research are to i) quantify the connection between glass forming properties such as the glass transition temperature and the fragility as a result of the variation of molecular structure, ii) analyse the nature and behaviour of the structural and secondary relaxation mechanisms and evaluate the connection between them and iii) observe the difference in glass forming dynamics with different types of structure variations.

Chapter 2

Experimental Techniques I: Broadband Dielectric Spectroscopy

2.1 Introduction

Glass forming liquids often demonstrate a dramatic increase in the structural relaxation timescale as temperature is decreased towards their glass transition temperature. Broadband Dielectric Spectroscopy (BDS) is a useful technique for the study of glass-forming systems as its operational frequency range can be between 10^{-6} and 10^{11}Hz allowing the dynamics of glass forming systems to be studied over a large range of timescales [93]. The spectrometers used in this study have a frequency range of 10^{-2} to 10^{6}Hz corresponding to timescales between $\sim$15s and $\sim$0.15μs. BDS involves the application of a harmonic electric field to a material. This perturbation results in a macroscopic polarisation. The equilibrium polarisation depends on the structure and temperature of the material and the underlying microscopic dynamics determine the timescale at which equilibrium is attained. Thus, through measurement of the macroscopic polarisation as the result of an applied electric field, one can gain structural and dynamic information about a material.

This chapter is split into several sections. Firstly, the theory of dielectric relaxation will be introduced and this will mainly follow the books of Kremer

and Schönhals [94], Böttcher, Bordewijk and Rip [95], Runt and Fitzgerald [96] and also the theses of Gainaru [97] and Blochowicz [98]. Next, the different components of the spectrometers used in this research will be explained. Finally a brief compilation of functions used to describe dielectric spectra will be given with an explanation of how the dielectric spectra were analysed in this research.

2.2 Dielectric properties of matter

Consider a charge, q, *in vacuo*. If another similar charge, q' is placed nearby, there will be a force between the two charges, according to Coulombs inverse square law [95]:

$$\mathbf{F} = \frac{qq'}{4\pi\varepsilon_0 r^2}\hat{\mathbf{r}}, \tag{2.1}$$

where r is the distance between the two charges and ε_0 is the permittivity of free space. The electric field, $\mathbf{E}$ resulting from the charge q at a distance r is defined as the force acting on a small positive test charge q' divided by the test charge,

$$\mathbf{E} = \frac{q}{4\pi\varepsilon_0 r^2}\hat{\mathbf{r}}. \tag{2.2}$$

If the assumption that the electric field intensity resulting from a distribution of charges in a certain volume of space is an additive combination of the contributions from these charges, then the divergence of the total electric field is equal to the charge density. In order to determine the electric field within matter, Maxwell introduced a vector field termed the electric displacement field, $\mathbf{D}$, which would satisfy the condition that its divergence would be related to the charge density [95]. This leads to the definition of Maxwell's so-called 'source equation':

$$\nabla \cdot \mathbf{D} = \rho_e \tag{2.3}$$

In the linear response regime, for relatively small electric field strengths, there

is a linear relationship between an applied electric field, $\mathbf{E}$, and $\mathbf{D}$ [94, 95]:

$$\mathbf{D} = \varepsilon_s \varepsilon_0 \mathbf{E}, \tag{2.4}$$

where ε_0 is the permittivity of free space and ε_s is the static dielectric permittivity.

As mentioned in the introduction, a material subjected to an external electric field results in a macroscopic polarisation, $\mathbf{P}$, of the material. The polarisation of dielectric, or insulating, materials occurs through several mechanisms [18, 94, 95, 97]:

1. the reorientation of permanent dipoles, μ,
2. a displacement of the electrons clouds relative to their nuclei and,
3. a displacement of the nuclei relative to each other.

Through these mechanisms, the electric field polarises the material. In the study of glass forming materials, we are interested in the polarisation due to the reorientation of permanent dipoles as this is the important mechanism of polarisation within the relevant frequency range and it probes the underlying microscopic dipoles and thus molecular dynamics. Mechanisms 2 and 3 give rise to a so-called induced polarisation, $\mathbf{P}_\infty$. These mechanisms occur on timescales ($< 10^{-13}$s) which are inaccessible in the frequency range of the dielectric spectrometers used in this research.

Additional mechanisms can also give rise to macroscopic polarisation. If a polar material contains charged species, then the application of an electric field will cause these species to diffuse. This so-called DC-conductivity is an important consideration for many of the glass formers studied in this research as will be shown in latter sections of this chapter. At very low frequencies, and thus very long timescales, these charged species can accumulate at the boundaries set by the containing electrodes. This is termed electrode polarisation. Furthermore, if a material contains different structural domains, accumulation of charge at the interfaces between domains can occur. This interfacial polarisation is called Maxwell-Wagner polarisation [97, 99].

2.2.1 The static case

We will now address what happens to a dielectric or insulating material under the application of an electric field **E** . Firstly, let us consider the static case, in which variations in applied electric field occur on greater timescales than those of the microscopic mechanisms within the dielectric material. For the purposes of the following discussion, it will be assumed that the material consists of rigid molecules with permanent dipole moments. Let us also assume that the material does not contain free charges. Thus we can neglect contributions to the polarisation due to conductivity.

Before an electric field is applied, the permanent dipoles within the material are effectively randomly oriented. When an electric field is applied, the dipoles will preferentially orient in the direction of the applied field, creating a macroscopic dipole moment. This creates a so-called orientational polarisation of the material, $\mathbf{P_0}$.

Under the application of an electric field, the total macroscopic polarisation of the material, **P**, increases proportionally to the strength of the applied field, **E**.

$$P = D - \varepsilon_0 \mathbf{E} = (\varepsilon_s - 1)\varepsilon_0 \mathbf{E} \tag{2.5}$$

The term $(\varepsilon - 1)$ in Equation 2.5 is a measure of how susceptible a particular material is to polarisation by an applied field. One can define the static dielectric susceptibility: $\chi_s = (\varepsilon - 1)$. In general, as **E** and **P** are vectors, ε_s (and therefore χ_s) are thus tensors. However, given that the glass-forming materials we consider in this work are macroscopically isotropic, the directionality of ε_s can be ignored [99].

The absolute magnitude of the total macroscopic polarisation is the summation of the orientational polarisation and the induced polarisation, $P = P_\infty + P_0$. Let us introduce the quantity $\Delta\varepsilon = \varepsilon_s - \varepsilon_\infty$, which is often termed the dielectric relaxation strength or dielectric loss [94–96]. ε_∞ is the dielectric permittivity associated with the response at much higher frequencies than those associated with

dipolar reorientation. We can now express the total macroscopic polarisation by substituting $\varepsilon_s = \Delta\varepsilon + \varepsilon_\infty$ into Equation 2.5:

$$\mathbf{P} = \mathbf{P}_\infty + \mathbf{P_0} = \varepsilon_0(\varepsilon_\infty - 1)\mathbf{E} + \varepsilon_0\Delta\varepsilon\mathbf{E}. \tag{2.6}$$

The orientational polarisation, $\mathbf{P_0}$, is the vectorial sum over all dipole moments, μ within the material per unit volume. For the purposes of this discussion we shall consider that the electric field E acts in the 'z' direction and the projection of P_0 on this direction is thus:

$$\mathbf{P_0} = \frac{1}{V}\sum_{i=1}^{N}\mu_i \cdot \mathbf{z} = \frac{N}{V}\langle\mu\rangle_z \tag{2.7}$$

Here, $\langle\mu\rangle_z$ denotes the average over all dipole moments in the z-direction and N is the total number of dipoles.

The permanent dipoles are never all fully aligned with the applied electric field due to thermal fluctuations . Therefore, we can consider the orientations of these dipole moments as a distribution within a solid angle $\mathrm{d}\Omega = 2\pi\sin\theta\mathrm{d}\theta$ around the direction of the applied field, z [97]:

$$\langle\mu\rangle_z = \frac{\int_0^\pi \mu_z e^{\left(\frac{\mu_z E}{k_B T}\right)} 2\pi\sin\theta\mathrm{d}\theta}{\int_0^\pi e^{\left(\frac{\mu_z E}{k_B T}\right)} 2\pi\sin\theta\mathrm{d}\theta} \tag{2.8}$$

Here, $\mu_z = \mu\cos\theta$. If it is assumed that the permanent dipoles within a material are non-interacting, then one can define the potential energy of each dipole as $U = -\mu E\cos\theta$ [98]. Therefore an equilibrium value of $\langle\mu\rangle_z$ can be calculated and Equation 2.8 reduces to [94, 95]:

$$\langle\mu\rangle_z = \frac{\mu^2}{3k_B T}E \tag{2.9}$$

Through substitution of Equation 2.9 into Equation 2.7 we can obtain a relationship between P_0 and E in terms of the dipole moment, μ [94].

$$P_0 = \frac{\mu^2}{3k_B T}\frac{N}{V}E \tag{2.10}$$

Thus, we can also define an equation relating the dipole moment to the dielectric strength, $\Delta\varepsilon$ by using Equation 2.6.

$$\Delta\varepsilon = \frac{\mu^2}{3\varepsilon_0 k_B T}\frac{N}{V} \tag{2.11}$$

This is known as the Curie law [94, 95]. Although this provides a means to describe the dielectric strength in terms of the orientational polarisation created by the motion of permanent dipoles, it does not take into account the interaction between these dipoles and assumes that local field effects can be ignored. Firstly, let us address the local field effects. Due to so-called shielding effects [94], there is a difference between the applied field, E, and the electric field which affects a specific dipole. Lorentz considered a 'spherical cavity' within a infinitely extended medium with a homogeneous polarisation [94, 98]. The 'local' electric field in the cavity, E_{loc}, is proportional to the applied electric field in the following manner [94]:

$$E_{loc} = \frac{\varepsilon_s + 2}{3}E. \tag{2.12}$$

If we now substitute E for E_{loc} in Equation 2.10 and consider the orientational polarisation given in terms of the dielectric strength $\Delta\varepsilon$ (Equation 2.6) we obtain the so-called Curie-Weiss law for $\Delta\varepsilon$ [98]:

$$\Delta\varepsilon = \frac{(\varepsilon_\infty + 2)T_{CW}}{T - T_{CW}}, \tag{2.13}$$

where $T_{CW} = \frac{n\mu^2}{9\varepsilon_0 k_B}$ and n is the number density of dipoles, $n = N/V$.

Another general extension of the relationship between μ and $\Delta\varepsilon$ was postulated by Onsager [100] to describe materials containing polar molecules. This extension considers the polarisation of the environment surrounding a permanent dipole by introducing the so-called reaction field [94, 95] in which the dipole moment of a molecule, $\mu = \mu_0 + \alpha E_{loc}$. The Onsager equation is defined as follows:

$$\Delta\varepsilon = \frac{\varepsilon_s(\varepsilon_\infty + 2)^2}{(2\varepsilon_s + \varepsilon_\infty)}\frac{n}{9k_B T\varepsilon_0}\mu^2. \tag{2.14}$$

In order to correctly determine the relationship between the permittivity and the average dipole moment we must also consider that each permanent dipole

within a material is surrounded by other dipoles and therefore dipole-dipole interactions are important. These interactions are not taken into account in Equation 2.14. Kirkwood and Frölich [94, 96, 100–103] introduced the factor, g_K, in order to model the interaction between dipoles:

$$\Delta\varepsilon = \frac{\varepsilon_s(\varepsilon_\infty + 2)^2}{(2\varepsilon_s + \varepsilon_\infty)} \frac{n}{9k_B T\varepsilon_0} g_K \mu^2. \tag{2.15}$$

In general g_K can be greater or less than one depending on whether permanent dipoles have a tendency to orient parallel or anti-parallel to each other.

2.2.2 The time/frequency dependent case

So far we have defined the polarisation of a dielectric material based on the assumption of an applied electric field with no frequency or time dependence. Firstly, we can consider the application of an electric field to a material and then subsequent removal of that field. A diagram of this situation is shown in Figure 2.1.

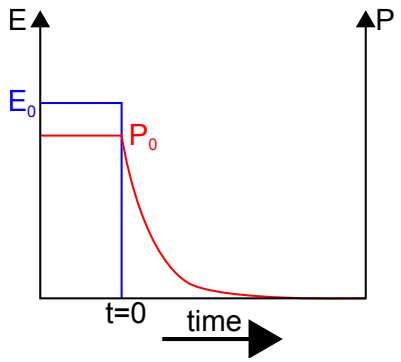

Figure 2.1: Diagram showing the effect of application and then subsequent removal (at $t = 0$) of an electric field on the orientational polarisation, P_0.

When the field is applied, the macroscopic polarisation due to the orientational polarisation, P_0, will not instantaneously reach its equilibrium value as it takes a certain amount of time for the dipoles within the material to align with the field. Alternatively one can investigate the case where an initially static applied field is turned off and study how the polarisation relaxes towards its equilibrium value. When the field is removed, the polarisation decays [97]. For the purposes of this

discussion, by analogy with a so-called 'step-off' experiment, we can introduce the relaxation function, $\Phi(t)$, where:

$$\Phi(t) = \frac{P_0(t)}{P_0(t=0)}. \tag{2.16}$$

If the magnitude of the applied electric field, E, is relatively small then the response of a material to this external perturbation is governed by the fluctuation-dissipation theorem [94, 97]. This means that the response to the perturbation results from the same mechanisms that control equilibrium fluctuations of the polarisation (i.e. without the application of an applied field). This is important as it means perturbation due to an applied field and analysis of the resulting polarisation gives information about the microscopic motions of dipoles and thus molecules within a material but does not change the fundamental nature of these motions. In this regime, the relaxation function can instead be expressed as an autocorrelation function, ϕ_P, of the orientational polarisation, where,

$$\Phi(t) = \phi_P(t) \equiv \frac{\langle \mathbf{P_0}(0) \cdot \mathbf{P_0}(t) \rangle}{\langle \mathbf{P_0}(0)^2 \rangle}. \tag{2.17}$$

If one ignores inertial effects, the rate of change of the polarisation of a material subjected to an externally applied field is proportional to the polarisation at a given time [94]:

$$\frac{dP(t)}{dt} = -\frac{P(t)}{\tau_D} \tag{2.18}$$

Where τ_D is the Debye characteristic relaxation time. If Equation 2.18 holds, there will be a single exponential decay of the autocorrelation function, ϕ_P in the time-domain, occurring at $t = \tau_D$. Furthermore, as the orientation polarisation is due to the reorientation of permanent dipoles, μ, in the direction of an applied electric field, ϕ_P can be expressed in terms of the autocorrelation of dipole

moments instead [95, 97]:

$$\phi_p(t) = \frac{\sum_{i,j}^{N} \langle \boldsymbol{\mu}_i(0) \cdot \boldsymbol{\mu}_j(t) \rangle}{\sum_{i,j}^{N} \langle \boldsymbol{\mu}_i(0) \cdot \boldsymbol{\mu}_j(0) \rangle} = \frac{\sum_{i}^{N} \langle \boldsymbol{\mu}_i(0) \cdot \boldsymbol{\mu}_i(t) \rangle + \sum_{i \neq j}^{N} \langle \boldsymbol{\mu}_i(0) \cdot \boldsymbol{\mu}_j(t) \rangle}{N\mu^2 + \sum_{i \neq j}^{N} \langle \boldsymbol{\mu}_i(0) \cdot \boldsymbol{\mu}_j(0) \rangle}. \tag{2.19}$$

In this manner, a connection between the effect of an applied electric field on the macroscopic orientational polarisation has been intrinsically linked to the microscopic dynamics within a material. It should be noted that this equation contains not only autocorrelation terms but also cross-correlation terms between different dipole moments. If it is assumed that cross-correlation terms can be neglected [95, 97], the autocorrelation function of the orientational polarisation is equivalent to the autocorrelation of dipole moments, $\phi_\mu(t)$ [97]:

$$\phi_\mu(t) = \frac{1}{N\mu^2} \sum_{i}^{N} \langle \boldsymbol{\mu}_i(0) \cdot \boldsymbol{\mu}_i(t) \rangle = \frac{1}{\mu^2} \langle \boldsymbol{\mu}(0) \cdot \boldsymbol{\mu}(t) \rangle . \tag{2.20}$$

Therefore, to a good approximation, through measurement of the macroscopic polarisation, dielectric spectroscopy also indirectly probes dipole-dipole reorientations and thus probes the microscopic dynamics by probing molecular reorientations. In the research presented here, dielectric spectroscopy was performed in the frequency domain in order to access timescales shorter than can be measured in the time domain. Measurements in the frequency domain involve determination of the complex dielectric permittivity, ε^*.

If we instead consider a harmonic applied electric field of the form $E^*(\omega) = E_0 e^{i\omega t}$, the polarisation becomes frequency dependent, according to Equation 2.5.

$$P^*(\omega) = (\varepsilon^* - 1)\varepsilon_0 E^*(\omega) \tag{2.21}$$

As the applied field is frequency dependent, it follows that the polarisation as a result of that field must also vary harmonically. The response of a material to the applied field, E^* is characterised by the complex dielectric permittivity, ε^*,

which can be split into its real and imaginary parts.

$$\varepsilon^* = \varepsilon' - i\varepsilon'' \tag{2.22}$$

The real part of the permittivity, ε', is a measure of the energy stored in the system as a function of frequency. In the static case ($\omega = 0$), ε' is equivalent to ε_s as defined in Equation 2.4 [95, 99]. The imaginary part, ε'' is proportional to the energy dissipated as a function of frequency. In terms of Equation 2.4, ε'' is a measure of the amplitude of the component of the displacement field, D, with a $\pi/2$ phase difference to the applied electric field, E. The imaginary term is often called the dielectric loss factor [95]. The complex dielectric permittivity can be related to the response function, $\Phi(t)$ (as defined in Equation 2.16) in the following manner, [94]:

$$\frac{\varepsilon^*(\omega) - \varepsilon_\infty}{\Delta\varepsilon} = 1 - i\omega \int_0^\infty \Phi(t) e^{-i\omega t} \mathrm{d}(t) \tag{2.23}$$

The real and imaginary components of ε^* are related by the so-called Kramers/Kronig relations [18, 94] and as a result of this carry equivalent information about the relaxation dynamics in materials. In summary, dielectric spectroscopy in the frequency domain measures the complex dielectric permittivity, ε^*, which is related to the change in the macroscopic polarisation, P, as a result of an applied frequency dependent electric field, E^*. As the autocorrelation function of P, ϕ_p, is related to the reorientation of permanent dipoles, this allows information about the microscopic dynamics within a material to be probed.

2.2.3 The Debye response

If one ignores inertial effects, the rate of change of the macroscopic polarisation, $\mathbf{P}$, is proportional to its absolute value at a given time [94],

$$\frac{\mathrm{d}\mathbf{P}}{\mathrm{d}t} = -\frac{1}{\tau_D}\mathbf{P}(t), \tag{2.24}$$

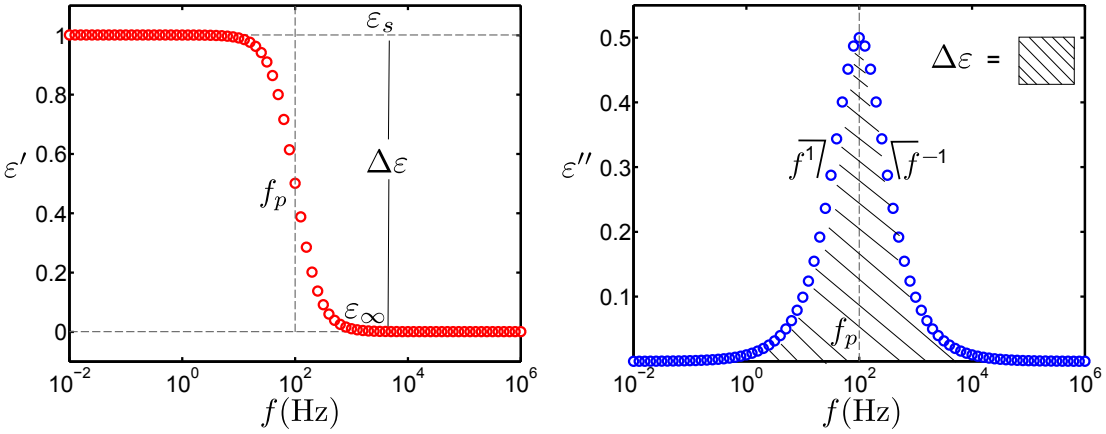

Figure 2.2: Figure showing the real and imaginary parts of the Debye function for ε^*.

where, τ_D, is the characteristic Debye timescale. This equation means that the response function, $\Phi(t)$, decays in an exponential manner:

$$\Phi(t) = e^{-\frac{t}{\tau_D}}. \tag{2.25}$$

Through substituting this behaviour of $\Phi(t)$ into Equation 2.23, this yields the following behaviour of ε^*:

$$\varepsilon^*(\omega) = \varepsilon_\infty + \frac{\Delta\varepsilon}{1 + i\omega\tau_D}. \tag{2.26}$$

This is the so-called Debye function. An example of the dielectric spectra predicted by Debye function in the real and imaginary parts of ε^* as a function of frequency are shown in Figure 2.2.

The Debye function is manifested as a step-like exponential decay in ε' and a peak in the dielectric loss,ε''. The low and high frequency power-law flanks of the loss peak follow a f^1 and f^{-1} frequency dependence respectively. It is often observed that the dielectric loss peak is broader than that predicted by the Debye function. This will be fully discussed in Section 2.5.

The dielectric strength, $\Delta\varepsilon$, can be determined by taking the difference between the limiting values of ε' at low and high frequencies $(\varepsilon_s - \varepsilon_\infty)$. This is equivalent to integrating the respective peak in ε'' using an integral of the follow-

ing form:

$$\Delta\varepsilon = \frac{2}{\pi}\int_0^\infty \varepsilon''(\omega)\frac{\mathrm{d}f}{f} \tag{2.27}$$

As ε' and ε'' are related through Kramer/Kronig relations it can be said that the same physical information is contained within both ε' and ε''. Therefore, in the remainder of this chapter (and in the subsequent analysis of the obtained results) only the imaginary contributions to ε^* will be considered. One advantage of considering only ε'' is that the value for the limiting dielectric constant at high frequencies, ε_∞, can be neglected as this only applies in ε' and thus removes a fitting parameter required to describe the spectra obtained through dielectric spectroscopy [104]. Another advantage is that the shape parameters needed to describe ε^* are very well defined in the imaginary part.

2.2.4 DC conductivity

In Section 2.2.1 the discussion of the macroscopic polarisation was conducted under the assumption of no charged species within a material. This is often not the case in reality and a contribution due to ionic conductivity is normally observed:

$$\varepsilon^*_{cond}(\omega) = -i\frac{\sigma_0}{\varepsilon_0\omega}. \tag{2.28}$$

Therefore conductivity contributions are only observed in the dielectric loss, ε'' and are manifested as a power-law flank at low frequencies with an exponent of unity. In samples containing a high number of mobile charge carriers, the conductivity contribution can dominate ε'' such that the contributions due to the orientation of permanent dipoles can be obscured [18]. In such cases, it is preferable to remove the charged species within a material in order to analyse the relaxation phenomena due to dipolar orientation. Note that for a high degree of conductivity particularly at low frequencies where there is enough time for the charged species to move across the cell, polarisation effects can occur and these will be observed in both the real and imaginary part of the permittivity.

2.3 Experimental technique

In simple practical terms, a dielectric spectroscopic experiment involves placing a sample of material between two electrically conducting electrodes and applying a sinusoidally varying voltage across these electrodes. The sample volume is effectively a filled capacitor with a complex capacitance, C^*, which is related to the surface area of the electrodes, A, the separation between the electrodes, d and the complex dielectric permittivity, ε^*:

$$C^* = \frac{\varepsilon^* \varepsilon_0 A}{d} \tag{2.29}$$

If two identical metal plates are placed parallel to each other and subjected to a voltage, there will be a homogeneous accumulation of charge on each plate. The voltage, V_0 is related to the charge, Q_0: $V_0 = Q_0/C_0$ where C_0 is the capacitance of this empty capacitor [18]. If a material is placed between the plates, the capacitance will increase and will scale with the dielectric permittivity of the material, ε [49]. If we instead apply a sinusoidally varying voltage of the form [18, 94, 98]:

$$V(\omega) = V_0 e^{i\omega t} \tag{2.30}$$

Then one can measure the resulting complex current, with a phase difference, $\phi(\omega)$, to the applied voltage [98].

$$I(\omega) = I_0 e^{i(\omega t + \phi(\omega))} \tag{2.31}$$

Using Ohm's law, the complex impedance, Z^* of the sample can be determined and this in turn can be related to ε^* [94].

$$\epsilon^*(\omega) = \frac{1}{i\omega Z^*(\omega) C_0}. \tag{2.32}$$

2.3.1 The dielectric spectrometer

BDS was performed both at the University of Leeds and Chalmers Institute of Technology. The dielectric spectrometers used were manufactured by Novocon-

trol. The spectrometers consist of a frequency analyser (Novocontrol Alpha-N (Leeds) or Alpha-S (Chalmers)) connected to a 'sample cell' through a high impedance active test interface which is either part of the sample cell itself (Active Sample Cell ZGS, Novocontrol: used at Chalmers) or connected separately (Novocontrol 2-Wire Test Interface ZG2: used in Leeds) to a standard sample cell (Novocontrol BDS 1200). The test-interface is required for high accuracy measurements of the complex impedance, Z^* [96].

The dielectric active test interface and frequency response analyser.

A schematic circuit diagram of the active test interface for the spectrometer is shown in Figure 2.3. The interface function is based on the principles of Fourier correlation analysis [94, 96]. Firstly we can consider the simpler case in which the current to voltage converter is removed from the circuit and the reference capacitor is replaced by a simple resistor of resistance, R. A sinusoidally varying voltage V_1^* is applied to the sample via a generator. The complex current, I_S^* which results from the application of V_1^* to the sample is then converted into a second complex voltage, V_2^*. The voltages V_1^* and V_2^* are measured by two phase sensitive sine wave correlators [94]. The complex sample impedance can thus be calculated [18, 94, 96]:

$$Z_S^* = \frac{V_S^*}{I_S^*} = R\left(\frac{V_1^*}{V_2^*} - 1\right) \tag{2.33}$$

To provide a more accurate determination of Z_S^* at lower frequencies (<100 kHz [94]) of the applied harmonic voltage, the simple resistor can be replaced by a current to voltage converter with a variable impedance, Z_X^* which can be modified in resistance and capacitance [96] such that the output voltage, V_2^*, can be well matched to the input channels of the frequency analyser [18]. The sample impedance can then be determined in a similar manner to Equation 2.33 [96]:

$$Z_S^* = -\frac{V_{1S}^*}{V_{2S}^*} Z_X^* \tag{2.34}$$

Although this method leads to a more accurate determination of Z_S^* one is still limited to some extent by phase errors in the frequency analyser and the

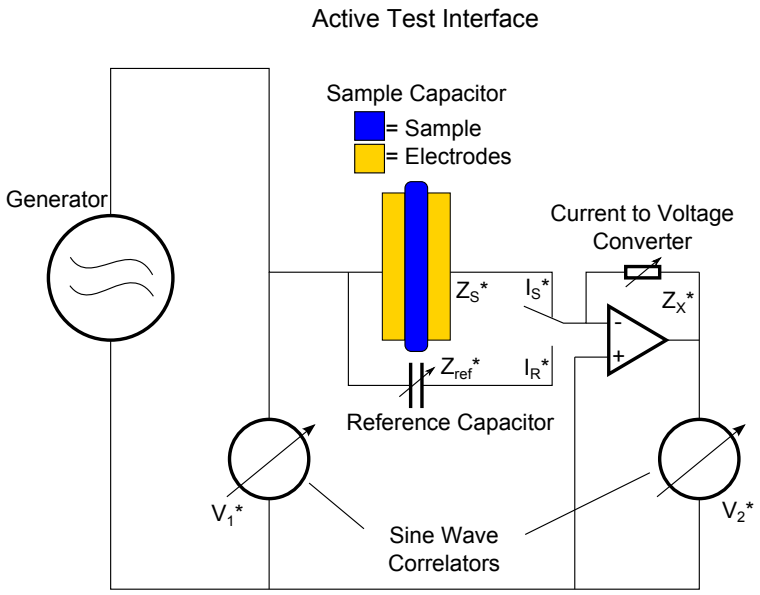

Figure 2.3: a)Schematic of the circuitry involved in the dielectric analyser.

current to voltage converter itself [96]. In order to remove these limitations in the accuracy of the determination of the impedance a low-loss reference capacitor can be introduced with a variable impedance, Z^*_{ref}. After each measurement point of the sample impedance Z^*_S, a measurement of the reference impedance is made [105]. The capacitance of the reference capacitor can be varied such that it is similar to that of the sample [96]. As both measurements involve the same systematic phase-errors associated with the correlators and the current to voltage converter, these deviations can be eliminated [18, 94, 96]. The complex impedance of the reference capacitor can be determined in a similar manner to Equation 2.34.

$$Z^*_{ref} = -\frac{V^*_{1ref}}{V^*_{2ref}} Z^*_X \tag{2.35}$$

By combining Equations 2.34 and 2.35 an expression relating Z^*_S and Z^*_{ref} can

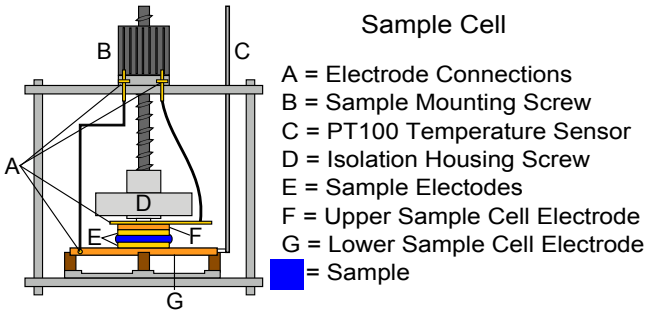

Figure 2.4: Schematic diagram of the dielectric sample cell.

be defined [94]:

$$Z_S^* = \frac{V_{1S}^*}{V_{2S}^*}\frac{V_{2ref}^*}{V_{1ref}^*}Z_{ref}^* \tag{2.36}$$

The frequency response analysers used in this research (Alpha-A (Leeds) or Alpha-S (Chalmers)) have a nominal an operating frequency range of 3μHz to 40MHz.

Sample cell

The lower portion of the sample cell (either BDS 1200 or the 'Active Sample Cell') is shown in Figure 2.4. The cell consists of two sample cell electrodes through which the voltage, V_{1S}^* is applied and the complex current,I_S^* is measured through the appropriate electrical connections. The electrodes can be tightened together such that there is good surface contact between the electrodes and the measurement sample. Rather than placing a material directly between the two sample cell electrodes, specific sample geometries can be used depending on the nature of the material to be measured (see Section 2.3.2). The top electrode is held in position by an isolation housing to prevent electrical conduction through the sample cell housing.

During measurement, the sample cell is placed into a cryostat and a temperature control system (Novocontrol Quatro) regulates the temperature of the

sample cell using pressurised nitrogen gas supplied by a connected liquid nitrogen dewar. The pressure of the gas flow is regulated by a heater at the bottom of the nitrogen dewar. A second heater is placed between the dewar and the cryostat such that the temperature of the gas can be finely tuned in order to control the temperature of the sample cell. The temperature of the sample cell itself is measured using a PT100 thermocouple connected to the lower sample cell electrode. In this manner, the temperature of the sample cell can be controlled over a wide range of operating temperatures, 100 K to 700 K, with an accuracy of $\pm$0.1K.

2.3.2 Sample preparation

One of the major advantages of using dielectric spectroscopy in order to study the dynamics of glass forming systems, aside from the wide frequency range, is the ability to measure on a huge variety of different samples. BDS can be used to study samples ranging from simple molecular liquids with a viscosity similar to that of water at room temperature to high molecular weight, high viscosity polymers. In order to measure the samples successfully, certain dielectric geometries must be used depending on the behaviour of the material to be studied.

Polymeric samples

The basis of a dielectric experiment, as described in Section 2.3, is to place a sample between two parallel electrodes such that a sinusoidally varying voltage can be applied. For the polymeric samples studied during this research project, the sample geometry was very simple. Polymeric samples were placed between two circular electrodes with diameters of 20mm and 40mm and a thickness of 2mm. In order to maintain a fixed separation between the electrodes, several silica spacers with a thickness of 50 or 100μm were placed between the electrodes in a star-like formation such that the separation between the electrodes would be maintained after applying pressure. A constant sample volume was achieved by first placing the polymer on the bottom electrode and heating the sample significantly above its expected glass transition temperature ($\sim$ 473K). The silica spacers and the top electrode were placed on top of the heated polymer. Pressure was then applied to the top electrode to ensure a consistent sample thickness

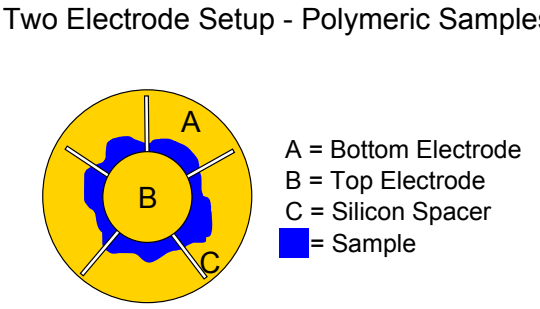

Figure 2.5: Schematic of the two-electrode set-up as described in the text

between the two electrodes. A schematic diagram of this setup is shown in Figure 2.5.

Removal of Ionic Conductivity

In some cases, the polymeric samples showed a significant conductivity contribution in ε'' such that the α relaxation was completely obscured at low temperatures. This conductivity contribution was attributed to ionic impurities within the polymeric samples. In order to remove this contribution, methanol precipitation of the samples was conducted. The samples to be cleaned were dissolved in toluene at a concentration of 3 wt % and then added to significantly larger volume of methanol. The polymeric samples used in this research do not dissolve readily in methanol and thus precipitated out of solution. The polymer/toluene/methanol solution was allowed to sit undisturbed until the polymer had completely precipitated and then the supernatant was pipetted off. The resulting polymer was then dried in a vacuum oven at a temperature significantly above the glass transition ($\sim$ 473K) in order to remove any excess solvent. The dried polymer was then redissolved in toluene at a concentration of 5 wt%, solution cast onto a 40mm electrode and allowed to dry. The resulting solution cast sample was then placed into a vacuum oven again in order to remove all traces of solvent. The dielectric spectra for polystyrene shown before and after this cleaning procedure are shown in Figure 2.6. The conductivity contribution to ε'' is reduced by around a decade thus leading to a more accurate determination of the position and strength of the α relaxation peak.

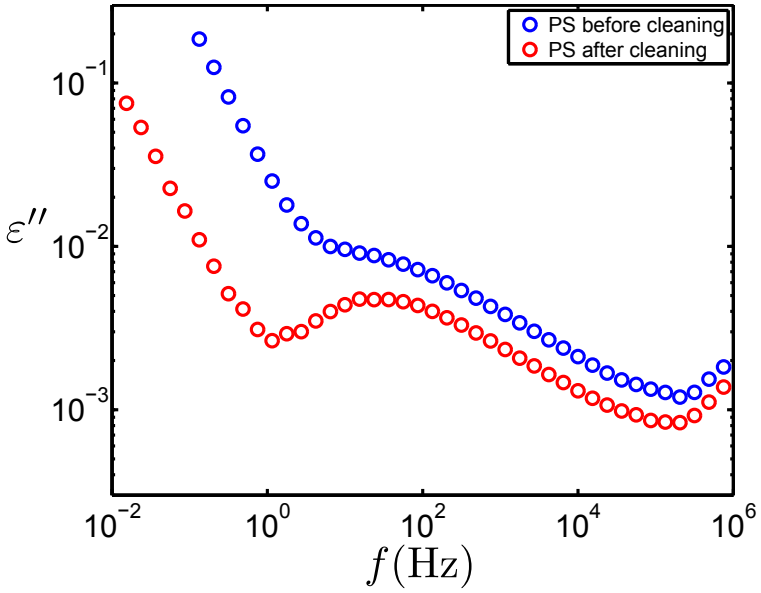

Figure 2.6: Comparison between dielectric spectra for both untreated and cleaned polystyrene.

A similar approach to remove the conductivity contribution was also completed for another related research project (the results of which are out of the scope of this thesis) based on a procedure published by Matsumiya *et.al.* for the cleaning of bulk polystyrene [106]. In this procedure, the polystyrene is dissolved in a solvent in a similar manner to the methanol precipitation procedure (in this case, the solvent was cyclohexane). The dissolution of the polymer was completed in a beaker which had been thoroughly cleaned and baked at 120°C for 4 hours prior to the experiment. The idea behind this procedure was that any ionic impurities within the polymer would diffuse preferentially towards the edges of the beaker. The solution was left undisturbed in the beaker for 24 hours before being pipetted into another baked conical flask and concentrated under reduced pressure. The resulting concentrated solution was then concentrated by evaporation under vaccum using a cold trap to stop the removed solvent from entering the pump. Finally, the sample was placed in a vacuum oven in order to remove all solvent. It was found that this procedure also yielded a reduction of the conductivity by an order of magnitude and is in this sense equivalent in efficiency to the precipitation procedure. The precipitation procedure was chosen to clean

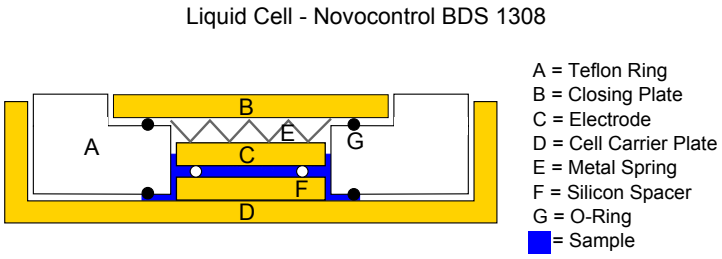

Figure 2.7: Schematic of the dielectric liquid cell (BDS 1308, Novocontrol)

the polymeric samples used in this research as it was more easily implemented.

Low Molecular Weight Glass Formers

Many of the molecular glass formers in this work had a relatively low viscosity (on the order of that of water) at room temperature and therefore could not be simply applied to the electrodes in the same way as the polymeric samples. In this case, a so-called 'liquid-cell' was used (BDS 1308, Novocontrol). A schematic diagram of the cell is shown in Figure 2.7.

The basic functionality of the liquid cell is very similar to that of the two-electrode method used to measure the polymeric samples. The sample measurement volume sits between two circular gold-plated electrodes with a fixed separation achieved through use of silicon spacers. In order to contain the liquid and to account for thermal expansion, the electrodes sit within a Teflon ring with O-rings above and below the ring in order to render the cell reasonably air tight and prevent evaporation of the sample. The Teflon ring and electrodes sit within a dish-like carrier plate. The cell is closed by fitting a closing plate to the top of the set-up and electrical contact between this closing plate and the top electrode is ensured by using a metal spring which accounts for uneven tightening of the sample cell around the liquid cell. In order to get an accurate determination of the capacitance (and therefore the permittivity) of a sample contained within the liquid cell, the 'stray' capacitance of the cell had to be taken into account: i.e. the capacitance of the sample-less cell. The stray capacitance of the liquid cell could be determined by changing the compensation for the capacitance within the dielectric control software and observing the behaviour of the real part of the permittivity, ε', between 10Hz and 100kHz [107]. A correct setting of the stray

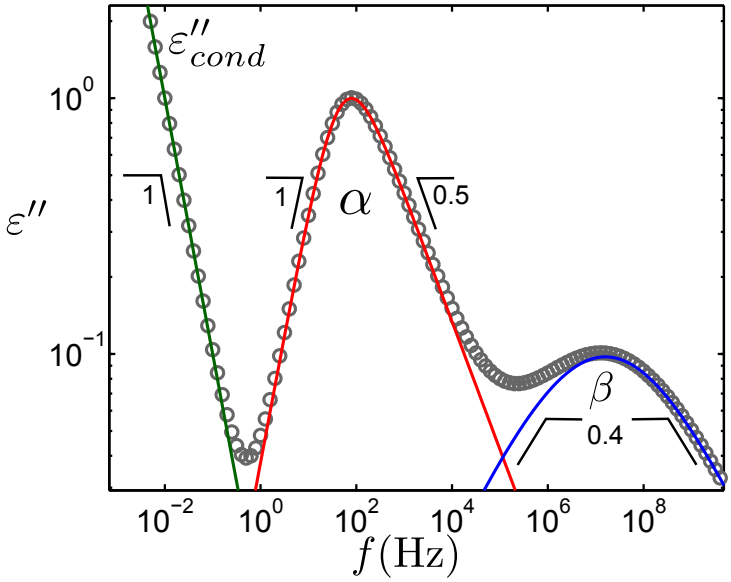

Figure 2.8: Figure showing a typical dielectric spectrum in ε''. The grey points are generated from an additive combination of a conductivity contribution (green line) and examples of a typical α relaxation loss peak (red line) and a typical secondary β peak (blue line).

capacitance would lead to a value of 1 in ε': the correct setting of this particular liquid cell was 4.25 pF.

2.4 Characteristics of dielectric spectra

Figure 2.8 shows an example of a typical spectrum obtained from dielectric spectroscopy. Temperature and frequency dependent relaxation processes within a material are manifested as peaks in ε''. In this case, contributions to the spectra include the loss peaks in ε'' relating to the primary α relaxation and a secondary β relaxation in combination with a low frequency power law flank which can be attributed to ionic conductivity. In Section 2.2.2, the Debye function was introduced as a means of describing the frequency dependent behaviour of ε^* as a result of the reorientation of permanent dipoles, and thus relaxation processes within a glass forming material. In general, the loss peaks in ε'' relating to relaxation processes have a more complicated functional shape than that described by the Debye relaxation. For example, the loss peak related to the structural or

α relaxation of a material is, in general, anti-symmetric with a high frequency flank described by a power law whose exponent is less than that of the exponent used in the power law description of the low frequency flank. In contrast to this, the loss peak relating to the β relaxation is usually symmetrically stretched in a double logarithmic plot with an exponents that are different from the -1 and 1 values of a Debye expression. Therefore, in order to describe the functional shape of these relaxation phenomena, modifications to Equation 2.26 are required.

2.5 Analysis of dielectric spectra

In this section a selection of susceptibility functions used to describe the relaxation mechanisms observed in the dielectric spectra will be introduced. Firstly, empirical functions derived from the simple Debye description of the dielectric permittivity will be explained and then a selection of other examples of functions used to describe relaxation mechanisms will be shown.

2.5.1 Empirical response functions based on the Debye function

In the imaginary part of the permittivity, ε'', the so-called Debye relaxation is manifested as a peak with a value of 1 and -1 for the gradients of the low and high frequency flanks in a double logarithmic plot and with a peak position relating to the characteristic relaxation time: $\omega_p = \frac{1}{2\pi\tau_D}$. In most cases the peaks observed in ε'' corresponding to relaxation phenomena have a shape which cannot be completely described through use of Equation 2.26. For example, the characteristic loss peak of the α relaxation is usually asymmetric with a high frequency gradient significantly less than the gradient of the low frequency flank. In order to describe the spectral shape of such relaxation phenomena more thoroughly, several empirical generalisations to Equation 2.26 have been made.

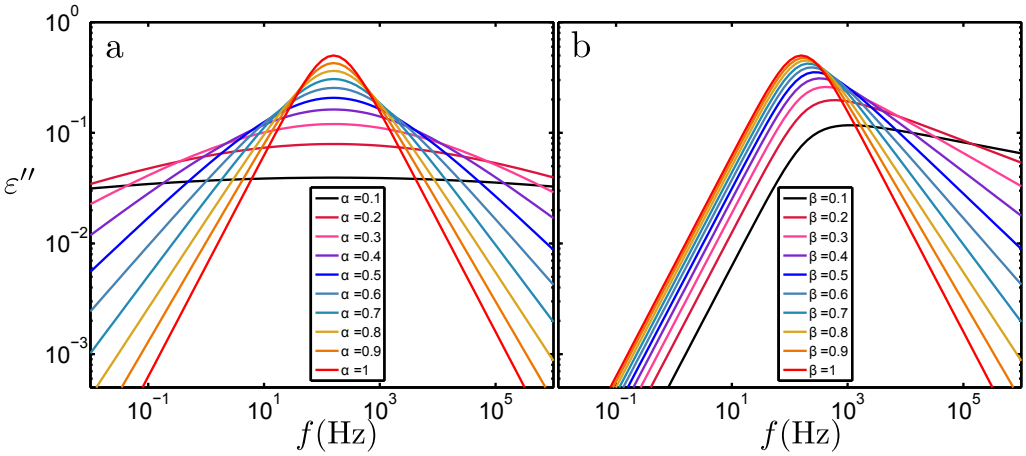

Figure 2.9: The functional shapes of the a) Cole-Cole function with varying symmetric stretching parameter, α and b) the Cole-Davidson function with varying anti-symmetric stretching parameter, β.

Cole-Cole function

The so called Cole-Cole (CC) function is an empirical extension to the Debye function, which describes symmetric broadening of the relaxation peak in ε'' [108].

$$\varepsilon^*_{CC}(\omega) = \varepsilon_\infty + \frac{\Delta\varepsilon}{1 + (i\omega\tau_{CC})^\alpha} \tag{2.37}$$

The symmetric stretching parameter, α, can vary between 0 and 1 and τ_{CC} is equivalent to the peak frequency. Equation 2.37 reduces to the Debye function if $\alpha = 1$. The loss peak relating to the β relaxation is often observed as a symmetrically stretched relaxation and therefore Equation 2.37 is well suited to describe its spectral shape. The variation of the functional shape of Equation 2.37 with different values of α is shown in Figure 2.9a).

Cole-Davidson function

Many examples of dielectric loss peaks exhibit anti-symmetric stretching. In order to describe their spectral shape, another empirical modification of Equation 2.26 is often used, the Cole-Davidson (CD) function [109].

$$\varepsilon^*_{CD}(\omega) = \varepsilon_\infty + \frac{\Delta\varepsilon}{(1 + i\omega\tau_{CD})^\beta} \tag{2.38}$$

Here, the β parameter describes the anti-symmetric stretching of the peak. In this formulation, the β parameter is the gradient of the high frequency flank in a log-log plot and a value of $\beta = 1$ reduces Equation 2.38 to the Debye relaxation. The variation of the functional shape of Equation 2.38 is shown in Figure 2.9b. It is clear from this figure that, for decreasing values of β, the peak position in frequency increases. In order to obtain the position of maximal loss for the peak, a transformation of τ_{CD} must be made [94]:

$$\omega_p = \frac{1}{\tau_{CD}} tan\left[\frac{\pi}{2\beta + 2}\right]. \tag{2.39}$$

Havriliak-Negami function

In order to completely describe the shape of a dielectric loss peak for which both the low and high frequency powerlaws might differ from the Debye behaviour, a further empirical generalisation was made by Havriliak and Negami [110] to combine the stretching effects of both the CC and CD functions.

$$\varepsilon^*_{HN}(\omega) = \varepsilon_\infty + \frac{\Delta\varepsilon}{\left(1 + (i\omega\tau_{HN})^\alpha\right)^\beta} \tag{2.40}$$

In this formulation the gradients of the low and high frequency flanks of the loss peak in a log-log plot of ε'' are set by α and $\alpha\beta$ respectively. As the Havriliak-Negami (HN) function involves an anti-symmetric stretching term a correction must be applied to the characteristic timescale, τ_{HN}, in order to obtain the peak frequency, involving both shape parameters in a similar manner to Equation 2.39.

$$\omega_p = \frac{1}{\tau_{HN}} \left[sin\left(\frac{\alpha\pi}{2 + 2\beta}\right)\right]^{\frac{1}{\alpha}} \left[sin\left(\frac{\alpha\beta\pi}{2 + 2\beta}\right)\right]^{-\frac{1}{\alpha}} \tag{2.41}$$

In most cases, the HN function is adept at fitting most relaxation spectra and it could be said that in order to fit the dielectric loss peak relating to the α relaxation, a function with no less than four shape parameters is required in order to describe the shape of the relaxation peak over a wide range of frequencies [94, 96, 111].

2.5.2 Empirical response functions formulated to describe the dielectric loss

So far, empirical functions derived from the Debye function have been presented which describe the complete complex dielectric permittivity, ε^*, so that the real and imaginary parts can be fit with the same function. In addition to these functions, there are a range of other often used empirical equations which are derived to describe loss peaks in the imaginary part of the permittivity directly.

Fuoss-Kirkwood function

The Fuoss-Kirkwood (FK) expression [104, 112] is an example of a function which can be used to fit a symmetrically stretched dielectric loss peak in ε'', with a similar functional shape to that of the CC function.

$$\varepsilon''(\omega) = \frac{2\varepsilon''_p \left(\omega\tau\right)^m}{1 + \left(\omega\tau\right)^{2m}} \tag{2.42}$$

Here, ε''_p is the maximum of the dielectric loss peak and the stretching parameter, m, can vary between 0 and 1. In a log-log plot, m sets the gradient of the high and low frequency flank. Interestingly, although the CC and FK functions essentially describe the functional shape of a dielectric loss peak in a similar fashion, the shapes show a slight but significant difference in the 'bluntness' of the peak, even if the stretching parameters are set to the same value for each function [104].

Jonscher function

The analogous expression to the HN function, for the description of a loss peak which contains components of both symmetric and anti-symmetric stretching, in ε'' is the Jonscher (J) expression [104, 113].

$$\varepsilon''(\omega) = \frac{K_J}{\left(\frac{\omega}{\omega_1}\right)^{-m} + \left(\frac{\omega}{\omega_2}\right)^{1-n}} \tag{2.43}$$

The shape parameters (often termed the Jonscher parameters [94, 96]) $-m$ and $1-n$ describe the gradients of the low and high frequency flanks (in a log-log

scaling) respectively. The parameter K_J is a rescaling parameter proportional to the amplitude of the loss peak in ε'' and ω_1 and ω_2 are described as 'thermally activated characteristic frequencies' [113]. Again, a comparison between the HN and Jonscher functions with identical values of the shape parameters leads to a slightly different widths of the resulting description of the dielectric loss peak [104].

Rikard Bergman function

In general, when fitting experimental data with empirically derived equations, it is best to reduce the number of fitting parameters in order to be able to relate these parameters to physical properties of a material in an objective manner. Indeed, one could create an empirical expression with a high number of free parameters which would fit any spectral shape but this does not aid any physical description of the system with the possible exception of a better determination of the timescale of the maximal loss in ε''. Having said that, the functions described thus far seem to have a similar failing in that they do not directly account for differences in the bluntness of the dielectric peak. Instead, the bluntness is approximated through variations of the gradients of the high and low frequency flanks. Therefore, in order to follow the development of the shape parameters describing the dielectric loss peak it seems logical that one at least for some systems must include a separate description of the bluntness.

An empirical function which, rather than being derived from the Debye expression for the dielectric loss, describes the shape of the peak directly was developed by Rikard Bergman (RB) [104]. This function has a simple and elegant derivation which starts from a complete description of all the shape parameters of the peak: amplitude, peak frequency, bluntness and the gradients of the high and low frequency flanks. The number of the free parameters in a fitting procedure can then be reduced if a selection of the parameters are locked appropriately. The derivation begins with a description of the inverse loss peak rescaled by the amplitude, $\frac{\varepsilon''_p}{\varepsilon''}$ which can mathematically easily be described as:

$$\frac{\varepsilon''_p}{\varepsilon''} = A\omega^{-a} + B\omega^{b} + C \tag{2.44}$$

The first and second terms in this equation relate to the power laws describing the flanks of the minima, with the parameters a and b used to describe the gradients of these flanks in a log-log representation and thus the powerlaw exponents. The parameter C does not affect the gradients of these flanks at frequencies significantly different from the frequency of the minimum, ω_p. The amplitude parameters, A and B can be determined by differentiating Equation 2.44 given that the resulting derivative should be zero at ω_p:

$$A = \left(\frac{b\,(1-C)}{a+b}\right)\omega_p^{a} \tag{2.45a}$$

$$B = \left(\frac{a\,(1-C)}{a+b}\right)\omega_p^{-b} \tag{2.45b}$$

By substituting these relationships into Equation 2.44 and rearranging for ε'' a function can be obtained to describe the shape of a dielectric loss peak.

$$\epsilon''(\omega) = \frac{\epsilon''_p}{\frac{(1-C)}{a+b}(b(\frac{\omega}{\omega_p})^{-a} + a(\frac{\omega}{\omega_p})^{b}) + C} \tag{2.46}$$

In this formulation, the C parameter relates to the bluntness of the peak in ε''. The Debye loss peak shape is achieved when $a = b = 1$ and $C = 0$. The affect of variation of the parameters in Equation 2.46 is shown in Figure 2.10. The figure showing the variation of the C parameter (Figure 2.10c) demonstrates how the bluntness affects the shape of the dielectric loss peak. It should also be noted that for particularly low values of the a and b parameters, the breadth of the peak also increases to some degree.

The RB function provides a complete description of loss peaks in ε''. Equation 2.46 can be adapted to suit specialised fitting situations if certain assumptions are made. For example, in many cases the low frequency flank of the α relaxation loss peak can be described by a power law with an exponent, or a parameter, of 1. If this assumption is made, it can be shown that $C = 1 - b$ and thus, Equation 2.46 reduces to just three fitting parameters: b, ω_p and ε''. This 3-parameter representation of the RB function can be shown to be a good approximation for

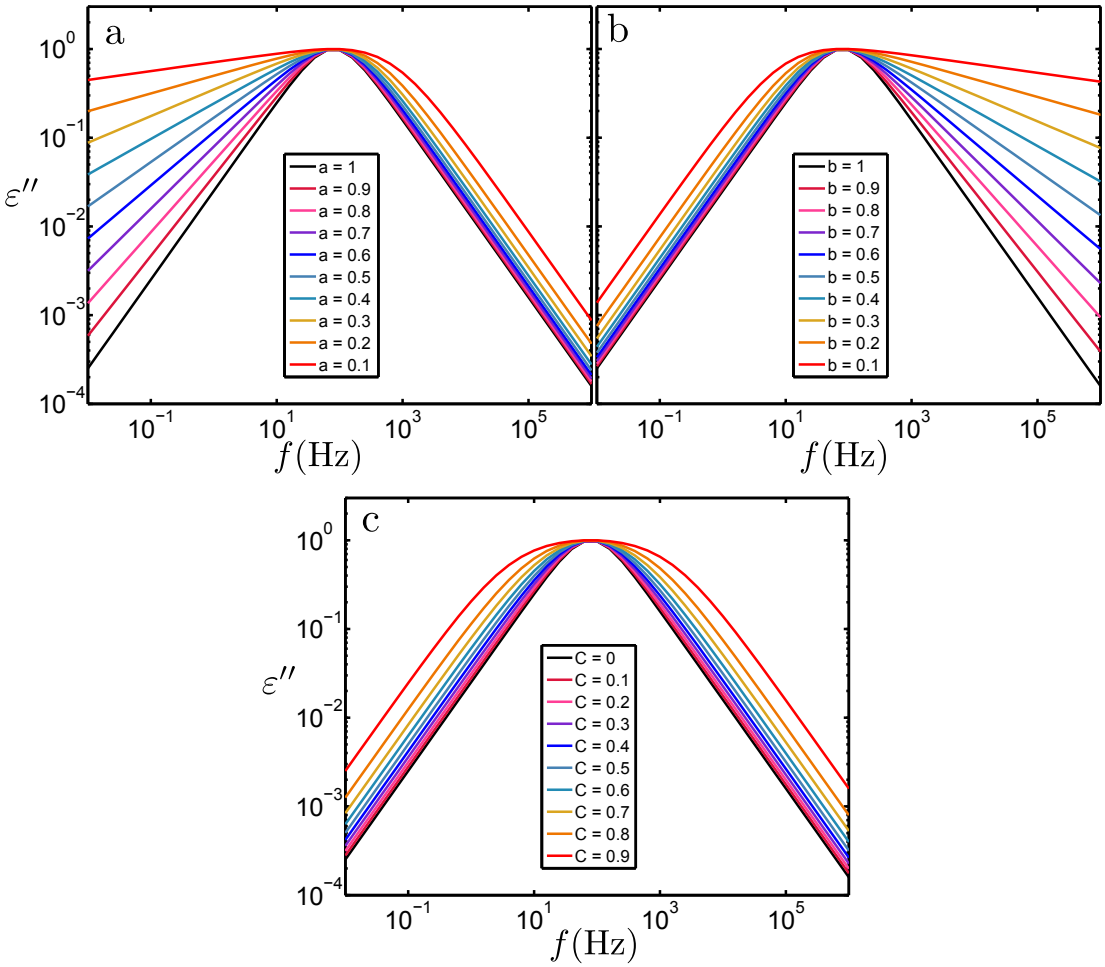

Figure 2.10: Figures showing the affect of variation of the different shape parameters in Equation 2.46: a) $a = 0.1 \rightarrow 1$, $b = 1$, $C = 0$ b) $a = 1$, $b = 0.1 \rightarrow 1$, $C = 0$ c) $a = b = 1$, $C = 0 \rightarrow 0.9$

the Kohlrausch-Williams-Watts (KWW) function (Section 2.5.3) in the frequency domain [104].

2.5.3 Time domain analysis

So far, we have only considered fitting of the dielectric spectra in the frequency domain of ε. One can achieve a similar description of the loss peaks in the spectra by transforming the data into the time-domain followed by a fit of the response function, $\Phi(t)$, in the time-domain.

Kohlrausch-Williams-Watts Function

The response function, $\Phi(t)$ often exhibits non-Debye like behaviour and this is characterised by a stretched exponential decay in the time-domain as first described by Kohlrausch in 1854 [41].

$$\Phi(t) = e^{-\left(\frac{t}{\tau}\right)^{\beta}} \tag{2.47}$$

Where, τ is a characteristic relaxation time and β describes the degree of stretching. Williams and Watts were the first to apply this form of stretched exponential to describe the dielectric relaxation behaviour in molecular glass formers in the frequency domain by applying a Laplace transform to Equation 2.47 [42, 98, 114, 115]. An analytical solution to the transformation of Equation 2.47 into the frequency domain is only available for the specific case where $\beta = 0.5$.

Generalised Gamma Distribution

Another example of a fitting approach defined in the time-domain assumes that $\Phi(t)$ can be described using a distribution of Debye-like single exponential decays. It uses the so-called generalised gamma (GG) distribution of timescales [97, 98]:

$$G_{GG}(ln\tau) = N_{GG}(\alpha, \beta) e^{\frac{-\beta}{\alpha}\left(\frac{\tau}{\tau_0}\right)^{\alpha}} \left(\frac{\tau}{\tau_0}\right)^{\beta} \tag{2.48}$$

The normalization factor N_{GG} is constructed such that integration of Equation 2.48 over all possible timescales yields a value of 1 and τ_0 is the timescale

corresponding to the maximum of the distribution. The shape parameters α and β describe the width and stretching of the distribution respectively. One can transform the GG distribution such that it can be used to describe the complex dielectric permittivity in the frequency regime [97]:

$$\frac{\varepsilon^*(\omega) - \varepsilon_\infty}{\Delta\varepsilon} = \int_{-\infty}^{\infty} \frac{1}{1 + i\omega\tau} G_{GG}(ln\tau) \mathrm{d}ln\tau \tag{2.49}$$

Through such a transformation the β parameter describes the gradient of the high frequency flank of a loss peak in ε'' and it can be shown that for values of $\beta < 0.7$, this shape parameter is a close approximation to the anti-symmetric stretching parameter in the CD function.

2.5.4 Functional description of the excess-wing

In some instances the α relaxation loss peak in ε'' exhibits a change in the power-law exponent of its high frequency flank (see Chapter 1). In these cases, it is necessary to fit the loss peak with appropriate functional descriptions of the change in the power-law exponent. Examples of this include a modified version of the G_{GG} distribution [97, 98] and a modified version of the CD expression [55]. The function used for samples that show an excess-wing behaviour in the results presented in this thesis were fit using a modified version of the RB function.

In order to construct this modification, it was assumed that the excess-wing was due to an underlying β relaxation and that the contributions to the spectra would follow the Williams-Watts ansatz [115]:

$$\Phi(t) = A\Phi_\alpha(t) + (1 - A)\Phi_\alpha(t)\Phi_\beta(t) \tag{2.50}$$

Here, the relaxation functions due to the α and β relaxation mechanisms, Φ_α and Φ_β are related by a correlation factor, A which sets the fraction of the decay of the correlation function attributed to each relaxation process in the time domain.

This ansatz assumes no interaction between the α and β relaxations and that the nature of the β relaxation would remain the same even when the two relaxations are completely merged. Equation 2.50 implies that the observed excess-

wing in the dielectric loss is not due to the *actual* β relaxation but a result of the so-called effective β relaxation, ε''_{eff}. In the time-domain, the response function of the effective β relaxation, $\phi_{\beta_{eff}}(t)$, which is obtained through a multiplication of $\phi_\alpha(t)$ and $\phi_\beta(t)$:

$$\phi_{\beta_{eff}}(t) = \phi_\alpha(t) \cdot \phi_\beta(t) \tag{2.51}$$

At temperatures far below T_g, $\phi_\alpha(t) = 1$ and this means that $\phi_\beta(t) = \phi_{\beta_{eff}}(t)$. However, at higher temperatures the α and β relaxations are much closer together in timescale and therefore $\phi_\beta(t) \neq \phi_{\beta_{eff}}(t)$.

Equation 2.51 corresponds to a mathematical convolution in the frequency domain: $\varepsilon_{\beta_{eff}}(\omega) = \varepsilon_\alpha(\omega) \otimes \varepsilon_\beta(\omega)$. In the case of merging of the α and β processes in the frequency domain, the low frequency shape of the β loss peak is largely set by the α relaxation whereas the high frequency shape is set by the underlying β relaxation. This behaviour can be modelled in the dielectric loss through an addition of functional components describing the α relaxation and the effective β relaxation: $\varepsilon''(\omega) = \varepsilon''_\alpha + \varepsilon''_{\beta_{eff}}$.

The functional form of the modified RB function is as follows [18]:

$$\varepsilon''(\omega) = \frac{\varepsilon''_p}{\frac{(1-C)}{a+b}\left(b\left(\frac{\omega}{\omega_p}\right)^{-a} + a\left(\frac{\omega}{\omega_p}\right)^{b}\right) + C} + \frac{\varepsilon''_{wing}}{\frac{(1-C_{eff})}{a+g}\left(g\left(\frac{\omega}{\omega_p}\right)^{-a} + a\left(\frac{\omega}{\omega_p}\right)^{g}\right) + C_{eff}} \tag{2.52}$$

The first component of this equation is identical to the 'unmodified' RB function given in Equation 2.46, with parameters describing the exponents of the high and low frequency power-law flanks, a and b, the bluntness of the peak, C and the amplitude, ε''.

The second component describes the contribution of the 'effective' β relaxation. In this component, the exponent of the low frequency power-law is also described by the a parameter in the first component. Furthermore, the peak frequency, of both contributions is set by one parameter, ω_p, thus assuming a strong merging of the two relaxations. As discussed, the low frequency behaviour of the effective β loss would be set by the shape of the α loss in a frequency convolution.

The g parameter is the exponent of the power law describing the high frequency flank of the effective β relaxation and thus the excess-wing. The amplitude is set by ε''_{wing}.

If the α and β relaxations are strongly merged, one could assume that the bluntness of the effective β relaxation, C_{eff}, could approximately be determined as the bluntness of the α and underlying β relaxations weighted by the strength of the two contributions. This is defined as follows:

$$C_{eff} = \frac{C\varepsilon''_p + C_\beta \varepsilon''_{wing}}{\varepsilon''_p \varepsilon''_{wing}} \tag{2.53}$$

Here, it was assumed that the underlying β relaxation would be symmetrically stretched and well described by the CC function as is often observed in the literature [33, 61, 94, 96, 116, 117]. An analytical description of the CC function using the RB function yields a bluntness: $C_\beta = \frac{1}{2}\left[1 - \tan^2\left(\frac{g\pi}{4}\right)\right]$, for the underlying β relaxation. Note that the 'amplitude' of the excess-wing, ε''_{wing} has been assumed to be equivalent to the amplitude of the underlying β relaxation.

2.5.5 Fitting procedure

Dielectric spectra were fit using an additive combination of functional descriptions of the observed contributions to the dielectric loss. In general, the anti-symmetrically stretched α relaxations were described using the RB function in order to provide a complete description of the loss peak, including the 'bluntness' described by the C parameter. In order for comparison, the loss peaks were also fit using the HN function, as it is often used in the literature [33, 61, 94, 96, 116, 117]. The β relaxation is manifested as a symmetrically stretched loss peak and therefore the CC function was used in order to describe it.

In the case demonstrated in Figure 2.8, fitting would require an additive combination of the RB or HN functions to describe the α loss peak, the CC function to describe the β loss peak and a power law flank to describe the conductivity flank observed at low frequencies of the form described by Equation 6.1. This equation suggests that the conductivity should follow a ω^1 behaviour: the gradient of the power law flank in a log-log scaling should be 1. In some instances it was necessary to generalise the behaviour by fitting a power-law of the form

$\varepsilon'' = A\omega^k$. Samples for which the α loss exhibited excess-wing behaviour were fit using the modified RB expression described in Section 2.5.4.

Fitting of the various dielectric spectra obtained in this research was completed using the Novocontrol WinFit software which optimises a set of initial parameters based on the local minimisation of the mean squared deviation (MSD) between the total fit function and the measured data points [118]. Winfit uses non linear curve fitting algorithms based on the Gauss or Newton method. Further data analysis of the spectra was performed using MATLAB [119].

2.6 Summary

Dielectric spectroscopy is a highly appropriate experimental technique for the study of glass-forming liquids as its large operating frequency range means that the dynamics of such materials can be analysed over a wide range of timescales. The nature of the BDS set-up is such that one can measure on a variety of different sample geometries meaning that it is an ideal technique for measurement of samples ranging for low molecular weight liquids to bulk polymers.

2. EXPERIMENTAL TECHNIQUES I: BROADBAND DIELECTRIC SPECTROSCOPY

Chapter 3

Experimental Techniques II: Thermal Analysis

3.1 Introduction

In the following chapter, the theory and experimental techniques for two different forms of thermal analysis, Differential Scanning Calorimetry (DSC) and Thermogravimetric Analysis (TGA), will be explained. DSC was used in order to characterise the *calorimetric* glass transition of the systems studied and TGA was used in order to facilitate the sample preparation for measurements using Broadband Dielectric Spectroscopy (see Chapter 2).

3.2 Differential Scanning Calorimetry

Differential scanning calorimetry (DSC) is a technique used to measure the difference between the heat flow through a sample and a reference sample resulting from a systematic change in the temperature of the system. DSC is a particularly applicable technique for the measurement of glass-forming systems as the glass transition is manifested as a step-like transition in the heat flow, q, and the specific heat capacity, C_P; thus, T_g can be determined very accurately.

3.2.1 Heat flow as a function of temperature

As mentioned in the introduction, DSC involves the measurement of the difference in the heat flow through a sample and a reference sample. The sample is placed in a closed aluminium pan (see Section 3.2.5) and the reference sample is often just an empty pan. Calculation of the difference in heat flow through both the sample and the empty reference pan allows the *actual* heat flow through the sample to be determined. This will be explained in more detail in Section 3.2.4.

A typical DSC trace of the heat flow, q ,is shown in Figure 3.1a for hexylbenzene. This measurement was conducted upon heating of the sample. Firstly, we note that the trace of q is negative at the beginning of the trace (low temperatures). This is because heat has to be supplied to the sample in order to raise its temperature and in the figure we define the heat flow as negative when it flows into the sample. The heat flow is related to the rate of change of the enthalpy, H: $q = \frac{\mathrm{d}H}{\mathrm{d}t}$ and the specific heat capacity at constant pressure, C_p, can be expressed as the change of enthalpy as a function of temperature:

$$C_P = \left(\frac{\partial H}{\partial T}\right)\Big|_P. \tag{3.1}$$

Therefore, C_p can also be obtained from a DSC measurement by dividing the heat flow, q, by the heating/cooling rate:

$$C_P = \frac{q}{\frac{\mathrm{d}T}{\mathrm{d}t}}. \tag{3.2}$$

The equivalent trace in the specific heat capacity, C_p is shown in Figure 3.1b.

There are three distinguishable features in Figures 3.1a and b. Firstly there are two prominent peaks relating to first order thermodynamic transitions. The first of these indicates crystallisation of the sample and thus results in an exothermic peak in q as the sample releases heat. Correspondingly for crystallization an exothermic peak in C_p is observed. At higher temperatures there is another peak that indicates melting of the sample and is characterised by an endothermic peak, as heat is absorbed by the sample. Again, we see a corresponding endothermic peak in C_p. If the material shown in Figure 3.1 is fully amorphous a the beginning

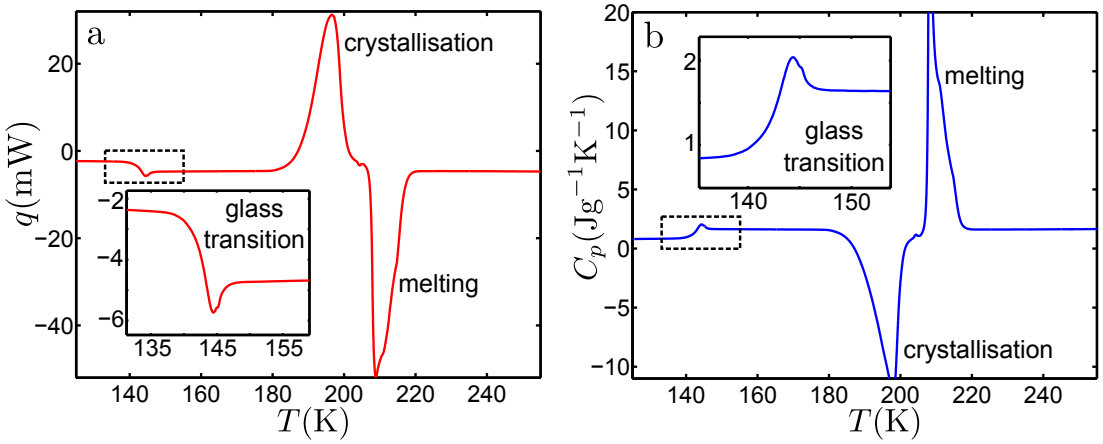

Figure 3.1: a) The heat flow, q, trace for hexylbenzene. b) The equivalent C_p trace for hexylbenzene.

of the temperature run, the area of these peaks is equivalent to the enthalpy of fusion, ΔH_{fus}.

At low temperatures, we observe a 'step' in the trace of both q and C_p. This indicates the glass transition as shown clearly in the insets of Figures 3.1a and b. The calorimetric glass transition temperature, T_g is often defined as the 'onset' temperature of the step in C_p or q (see Section 3.2.2). The height of the step in ΔC_p can be related to the degrees of freedom released in the transition [120]. It has also been used to define the so-called thermodynamic fragility of glass-formers [91], with more fragile glasses having a greater difference between the heat capacities in the glass and the supercooled liquid. This usually corresponds well to dynamic definitions of the fragility, such as the m parameter introduced in Chapter 1, for simple molecular glass formers [121] but can exhibit the opposite behaviour for some polymeric systems [122]. This will be discussed further in Chapters 4 and 6.

Importantly, one can determine the entropy at a specific temperature, $S(T)$,

by integrating the DSC trace of C_p:

$$C_p(T) = T\left(\frac{\partial S}{\partial T}\right)\Big|_P \tag{3.3a}$$

$$S(T) = \int_0^T \frac{C_p(T)}{T}\mathrm{d}T \tag{3.3b}$$

Note that here a 'reference' temperature of $T = 0$ K has been used in order to define the actual value of $S(T)$. In principle, this is valid as the third law of thermodynamics states that $S = 0$ at 0 K [123]. However it is often difficult to determine the development of C_p to very low temperatures. This will be explored in more detail in Chapter 4. Furthermore, one can define the so-called excess entropy, S_x, as the difference in entropy between the supercooled liquid and the corresponding crystal: $S_x = S^{liquid} - S^{cryst}$. The total entropy S_{tot} in the liquid can be thought of as the combination of the vibrational and configurational entropies [2]. The excess entropy can be shown to decrease strongly as the liquid approaches the glass-transition and this property has been used in models to try and understand the slowing down in the dynamics. There are even theories for the glass-transition that are based on the idea that the configurational entropy, S_c of a system should become zero when a supercooled liquid forms a glass even though this is not the case since there are still configurational degrees of freedoms remaining in the glassy state, as further described in more detail in Chapter 4.

3.2.2 Analysis of the observed glass transition

The DSC traces obtained in this research were analysed using TA's Universal Analysis software. A graphical representation of the approach used to analyse the glass transitions are shown for the step in C_p observed for the liquid hexylbenzene, as shown in Figure 3.2a. Steps in C_p were analysed by first choosing two points within the analysis software at the low and high temperature baselines either side of the glass transition step. The software determines tangents to these points and also a tangent to the inflection point of the C_p step, as denoted by the dashed red lines in Figure 3.2a. The point at which the extrapolated tangent line of the glass

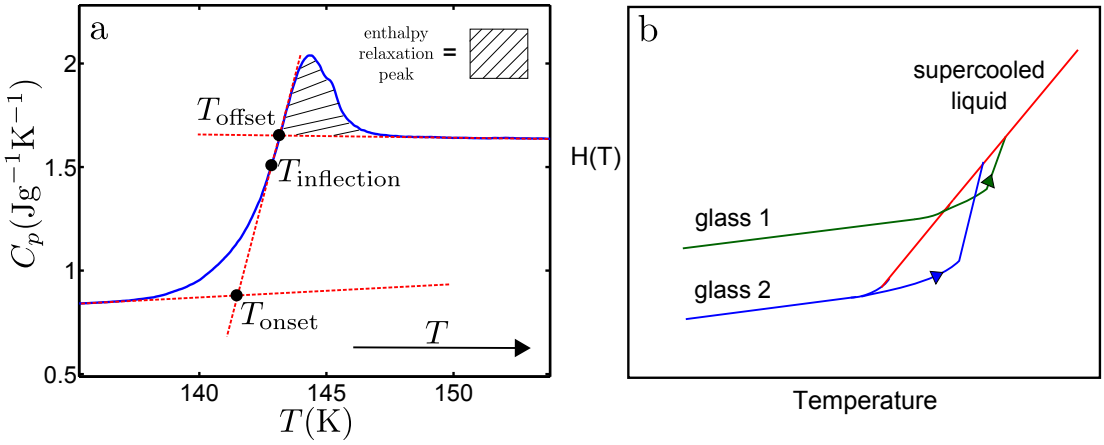

Figure 3.2: a) Glass transition step in C_p for hexylbenzene, indicating how analysis was performed. b) Diagram of the change in enthalpy as temperature is increased for two different glasses as explained in the text.

baseline (low T) crosses the inflection tangent is known as the onset temperature, T_{onset}. The point at which the extrapolated tangent of the supercooled liquid baseline crosses the inflection tangent is known as the offset temperature, T_{offset}.

In general, the extrapolated onset temperature of the endothermic step in C_p is used to define T_g [32, 124]. Although the use of different rates of cooling and heating a molecular glass-former into and out of the glassy state will change the shape of the step in C_p at the glass transition [125], the onset temperature is relatively insensitive to reasonable variation of the material's thermal history [126]. It has been shown that the repeatability of DSC analysis is such that the onset temperature can be determined within an error of 1K [127].

Although the onset temperature is used to define T_g in most cases, there are examples of different choices of T_g in the literature such as at the temperature at half of the step height, $\Delta C_p/2$ [128]. Also, if the derivative of C_p is taken, then there will be a peak corresponding to the inflection point of the glass transition step and one can define T_g as the temperature at which the peak occurs [129]. It could be argued that this is a better method for determining T_g as it does not depend on the somewhat arbitrary positioning of the tangents used to determine the onset temperature. However, the inflection point of the step in C_p is much more dependent on the thermal history of the material than the onset temperature

and this method involves taking the derivative of the data which introduces errors. Thus, in this study, the T_g, as obtained from analysis of DSC data, will be taken as T_{onset}.

In some cases, an extra contribution to C_p is observed after the glass transition. This so-called enthalpy relaxation peak (as shown in Figure 3.2a) can be explained by considering the variation of enthalpy with increasing temperature for different glasses [125]. A diagram depicting the variation of H with temperature (as introduced in Chapter 1) is shown in Figure 3.2b. As a supercooled liquid is cooled, H decreases at a certain rate. At T_g, there is an observed change in the temperature dependence of H. Faster cooling rates lead to higher observed glass transition temperatures and thus the change in the temperature dependence of H occurs at a higher temperatures [130]. For example, in Figure 3.2b, 'glass 1' is formed with a faster cooling rate than 'glass 2'. If these glasses are then heated at the same rate, the change in the temperature dependence of H at T_g is not necessarily reversible. One can sometimes observe 'superheated glass' behaviour of H where H increases at the same rate above T_g because the equilibrium liquid behaviour of H can not be realised at the temperature at which vitrification occurred on cooling [125]. At a certain temperature ($T > T_g$), the temperature dependence of H rapidly falls back onto the expected temperature dependence of H for the supercooled liquid. This is manifested as a peak in C_p, as shown in Figure 3.2a. Therefore this effect is an indication of the thermal history of a glass.

3.2.3 Different methods of calorimetry

Differential scanning calorimeters are generally manufactured using two different principles of determining the heat flow through a sample. Power compensation DSC involves placing the sample and reference in two separate furnaces and monitoring the temperature difference between the sample and the reference, ΔT. The electrical power supplied to the sample furnace, P_S ,and the reference furnace, P_R, are varied such that $\Delta T = 0$. Measurement of the differential between P_S and P_R yields the differential heat flow between the sample and the reference [131].

Heat-Flux DSC on the other hand involves placing the sample and reference onto platforms with high thermal conductivity within the same furnace and measuring ΔT directly, in order to determine the difference in heat flux [132]. In this research, a turret-type heat-flux DSC was used and therefore the following explanation of the determination of the heat flow through a material will be conducted with reference to the direct measurement of ΔT between a sample and a reference sample.

3.2.4 Accurate determination of the heat flow

The following description of the determination of the heat flow is based on the work of Danley [132] and Hohne *et. al.* [130].

The measured heat flow in a DSC experiment, q, is the difference between the heat flow through the sample, q_S and the heat flow through a reference sample, q_R, as determined through measurement of the difference in the temperature of the sample and the reference sample (T_S and T_R). In the simplest approximation of steady-state heat flow, the conduction of heat can be described by the Biot-Fourier equation (in this formulation of the equation, vector notation has been ignored)[130, 133]:

$$\frac{q}{A} = -\lambda \nabla \cdot T \tag{3.4}$$

Here, A is the cross-sectional area of the connecting path between the heat source and sink and thus the quantity $\frac{q}{A}$ is the heat flux. λ is the thermal conductivity. A diagram depicting this scenario is shown in Figure 3.3a If we consider that, in a DSC experiment, heat flows between the DSC furnace and the sample and the reference respectively and that the lengths of the paths, Δl, between the sample/reference and the furnace are equivalent, one can construct

expressions for q_s and q_R [130].

$$q_S = -\lambda A \frac{\Delta T_{SF}}{\Delta l} \tag{3.5a}$$

$$q_R = -\lambda A \frac{\Delta T_{RF}}{\Delta l} \tag{3.5b}$$

$$\tag{3.5c}$$

Here, ΔT_{SF} and ΔT_{RF} are the temperature differences between the sample/reference and the furnace. We can now construct an expression for the differential heat flow, $q = q_S - q_R$.

$$q = \frac{-\lambda A}{\Delta l}(T_S - T_R) \tag{3.6}$$

One can approximate the quantity $-\frac{\Delta l}{\lambda A}$ as some thermal resistance in the system, R. If we assume that the thermal resistances between the furnace and the sample, R_{SF} and the reference, R_{RF} are equivalent (i.e. $R = R_{SF} = R_{RF}$), q is linearly related to the difference in temperature between the sample and the reference, ΔT, with R as the proportionality factor [130, 132]:

$$q = \frac{\Delta T}{R} \tag{3.7}$$

This equation for q is what all calorimeters are based on. We have made a number of assumptions when constructing this equation, namely: i) the thermal resistances R_{RF} and R_{SF} are the same, ii) the rate of heating in both the sample and reference are the same and iii) the heat capacities of the sample and reference are balanced. In order to get the most accurate determination of the heat-flow, these assumptions need to be addressed. In general, one must consider the *rate* of heat flow, $\dot{q} = \mathrm{d}q/\mathrm{d}t$, as ΔT would not be constant in time when endo- or exothermic transitions occur within a sample. The different thermal considerations can be described in simple terms using a circuit diagram [132]. This interpretation is valid, from a physical point of view, as heat transfer and charge transfer are analogous [130]. In this manner, q and ΔT are analogous to the charge current and the voltage respectively and therefore Equation 3.7 is the thermal equivalent

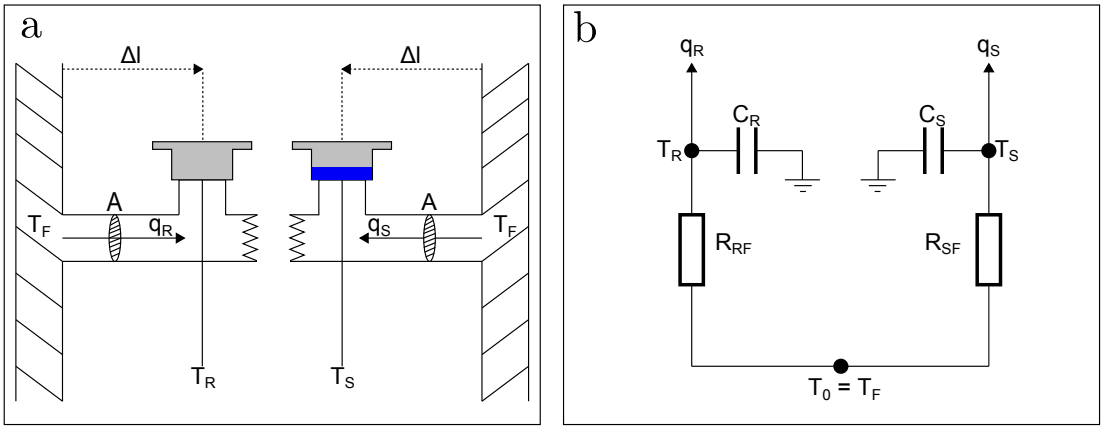

Figure 3.3: a) Diagram of the functionality of the turret-type heat flux DSC as explained in the text. b) Circuit diagram showing the thermal components of the DSC.

to Ohm's law. If we assume that the thermal resistances between the furnace and the sample and the reference are not identical and that the heat capacities of the sample and reference can be approximated as capacitors with so-called heat capacitances, C_S and C_R, then we can form equations which describe the heat flow through the sample, q_S and reference, q_R, in the circuit in a similar manner to using Kirchoff's laws to determine the flow of charge. We can also define T_0 as the temperature of the furnace (as shown in Figure 3.3b). The equations for q_S and q_R can be written as follows [132]:

$$q_S = \frac{T_0 - T_S}{R_{SF}} - C_S \frac{\mathrm{d}T_S}{\mathrm{d}t} \tag{3.8a}$$

$$q_R = \frac{T_0 - T_R}{R_{RF}} - C_S \frac{\mathrm{d}T_R}{\mathrm{d}t} \tag{3.8b}$$

For further simplification the differential temperatures ΔT and ΔT_0 can be

introduced where:

$$\Delta T = T_S - T_R \tag{3.9a}$$

$$\Delta T_0 = T_0 - T_S \tag{3.9b}$$

We can now form an equation for the differential heat flow: $q = q_S - q_R$ [132].

$$q = -\frac{\Delta T}{R_{RF}} + \Delta T_0 \left(\frac{1}{R_{SF} + R_{SR}} \right) + (C_R - C_S)\frac{\mathrm{d}T_S}{\mathrm{d}t} - C_R \frac{\mathrm{d}\Delta T}{\mathrm{d}t} \tag{3.10}$$

The consideration of the temperature of the furnace T_0 when calculating the heat flow to correct for the influence of thermal inertia is the so-called TZero$^{\mathrm{TM}}$ DSC technology invented by TA Instruments and is the fundamental basis for measurement of the DSC used in this research (as will be described in section 3.2.5) [134]. The reasoning for measuring T_0 as well as T_S and T_R is that the measurement of the sample temperature is not strictly determined at the sample itself: rather, it is determined at a thermocouple which sits below the sample crucible. There are several components which could lead to some thermal resistance between the thermocouple and the sample itself. Thus, due to the flow of heat, the measurement of the temperature of the sample will be slightly delayed in comparison to the *actual* sample temperature. One can picture this 'delay' as follows [130]. If we consider the *measured* sample temperature, T_S^m and define a characteristic time-constant τ_m to describe the temperature relaxation between the sample and the measurement point, we can describe the difference between T_S^m and T_S:

$$T_S^m = T_S - \tau_m \frac{\mathrm{d}T_S^m}{\mathrm{d}t} \tag{3.11}$$

By defining an analogous equation to describe the measured reference temperature T_R^m and introducing the quantity $\Delta T^m = T_S^m - T_R^m$ one can obtain an expression for the difference in temperature between the sample and the reference,

ΔT:

$$\Delta T = \Delta T^m - \tau_m \frac{\mathrm{d}\Delta T^m}{\mathrm{d}t} \tag{3.12}$$

Therefore an accurate determination of ΔT (and thus the heat flow q) can be obtained through knowledge of the time constant, τ_m. If this method of measuring T_0 is not used, then one can get smearing of the features in a DSC trace, the level of which is set by τ_m.

Although we now have a more accurate way of determining the differential heat flow than Equation 3.7, it has been based on the assumption that the sample and reference are in direct contact with their respective 'platforms' within the sample cell of the calorimeter. In an actual DSC measurement, a material to be measured is placed into a 'pan' of some kind. The reference is most often just an empty pan, of the same material as the sample pan. Therefore by calculating the differential heat flow, the effects of the sample and reference pans can be factored out of the heat flow through the sample q_{sam}, which is the quantity we wish to obtain.

One can construct a similar circuit diagram to that shown in Figure 3.3b in order to describe the added effects of the sample and reference pans and therefore we can define the associated thermal resistances and capacitances associated with the sample pan, C_{SP} and R_{SP} and those associated with the reference pan C_{RP} and R_{RP}.

The heat flow through the sample pan q_{SP} is the product of the mass of the sample pan, m_{SP}, the specific heat capacity of the pan material, c_{pan}, and the heating rate of the pan. Thus q_{sam} can be expressed in terms of the measured sample heat flow as $q_S - q_{SP}$. If the reference sample pan is empty, then the measured reference heat flow, q_R is equivalent to the heat flow through the reference pan. Therefore we can construct the following equations:

$$q_S = q_{sam} + m_{SP} c_{pan} \frac{\mathrm{d}T_{SP}}{\mathrm{d}t} \tag{3.13a}$$

$$q_R = m_{RP} c_{pan} \frac{\mathrm{d}T_{RP}}{\mathrm{d}t} \tag{3.13b}$$

Equation 3.13b can be rearranged in order to obtain an expression for c_{pan} and therefore this can be eliminated from Equation 3.13a as the sample and reference pans are made of the same material. We can then reformulate Equation 3.13a in order to obtain an expression for q_{sam}, which takes the difference between the masses of the pans and the difference in the heat flow through each pan into account [132].

$$q_{sam} = q_S - q_R \left(\frac{m_{SP}}{m_{RP}}\right) \left(\frac{\mathrm{d}T_{SP}}{\mathrm{d}t}\right) \left(\frac{\mathrm{d}T_{RP}}{\mathrm{d}t}\right)^{-1} \tag{3.14}$$

In order to determine the temperatures T_{SP} and T_{RP}, relations must be constructed using the values of the measured temperatures T_S and T_R. This can be realised by applying Equation 3.7, using the resistances R_{SP} and R_{RP}. In this case, ΔT would be the difference between T_S and T_{SP} or T_R and T_{RP}. The resistance associated with the pans can be constructed thorough addition of the resistances due to the pan itself, the resistance of the temperature sensor and the resistance associated with the gas layer between the pan and the sensor. These resistances can be determined using the appropriate thermal conductivities and geometries of the different components [132].

3.2.5 Measurement technique

The DSC used to complete the work presented in this thesis is a Q2000 from TA Instruments. The DSC operates using the TZero^{TM} principle as explained in Section 3.2.4. This type of calorimeter has a sample cell containing a turret type heat-flux set-up [130] as depicted in Figure 3.4a.

Calorimeter sensor and measurement chamber

A diagram showing the measurement chamber of the Q2000 DSC is shown in Figure 3.4a. The sample and reference platforms sit on a constantan base such that the sample and reference are not in thermal contact with each other. In this manner, one does not get so-called 'cross-talk' between the sample and the reference as the heat flow through the sample does not affect the heat flow through the

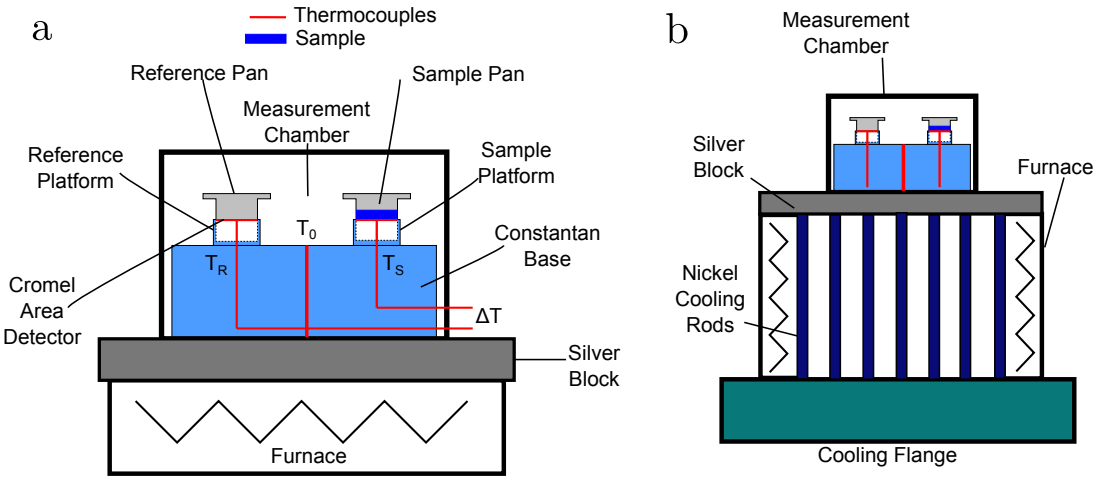

Figure 3.4: a) Diagram of the calorimeter sensor and the measurement chamber. b) Diagram depicting how the measurement chamber is cooled/heated

reference and vice versa. The temperatures, T_0, T_S and T_R are measured using thermocouples. A thermocouple is constructed by connecting two different metals and recording the potential between them, which scales with the temperature of the surface that they are connected to [135]. In the Q2000 DSC constantan and cromel are used to construct the thermocouples as they have a higher potential per unit change of temperature than any other thermocouple combination over the temperature range of the DSC [136]. The temperature of the base (and thus the furnace), T_0 is measured between the cromel and constantan wires connected to the base, equidistant between the sample and reference platforms. The temperature of the sample and reference pans are measured between the cromel 'area detectors' which are welded onto the underside of the respective platforms and the base constantin wire. The sample cell is purged with either nitrogen or helium (depending on the cooling system used) to prevent ice formation or condensation and to ensure even heating of the cell [137].

Temperature Control

A diagram showing how the temperature of the measurement chamber is controlled in the Q2000 DSC is shown in Figure 3.4b. The DSC was run with either a refrigerated cooling system (RCS) or liquid nitrogen cooling system (LNCS).

Unlike other types of heat-flux DSC, the furnace in the Q2000 system sits below the sample chamber rather than surrounding it and is connected to the calorimeter sensor via a silver block to ensure good thermal conductivity. The furnace block sits on top of a cooling flange plate, the temperature of which is kept at close to the lowest operating temperature of the DSC cooling system (-180 °C for the LNCS and -90°C for the RCS). This cooling flange is connected to the furnace and silver block by 54 nickel rods which enable rapid cooling of the sample cell and allow greater rate dependent control of the temperature of the DSC. Although the Q2000 can attain reasonably fast heating/cooling rates, the cooling rate is limited close to the operating temperature of the flange. In this research however, we only consider the DSC traces on heating of the samples.

Sample preparation and operating procedure

For the research presented in this thesis, the samples were all prepared in hermetically sealed aluminium pans (see Figure 3.4a). This ensured that evaporation of the lowest molecular weight samples measured could be prevented. Although it is not strictly necessary to use hermetically sealed pans to measure polymeric samples, the same pans were used for all samples to ensure comparability between the obtained data. Samples of between 5 and 15mg were placed into the pans. In the case of the polymeric samples, it was necessary to 'pre-melt' the sample in order to guarantee good thermal contact between the sample and the bottom of the pan.

In all cases for this research, samples were run with a heating/cooling rate of 10 K per minute as it has been shown that this rate corresponds to a structural relaxation timescale of 100s [138–141], corresponding to the timescale at which the dynamic T_g is often defined. The samples were first cooled below their expected glass transition temperatures and then measurements were performed whilst cycling the temperature around this transition.

Calibration

In order to obtain an accurate value for the heat flow through the sample, the calorimeter must be calibrated in order to determine values for the machine spe-

cific unknowns from Equation 3.10, namely the thermal capacitances associated with the sample and reference measurement platforms, C_S and C_R, and the thermal resistances between the furnace and the sample and reference, R_{SF} and R_{RF}. The calibration involves first running the DSC with no sample or reference pans. In this manner, the heat flows of both the sample and reference are effectively zero and so Equations 3.8a) and b) can be rearranged such that an expression for the so-called time constants of the calorimeter can be obtained where, for example, $\tau_S = C_S R_S$ [132]:

$$\tau_S = \Delta T_0 \left(\frac{\mathrm{d}T_S}{\mathrm{d}T} \right)^{-1} \tag{3.15a}$$

$$\tau_R = (T_0 - T_R) \left(\frac{\mathrm{d}T_R}{\mathrm{d}T} \right)^{-1} \tag{3.15b}$$

$$= (\Delta T_0 - \Delta T) \left(\frac{\mathrm{d}T_S}{\mathrm{d}t} - \frac{\mathrm{d}\Delta T}{\mathrm{d}t} \right)^{-1} \tag{3.15c}$$

The next step in the calibration is to determine the thermal capacitances directly. This can be achieved by placing sapphire disks with well known mass onto the sample and reference platforms. The heat flow through the sapphire disks, can be determined as a product of the mass of the disks,m_{sapp}, the specific heat capacity of sapphire, c_{sapp} and the heating rate. Sapphire has no phase transitions in the temperature region of measurement for this calorimeter and therefore the assumption made during this calibration is that the rate of heating of the sapphire disks is equivalent to the rate of heating through the sample and reference platforms. We can thus set the heat flow in Equations 3.8a) and b) equal to the heat flow expected for the sapphire disks and solve the equations for C_S and C_R. As we have determined the time constants for the calorimeter, τ_S and τ_R, we can now obtain expressions for the determination of the thermal

resistances, R_{SF} and R_{RF} [132]:

$$R_{SF} = \frac{\tau_S}{C_S} \tag{3.16a}$$

$$R_{RF} = \frac{\tau_R}{C_R} \tag{3.16b}$$

$$\tag{3.16c}$$

Therefore, by calibrating the machine using an empty sample cell (i.e. no sample or reference) and then calibrating with sapphire disks with well defined thermal properties, we can determine all the machine dependent thermal unknowns required to correctly measure the heat flow. This has the added advantage of setting the baseline of the DSC measurement to (effectively) zero and thus this type of DSC does not require the removal of a baseline from the resulting traces in heat flow.

Further calibration

Although the method described above yields an essentially perfectly flat baseline ($q = 0 \pm 10\mu W$), there could still be some discrepancy of the measurement of the onset temperature or enthalpy change ΔH of a transition, such as melting. In order to account for this, a DSC can be calibrated using samples with a very well defined melting temperature and enthalpy of fusion ΔH_{fus} [142]. Typically, indium is used for such a calibration with a melting temperature of 156.6 °C and a ΔH of 28.47 kJ/kg. One can measure a sample of indium and then adjust the temperature correction and the so called 'cell-constant' of the calorimeter in order to ensure a correct determination of the transition temperatures and enthalpies for future measurements. Although this method is valid, by only applying the temperature correction of the calorimeter with one reference material we are assuming that the temperature correction is the same across the entire operating temperature range. This is not always the case and often it is necessary to do a multi-point calibration of the temperature correction of the calorimeter, especially

for low temperature measurements [128, 143]. For this reason, adamantane was also used to calibrated the temperature correction of the calorimeter.

3.3 Thermogravimetric Analysis

The term *Gravimetric Analysis* refers to the accurate determination of the mass of a sample and therefore *Thermogravimetric Analysis* is the determination of the mass of a sample as a function of temperature [144].

TGA was used to determined the degradation temperature, T_D, of polymeric samples to aid the sample preparation of these samples for measurement using Broadband Dielectric Spectroscopy. In order to measure polymeric samples using, BDS, the samples were applied to 40mm diameter electrodes with silicon spacers and heated to temperatures significantly higher than their expected glass transition temperatures. A smaller 20mm diameter electrode was then placed onto the polymer/spacer set up and pressure was applied in order to ensure a constant sample thickness between the two electrodes. The inherent problem with this procedure was that the temperature required in order to decrease the viscosity of the polymeric samples enough such that an even sample thickness could be attained was close to the degradation temperature of the polymers. Therefore, in order to avoid degradation of the samples, thermal gravimetric analysis (TGA) was performed to determine the temperatures at which they would degrade. This provided an upper-bound for the temperature in the sample preparation process.

A diagram of a typical TGA set-up is shown in Figure 3.5a. A TGA instrument consists of a sample platform which is connected to a balance in order to measured the change of mass of the sample, contained within a metal pan. A furnace is used to vary the temperature of the sample. This temperature, T_s, is recorded by a thermocouple connected to the sample platform.

The mass of the sample is recorded through an electrobalance connected to the sample platform via the 'sample carrier'. In order for an accurate determination of the sample mass, buoyancy corrections must be made. During measurement, the apparent mass of a sample can appear to increase due to Archimedes' Principle [145]. As the sample is heated, the density of the surrounding gas decreases whereas the density of the sample does not change at the same rate. This means

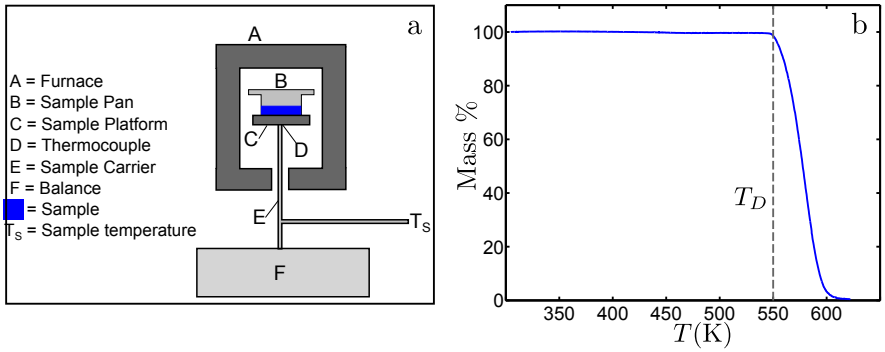

Figure 3.5: a) Diagram showing a typical TGA set-up as described in the text. b) TGA data for a sample of poly(α-methylstyrene) (M_w = 28000) with the degradation temperature, T_D, indicated by the dashed line.

that the 'upthrust' due to the mass displacement of the gas will decrease with increasing temperature leading to an apparent increase in the mass of the sample. This effect can be reduced by using a small sample mass ($\sim$ 10mg) and by performing a baseline calibration by measuring a sample which will not change in mass over the measured temperature range.

In this research, a Netzsch TG 209 F1 Libra® TGA instrument was used. The instrument has an operational temperature range of 283 - 1373 K and the heating rate can be varied between 0.001 to 200 K/min. Measurements of the samples in this research were placed into aluminium sample pans and heated to a temperature of 620 K at a rate of 10 K/min. The result of this for a sample of poly(α-methylstyrene) (M_w = 15900) is shown in Figure 3.5b. The percentage mass remains at 100% for most of the temperature range measured before rapidly decaying to 0 at a certain temperature. The temperature at which an appreciable decrease of the mass was observed was defined as the degradation temperature, T_D, as shown in the figure.

3.4 Summary

Differential Scanning Calorimetry (DSC) and Thermogravimetric Analysis (TGA) are useful tools in the determination the thermal properties of materials. Firstly, this chapter included an explanation of how the heat flow is determined in a heat-

flux DSC and a description of the TA Q2000 heat-flux DSC that was used in order to determine the nature of the characteristic steps in the heat capacity relating to the glass transition. Secondly, a brief description of the principles of TGA was given which was used in order to determine the degradation temperature, T_D, for the polymeric samples measured in this research.

Chapter 4

Results I: Relaxation dynamics in a systematic series of simple molecular glass formers

4.1 Introduction

In Chapters 4, 6 and 7 the dynamics of glass-formers as a function of the 'size' of their constituent molecules will be considered. Chapter 4 focuses on a series of alkylbenzenes where the alkyl tail attached to a phenyl ring is varied systematically. In contrast, Chapters 6 and 7 focus on chain-length series of oligomers or polymers either of poly(styrenes) (Chapter 6) or poly($\alpha-$methylstyrenes) (Chapter 7). This choice of systems makes it possible to systematically investigate both how small structural modifications changes the glass transition temperature, T_g, and how the building up of polymeric chains by adding monomers together changes T_g.

An increase of the glass transition temperature, T_g, with increasing molecular weight is a feature common to low molecular weight glass forming liquids. From a simplistic point of view it makes sense that a higher temperature is necessary to bring a system of larger molecules from the glassy to the fluid state. However, there are no established theories or models that both describe this molecular weight or size variation in detail and fit experimental data well. Figure 4.1a shows a compilation of data obtained from the literature [146] for a large compilation

of glass-forming liquids that interact through van der Waals interactions. Based on this, Novikov *et. al.* suggest that the relationship between T_g and molecular weight can be described by a simple power law expression: $T_g \propto M^{\alpha}$, where $\alpha = 0.51 \pm 0.02$. This behaviour is denoted by the red dashed line in Figure 4.1a. The authors provide some qualitative explanations for the general observed trend of an increasing T_g with increasing M_w. One is based on the so called Lindemann criterion for melting, which states that as the atomic mean square displacement $< x^2 >$ reaches 10% of the squared inter-atomic distance a^2 the system melts [147]. The mean square displacement can be approximated as $< x^2 > \propto T/M_w\omega_D^2$, where T is the temperature and ω_D the Debye frequency [148]. This means that the melting temperature $T_m \propto M_w$. Moreover, it is well known that to a good approximation there is a simple relationship between the melting temperature and the glass-transition temperature, $T_g \approx 2T_m/3$ [149]. Following this simple reasoning, one would thus expect that approximately $T_g \propto M_w$. Another simple argument is based on the fact that one can both motivate theoretically [2] and show experimentally that T_g [2, 146] is proportional to a material's elastic moduli, e.g. a bulk modulus or a shear modulus, multiplied by a relevant volume where the latter has a size of the order of the molecular volume. Novikov *et. al.* make the argument that if the molecules interact through van der Waals interactions a simple relationship between T_g and the molecular weight of the molecule can be derived. The argument is that the bulk modulus B is proportional to the volumetric density of the intermolecular interaction energy, U, so that $B \propto U/V$, and U in turn is proportional to the surface of a molecule. Thus, one obtains an approximate scaling $B \propto V^{1/3}$, where V is a molecular volume. Using the general relationship between T_g and modulus, one finally obtains, $T_g \propto B \propto V^{2/3} \propto M_w^{2/3}$. The authors state that these explanations are speculative and only a very rough estimates but they do support the growth of T_g with increasing M_w.

Larsen *et. al.* also provide an argument for the increase of T_g for a range of molecular glass formers based on their size [150]. The authors collate T_g data for 13 non-polar glass formers [151–156] comprising of molecules which they approximate as rigid (based on the fact that the molecules contain alkane chains less than 3 carbons long) and characterise their size based on their effective hard sphere diameters, σ_0, where $\sigma_0 < 1$nm for the samples studied. The hard sphere

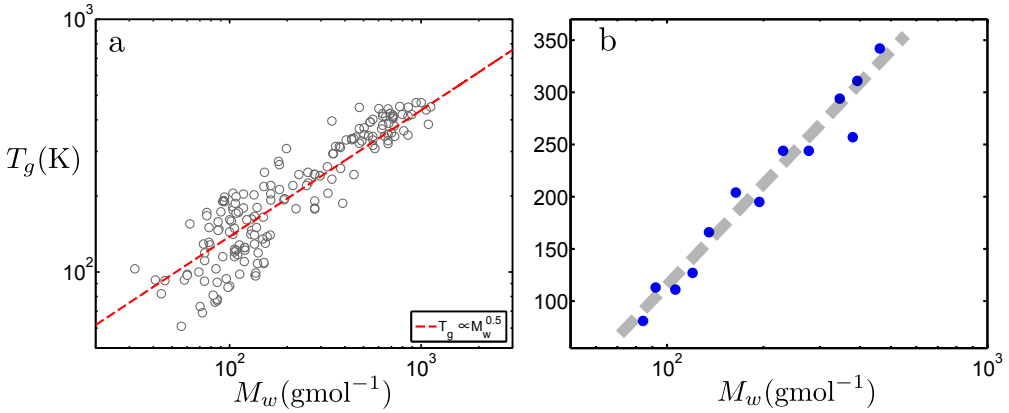

Figure 4.1: a) T_g as a function of molecular weight reproduced from Ref.[146]. The red line indicates the predicted $T_g \propto M_w^{\alpha}$ behaviour with $\alpha = 0.5$. b) T_g as a function molecular weight of a selection of molecular glass formers reproduced from Ref.[150]. The dashed guide to the eye indicates the linear behaviour of the T_g values with a $\log_{10}(M_w)$ scaling.

diameters are derived from analysis of high-pressure equation of state data [157]. The authors found a systematic growth of T_g with increasing σ_0. The authors further provide a very interesting idea for how to think of their data, which is based on the behaviour of the glass transition in colloidal systems. For suspensions of relatively mono-disperse hard-sphere colloids it is well known that glass formation occurs at a colloid volume fraction $\phi \sim 0.58$ [158]. Given the hard sphere sizes of the molecules in the series, a similar argument can be used here where one defines T_g as occurring when the molecules reach a $\phi \sim 0.58$. However, this approach could not quantitatively account for the data over the full range of molecular weights. Thus, for a more direct comparison to the discussions and data discussed in this work, we have in Figure 4.1b replotted the T_g values from the authors' compilation as a function of molecular weight on a logarithmic scale. This will later serve as a point of reference for the behaviour of a series of simple molecular liquids for which the molecules can be considered as rigid.

Several other compilations of T_g and other dynamic data obtained for molecular glass forming liquids exist in the literature (for example Refs. [25, 37, 52, 151]. However, comparison between very different types of samples is difficult due to their differing chemistries and interactions between constituent molecules. In or-

der to explore the variation of parameters such as T_g, the most logical approach should be to study series of samples where a quantifiable parameter relating to the molecular structure or interactions is systematically varied. In the results presented in the following chapters of this thesis, the parameter chosen for systematic variation was the molecular weight of a specific series of substances. In this manner, we have chosen to investigate systematic modifications of structure. Studies of a systematic nature exist particularly for polymeric systems where the effect of increasing the degree of polymerisation is explored. However, the existing studies generally focus on oligomeric chain-series where mainly the structural relaxation and the related glass transition temperature are investigated. Very few studies exist where the full relaxation behaviour is mapped out in detail and this lack of systematic investigations is even more clear for non-polymeric glass-forming systems.

To address this, in this chapter, an investigation of the effect of structure modifications in a series of simple molecular organic glass-forming liquids, alkylbenzenes, will be presented. The alkylbenzenes are most commonly used as solvents or as precursors in the synthesis of other chemicals. They also exist as integral components of petroleum products [159]. The common feature of the samples in this series is a single benzene ring covalently bonded to a 'tail' consisting of a differing number of backbone carbon atoms. A schematic representation of the chemical structure of the samples in this series is shown in Figure 4.2.

To facilitate the following discussion of the results for the alkylbenzenes, and focus the attention of the reader to the length of the alkyl-chain tail, the parameter M will be used to represent the different samples where M relates to the number of backbone carbon atoms in the tail (see Figure 4.2). For example, ethylbenzene consists of a benzene ring connected to a tail consisting of methylene (CH_2) and methyl (CH_3) groups. The number of carbon atoms in the backbone of the tail in this instance is 2 and therefore, using this nomenclature, ethylbenzene would be the $M = 2$ sample. Note that often, M, is used to refer to the molecular weight. To avoid confusion, the molecular weight will be referred to as M_w in this thesis. The samples for this study were all obtained from Sigma-Aldrich with a stated purity of better than 98%. Further details regarding

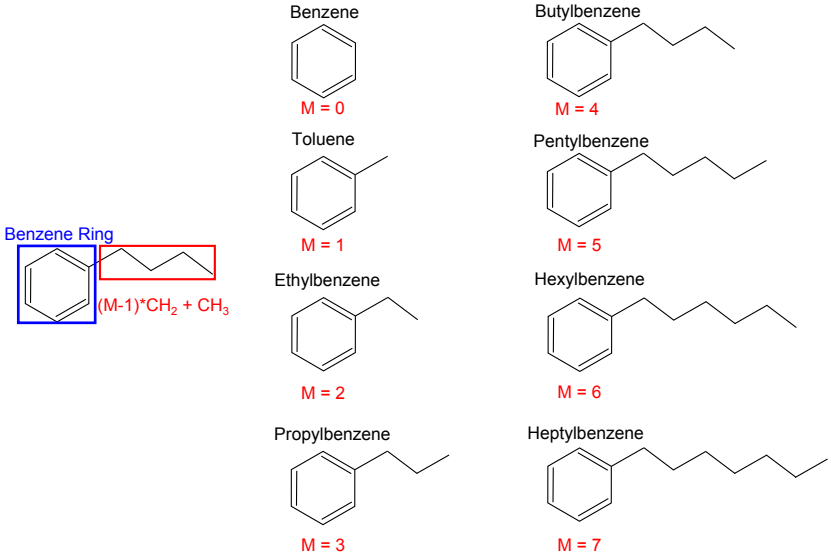

Figure 4.2: Schematic representation of the chemical structure of the samples in the alkylbenzene series.

the series, including their M value and values for the melting and boiling points quoted by the manufacturer are shown in Table 4.1.

Sample	M	M_w (g/mol)	Density at 298K (g/ml)	Stated Purity	T_m (K)	T_b (K)
Toluene	1	92.14	0.865	99%	180	383
Ethylbenzene	2	106.17	0.867	$> 99.5\%$	178	409
Propylbenzene	3	120.19	0.862	$> 99.5\%$	174	432
Butylbenzene	4	134.22	0.860	$> 99.8\%$	185	456
Pentylbenzene	5	148.24	0.863	$> 99.0\%$	198	478
Hexylbenzene	6	162.27	0.861	$> 99.8\%$	212	499
Heptylbenzene	7	176.30	0.860	98%	225	506

Table 4.1: Table showing specific details for the samples in the alkylbenzene series with the relevant quoted specifications from the manufacturer. All samples were obtained from Sigma-Aldrich.

The research presented here combine results obtained from Broadband Dielectric Spectroscopy (BDS) and Differential Scanning Calorimetry (DSC) in order to analyse the effects of increasing alkyl tail-length on the dynamics of the glass transition. A systematic investigation of the relaxation dynamics of the alkylbenzene series has not been reported before. However, data on some properties exist in the

literature on the M = 1-4 and 6 samples in the series [33, 34, 55, 61, 78, 98, 160–165]. These literature results will be discussed in relation to our new measurements when this is relevant throughout the chapter.

4.2 Dielectric Spectroscopy: α relaxation

In this section the dielectric measurements and analysis of the α relaxation for the alkylbenzene series will be discussed. Measurements were performed at both the University of Leeds and at Chalmers University of Technology, Gothenburg, using the Novocontrol Alpha-A and Alpha-S analysers (for more details, please refer to Chapter 2). The two dielectric set-ups have an operating frequency range of 10^{-2} to $\sim 10^{6}$Hz allowing the characteristic relaxation mechanisms of the glass-formers to be captured over a wide range of frequencies and timescales. As the experiments were performed on two different spectrometers, this enabled the repeatability of the obtained spectra with regards to different experimental set-ups to be determined. The low viscosity of the samples at room temperature meant that the samples had to be run using the dielectric liquid cell (BDS 1308, Novocontrol) as described in Chapter 2. The samples were placed between two 20mm diameter gold plated electrodes with a fixed separation of 100µm maintained through the use of silica spacers. The temperature of the dielectric sample cell was maintained using the Novocontrol Quatro cooling system with an operating temperature range of -160 to 400°C and an accuracy of $\pm$0.1°C.

4.2.1 Dielectric spectra

The dielectric response corresponding to the α relaxation manifests itself as a peak in the dielectric loss, ε''. In order to capture the development of the loss peak as a function of temperature, the samples were run at a selection of temperatures ranging from just below T_g to a temperature such that the α relaxation peak for each sample was no longer visible in the measurable frequency window. The dielectric measurements of this series in the α relaxation temperature regime were conducted by first cooling the samples at the maximum rate of the cooling system ($\sim$20K/min) to a temperature below their expected T_g in order to avoid

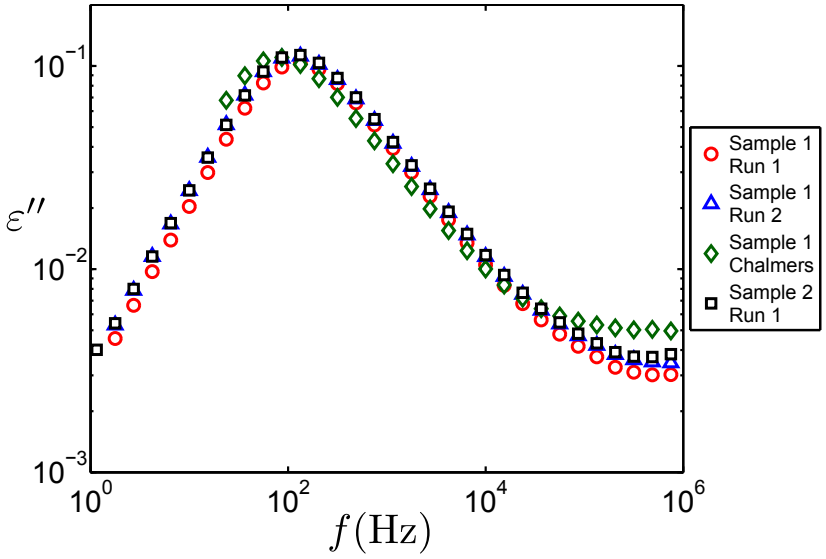

Figure 4.3: Dielectric spectra for different runs of $M = 5$ samples at 147 K in order to check the repeatability of the observed α relaxation peak. The different runs include comparisons between re-fillings of the liquid cell, the response from two different dielectric spectrometers and the response from two different batches of pentylbenzene.

crystallisation of the samples. The temperature was then increased in steps of 2 K and dielectric spectra were obtained at every temperature increment.

To illustrate the repeatability of the α relaxation spectra, several spectra obtained for pentylbenzene (M = 5) are shown in Figure 4.3. This figure shows spectra recorded on samples from the same batch in four separate runs, each including a re-filling of the liquid cell. Measurements were performed using both the two different dielectric set-ups at Leeds and Chalmers (as indicated in the figure) and a measurement performed on a separate batch of pentylbenzene is also shown in order to confirm that the obtained results were independent of the batch studied. This figure illustrates that the dielectric spectra in the α relaxation regime are highly repeatable between different spectrometers, different sample batches and re-fillings of the liquid cell. Slight variations in the peak frequency, particularly between the runs completed at Leeds and those completed at Chalmers, can be attributed to small variations in the measured absolute temperature of the spectrometer on the order of $\pm$0.5K.

Figure 4.4 shows the dielectric loss ε'' obtained for the alkylbenzene series (M = 2,3,4,5,6 and 7) in the temperature range for which the α relaxation was clearly visible within the measurable frequency range. The solid lines are the results of data fitting and the details of the fitting procedure will be described in Section 4.2.3. Data are not shown for toluene (M = 1) as the sample could not be quenched at a sufficient rate as to avoid crystallisation. As a result of this, the data for toluene shown in latter parts of this chapter were obtained from the two existing relevant literature studies on dieletric spectroscopy of toluene [33, 55, 61, 98]. The two literature studies addressed the problem with sample crystallization differently. In the Refs. [55, 61, 98], two partially silvered microscope glass plates were glued together at a fixed separation of 50μm. The sample was then introduced into the cavity and the filled cell was placed into a cryostat pre-cooled to 80K in order to quench the sample. With interfaces prepared in this manner, crystallisation could be avoided. Measurements were performed upon heating of the sample. In Ref. [33], the authors used small sample volumes to suppress crystallisation. Purified toluene was placed into thin-walled glass capillaries and measurements were performed by placing several of these capillaries between two metal plates acting as electrodes. Measurements were made upon lowering of the sample temperature. In this case, the effects on the electric field distribution introduced by the specific measurement geometry was taken into account by modelling the effect of a thin-walled cylinder in a parallel plate capacitor.

The most prominent features of Figure 4.4 are the clear loss peaks relating to the α relaxations. The samples all demonstrate a decrease in the peak frequency of these α relaxation loss peaks with decreasing temperature, and a slowing of the structural relaxation timescale is generally observed as the glass transition temperature is approached. This behaviour is characteristic of glass forming liquids [2]. In the case of the M = 3, 4, 5 and 6 samples, crystallisation of the samples was observed when the peak frequency of the α relaxation reached a value of 10^4 Hz. The loss peaks could be obtained beyond this frequency for the M = 3 and 4 samples by cutting the low frequency range at the appropriate temperatures and thus decreasing the measurement time at each temperature meaning that crystallisation could be avoided. However, the loss peaks for the M = 5 and 6 samples were unobtainable in this temperature/frequency region.

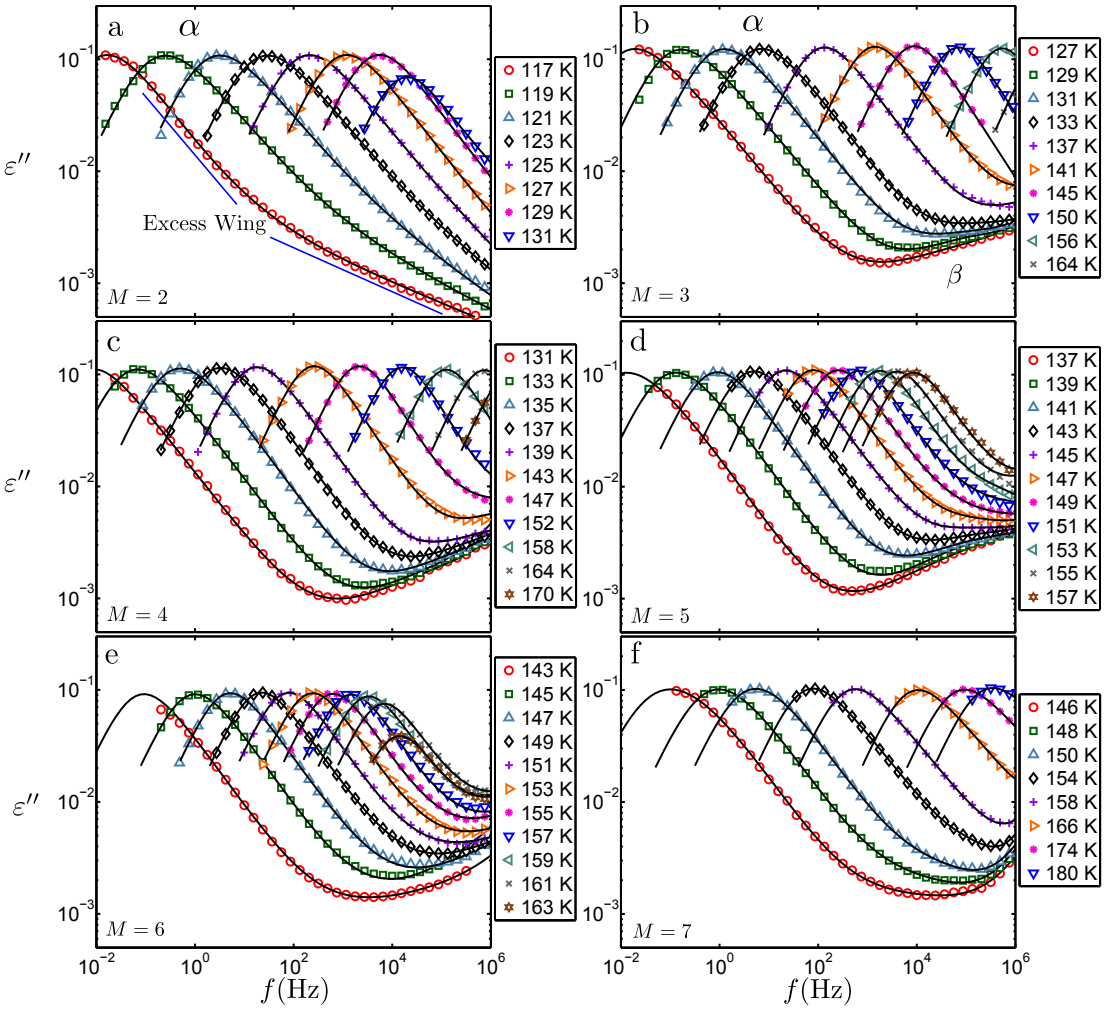

Figure 4.4: Dielectric loss spectra for the a) $M = 2$ b) $M = 3$, c) $M = 4$, d) $M = 5$, e) $M = 6$ and f) $M = 7$ samples in the α relaxation regime. Fits of the data are shown as solid lines in the figures and will be further described in the text.

The spectra for the M = 3 - 7 samples shown in Figures 4.4b-f additionally show two extra contributions to the dielectric loss. The first of these is an intermediate frequency relaxation contribution which is consistent with the secondary relaxation process clearly observed at lower temperatures for the M = 3, 4, 5 and 6 samples. This secondary relaxation could not be resolved for the M = 7 sample at lower temperatures, but the full spectra for this sample could not be described in the α relaxation range without the introduction of an intermediate relaxation process, which strongly suggests that the M = 7 sample has the same kind of relaxation contribution. The nature of the observed secondary relaxations will be discussed in Section 4.3. The second extra contribution to the spectra was a weak high frequency contribution. The origin of this contribution is unclear, but its existence and behaviour was repeatable through separate sample measurements.

The spectra for the M = 2 sample do not show any indications of the intermediate frequency contribution or the high frequency contribution. Instead, the loss peaks demonstrate a distinct change in the gradient of the high frequency flank of the α loss peak, a so-called 'excess-wing', as indicated by the solid blue lines in Figure 4.4a. This could be indicative of the merging of a secondary relaxation process as observed in an oligomeric chain series of propylene glycol based dimethyl ethers in research published by Mattsson *et. al.* [69]. In this study, samples with the degree of polymerisation N = 1, 2, 3, 7 and 69, were analysed using dielectric spectroscopy and it was observed that for the longer chain-length samples, a clearly separated α and β relaxation loss peak were observed. However, as the chains became shorter the two relaxations moved closer together and eventually the secondary contribution was submerged under the high-frequency flank of the α relaxation in effect leading to an excess wing. The implication was that the excess-wing observed for the smaller chain length samples was due to the merging of the α and β relaxations. Similar observations have also been made in a series of polyalcohols [166] and for an oligomeric series of propylene glycol [167]. Also, observations have been made in other systems where different routes were used to control the separation of the α and β relaxations. In a study by Schneider *et. al.* samples of propylene carbonate and glycerol were aged for up to 5 weeks at a temperature close to the glass-transiiton where aging leads to a significant slowing-down of the α relaxation, whereas the β relaxation shows a much

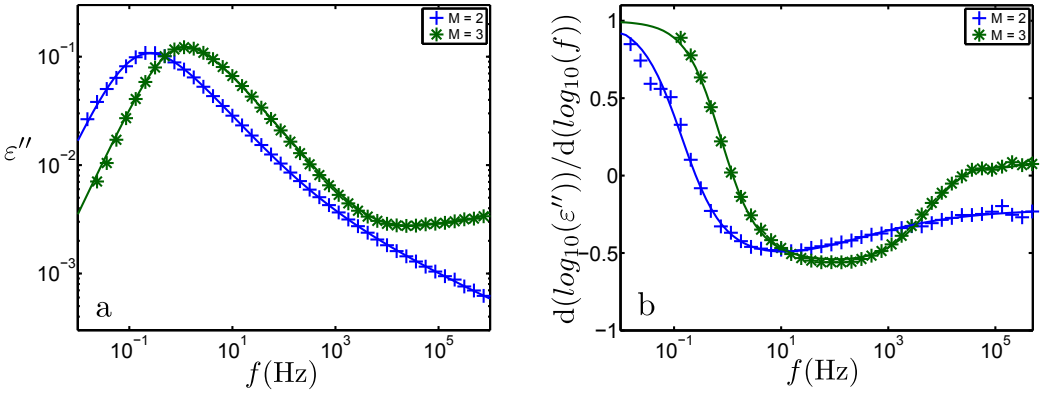

Figure 4.5: Figure showing a) the dielectric loss in the α relaxation regime and b) the derivative of ϵ'' against frequency for the $M = 2$ and 3 samples to demonstrate the difference between the spectra.

weaker dependence thus leading to a separation of the two relaxations for longer aging times [71]. In these experiments, the excess-wing observed for the samples becomes a 'shoulder' with ageing, hinting at an underlying β relaxation. Casalini *et. al.* studied the pressure evolution of the type B glass former, tripropylene glycol (tri-PPG) [70]. The sample was held at a temperature of 220.5 K and subjected from pressures increasing from atmospheric pressure to 591.3 MPa. At atmospheric pressure, the dielectric spectra for tri-PPG showed clearly defined loss peaks relating to the α relaxation and what the authors call the β relaxation. As pressure was increased, an excess-wing developed on the high frequency flank of the α relaxation. With further increasing pressure, this wing developed into another well defined relaxation process further indicating that the excess-wing is indicative of an underlying relaxation process.

The dielectric loss for the $M = 2$ and 3 samples are shown in Figure 4.5a and the different behaviour of the $M = 2$ sample is clear. In order to investigate the wing behaviour of the $M = 2$ sample further, the derivative of ε'' for the $M = 2$ and $M = 3$ samples was derived as shown in Figure 4.5b. The derivative spectra shows a minimum corresponding to the gradient of the high frequency flank close to the peak frequency, f_p, before increasing to a non-zero value which corresponds to the power-law exponent representing the excess wing, as shown in Figure 4.4a). In comparison, the $M = 3$ derivative spectra increases from the minima up to a value of around zero as a combined result of the secondary relaxation and high

frequency contribution entering the frequency window. We could not establish a clear indication of an excess wing in the temperature regions shown in Figures 4.4b-f for the $M = 3$ to 7 samples. If we assume that the excess wing in the dielectric spectra for the $M = 2$ sample is indicative of an underlying β relaxation then the absence of this behaviour for the higher molecular weight samples poses an obvious question: what happens to this secondary relaxation as tail-length is increased? One possible scenario is that, for the higher molecular weight samples in this series, the secondary relaxation becomes increasingly merged with the α relaxation and is therefore indistinguishable in the spectra. This hypothesis will be analysed in full in Section 4.3.7. Another hypothesis is that the secondary relaxation responsible for the excess wing in the $M = 2$ sample has a direct counterpart in the secondary relaxations directly observed for the other samples. We will investigate both these hypotheses in detail.

4.2.2 Rescaled spectra

To directly compare the dielectric spectra from the different samples, spectra corresponding to a peak frequency, f_p (Figure 4.6a) of approximately 1 Hz were chosen and rescaled both by their peak frequency and peak amplitude, ϵ''_{max} (Figure 4.6b), respectively. As shown in Figure 4.6a, the α relaxation amplitude and shape show relatively little variation between the different samples in the series with toluene as an exception and no systematic trend is observed in the amplitude of the loss peaks. We note that the density of the samples is nearly independent of the alkyl tail-length at 298K (see Table 4.1) and the molecular dipole moments should be very similar which together supports a similar dielectric strength. Again, the slight exception is the dielectric loss peak for toluene ($M = 1$) which appears to have a smaller amplitude. Furthermore, the gradient of the low frequency flank (in a log-log representation) for all spectra is very similar across the range of samples. This observation ties in well with the fact that the exponent of the power law describing the low frequency flank is normally consistent with a value of 1 [168]. It is important to realise however that this is not always true and in polymeric samples where a wider range of chain-related relaxation modes exist the behaviour can be more complex. Also in associating

systems extra long-time contributions could occur which will effectively change the low-frequency slope. Finally, the gradient of the high frequency flank varies across the range of samples increasing slightly with increasing molecular weight for the $M = 1$ to 6 samples, as shown in Figure 4.6b.

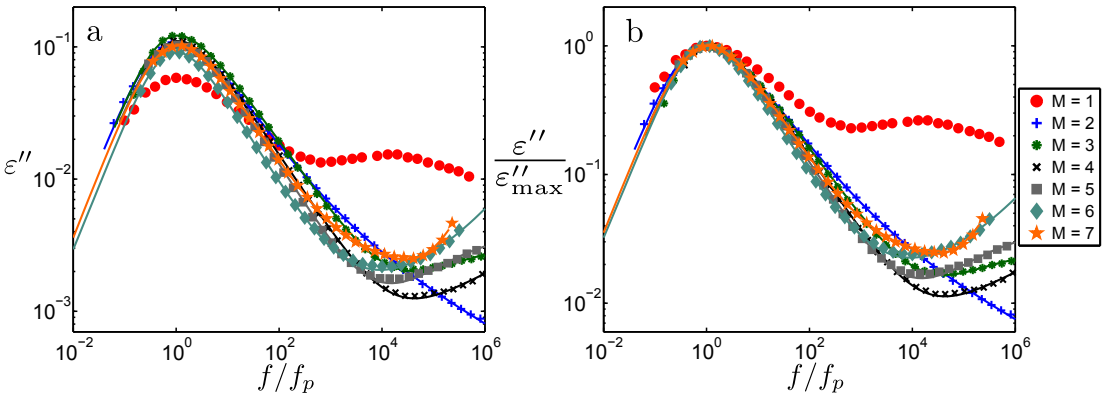

Figure 4.6: Dielectric spectra for the different samples rescaled by a) f_p and b) f_p and ϵ''_{max}. Data for toluene was obtained from [61].

The most prominent feature of this figure, however, is the relatively strong β relaxation observed for the $M = 1$ [61] sample. As discussed above, the $M = 3$ - 6 samples all demonstrate a secondary relaxation process which is clearly observed at lower temperatures and the timescales, τ_β, for the weak secondary contributions observed in Figure 4.6 are consistent with the τ_β observed at much lower temperatures (as shown in Figure 4.33 in Section 4.3.7). However, it is not clear what the relationship is between the different secondary relaxation contributions observed as separate but weak loss peaks for the M = 3-6 samples, an excess wing for the $M = 2$ sample and a relatively strong secondary loss peak for the $M = 1$ toluene sample. These relationships will be investigated in detail in latter sections of this chapter.

4.2.3 Fitting procedure

In this section, the fitting procedure used in order to describe the dielectric spectra in the α relaxation regime will be discussed. Firstly, a qualitative analysis of the development of the α loss peak will be shown. Following this, the functions used

to describe the spectra will be reintroduced. The full behaviour of these functions is described in Chapter 2 but are defined here again for clarity.

General shape of the α loss peak

In order to gain a qualitative impression of the variation of the α loss peak with increasing temperature for the samples in this series, the dielectric spectra for each sample were first rescaled in both frequency and ε''. As an illustration, the rescaled spectra for propylbenzene ($M = 3$) for a selection of temperatures in the α relaxation regime is shown in Figure 4.7a. The first thing we can see from this figure is that the low frequency flank of the α relaxation peaks fall onto a single curve which could be well expressed as a power law with an ω^1 behaviour, as indicated in the figure. The figure also shows that the peak becomes more narrow with increasing temperature. This is illustrated by the slight increase of the gradient of the high frequency flank and/or by the decreasing 'bluntness' of the peak with increasing temperature. The parametrisation of this variation for this series of samples will be shown in Sections 4.2.4 and 4.2.4.

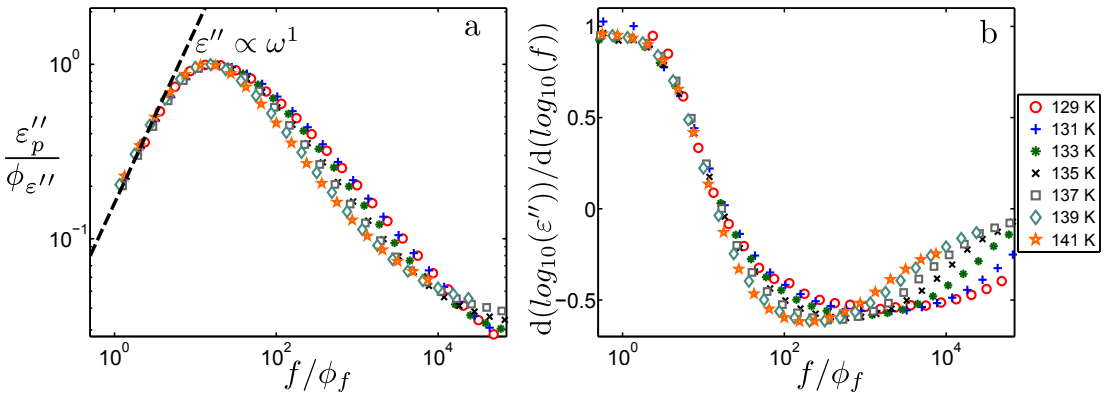

Figure 4.7: a) Plot showing a selection of dielectric spectra for propylbenzene, rescaled in both frequency and ε'' in order to collapse their low frequency flanks onto one single curve. The low frequency flanks can be described power law flank of the form $\varepsilon'' = A\omega^1$ as indicated. b) The derivative of the spectra shown in a).

Figure 4.7b shows the derivative of the spectra with the same scaling in frequency as in Figure 4.7a. The difference in the minimum value of the differential

spectra indicate that as temperature is increased the exponent of the high frequency power-law flank increases but the overlap of the derivative spectra at lower frequencies suggests that the relaxation peaks can be described with the same low frequency flank. All measured samples in the series (M =2-7) show similar behaviour to that shown in Figures 4.7a and b.

Figures 4.7a and b thus demonstrate that the spectra cannot be fully rescaled across the temperature range and therefore time-temperature superposition (TTS) does not hold. TTS is predicted from the simplest mode-coupling theory approximations (the so called ideal MCT) [13, 169], which can generally describe the response of glass-forming molecular liquids for temperatures above a critical temperature, T_c [169] that is typically situated at a temperature 1.2 - 1.6 times that of T_g [85]. The validy of TTS for polymeric glass formers has been widely assumed [170–173] and TTS has also been shown to apply to some molecular glass formers close to T_g [174] but the authors concede that the behaviour is most likely not universal of all molecular glass formers. The often observed break-down of TTS has in some cases been attributed to the presence of a secondary relaxation process [175]; the idea is either that TTS is broken due to interactions between the primary and secondary relaxation or that the presence of secondary relaxations makes the data fitting very difficult and a clear determination of the real shape of the α response becomes impossible. Either of the latter interpretations, raises the question of whether a secondary relaxation process is hidden within the high frequency flank of the α loss peaks for the M = 3 to 7 samples. Furthermore, it has been observed that if a sample appears to obey TTS in the data obtained from one technique, this is not necessarily the case for data obtained from another technique for the same sample [13]. If one make the assumption that TTS should hold for all glass forming systems, then one could fix the value of the parameters describing the 'stretching' of the α loss peak and ascribe any changes in the width of the spectra to some secondary process. However, given the lack of consensus as to whether this behaviour is to be expected the most pragmatic approach to fitting the dielectric spectra obtained in this work is to fit the spectra without such assumptions. The quantification of the lack of TTS for this series will be shown in Section 4.2.3.

The physical explanation underlying the stretching of the exponential decay of the relaxation function in the time domain or the broadening of the dielectric loss peak in the frequency domain is a controversial issue, as was explained in Chapter 1. On the one hand one could hypothesize that the relaxation function is inherently non-exponential. On the other hand, one could consider the possibility of so-called dynamic heterogeneity, suggesting that a supercooled liquid contains many dynamic regions each of which relaxes with an exponential nature and with its own relaxation time. This would therefore lead to a distribution of timescales and could explain the observed broadening [44]. For example, the generalised Gaussian distribution function sometimes used to describe ε'' assumes a distribution of relaxation timescales in order to parametrise the α relaxation loss peak [98]. Thus, one interpretation of the variation in the shape of the α loss peak as shown in Figures 4.7a and b is that the distribution of relaxation timescales becomes narrower with increasing temperature above the glass transition.

Fit functions

The fit functions used to describe the dielectric spectra will now be introduced. Although a full explanation of the typical fit functions used to describe dielectric spectra is available in Chapter 2, these will be redefined here for clarity. As shown in Figures 4.4b-f, the dielectric spectra for the M = 3 - 7 samples feature three contributions to ε'': a peak corresponding to the α relaxation, an intermediate frequency contribution corresponding to a secondary β relaxation and a high frequency contribution. The loss peak relating to the α relaxation was fitted using both the Rikard Bergman (RB) [104] and Havriliak-Negami [110] (HN) functions. The two separate fits were performed in order to investigate the effect the chosen fitting approach has on the resulting fitting parameter behaviours and to provide a comparison between two different fitting routines. The RB function was chosen since it has the flexibility to account for the peak bluntness whereas the HN function was chosen as it is the most commonly used empirical fitting function in the analysis of α relaxation loss peaks in dielectric spectra [33, 61, 94, 96, 116, 117]. The RB function is defined as follows, with parameters

relating to the amplitude, ε'', peak frequency, ω_p and power-law exponents of the low, a, and high ,b, frequency flanks of the dielectric loss peak:

$$\varepsilon''(\omega) = \frac{\varepsilon''_p}{\frac{(1-C)}{a+b}\left(b\left(\frac{\omega}{\omega_p}\right)^{-a} + a\left(\frac{\omega}{\omega_p}\right)^{b}\right) + C} \tag{4.1}$$

The parameter C relates to the 'bluntness' of the resulting loss peak. The HN function provides description of the dielectric loss peak in ε'' with parameters relating to the timescale of the relaxation, τ_{HN}, dielectric strength, $\Delta\varepsilon$ and shape parameters relating to the symmetric (α) and anti-symmetric (β) stretching of the peak:

$$\varepsilon^*_{HN} = \varepsilon_\infty + \frac{\Delta\epsilon}{(1 + (i\omega\tau_{HN})^\alpha)^\beta} \tag{4.2}$$

The symmetric stretching parameter, α, is the exponent of the low frequency power-law flank of the a loss peak and the exponent of the high frequency power-law flank can be obtained by multiplying the symmetric and anti-symmetric stretching parameters: $\alpha\beta$. The secondary contributions were fit using the Cole-Cole (CC) expression [176] which is obtained by setting the β parameter to 1 in Equation 4.2. The high frequency contribution was fit with a power law of the form: $\varepsilon'' = A\omega^k$. A full description of the dielectric spectra, as shown in Figure 4.4, was achieved by using an additive combination of these three fitting contributions.

As described above, the $M = 2$ sample displayed in Figure 4.4a) did not show the same contributions to the dielectric spectra as the other samples. Instead, a variation in the exponent of the high frequency power law of the α loss peak was observed indicating a so-called excess-wing. The α loss peak was again described using two different fitting approaches in order to facilitate comparison. In the first, a modified version of the RB function was used, which is fully described in Chapter 2. In order to construct this modification, it was assumed that the excess-wing was due to an underlying β relaxation and that the contributions to the spectra would follow the Williams-Watts ansatz [115] which is based on a convolution of the relaxation contributions in frequency space. The functional

form of the modified RB function is as follows [18]:

$$\varepsilon''(\omega) = \frac{\varepsilon''_p}{\frac{(1-C)}{a+b}\left(b(\frac{\omega}{\omega_p})^{-a} + a(\frac{\omega}{\omega_p})^{b}\right) + C} + \frac{\varepsilon''_{wing}}{\frac{(1-C_{eff})}{a+g}\left(g\left(\frac{\omega}{\omega_p}\right)^{-a} + a\left(\frac{\omega}{\omega_p}\right)^{g}\right) + C_{eff}} \tag{4.3}$$

The first component of this equation is identical to the 'unmodified' RB function given in Equation 4.1. The second component describes the contribution of the 'effective' β relaxation (see Chapter 2). The g parameter is the exponent of the power law describing the excess-wing and ε''_{wing} describes its amplitude.C_{eff} parametrises the bluntness of the 'effective' β relaxation (see Chapter 2).

For comparison the $M = 2$ sample was also fit with an additive combination of Havriliak-Negami (HN) functions [110] to describe both the α and underlying 'effective' β contributions. In this combination, the parameter corresponding to the exponent of the low frequency power-law flank, α, was set to the same value for each HN function in order to mimic the behaviour of a mathematical convolution of the two formulae in frequency.

In order to provide a more complete picture of the variation of the fitting parameters across the series, fitting parameters for the data obtained from the literature for toluene are also discussed and included in the plots. In Ref.[55], the toluene spectra were fit under the assumption of the Williams and Watts ansatz [60]. A generalised gamma (G_{GG}) distribution of timescales [98] was used to fit the α relaxation loss peak in which the parameter corresponding to the exponent of the low frequency flank was fixed to 1 and another G_{GG} distribution was used to fit the observed β loss peak. In Ref.[33], the data shown were fit by first rescaling the dielectric spectra onto a single master curve. The master curve was then fitted using the HN function as well as the CD function for comparison. The authors found that the HN fit provided a better interpolation of the data and for this reason the fit parameters quoted for the fit of the HN function will be used in this section in order to compare to the fit data presented for the other alkylbenzene samples.

4.2.4 Fit parameters

The following sections will detail the development of the fitting parameters from the two functional descriptions of the α loss peak constructed using the RB and HN functions.

Low frequency flank.

In this section, the fit parameters describing the exponent of the low frequency power-law flank will be discussed. The α loss peaks for the M = 3 - 7 samples were first fit using the RB function. Initially, the fits of Equation 4.1 were conducted with no constraints on the five fitting parameters. In these initial fits, the parameter relating to the exponent of the low frequency power-law flank of the α relaxation, a, showed very little variation in comparison to the other parameters and the spectra could generally be described well by setting $a = 1$. Indeed, many of the functional descriptions of the α loss peak including the CD function [109], the G_{GG} distribution [98], the KWW function [41, 42] are all based on the assumption that the low frequency flank of the α relaxation loss peak should have an ω^1 dependence. In subsequent fits, the value of a was fixed to 1 in order to enable a more constructive analysis of the variation of the other parameters.

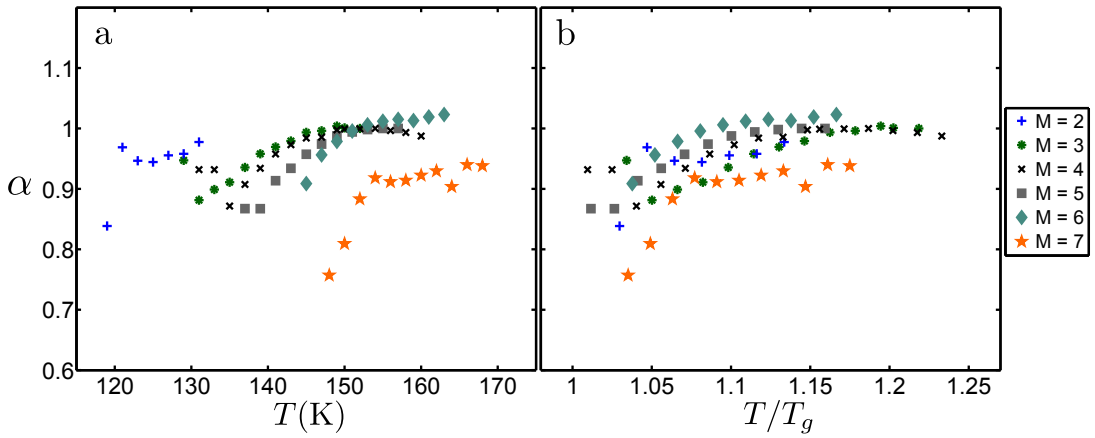

Figure 4.8: α parameters obtained through fits of the HN function to the dielectric spectra plotted against a) T and b)T_g/T.

The α parameter in a fit of the HN function is the exponent of the power law that describes the low frequency flank of a relaxation peak in ε'' [94]. In a loga-

rithmic plot, α becomes the gradient of the low frequency flank and is therefore comparable to the a parameter in Equation 4.1. The values for the α parameter are shown in Figure 4.8. In contrast to the behaviour of a for the alkylbenzene series, the α parameter is significantly lower than a Debye-like value of 1 at low temperatures, but increases towards 1 with increasing temperature. This behaviour demonstrates the narrowing of the α relaxation peak with increasing temperature. It also exemplifies the difference between the two functional descriptions of the α loss peak as the HN function does not take into account the bluntness of the peak. Therefore, the bluntness has to be approximated by the use of a combination of the α and β parameters in Equation 4.2.

The similar behaviour observed for the variation of the α parameter with temperature is emphasised through the T_g rescaling shown in Figure 4.8. Although the variation of the α parameter is similar for the samples in this series there is no discernible trend with increasing molecular weight. However the fact that the a parameter can be set to 1 and that the α parameter tends to 1 as temperature is increased is consistent with the increased bluntness observed for lower temperatures using the RB-expression and is consistent with the gradient of the low frequency flank reported in the literature for low molecular weight glass formers [96].

Bluntness

The bluntness of the α loss peaks will now be addressed and this is parametrised by the C parameter in the RB function. Values of C with temperature for the series are shown in Figure 4.9a. The values decrease from a non-zero value close to T_g to a value of 0 as temperature is increased indicating a narrowing of the response peaks. This is in contrast to previous fitting of dielectric data for a selection of dimethyl ethers, monomethyl ethers and glycols using the RB function in which the C parameter was invariant with temperature for a given sample [18]. The T_g scaled plot shown in Figure 4.9a demonstrate that the decrease of C takes place in a similar manner for all samples at temperatures above T_g. In order to confirm this behaviour, a number of spectra (in which the C parameter was non-zero) for the $M = 3$ sample were refitted with the C parameter locked to 0 and

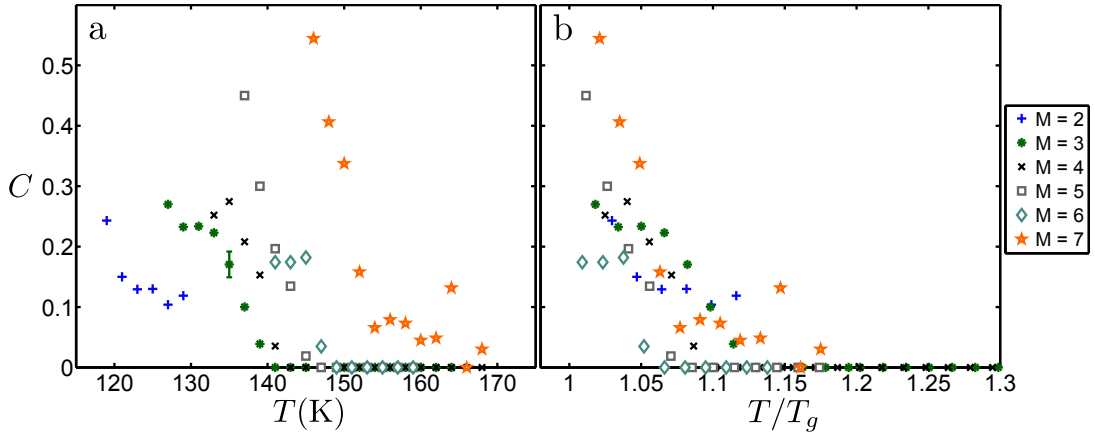

Figure 4.9: C parameters obtained through fits of the RB function (modified for the $M = 2$ sample) to the dielectric spectra plotted against a) T and b) T_g/T.

the a parameter left free instead. In this case, the spectra could not be well described. The spectra were then fitted with all parameters set to vary freely. In this case, the a parameter always tended to a value of 1 whereas the C parameter demonstrated the variation shown in Figure 4.9a. This suggests that in order to provide a full description of the spectra, the varying bluntness of the α loss peak requires consideration.

The HN function does not contain a parameter relating to the bluntness of the peak itself, unlike Equation 4.1 in which the bluntness is described by the C parameter. It therefore follows that in order to fit an α relaxation peak with Equation 4.2, the bluntness must be fit through variations of the α and β parameters describing anti-symmetric and symmetric stretching of the peak. The variation of the low frequency power-law exponent, α, from the HN function shown in Figure 4.8 can therefore be explained by the narrowing of the α relaxation peak with increasing temperature: at temperatures close to T_g where the peak is broadest, a lower value of the gradient of the low frequency flank is required to successfully describe the shape of the peak.

The indication of these fits is that, for these low molecular weight glass forming liquids, a range of α relaxation loss peaks over a range of temperatures cannot be described by a function with a single shape parameter such as the Cole-Davidson equation [109] and this is consistent with what has been reported previously

[94]. Havriliak *et. al.* demonstrated for 1000 sets of unbiased relaxation data that both the α and β parameters in the HN function are required in order to fit the spectra over an appreciable frequency range [111]. Furthermore it seems that the variation in shape of the loss peak, for this series, is almost entirely dependent on the bluntness and high frequency flank of the peak. We note that the variation in bluntness or α parameter respectively might indicate the presence of some additional underlying relaxation contributions which starts to affect the spectral shape at the lower temperatures. As will be discussed in more detail later on, we indeed find also other evidence supporting the the existence of an extra contribution. Note however that it does not make sense to introduce any extra relaxation contributions in the fitting procedure since the three introduced contributions describe the data well and adding further contributions would only introduce more fitting parameters without adding anything to the understanding.

High frequency flank.

In this section the exponent of the high frequency power-law of the α loss peak will be discussed. In the RB function, this exponent is set by the b parameter in Equation 4.1. The b parameters obtained through fits of the dielectric spectra for the different samples are shown in Figure 4.10a and shows an increase with increasing temperature. To further analyse the temperature dependence of the b parameter, the values were rescaled by T_g as shown in Figure 4.10b. The indication from this figure is that the b parameters show a similar temperature dependence for the $M = 1$ (from Ref. [98]), 2, 3, 4, 5 and 6 samples. The b parameter for the $M = 7$ sample appears to show slightly different behaviour as it is largely invariant with increasing temperature. The horizontal dashed red line in Figures 4.10a and b is indicates the value for the exponent of the high frequency flank obtained from Ref. [33].

The high frequency power-law exponent of the α relaxation is the product of the α and β parameters in the HN function. Values of $\alpha\beta$ are shown in Figure 4.11 and the trends of this parameter with increasing temperature are generally similar to the trends observed in the b parameter, as is to be expected. Again,

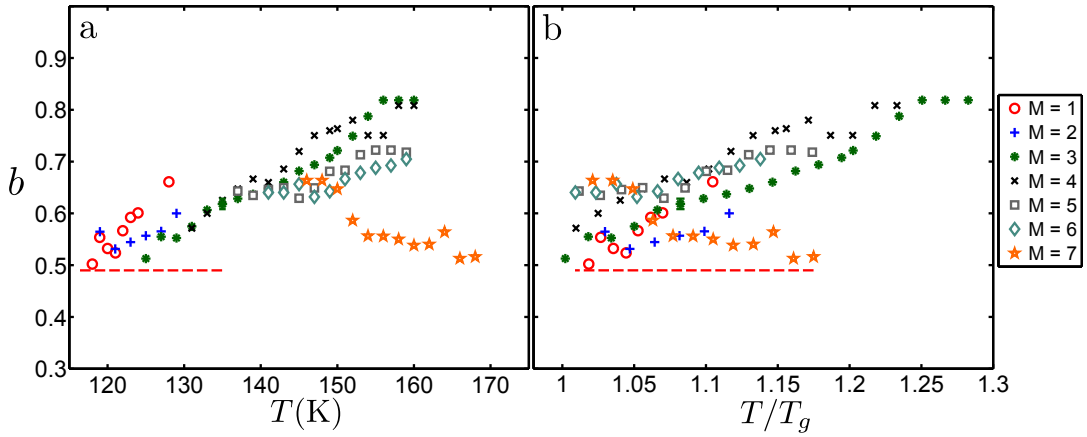

Figure 4.10: b parameters obtained through fits the RB function to the dielectric spectra plotted against a) T and b) T_g/T. Also shown are the fit parameters obtained from the literature for toluene, where the red circles denote data from [98] and the red dashed line denotes data from [33].

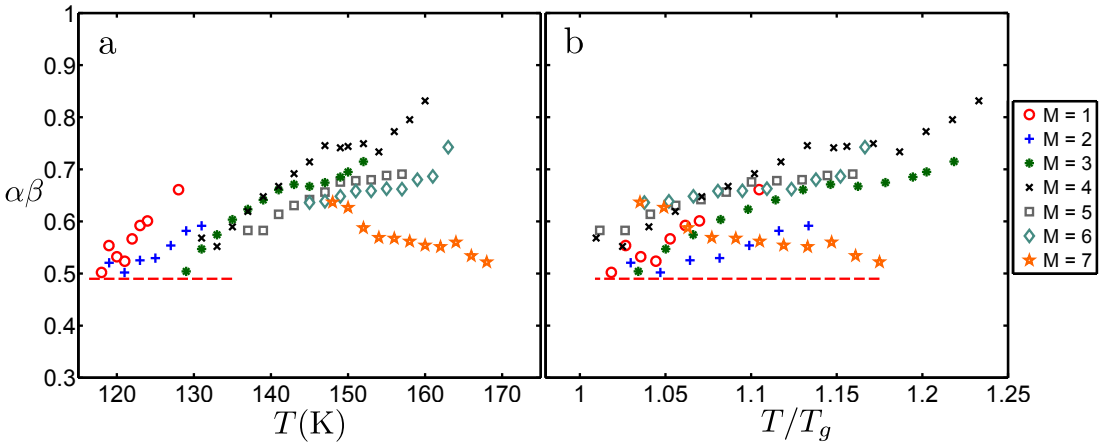

Figure 4.11: $\alpha\beta$ parameters obtained through fits of the HN function to the dielectric spectra plotted against a) T and b) T_g/T. Also shown are the fit parameters obtained from the literature for toluene, where the red circles denote data from Ref.[98] and the red dashed line denotes data from Ref. [33].

literature data for the high frequency flank exponent for the $M = 1$ sample are shown in a similar manner to Figure 4.10.

Although these two separate descriptions of the high frequency power-law exponent show the same temperature dependence, there is no particular trend with molecular weight. The sample M = 3 to 6 demonstrate a very similar variation of the high frequency flank as is shown very clearly in the rescaling of the parameters by T_g. The $M = 7$ sample shows a much less pronounced trend than the other samples however, suggesting that the exponent is almost invariant with increasing temperature.

The fitting results for the M = 2-7 samples agree well with the literature results for toluene from Ref.[98] (see the data points marked in red circles). In Ref.[33], the authors obtained a single value of the exponent by assuming TTS and rescaling the obtained spectra on top of eachother to create a master curve; the resulting master curve was fit with the HN function. The value for the high frequency exponent falls below the values obtained for the other samples, but appears consistent near the glass transition temperature. Moreover, in the analysis of Ref.[33], spectra were cut at a frequency of 100Hz, meaning that for higher temperatures, a significant proportion of the α loss peak was cut before the rescaled master curve was produced. The lower value obtained for the exponent therefore makes sense as the fitting of the HN function to these rescaled spectra would be largely dependent on the spectra at lower temperatures, presumably (given the temperature dependence of the b parameters for the other samples shown) with lower values of the high frequency exponent.

For the M = 1-7 samples we obtain a monotonic increase of the high frequency exponent with increasing temperature and α loss peak becomes narrower with increasing temperature as quantified by the C, b and $\alpha\beta$ parameters. This behaviour is a common feature of glass forming systems [13, 68]. One can conceptualise this as a narrowing of the distribution of time-scales as the sample temperature increases away from T_g; this would imply that the degree of dynamic heterogeneity decreases with increasing temperature which is a well known observed trend [21, 44]. Also, Ngai's coupling model links the increase of the KWW stretching parameter, β, to the level of cooperative motions involved in

the α relaxation, where a lower value of β indicates a greater degree of cooperativity [83]. With regards to this model, the results presented in Figures 4.10 and 4.11 indicate that the degree of cooperativity decreases with increasing temperature for the samples in this series, which is indeed expected since less cooperative motions are needed for motions to take place at higher temperatures. The high frequency power-law exponent of the α loss peak has also been shown to be correlated to the dynamic fragility parameter, m [11]. It has been found that for a range of glass formers a lower value of the exponent corresponds to a high value of m. In the latter sections of this chapter, results of m will be presented that indicate an increase of the fragility with increasing alkyl tail-length (Section 4.2.7). We will also demonstrate that this holds also for a thermodynamic fragility metric (Sections 4.4.2 and 4.4.3). Interestingly, since we do not observe a clear trend in either the b or $\alpha\beta$ parameters with increasing alkyl tail-length, we do not find support for this correlation for the glass-formers investigated here.

In some systems, it is observed that, close to T_g, the stretching of the α loss peak is temperature independent, implying that TTS should hold at these temperatures. Olsen *et. al.* show that for a number of liquids that show TTS, a high frequency power-law exponent of ~ 0.5 is expected [174]. Indeed, it is clear from Figures 4.10b and 4.11b that the exponents obtained through fits of the HN and RB functions decrease to a value of 0.5. Furthermore, the stretching exponent for toluene obtained from Ref.[33] (in which TTS was assumed over the measured temperature range) is very close to a value of 0.5. Similar behaviour is also observed for the $M = 7$ sample. However the increase of the exponent of the high frequency power-law of the α loss peak for the other samples shown extends across the whole temperature range.

Furthermore, above the critical temperature T_c , ideal mode-coupling theory (MCT) predicts that the value of the high frequency exponent of the relaxation function should 'level off' at a fixed value (less than 1) and and example of the quantification of this has been observed for glycerol and propylene carbonate [93]. However, other measurements of the same samples have yielded high frequency flank parameters which increase consistently towards a value of unity [177]. This has also been shown for a wide range of glass forming liquids by Wang *et. al.* [178] and light scattering measurements of another small molecule glass-former, salol,

yield a consistently increasing 'width' of the relaxation function with increasing temperature [179]. There is some slight indication of the levelling off of the gradient of the high frequency flank in both representations shown in Figures 4.10 and 4.11 for the $M = 3$ to 6 samples but the data are not conclusive in this regard.

Dielectric strength

The dielectric strength, $\Delta\varepsilon$, of the α relaxation will now be considered. In Chapter 2 it was shown that $\Delta\varepsilon$ corresponds to the area underneath a loss peak in ε''. The first determination of $\Delta\varepsilon$ was performed by numerical integration of the fits of RB function in ε'', parametrised using the a, b and C parameters described in the previous sections and the amplitude, ε'', and peak frequencies, ω_p, which will be considered in later sections. This integral has the following form [18, 180]:

$$\Delta\varepsilon = \frac{2}{\pi}\int_0^\infty \varepsilon''(\omega)\frac{\mathrm{d}f}{f} \tag{4.4}$$

Values of $\Delta\varepsilon$ obtained from numerical integration are shown in Figure 4.12a. The values decrease with increasing temperature for all samples. In order to further analyse their development, the values were also rescaled by T_g as shown in Figure 4.12b. It is clear from this figure that the temperature dependence of $\Delta\varepsilon$ is similar for the $M = 2$, 3, 4, 5 and 6 samples. Also shown are dielectric strength values obtained from Ref. [55] for the $M = 1$ sample. The dielectric strength for the $M = 1$ sample appears to have a stronger temperature dependence than that of the other samples. Another feature of Figure 4.12b is the systematic decrease of $\Delta\varepsilon$ with increasing alkyl tail-length for the $M = 3$, 4, 5 and 6 samples. However, the values for the $M = 1$, 2, and 7 samples do not follow this trend.

The observed approximate $1/T$ behaviour of the dielectric strength is consistent with the Kirkwood-Frölich generalisation of the Onsager relation between $\Delta\varepsilon$ and the dipole moment, μ [94, 96, 100–103]:

$$\Delta\varepsilon = \frac{\varepsilon_s(\varepsilon_\infty + 2)^2}{(2\varepsilon_s + \varepsilon_\infty)}\frac{\rho N_A}{9k_B T\varepsilon_0 M_w}g_K\mu^2 \tag{4.5}$$

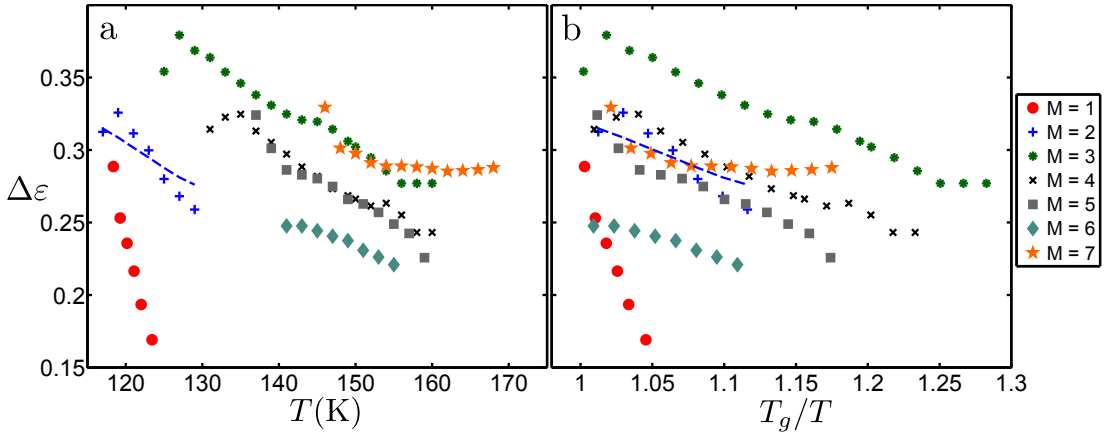

Figure 4.12: $\Delta\varepsilon$ parameters obtained from integration of the fits of the RB function to the dielectric spectra plotted against a) T and b) T/T_g. The dashed blue line indicates a fit of the Onsager equation (Equation 4.5) to the $M = 2$ data.

Where ρ is the density of the material, N_A is Avogadro's number, ϵ_0 is the permittivity of free space and M_w is the molecular weight. ε_s and ε_∞ are the limiting values of ε' at low and high frequency respectively (where $\Delta\varepsilon = \varepsilon_s - \varepsilon_\infty$) [94]. g_K is the so-called Kirkwood/Frölich correlation factor. In a system containing non-interacting dipoles, g_K would be equal to 1. In other systems, g_K can become greater or less than 1 depending on whether the dipoles align parallel or anti-parallel to each other [94, 96].

In order to test how well the $\Delta\varepsilon$ data conformed to the Onsager description of dielectric strength, Equation 4.5 was tested using the $M = 2$ sample as an example. A dipole moment of 0.59D was obtained from the literature [181]. The temperature dependent density for this sample was also obtained from the literature between 273 and 178K [182]. In order to evaluate the density in the same temperature region as the measurement of the $M = 2$ sample, the density values were extrapolated with a linear fit. Values of ε_s and ε_∞ were determined from the real part of the dielectric spectra, ε' (a figure depicting how these values can be obtained from ε' has been shown in Chapter 2). The dashed blue lines in Figures 4.12a and b are the resulting values obtained from Equation 4.5. The $\Delta\varepsilon$ data are reasonably well described by this interpretation of the dielectric strength. A g_K value of 0.3 was used to scale the behaviour to the correct magnitude in $\Delta\varepsilon$, suggesting anti-parallel alignment of the dipoles within the sample. However, it

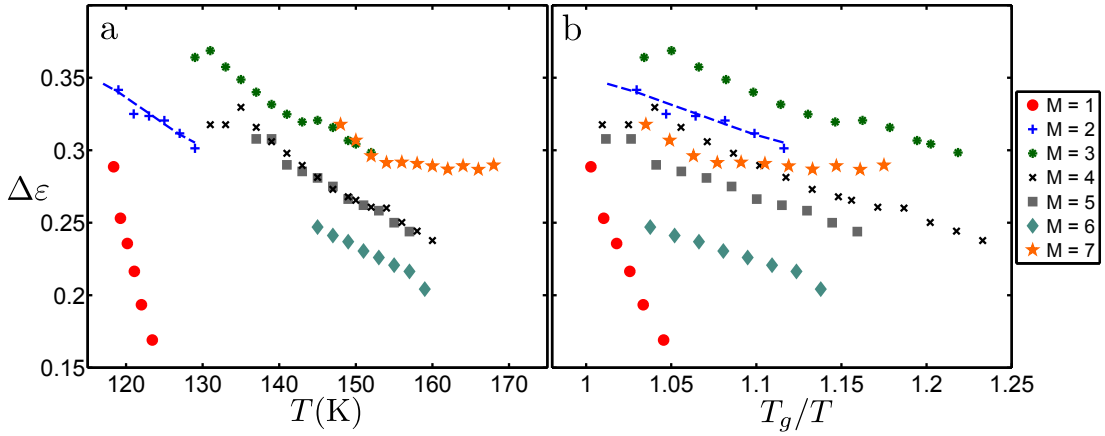

Figure 4.13: $\Delta\varepsilon$ parameters obtained from fits of the HN function to the dielectric spectra plotted against a) T and b) T/T_g. The dashed blue line indicates a fit of the Onsager equation (Equation 4.5) to the $M = 2$ data.

is not clear that the density of the $M = 2$ sample would scale linearly to this temperature range and therefore this could have lead to an incorrect determination of g_K. For example, if the density in this temperature range was significantly higher than predicted, a g_K value closer to 1 would be expected. The general conclusion that the dielectric strength can be reasonably well described using the Kirkwood-Frölich generalisation of the Onsager relation is clear.

Values of $\Delta\varepsilon$ were also determined through fitting of the HN function to the dielectric spectra, as $\Delta\varepsilon$ is one of the fitting parameters. These values are shown in Figure 4.13 and show a very similar temperature dependence to the values obtained through numerical integration of the fits of the RB function to the dielectric spectra. The only noticeable difference between these two interpretations of the dielectric strength is in the determined values for the $M = 2$ sample, which are better approximated by the generalised Onsager equation in Figures 4.13a and b.

Amplitude

Although one usually considers the dielectric strength as a means to analyse the 'size' of a dielectric loss peak, another quantification of the size can be gained from the amplitude of the peaks, ε''_p. This parameter is advantageous in some

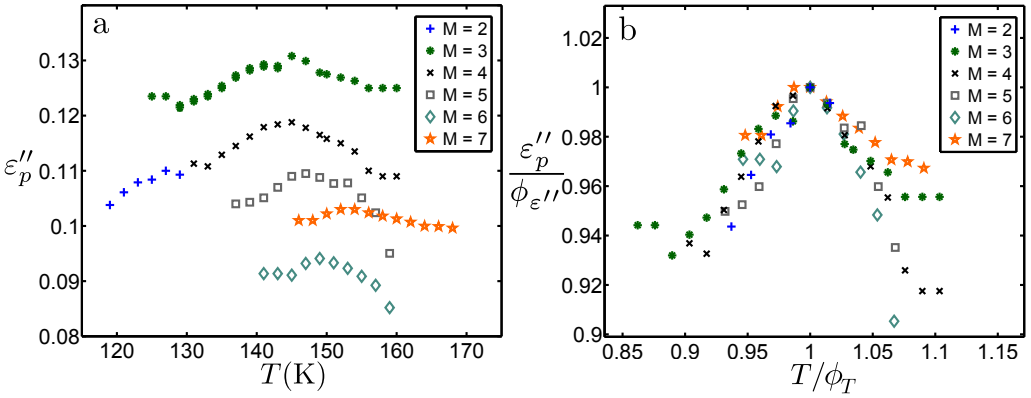

Figure 4.14: a) Amplitude, ϵ''_p, parameters obtained through fits of the RB function to the dielectric spectra. b) Amplitude parameters rescaled by the peak in the values, $\phi_{\varepsilon''}$ and the temperature at which this occurs, ϕ_T.

respects as it can be directly 'read off' from the dielectric spectra without recourse to integration or fitting and it is more sensitive to subtle variations in the temperature dependence of the loss peak. Figure 4.14a shows the variation of ε''_p, with temperature. In general, this parameter indicates a decrease in the amplitude of the α relaxation with increasing alkyl tail-length for the $M = 3$, 4, 5 and 6 samples. The $M = 2$ and 7 samples do not conform to this trend but the values show a similar temperature dependence to the others in the series. The most striking feature of this figure is that there appears to be a maximum in the amplitude at some intermediary temperature above T_g. This could be indicative of the merging between the α relaxation and some underlying secondary relaxation. The idea of an underlying largely 'hidden' secondary relaxation is discussed further in Section 4.3.7. The amplitude values are also displayed in a rescaled manner where both the amplitude and the temperature scaling factors, $\phi_{\varepsilon''}$ and ϕ_T, are introduced in Figure 4.14b. This scaling figure is used to approximately determine the temperatures at which the peak in the amplitudes are observed. See Section 4.3.7 for a more detailed discussion about these results.

4.2.5 Relaxation timescales

In the following section, the timescales corresponding to the peak position of the α loss peak will be discussed. So far, we have observed that the two fitting ap-

proaches used to describe the α relaxation loss peak give very similar values for the parameters used to describe the shape of the loss peaks. Only small differences were observed, such as the variation of the exponent of the low frequency flank and these were easy to conceptualise based on the differences in the fit function parametrisation. In order to quantify the similarities between the separate functional descriptions of the α loss peak, the peak timescales, obtained from each fitting routine were compared. The peak timescales can be directly acquired through fits of the RB function. However, the characteristic timescale obtained thorough fits of the HN function, τ_{HN}, must be transformed as a function of the α and β parameters in order to gain the peak timescale. This transformation is performed in the following way:

$$\omega_p = \frac{1}{\tau_{HN}^p} = \frac{1}{\tau_{HN}} \left[sin\left(\frac{\alpha\pi}{2+2\beta}\right)\right]^{\frac{1}{\alpha}} \left[sin\left(\frac{\alpha\beta\pi}{2+2\beta}\right)\right]^{-\frac{1}{\alpha}} \tag{4.6}$$

Values for the peak timescales obtained from both the RB and HN fit functions, τ_{RB} and τ_{HN}^p, are shown in Figure 4.15. These values are in excellent agreement with one another. The characteristic timescale for the HN function, τ_{HN}, are also shown as a point of comparison but are also very similar to τ_{RB} in this scaling. We note that sometimes the average relaxation times are determined instead of the time-scales corresponding to the maximum of the loss peak. However, we choose here to consistently use the peak timescales since the determination of the average relaxation times depends on the full shape of the peak and the sensitivity of the shape parameters to the used fitting function and additional relaxation contributions makes the average relaxation times more difficult to determine with a similar accuracy as the peak timescales.

Figure 4.15 together with the previous discussion of the variation of the shape parameters demonstrate that choosing empirical fitting approaches which include four free fitting parameters enable the full shape of the α relaxation loss peaks to be described well. Indeed, it has been stated previously that one can not fit the α loss peak over an appreciable frequency range with a function with less than four free parameters [94, 96, 104, 111]. The figure also shows that almost identical values of the peak timescale can be obtained from two separate fitting approaches.

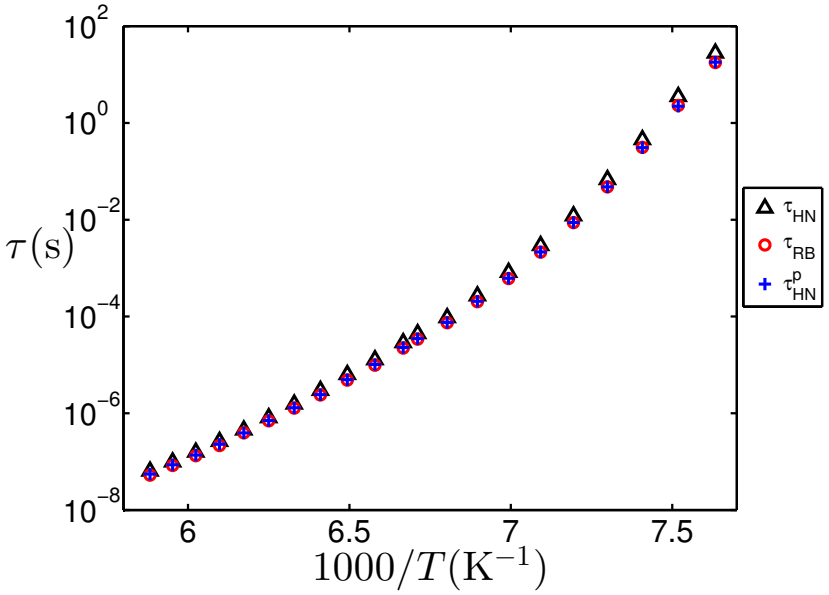

Figure 4.15: Figure showing the timescales for the α relaxation obtained from fits of the dielectric loss peak of the $M = 4$ sample with both the RB and HN functions. It is clear from this figure that both fit functions yield the same timescales.

The relaxation timescales, τ_α, obtained through fitting of the dielectric loss peaks corresponding to the α relaxations for the alkylbenzene series are shown in Figure 4.16. Data for τ_α shown for toluene ($M = 1$) were taken from Refs.[55] and [33]. Also shown is the T_g for benzene ($M = 0$) obtained from a DSC study in the literature [183] involving the confinement of benzene within a microemulsion in order to suppress crystallisation. The τ_α data move systematically to higher temperatures with increasing alkyl tail-length indicating an increase of the glass transition temperature. However, it appears the T_g values for the $M = 0$ sample does not follow this trend. This will be discussed further in Section 4.2.6. The horizontal dashed line in Figure 4.16 denotes $\tau_\alpha = 100$s, the point at which T_g is often defined [2].

One of the fundamental characteristics of τ_α for glass forming materials is that there is often a dramatic increase of τ_α as the glass transition is approached [2, 13]. This is clearly observed for the τ_α data shown in Figure 4.16. In many cases, τ_α data are well described by the empirically derived Vogel-Fulcher-Tammann (VFT)

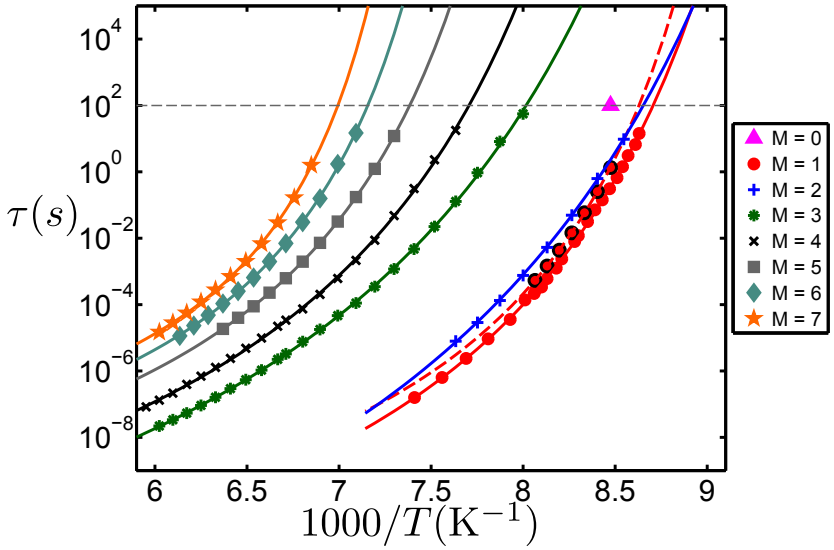

Figure 4.16: τ_α data for the alkylbenzene series, obtained through fits of the RB function to the dielectric spectra. Plot includes data from literature [33, 55] for toluene ($M = 1$) and the T_g value for benzene ($M = 0$) [183]. Solid lines indicate fits of the VFT equation to the data.

equation [27–29] as introduced in Chapter 1.

$$\tau_\alpha = \tau_0 e^{\frac{DT_0}{T-T_0}} \tag{4.7}$$

T_0 refers to the temperature at which τ tends to infinity, τ_0 is the limiting timescale at high temperatures and D is the so-called strength parameter. The solid lines result from fitting of the τ_α data in Figure 4.16 to the VFT function; it is clear that the data can be well described using such a description. The resulting fit parameters are shown in Table 4.2. The values of T_0 increase systematically with increasing alkyl tail-length for the $M = 2$ to 7 samples but appear to be higher for the two descriptions of the $M = 1$ sample. The values for τ_0 adhere to values close to typical microscopic timescales at high temperatures [2, 24–26] for the $M = 1$, 2, 3, and 4 samples but are higher than the typical range (10^{-12} to 10^{14}) for the $M = 5$, 6 and 7 samples and lower for the $M = 2$ sample. Also shown are the determined values for T_g and the fragility parameter, m. These parameters will be discussed in full in the following sections.

M	$log_{10}\tau_0(s)$	D	$T_0(K)$	$T_g(K)$	m	References
0				118 ± 5		[183]
				131		[184]
1	$-(14.8 \pm 0.3)$	7.3 ± 0.4	96.6 ± 0.6	115		[184]
				117		[78]
	$-(12.8 \pm 0.4)$	5.0 ± 0.3	$101.2 \pm (0.6)$	114.9	105.6	[33]
				115.9	116.8	[55]
				117.5		[185]
				113		[186]
2	$-(17.1 \pm 0.5)$	12.7 ± 0.9	90 ± 1	113		[184]
				115		[78]
				115.6	85.2	
				111		[186]
				115.7		[187]
3	$-(14.5 \pm 0.2)$	11.6 ± 0.4	95.6 ± 0.7	122	69	[188]
				124.7	70.7	
				122		[186]
				122.5		[187]
4	$-(13.1 \pm 0.2)$	8.5 ± 0.3	104.3 ± 0.6	125		[186]
				129.8	76.9	
				129.6		[187]
				127.5		[184]
5	$-(11.5 \pm 0.1)$	5.9 ± 0.1	113.9 ± 0.2	128		[186]
				135.4	84.5	
				135.7		[187]
6	$-(10.4 \pm 0.3)$	4.4 ± 0.3	121.2 ± 0.9	137		[186]
				139.7	93.7	
				140.4		[187]
7	$-(9.5 \pm 0.2)$	3.3 ± 0.2	127.0 ± 0.6	143.0	102.9	

Table 4.2: Fit parameters from the VFT fit of the τ_α data as well as T_g and the fragility parameter, m. The reported errors were obtained from a least mean squares fit of Equation 4.7 to the τ_α data.

4.2.6 Glass transition temperature

The horizontal dashed grey line in Figure 4.16a marks a time-scale of 100s, which corresponds to the time-scale for which the glass transition temperature, T_g, is normally defined; thus, the temperatures at which the VFT fits cross this line indicate T_g for the different samples. This timescale is commonly used to define the point at which the dynamics of a supercooled liquid become slower than experimentally attainable timescales [189]. The values extracted from this analysis are shown in Figure 4.17a in comparison with values obtained through analysis of the DSC traces obtained for the series (as described in Section 4.4.1) and values for the $M = 1$ [33, 55] and $M = 0$ [183] obtained from the literature .

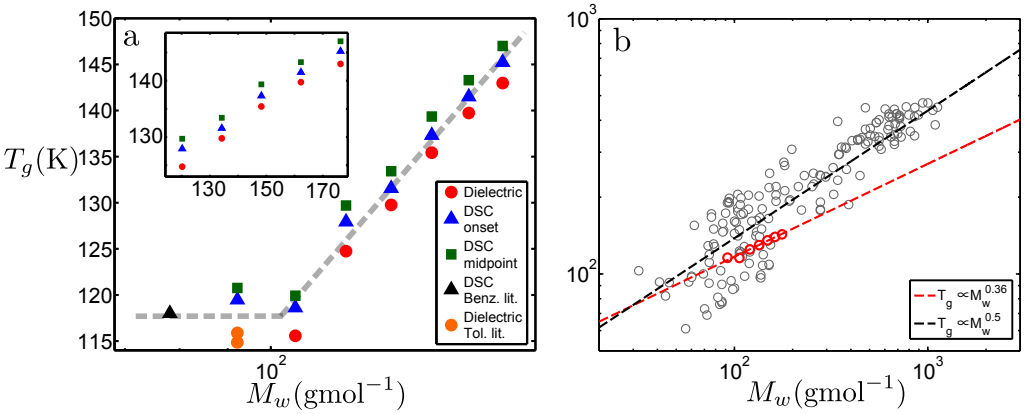

Figure 4.17: a) T_g values obtained through VFT fits of the τ_α data in comparison with values obtained through analysis of the DSC traces (both midpoint and onset as described in Chapter 3). Also shown are T_g values for the $M = 0$ [183] and $M = 1$ [33, 55] samples obtained from the literature b)T_g values for a variety of molecular glass formers in comparison to the T_g values obtained for the $M = 2$ to 7 samples shown in a). Also shown are fit lines based on the power-law relationship $T_g \propto M_w^a$ postulated by Novikov *et. al.* [146].

For samples with alkyl tails longer than 2 units (i.e. $M = 3$ to 7) T_g increases systematically with increasing molecular weight. Figure 4.17a shows the data in a semilogarithmic representation on which the behaviour for $M > 2$ can be well described by an exponential behaviour as represented by the dashed guide to the eye. The inset shows the behaviour for the $M > 2$ samples also in a linear plot. This indicates a weak bending over of the T_g values towards higher molecular

weight indicating that the relationship might be better described using a non-linear relationship. For the shortest tail-length samples with $M \leq 2$ data appears to show a limiting tail-length below which the glass transition temperatures no longer decrease. The observed trends are indicated by the dashed guides to the eye in Figure 4.17a.

A relationship between T_g and molecular weight of the form $T_g \propto M_w^{\alpha}$ was observed by Novikov *et. al.* [146] for a range of molecular glass-forming liquids as described in Section 4.1. Figure 4.17b shows T_g values obtained for this range of liquids in comparison with the T_g values obtained for the $M = 2$ to 7 samples from VFT fits of the τ_α data. The dashed black line indicates a fit of the literature data using the quoted value of $\alpha = 0.5$. The red dashed line indicates a similar fit of the T_g data obtained for the $M = 2$ to 7 samples. This fit demonstrates that the obtained T_g values could be described by a similar relationship, with an exponent $\alpha = 0.36$.

Larsen *et. al.* [150] present a relationship between T_g and the effective hard-sphere radius, σ_0, of constituent molecules in a glass forming system. This implies, from the results shown in Figure 4.17a, that σ_0 increases for samples with an alkyl tail-length of 2 units or more. A further implication of this is that the effective size of the $M = 0$, 1 and 2 samples are similar, as T_g no longer demonstrates a linear increase with increasing molecular weight for these samples. Interestingly a similar molecular weight dependence of T_g has been observed for short-chain polymeric samples as will be shown in Chapters 6 and 7.

4.2.7 Fragility

We have observed that the development of the τ_α values is in general non-Arrhenius. To describe this variation in the temperature dependence of the alpha relaxation time and the deviation from Arrhenius behaviour, the concept of 'fragility' is introduced, as was described in detail in Chapter 1. The key concept of fragility of glass forming materials will be reiterated here to aid the discussion. Strong glass formers are defined as having a near Arrhenius dependence of the structural relaxation timescale and fragile glass formers show the most significant departure from Arrhenius-like behaviour. The fragility of glass

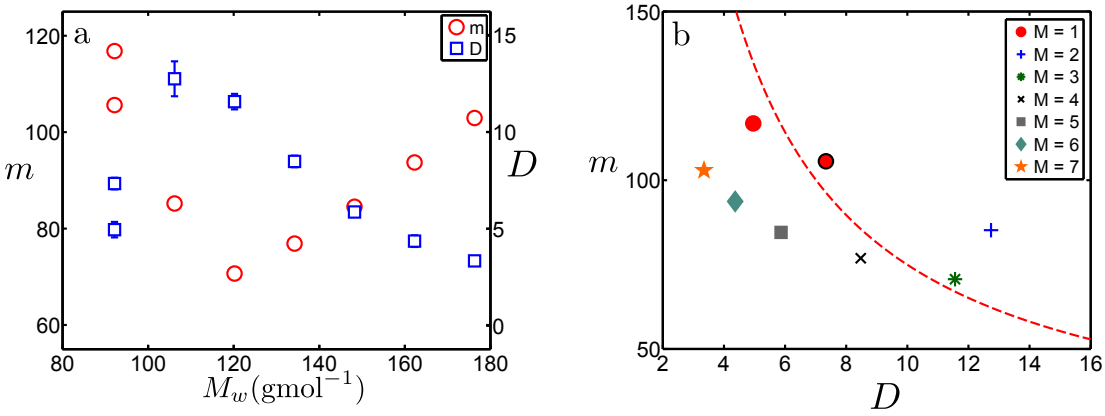

Figure 4.18: a) Comparison between the D and m parameters obtained through fitting of the VFT function to the τ_α data. b) Plot of m versus D in order to test the relationship proposed by Böhmer *et. al.* [11]. The dashed red line indicates a parametrisation of Equation 4.9.

formers can be parametrised by the fragility index m, which gives the gradient at T_g of the temperature dependent α relaxation time scale in an Arrhenius plot [2, 11, 13, 190, 191]:

$$m = \left.\frac{\mathrm{d}(log\tau_\alpha)}{\mathrm{d}(\frac{T_g}{T})}\right|_{T=T_g} \tag{4.8}$$

The fragility parameter or 'steepness index', m and the strength parameter in the VFT equation, D, both quantitatively describe the departure of the behaviour of τ_α from an Arrhenius description. The values for both the D and m parameters are displayed in Figure 4.18a. The m parameters show a linear molecular weight dependence for the $M = 3$ to 7 samples. However, this trend does not hold for the $M = 1$ and $M = 2$ samples, which display higher values of m. This could be indicative of some fundamental change in the dynamics of the alkylbenzene series beyond a tail length of 2 carbon atoms as was observed from the variation of the T_g values. Correspondingly, the D parameters show a decrease with increasing molecular weight for the $M = 2$ to 7 samples.

Generally, for the higher tail length samples, the D and m parameters appear to be inversely proportional to each other. This is not surprising since given that the α relaxation follows a VFT behaviour one can calculate an expression for the

fragility index m based on its definition and derive the following expression for m as a function of D[11],

$$m = m_{min} + \frac{m_{min}^2 ln(10)}{D} \tag{4.9}$$

Here, m_{min} is the lower limit of the fragility which would occur for a completely Arrhenius process, where $m_{min} \approx 16$ (if $\tau_0 = 10^{-14}$s is assumed) [2, 11]. In order to test this relationship, a plot of m versus D was made as shown in Figure 4.18b. The overall trend is captured, but it appears the dependence of m with D is far weaker than predicted by Equation 4.9. Note that the simple relationship assumes that the microscopic time-scale τ_0 is fixed at a certain value which is not generally true and is only an approximation. Also, a general problem with using D as a fragility metric is that it is a fitting parameter in the VFT expression and as such is correlated to the values of the other two VFT fitting parameters, τ_0 and T_0, which generally doesn't make it ideal as a fragility metric. However, it does to some extent parametrise the relaxation behaviour of the timescale of the structural relaxation over the full temperature regime, if the τ_α data can be described by the VFT function. On the other hand, the m parameter only considers the gradient at a specific point in temperature, T_g [192] which can be both be an obvious weakness even though the strength is that as the gradient at one particular temperature it is largely model independent and can be determined directly from the raw data if these are available near T_g.

4.2.8 Linearisation of the timescale Values.

An alternative and sometimes powerful method used in order to analyse the rate of increase of the structural relaxation timescale with decreasing temperature is is to plot the data in such a manner that if the data follows a VFT behaviour it automatically results in a straight line. Such a linearisation of a VFT behaviour is often called a Stickel analysis [31]. To linearise a VFT behaviour, the quantity Z is determined by taking the temperature derivative of the timescale data in the

following manner:

$$Z = \left(\frac{dlog\tau_\alpha}{d(\frac{1}{T})}\right)^{-\frac{1}{2}} = \left(\frac{loge^1 DT_0}{(\frac{T_0}{T}-1)^2}\right)^{-\frac{1}{2}} \tag{4.10}$$

We see from this expression that Z describes the development with temperature of the slope of the relaxation time curve in an Arrhenius plot. This way of plotting the data transfers a VFT behaviour into a straight line with a certain slope and an Arrhenius behaviour into a horizontal straight line thus with a slope of 0. The linearisation involves taking a derivative of the τ_α data which introduces noise. However, it is easy to analytically derive the relationship between the straight line parameters and the VFT parameters and in a plot of Z versus $1/T$, the gradient S is related simply to the VFT strength parameter D and T_0 as,

$$S = \left(\frac{T_0}{loge^1 D}\right)^{-\frac{1}{2}} \tag{4.11}$$

Since an Arrhenius behaviour of τ would lead to a horizontal line of fixed Z, the gradient in the resulting linearized Stickel plot represent in one parameter the deviation from Arrhenius behaviour and this one parameter in contrast to the fragility parameter m is defined over the full temperature range of interest and in contrast to the VFT parameters the parameter S is well defined. The linearisation of the τ_α data for the alkylbenzene series is shown in Figure 4.19a. The solid lines show the linearised VFT fits, constructed using Equation 4.10. It is clear that for the $M = 2$ to 7 samples the S parameter giving the gradient of the linearised τ_α data and representing the 'degree of non-Arrheniusness'. We see that $-S$ increases systematically with increasing alkyl tail-length indicating an increased departure from Arrhenius behaviour and therefore a more temperature dependent slowing down of dynamics for longer alkyl tails.

The gradient parameter, $-S$, as determined from Equation 4.11 is shown in Figure 4.19b and demonstrate an approximately linear growth with increasing molecular weight, shown in Figure 4.19a. The fragility parameter m is also shown for comparison and appears to obey a similar linear trend with increasing alkyl tail-length for the higher molecular weight samples. As discussed above, for the

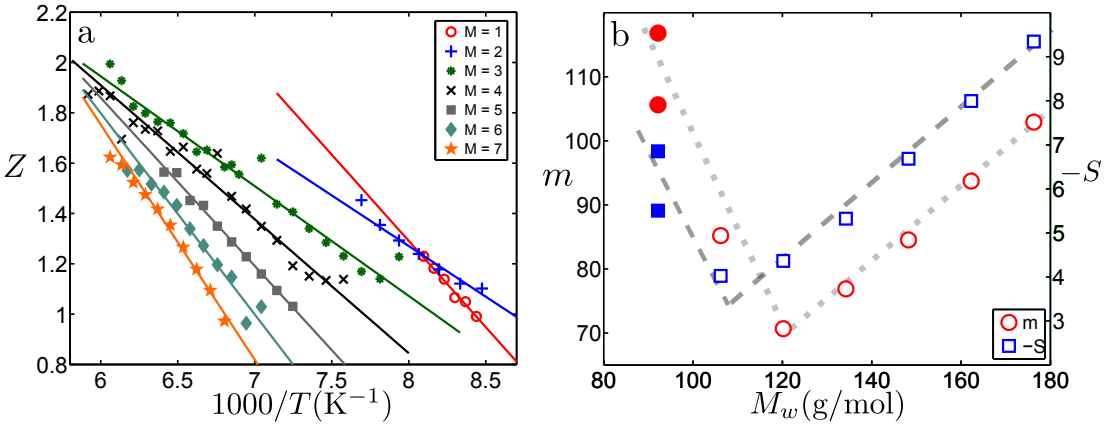

Figure 4.19: a) Stickel analysis of the τ_α data. b) Stickel parameter S in comparison with the fragility parameter m.

variation of the T_g values, there appears to be a comparable change of behaviour for the lowest molecular weights.

Furthermore, the linearisation of the τ_α data in the manner described above is often used to determine subtle changes in the temperature dependence of τ_α, which can be more easily resolved in a linearised Stickel representation than in an Arrhenius plot. Of course it is important to keep in mind that the linearisation requires a derivative so to be able to perform this constructively high quality experimental data with a good temperature resolution is needed.

For a wide range of molecular liquids where the temperature dependent τ_α values are available over a wide enough range of temperatures, a change in the temperature dependence is observed, which is clearly seen as a change from one straight line to another straight line where the change is observed at a temperature termed the crossover temperature, T^* [30, 35, 36]. Of course this temperature can be observed by fitting the data directly with VFT expressions, but the behaviour is more clearly and easily observed by using the linearised representation. It is important to note that in addition to a change of the temperature dependence of τ_α, a number of dynamic properties have been observed to change at this particular temperature [37]: i) the decoupling or bifurcation of the α and β relaxations [30], ii) the decoupling of rotational and translation diffusion [38] and iii) changes in the temperature dependence of the dielectric strength [37, 39].

For alkylbenzenes, the crossover regime has been shown previously for the $M = 3$ and 4 samples by Hansen *et. al.* [34]. Indeed, the authors show the existence of two crossover points, one associated with T^* and another at higher temperatures at which there is a zero gradient in Z and thus the behaviour becomes purely Arrhenius. For all alkylbenzene samples, we obtain data only in a temperature range close to T_g, below the crossover temperatures. As we will demonstrate for the alkyl benzenes and also for the oligostyrenes, it is still sometimes possible to resolve small changes in the VFT behaviour also at temperature below T^*. This has been observed for a few systems [193] and the change in the temperature dependence of the α relaxation have been shown to closely correspond to the decoupling of a secondary relaxation. However, this is an area of research which needs much more focus and investigation since we do not presently understand when and how the temperature dependence changes and when this is linked to the decoupling or merging of a secondary relaxation mode.

To obtain a physical picture of what the variation in fragility means, one sometimes refers to the energy landscape model as suggested by Goldstein (a more thorough explanation of this is available in Chapter 1) [89]. In this model, a viscous liquid is described by means of a 3N + 1 dimensional potential energy hypersurface [13, 18, 90]. This landscape can be considered as virtually independent of temperature and thus the temperature of the liquid only affects the resolution at which the liquid 'feels' the landscape [17]. The energy minima in this landscape correspond to various glassy states; there will also be minima associated with the crystallised state of the liquid and the so-called thermodynamically 'ideal' glassy state [18]. In terms of the fragility, the density of these glassy minima will depend on whether the glass-forming liquid is strong or fragile and where a more fragile system is characterised by a greater density of minima [13, 91, 92]. Thus, the increasing fragility observed through the m, D and S parameters for the $M = 3$ to 7 samples indicates that the density of the minima in the potential energy landscape increases with increasing alkyl tail-length.

4.3 Dielectric spectroscopy: β relaxation

In this section the measurement and analysis of the β relaxation for the alkylbenzene series will be discussed. In order to obtain dielectric spectra for this secondary process, the samples were cooled to 125 K and then measurements were performed upon lowering the temperature of the sample to 101 K in steps of 2 K.

4.3.1 Dielectric spectra

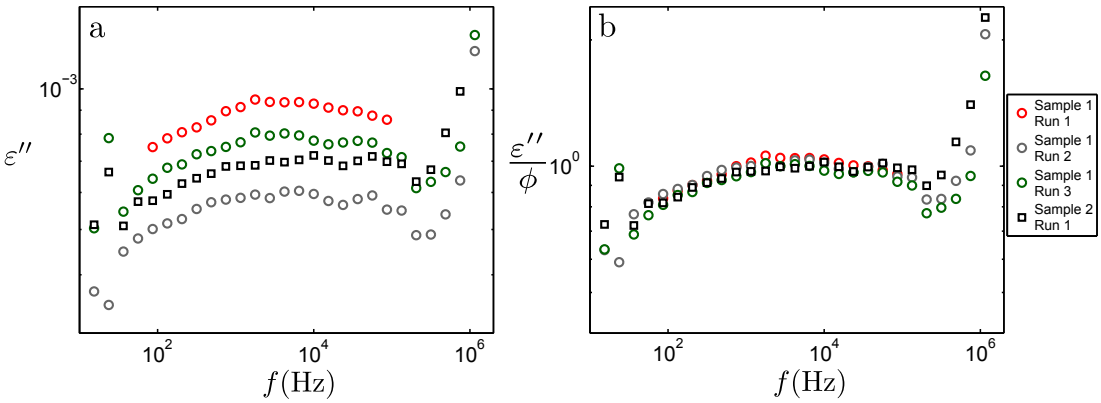

Figure 4.20: a) Comparison between dielectric spectra obtained for separate measurements of pentylbenzene at 101 K and b) rescaled in ϵ'' by a shift factor, ϕ.

For the $M = 3$ to 6 samples, secondary relaxation peaks were clearly observed at low temperatures, in the range between 101 and 111 K. Although the β relaxations could be resolved also at higher temperatures with consistent timescales (see Figure 4.33), only analyses of spectra in which the loss peak of the β relaxation could be fully resolved are shown here. In general, the β relaxation peaks observed in the dielectric spectra for the samples had a much lower amplitude that the α relaxation and were therefore more difficult to resolve in ε''. In order to investigate the repeatability of the observed relaxation contributions, each measurement was repeated with separate re-fillings of the liquid cell. Figure 4.20a shows separate measurements of the $M = 5$ sample at 101 K, indicated by the 'run' numbers in the legend. A separate batch of $M = 5$ sample was also measured ('Sample 2' in the figure) in order to confirm that the observed loss peaks

were not batch specific. We can see that the amplitude of the loss peaks vary slightly between measurements, but the peak is consistently observed in the same frequency position and has the same overall shape. In Figure 4.20b, the displayed spectra were rescaled in ε'' by a shift factor, ϕ. It is clear from this rescaling that although the amplitudes of the loss peaks vary somewhat, the shape and peak timescales are very similar meaning the spectra can be completely rescaled on top of each another. This serves to confirm that the same relaxation process is being probed in each measurement.

In order to determine the reason why the amplitudes of the relaxations in ε'' were different between runs, the spectra were also plotted as $tan(\delta) = \varepsilon''/\varepsilon'$. As both the real and imaginary parts of the dielectric permittivity are dependent on the sample area and thickness, rescaling in this manner removes this dependence meaning that any effect of loss of sample or inconsistent sample filling could be ruled out. However, it is clear from Figure 4.21 that there is still some small differences in the amplitudes. The reason for this variation is uncertain but it is important to remember that in the study of glass forming materials we are dealing with an inherently out-of-equilibrium structure and that supercooling a liquid into the glassy state twice will not result in the same structure [194]. For this reason, the difference in amplitude could be due to a difference in the number of dipoles that take part in this secondary relaxation process as a consequence of the differences in structure between the glassy state obtained after each supercooling of the sample. Ngai *et. al.* state that the dielectric strength $\Delta\varepsilon$ of a β relaxation process is expected to be dependent on the thermal history of a glass: a lower value of $\Delta\varepsilon$ is expected for a denser glassy state [51]. The idea that different supercooling scenarios could lead to different amorphous structures and therefore a variation in the strength of secondary, glassy relaxation phenomena has been studied with reference to salol by Wagner *et. al.* [195]. The majority of measurements of salol demonstrate that there is no indication of a Johari-Goldstein type β process either above or below the glass transition. However, upon quenching at an appropriately high rate (-490 K/min), the authors observed that a secondary relaxation process becomes visible at low temperatures. This is further evidence to suggest that the variation in the strength of the β process as observed in Fig-

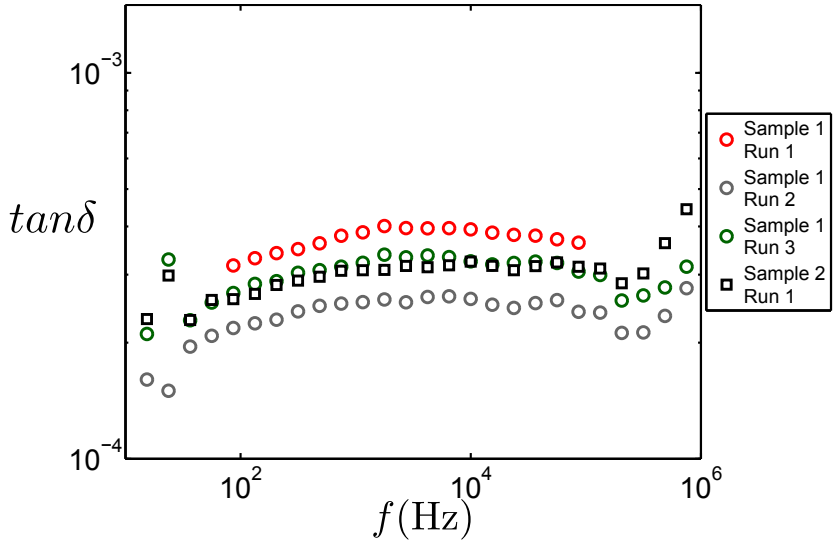

Figure 4.21: Figure showing $tan\delta = \varepsilon''/\varepsilon'$ for several separate runs of the $M = 5$ sample.

ures 4.20a and 4.21 could be due to the different thermal histories and therefore different obtained glassy structures.

4.3.2 Rescaled spectra

In order the analyse the development of the shape of the β relaxation prior to fitting, the β relaxation spectra for each sample were rescaled in both frequency and ε'' over the temperature range by the parameters ϕ_f and ϕ respectively. This rescaling is shown in Figure 4.22. We observe that the spectra can be scaled well for these samples. This scaling confirms that the relaxation peak can be resolved well in this temperature range and that their shape is largely invariant, with a slight broadening at higher temperatures. The overall breadth of the relaxation peak is much larger than that of the α relaxation which is consistent with what has been observed previously for secondary relaxations [51, 96, 196, 197].

4.3.3 Fitting procedure

To parametrise the development of the shape and timescale of the β relaxation further, the relaxation peak was fit using the Cole-Cole (CC) function [176] (ob-

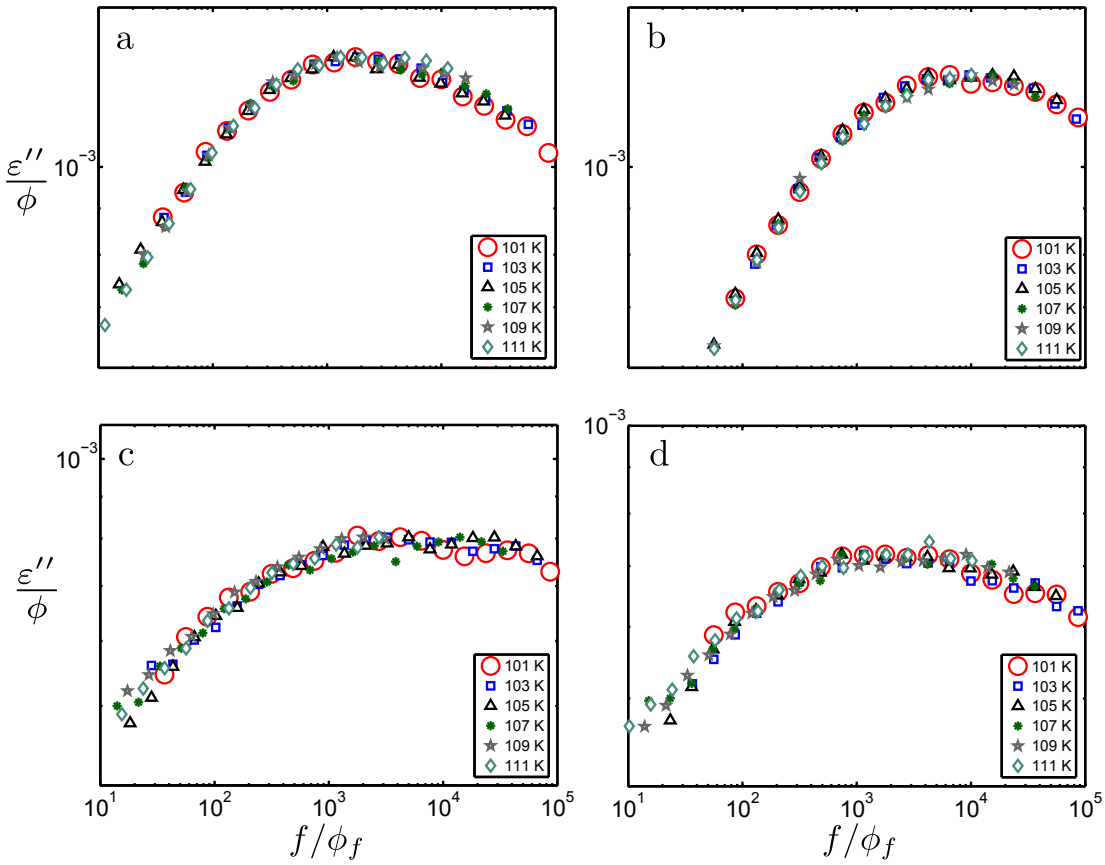

Figure 4.22: Dielectric spectra for the a) $M = 3$, b) $M = 4$, c) $M = 5$ and d) $M = 6$ samples in the β relaxation regime (111 K to 101 K) rescaled in both ε'' and f.

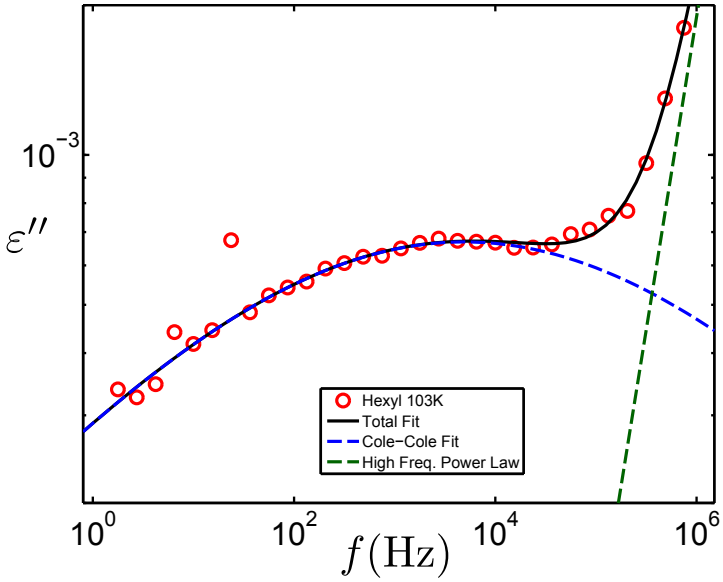

Figure 4.23: Dielectric spectra for the $M = 6$ sample at 101 K showing the different fit contributions.

tained by setting the β parameter in the HN function to 1), as is often used to describe secondary relaxation loss peaks [33, 61, 67, 94, 96, 116, 117]. The spectra also show a high frequency contribution (similar to that observed in the α relaxation regime) and this was fit using a power law of the form $\varepsilon'' = A\omega^B$. The full spectra for each sample were fit using an additive combination of both functional descriptions of the observed features. An example of a fit of the $M = 6$ sample at 101 K is shown in Figure 4.23, with the separate fit contributions indicated by dashed lines.

As temperature increases, the β relaxation becomes harder to resolve due to the proximity of the high frequency contribution. The values of A and B used to parametrise the high frequency power-law contribution were determined at the lowest measured temperature (101 K) and then kept constant for subsequent temperatures. In other words, the fits were conducted under the assumption that the shape of the high frequency flank was invariant with temperature and any changes to the spectra would be due to the secondary relaxation process. The dielectric spectra for all samples in the β relaxation regime could be well described based on the assumption of a fixed high frequency contribution. Furthermore,

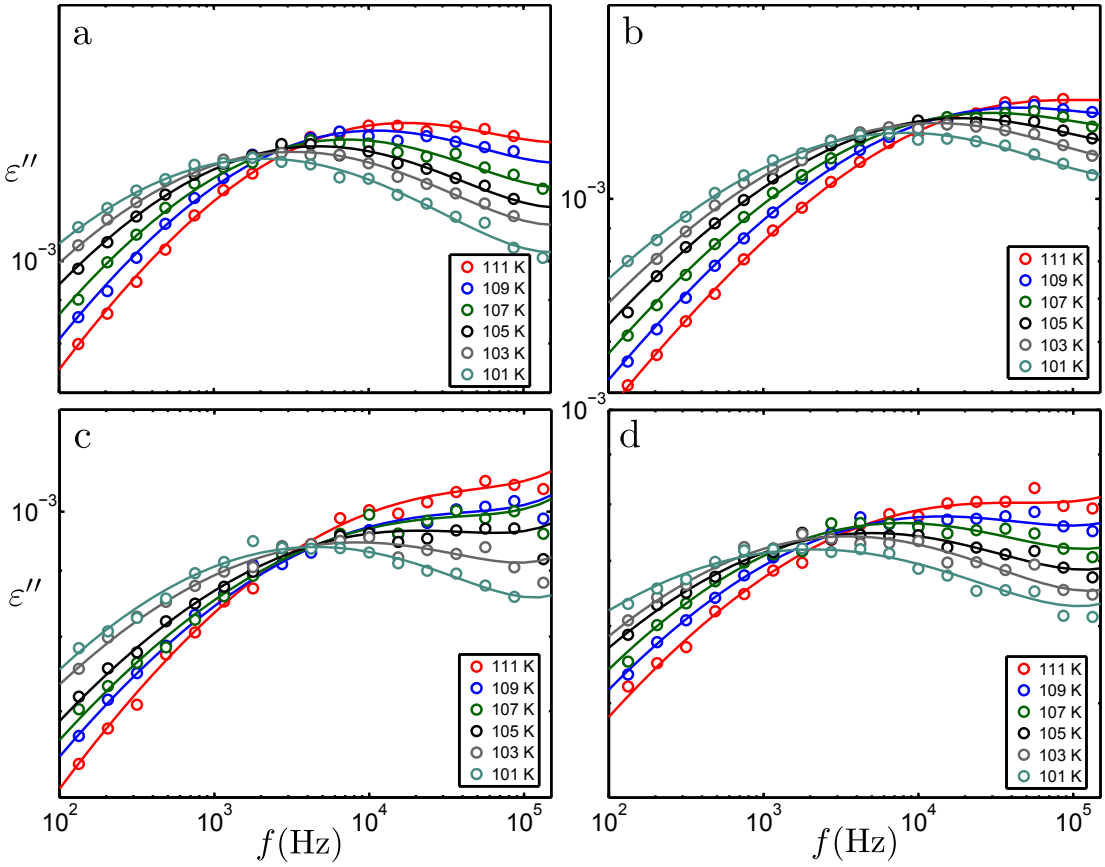

Figure 4.24: Dielectric spectra for the a) $M = 3$, b) $M = 4$, c) $M = 5$ and d) $M = 6$ samples in the β relaxation regime (111 K to 101 K). Fits through the data are a combination of a Cole-Cole and a high frequency power law fit.

the rescaling of the spectra shown in Figure 4.22 demonstrates that the high frequency contribution does not significantly affect the shape of the β loss peak.

The dielectric spectra and the resulting fits for the M= 3 to 6 samples are shown in Figure 4.24. The spectra are well described by the combination of a Cole-Cole function and a high frequency power law contribution. The peak frequency of the relaxation increases with increasing temperature as is expected. The β relaxation is completely resolvable for the $M = 3$ sample in the temperature range shown. The other samples also show resolvable β relaxations but at higher temperatures they become progressively hidden by the high frequency contribution.

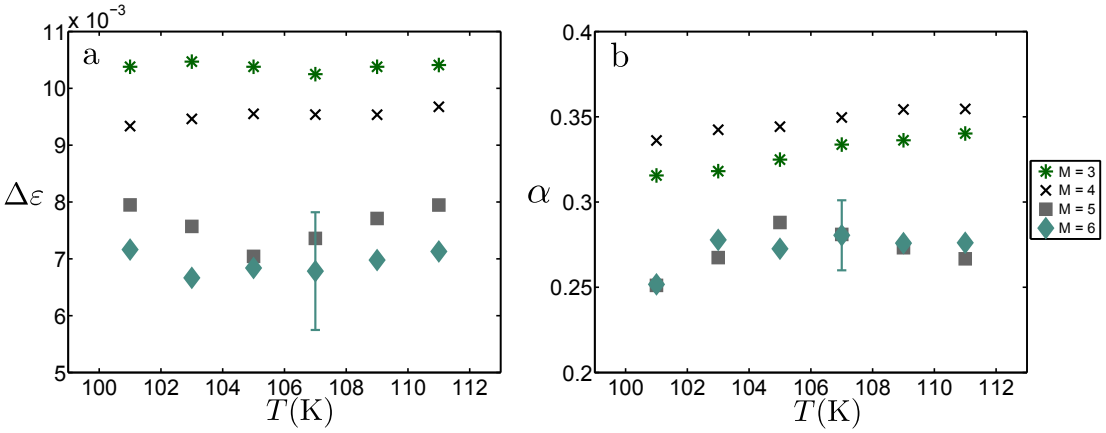

Figure 4.25: a) $\Delta\varepsilon$ values obtained through fits of the dielectric spectra. b) α values obtained through fits of the dielectric spectra. Errors for the values obtained from the hexylbenzene sample are the standard deviation between different runs.

4.3.4 Fit parameters

The dielectric strength and symmetric stretching parameters obtained through fits of the CC function to the the β relaxation peak are shown in Figures 4.25a and b. Error bars were determined by taking the standard deviation between fits using the CC function to separate measurements of hexylbenzene. The symmetric stretching parameter, α, does not appear to have any obvious temperature dependence suggesting that the shape of the relaxation peak is fairly invariant with increasing temperature, as was evident in the rescaling of the spectra (Figure 4.22). Also $\Delta\varepsilon$ is reasonably constant over the temperature range within the accuracy of its determination. This is consistent with previously observed behaviour of secondary relaxation processes, which often have a weak temperature dependence of their strength below T_g [51, 196, 198]. The dielectric strength of the secondary relaxations appears to get weaker with increasing alkyl tail-length and it appears that the α parameter becomes smaller for the higher tail-length samples. Murthy *et. al.* determined the $\Delta\varepsilon$ of the secondary relaxation for the $M = 3$ sample using dielectric spectroscopy [163] and this was reported to be 2×10^{-3} in a $tan(\delta)$ renormalisation. This value is sightly larger than the range of $tan(\delta)$ values observed in this research for the $M = 3$ sample which fell between 5×10^{-4} and 7×10^{-4}.

In order to test the robustness of the fits of the dielectric spectra in the β relaxation regime, the $\Delta\varepsilon$ values as determined from fitting the CC function to the dielectric spectra were compared to the rescaling parameters used to produce the rescaled spectra shown in Figure 4.22. In order to determine the dielectric strength, $\Delta\varepsilon$ from the rescaling parameter for the height of the peak, ϕ, the amplitude of the spectra were determined at 101 K using the following relationship determined by Bergman [104],

$$\varepsilon''_p = \frac{\Delta\varepsilon}{2} tan\left(\frac{\alpha\pi}{4}\right) \tag{4.12}$$

The obtained values of ε''_p were then multiplied by the rescaling parameters, ϕ, obtained for the higher temperatures (103 K, 105 K, 107 K, et.c.) for each sample, thus providing the variation of the amplitude with increasing temperature. These values were then used to calculate the equivalent $\Delta\varepsilon$ parameters using Equation 4.12 in order to compare with the fitted values of $\Delta\varepsilon$. A comparison between rescaled and fitted values of $\Delta\varepsilon$ for the different samples are shown in Figure 4.26. There is a very good agreement between the two sets of values suggesting that the fitting of the β relaxations is robust and confirms the trends observed in the parameters.

4.3.5 Comparison between samples.

We now consider the difference between the observed secondary relaxation processes for the $M = 3$, 4, 5 and 6 samples. In order to aid comparison, the dielectric spectra at two different temperatures, 101 K and 111 K, for each sample were plotted on the same axis. This is shown in Figures 4.27a and b. There appears to be a decrease in the amplitude of the secondary relaxation with increasing alkyl tail-length. This trend has already been quantitatively observed from the variation of the dielectric strength, $\Delta\varepsilon$, between samples (Figure 4.25a).

Further comparison was achieved by rescaling the spectra by the peak amplitude. This is shown in Figures 4.27c and d for 101 K and 111 K respectively. It is clear from these figures that the secondary relaxations observed in the $M = 3$, 5 and 6 samples occur with similar peak frequencies, suggesting that they are the

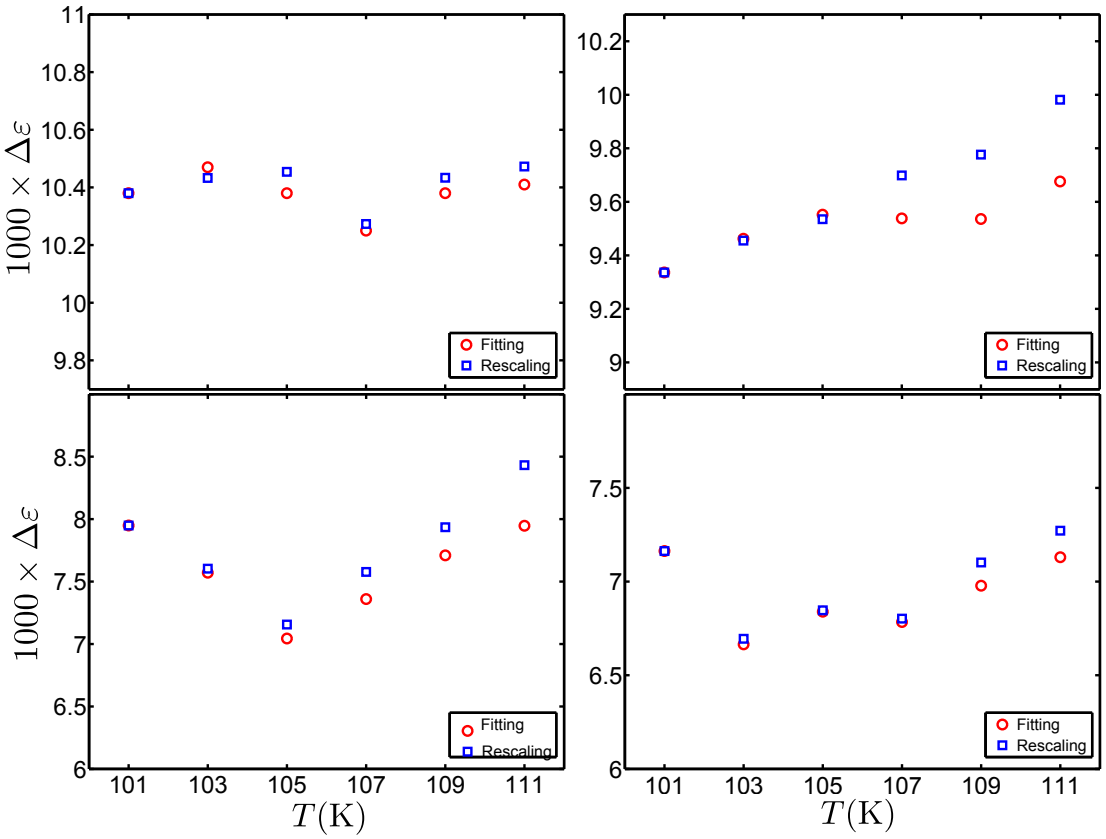

Figure 4.26: $\Delta\varepsilon$ values obtained from fitting and rescaling of the dielectric spectra for the a) $M = 3$, b) $M = 4$, c) $M = 5$ and d) $M = 6$ samples.

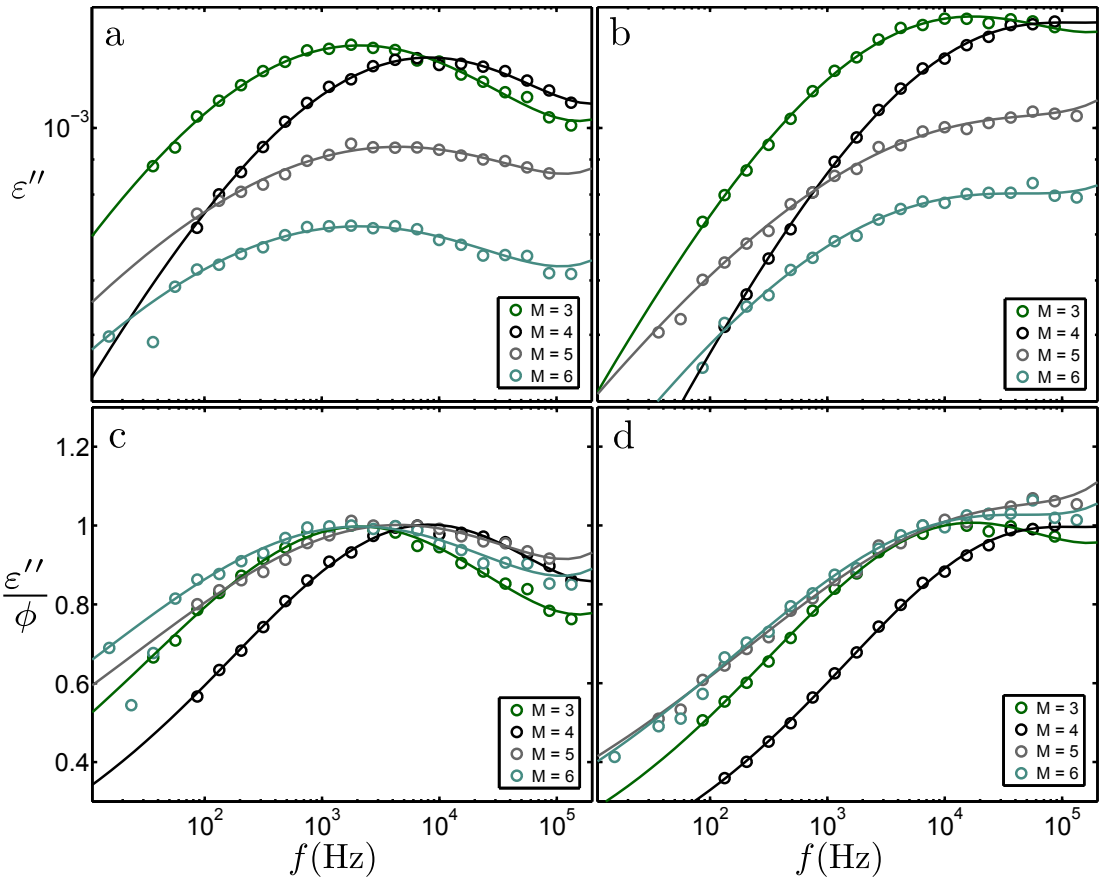

Figure 4.27: Dielectric spectra for the $M = 3$ - 6 samples at a) 101 K and b) 111 K. These spectra were then rescaled in ε'' in order to see whether they collapse (at c) 101K and d) 111 K). Samples $M = 3$,5 and 6 appear to collapse well at both temperatures indicating that the β relaxations occur with similar peak frequency for each sample.

result of the same relaxation mechanism and that the timescale of this mechanism is invariant with increasing molecular weight or alkyl tail-length. We also observed that the spectra have a slight increase in the breadth of the secondary loss peak with increasing alkyl tail-length, as quantified by the variation of the symmetric stretching parameter, α, obtained from the CC fits of the data (see Figure 4.25b). The peak frequency for the $M = 4$ sample, however, systematically occurs at higher frequencies than the other samples. This behaviour is repeatable at both 101 K and 111 K and in separate measurements of the sample.

4.3.6 Relaxation timescales

A full discussion of the timescales, τ_β obtained through analysis of the secondary relaxations for the $M = 3$ to 6 samples will now be presented. Firstly, the values obtained from the fits of the CC function to the dielectric spectra were compared to the values obtained through the rescaling parameters, ϕ_f, required to scale the dielectric spectra as shown in Figure 4.22. This was done so that the validity of the values obtained from the fitting procedure could be checked. In order to make this comparison, the τ_β value obtained at the lowest measured temperature (101 K) from fitting was multiplied by the values of ϕ_f for each sample. This comparison is shown in Figure 4.28. It is clear from this figure that the values obtained from fitting and rescaling correspond well with each other, confirming the validity of the fitting process. Therefore, quoted values of τ_β in the remainder of this chapter will be those obtained from fitting of the CC function.

An Arrhenius plot showing the τ_β values across the sample range in comparison with the τ_α values (as discussed in Section 4.2.5) is shown in Figure 4.29a. This figure shows that the timescale of the α and β relaxations occur at significantly different timescales and have a different temperature dependence. A separate plot featuring just the τ_β data is shown in Figure 4.29b. The timescales for the $M = 3$, 5 and 6 samples have similar values, quantifying the similar peak frequencies of the secondary loss peak shown in Figure 4.27. The values for the $M = 4$ are lower than those of the other samples again quantifying the observed behaviour of the spectra. Also shown are τ_β data for the $M = 1$ sample obtained

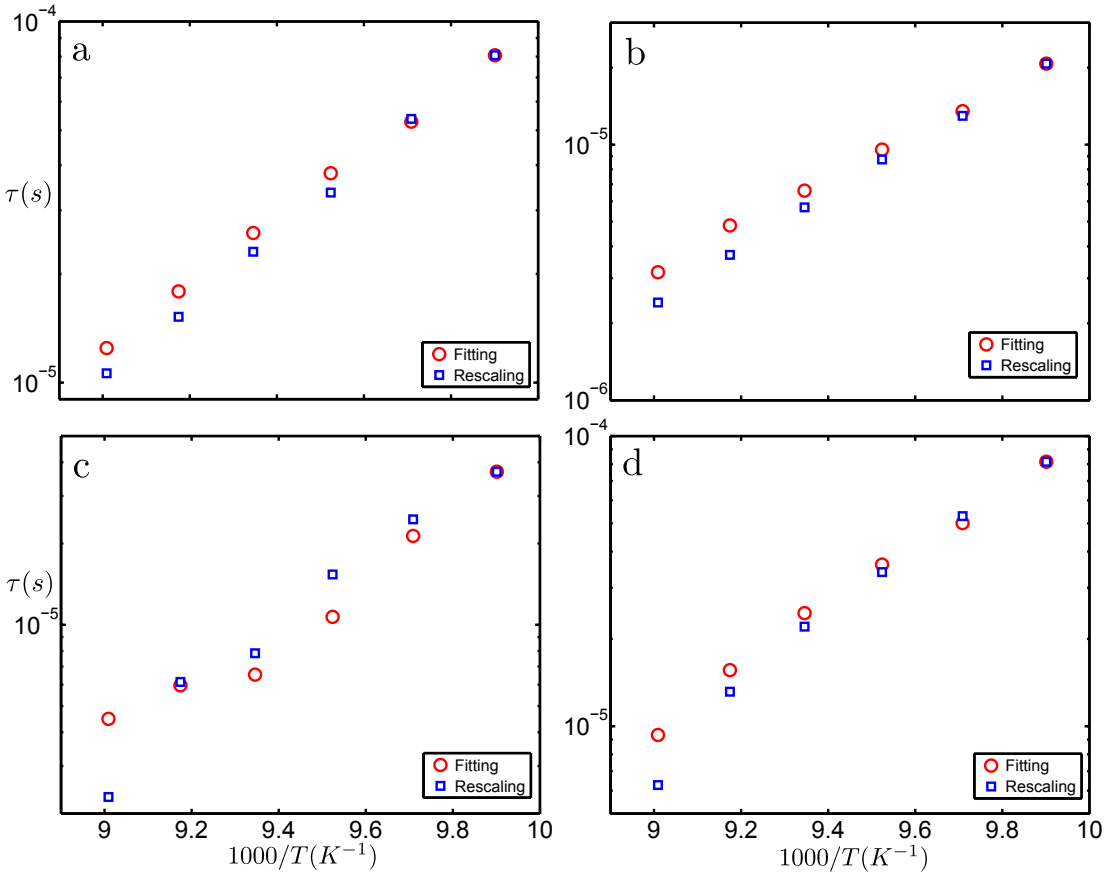

Figure 4.28: τ_β values obtained from fits (red circles) and rescaling (blue squares) of the dielectric spectra for the a) $M = 3$, b) $M = 4$, c) $M = 5$ and d) $M = 6$ samples.

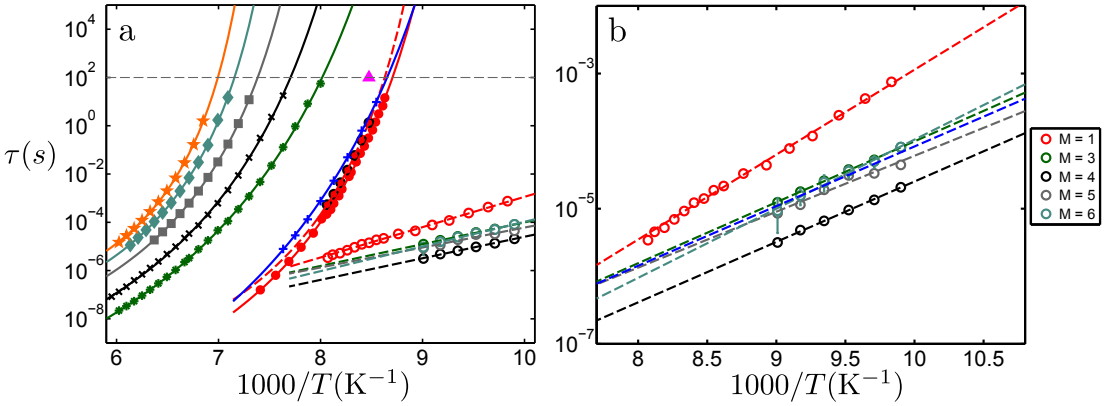

Figure 4.29: a) Values of τ_α and τ_β data for the alkylbenzene series. τ_β data are indicated by the open circles. b) Plot showing the values of τ_β separately. Plots include data from literature [33, 55] for the $M = 1$ sample. Dashed lines indicated fits of the Arrhenius equation to the τ_β data. Also plotted is an Arrhenius-like line indicating the supposed behaviour of the $M = 2$ sample had it shown a distinct secondary relaxation rather than an excess wing. A description of how this data were obtained is given in the text.

from the literature [55]. The observed peak timescales for this relaxation process are slower than those of the other samples. We saw in Section 4.2.1 that the $M = 2$ sample exhibited an excess-wing and did not show any signs of a secondary process at low temperatures. The dashed blue line indicates the hypothesized behaviour for a submerged secondary relaxation for the $M = 2$ sample as obtained through the analysis procedure detailed in Section 4.3.6. This line indicates that the expected values of τ_β for the $M = 2$ sample might also follow the timescales of the $M = 3$, 5 and 6 samples.

Dashed lines through the τ_β data indicate fits of the Arrhenius equation to the τ_β data. This equation was introduced in Chapter 1 but will be redefined here to aid the following discussion:

$$\tau = \tau_0 e^{\frac{E_A}{k_B T}} \tag{4.13}$$

Here, E_A, is the activation energy barrier and τ_0 is the limiting timescale at high temperatures. It is clear from Figure 4.29a that the data are well described by such an analysis, indicating that the observed secondary relaxation mechanism is an 'activated process' with a fixed temperature independent energy barrier.

M	$\log_1 0(\tau_0)$ (s)	E_A (kJ/mol)	T_g (K)	K (E_A/RT_g)	Reference
1	-15.5 ± 0.2	24.1 ± 0.5	115.9	25.0	[55]
3	-13.0 ± 0.1	17.3 ± 0.3	124.7	16.6	-
4	-13.5 ± 0.2	17.1 ± 0.4	129.8	15.9	-
5	-12.9 ± 0.9	16 ± 2	135.4	14.1	-
6	-14.2 ± 0.4	19.6 ± 0.8	139.7	16.9 ±	-

Table 4.3: Table showing the activation energies E_A and τ_0 obtained through fitting of the τ_β values and the constant, K, from the relationship between E_A and T_g (Equation 4.14) [15, 61]. Errors in the fitted parameters were obtained from the covariance matrix resulting from non-linear mean squares fitting of the data.

This is a feature common to secondary relaxation processes in the glassy state [51]. Fit parameters for the description of the τ_β data with the Arrhenius equation are shown in Table 4.3. The τ_0 data are close to the expected microscopic timescales of the bulk liquids at high temperature [2, 24–26]. The activation energies, E_A, show little variation between the $M = 3$ to 6 samples but is clearly higher for the $M = 1$ sample. The obtained value of E_A observed for the $M = 3$ sample is consistent with values published previously [163, 165].

It has been shown that for a number of molecular liquids that there is an empirical relationship between the activation energy and T_g [61]:

$$E_\beta = KRT_g, \tag{4.14}$$

where R is the universal gas constant. Kudlik *et. al.* compared the values of this constant for a selection of molecular glass formers and it was concluded that, in general, Equation 4.14 holds with a value of $K = 24 \pm 3$ [15, 55]. This is also consistent with a value of $K = 26 \pm 2$ obtained for a wide range of metallic glasses [9]. The important implication of Equation 4.14 is that it connects the activation energy of the β relaxation with T_g suggesting a fundamental connection between the α relaxation (the timescale of which governs T_g) and the β relaxation, where the general idea is that the secondary relaxation can be thought of as a a precursor to the structural relaxation [15, 51]. Values of K calculated using Equation 4.14 are shown in Table 4.3 for the alkyl benzenes. We find that the values of K deviate from the often observed value of around 24 and we find

smaller values of $\sim 16-20$ except for toluene which shows a value consistent with 24 ± 3. Such deviations of K (∼10-40) were also observed by Ngai *et. al.* when they looked a wide range of different types of glass-formers and relaxations, but the authors still assumed that Equation 4.14 holds [15]. Thus, it is not presently clear how unique a specific value of K is in terms of indicating a link between the primary and a generic secondary relaxation mechanism. However, it is an experimental fact that the M = 3-6 samples all have secondary relaxations with very similar activation energies within the glassy state, whereas toluene shows a higher activation energy. The former values are lower than that generally expected to fulfil the often observed scaling relationship with T_g, but the value of K for toluene is consistent with that of the standard values. These observations thus suggests a different origin of the secondary relaxation in the M = 3-6 samples and that in toluene, respectively. The behaviour for toluene suggest that the observed secondary relaxation corresponds to the standard beta-relaxation whereas the M = 3-6 sample secondary modes might be of a different origin, thus akin to what we observe and term the γ relaxation in the oligostyrenes. In fact, as described in more detail in Chapter 6, the activation energy of the γ relaxations and the secondary relaxation of the M = 3-6 samples is very similar. Thus, if the secondary relaxation observed for the majority of the alkyl benzenes is not the β relaxation, it suggest that this relaxation is instead hidden under the α response. Indeed, as discussed above, we have found several indications suggesting that another relaxation contribution is indeed present at time-scales intermediate between the α and the observed secondary relaxation.

Rescaling using the glass transition temperature

In order to further analyse the variation of τ_β, the data were plotted in a T_g rescaled Arrhenius plot as shown in Figure 4.30a. An interesting consequence of this rescaling of the timescale data is that the τ_β values appear to decrease systematically with increasing alkyl tail-length. This suggests an increased separation between the α and β relaxations with increasing tail-length. Of course, as discussed above it is not clear whether the secondary relaxation for toluene should be directly compared with those in the rest of the alkylbenzenes, but it

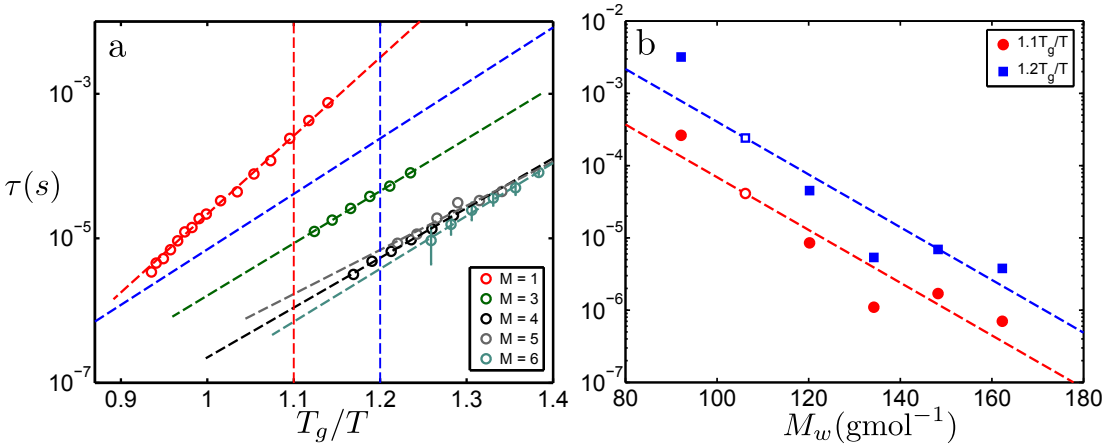

Figure 4.30: a)τ_β data for the $M = 1$, 3, 5, and 6 samples in a T_g rescaled Arrhenius plot. Vertical dashed lines indicate cuts taken at 1.1 and 1.2 T_g/T. b)τ_β data taken at cuts of $1.1T_g/T$ and $1.2T_g/T$. Open symbols refer to the estimated cut τ for the $M = 2$ sample, obtained by fitting the cut values for the other samples.

is still worth investigating this interpretation and in addition, it is important to note that we can not be certain that the secondary relaxation in toluene as reported in literature does not consist of several merged relaxation contributions. Thus, in order to quantify the observed variation of the relaxation behaviour with M-value, cuts of the data were made at specific values of T_g/T (1.1 and 1.2 T_g/T) indicated by the vertical dashed red and blue lines.

The τ_β values obtained from these cuts are shown in Figure 4.30b. Based on the hypothesis that the cut values decrease systematically with increasing tail-length then the data can be reasonably described by linear fits, as indicated by the dashed lines (corresponding to the cut lines in Figure 4.30a). Note that this is of course very speculative and for the highest M-values within the accuracy of the data it is difficult to talk about any variation with tail-length. Still, assuming that toluene can be compared to the other secondary relaxation, we do find a general speed up for higher M when the data have been shifted with regards to their T_g values. The open symbols in Figure 4.30b are extrapolations based on the linear fits to roughly estimate the expected τ_β values for the $M = 2$ sample. In turn, the two extrapolated values allowed expected τ_β values for the $M = 2$ sample to be generated and the dashed blue line in 4.30b. show the expected behaviour of

the τ_β values for the M=2 sample. The blue dashed Arrhenius behaviour is also added to Figures 4.29a and b.

Mixtures of toluene and polystyrene

It was shown in Section 4.3.6 that activation energy for the τ_β data for toluene ($M = 1$) is relatively different to that of the other samples. However, as discussed above toluene is the only sample which we have not measured ourselves due to the difficulty to avoid crystallization. That we need to rely on literature measurements and the fact that special approaches had to be adapted to avoid crystallization puts a question on how much we can trust the data for toluene. To investigate this we investigate our own data where toluene was mixed with polystyrene in different concentrations. The details of these experiments are published elsewhere [199]. The idea of mixing toluene with a polymer is that crystallization can be avoided and by performing measurements on samples with varying polymer concentrations we can quantify the effects that the polymer has on the observed behaviour. The τ_β data obtained through measurements of mixtures of toluene with differing amounts of polystyrene are shown in Figure 4.31 together with data for pure toluene, as obtained from literature and discussed previously [55]. Interestingly, we find that the time-scale of the β relaxation is largely unaffected by the addition of polystyrene. Importantly, we find that the temperature dependence of the τ_β values obtained from the mixtures are consistent with the data obtained for pure toluene from literature and this serves to confirm the τ_β data for the pure sample.

The similarities between the different sets of τ_β data were quantified by comparing the activation energies, E_A, obtained through fits of the Arrhenius equation to the data in Figure 4.31. The fitted parameters are shown in Table 4.4. Values for E_A show good agreement across the different samples, confirming the similar temperature dependence of τ_β. Furthermore, the values of τ_0 agree between the different samples but are lower than the typical range expected (10^{-12} to 10^{-14}) [2, 24–26].

The relationship between E_A and T_g (Equation 4.14) was also tested for this series and it was found that the constant of proportionality, K, was reasonably close to values found for other molecular glass formers [15] as shown in the table.

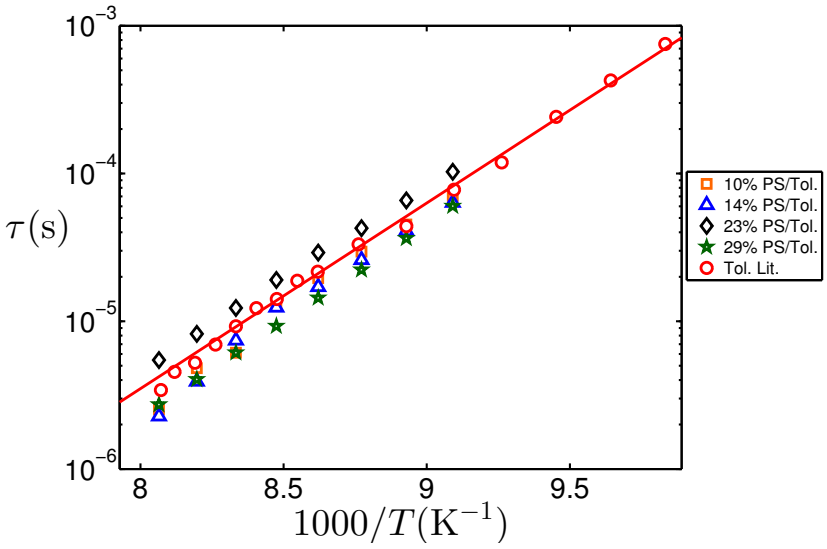

Figure 4.31: τ_β data obtained from the literature for toluene [55] in comparison with data obtained through dielectric measurements of samples containing a mixture of toluene and polystyrene.

PS/Toluene wt%	$\log_{10}(\tau_0)$(s)	E_A (kJ/mol)	T_g	K (E_A/RT_g)	Reference
0	-15.5 ± 0.2	24.1 ± 0.5	115.9	25.0	[55]
10	-16.8 ± 0.5	27 ± 1	118.7	27.1	[199]
14	-16.6 ± 0.6	26 ± 1	120.2	26.4	[199]
23	-15.2 ± 0.1	23.7 ± 0.3	124.1	23.0	[199]
29	-16.1 ± 0.1	25.0 ± 0.1	127.7	23.5	[199]

Table 4.4: Table showing the activation energy E_A and τ_0 values obtained through fitting of the τ_β values and the constant from the relationship between E_A and T_g (Equation 4.14) [15, 61] for mixtures of polystyrene and toluene. Also shown are determined values of T_g from the VFT descriptions of the τ_α data.

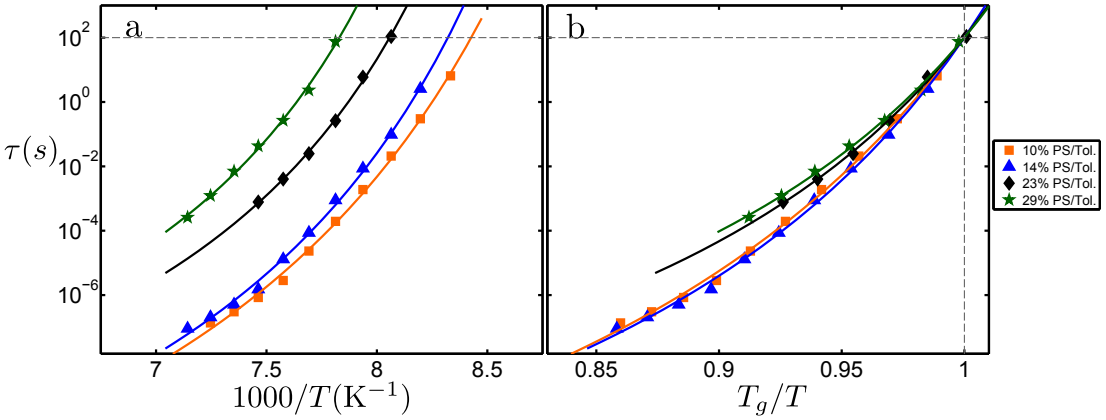

Figure 4.32: a) τ_α data obtained through dielectric measurements of samples containing a mixture of toluene and polystyrene. b) Data rescaled by T_g

The affect of the addition of polystyrene to toluene is much more pronounced in the timescale of the structural relaxation, as shown in Figure 4.32a. As a higher percentage of polystyrene is mixed with toluene, the α relaxation is shifted to longer timescales. This has the affect of increasing the glass transition of the mixture, as shown in Table 4.4. The τ_α data are again well described by the VFT expression (Equation 4.7) denoted by the lines through the data. In order to further analyse the τ_α data, a T_g rescaling was performed and this is shown in Figure 4.32b. This rescaling shows in a qualitative sense that as the percentage of polystyrene is increased, the fragility of the mixture decreases. Both systems also show an increase in the temperature regime of the α relaxation coupled to an increase in the glass transition temperature. This variable behaviour of the τ_α data is accompanied by τ_β data which, to a certain approximation, is invariant with polystyrene content. Even though the glass-transition increases the ratio between the determined activation energy and the glass transition temperature remains within the often observed 24 ± 3 range. If this relation holds one would expect a variation in the activation energy as the glass transition temperature varies. However, the varition in T_g is not enough to clearly determine whether any systematic variation in activation energy takes place. Within the accuracy of the measurement we do not observe a trend.

4.3.7 Further analysis of the α and β relaxation timescales.

In this section the timescales for the α relaxations obtained through fitting of the dilectric spectra, τ_α will be more closely compared with the the timescales of the secondary relaxations observed samples at low temperatures, τ_β. This comparison is shown in Figure 4.33a-f for the M = 2-7 samples. Also shown in the figures are τ_β values obtained through the fitting of the observed 'intermediate' contribution between the α relaxation loss peak and the high frequency power-law contribution, as described in Section 4.2.3. These timescales show a strong resemblance to the τ_β data observed at lower temperatures for the fully resolved β relaxation in the M = 3 to 6 samples. The resemblance is quantified by the fact the two sets of τ_β data can be described by the same Arrhenius fit, as indicated by the fit lines through the data.

An extrapolated crossing of the Arrhenius fit to the τ_β data and the VFT fit to the τ_α data are observed for the M = 3, 4 and 5 samples. This crossing point is indicated by the vertical dashed purple line. It was explained in Section 4.2.8 that the crossover temperature, T^*, has been associated with the decoupling or bifurcation of the α and β relaxations [30]. This crossover temperature is often defined as the point at which the temperature dependence of τ_α changes and is often observed through linearisation, or Stickel analysis, of the τ_α data [31]. In this manner, the crossover temperature, which is outside the dynamic range of our spectrometer, has been determined for the M = 3 and M = 4 samples by Hansen *et. al.* [34]. This point is denoted by the vertical dashed light blue lines in Figures 4.33b and c. For the M = 3 sample (Figure 4.33b) the crossover temperature determined through Stickel analysis and the crossover of the VFT and Arrhenius descriptions of the τ_α and τ_β data are in good agreement with each other. This provides evidence for the bifurcation scenario. However, there is less agreement between these two definitions of the crossover temperature for the M = 4 sample (Figure 4.33b). We note that although a secondary relaxation process could not be fully resolved for the M = 7 sample, the timescales obtained for the 'intermediate' contribution suggest an underlying secondary relaxation of a similar nature to that observed for the M = 3, 4, 5 and 6 samples even though

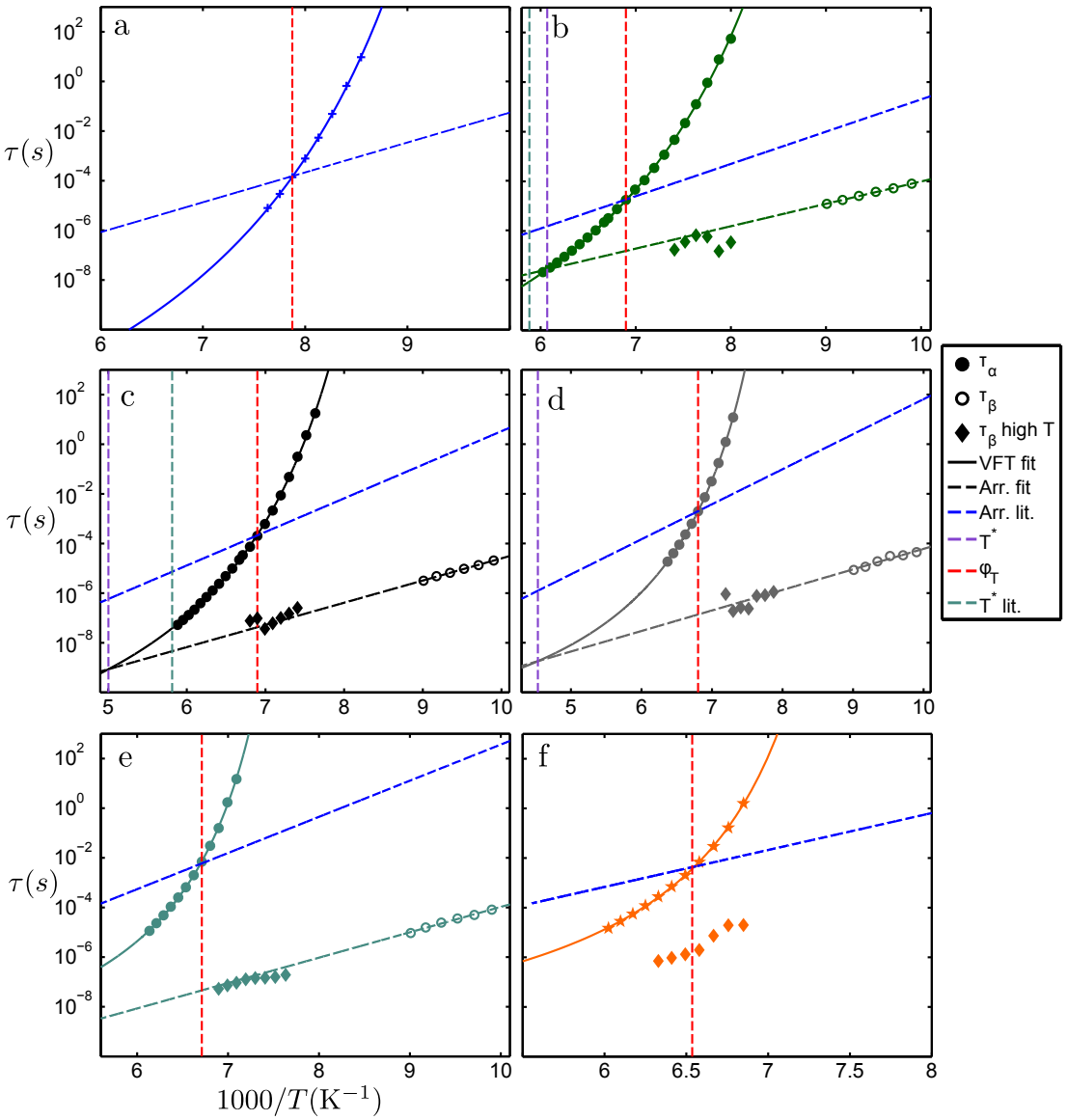

Figure 4.33: Values of τ_α and τ_β for the a) $M = 2$ b) $M = 3$, c) $M = 4$, d) $M = 5$, e) $M = 6$ and f) $M = 7$ samples including their VFT and Arrhenius fits respectively. Also shown are red dashed lines indicating the temperature of the maximum of ϵ''_p for each sample in Figure 4.14. The blue dashed lines indicated theoretical values of τ_β obtained through application of the Arrhenius equation with an activation energy determined using Equation 4.14. The vertical dashed purple lines indicate the crossing of the Arrhenius and VFT fit lines and the vertical dashed turquoise lines indicate crossover temperatures, T^*, determined by Hansen *et. al.* [34]

for the $M = 7$ it is difficult to assign the exact time-scale with any significant accuracy due to the weakness of the contribution.

In Section 4.2.4, a peak was shown in the fitting parameters describing the amplitude, ε''_p, of the α relaxation loss peak and it was speculated that this might be indicative of the merging of a 'hidden' secondary relaxation with the α peak. The temperatures at which the peaks in ε'' were observed are denoted by the vertical dashed red lines in Figures 4.33a-f. If this temperature was indicative of a merging of the observed secondary relaxation with the α relaxation then the extrapolated Arrhenius fit of the τ_β data should cross the VFT fit of the τ_α data at this temperature. The figures clearly show that the two fit lines do not cross at this temperature suggesting that the maximum in the amplitude is not due to merging of these two observed processes. This suggests that if the amplitude peak is due to a 'hidden' secondary relaxation, it will be an additional contribution separate from the secondary relaxations directly observed in the data.

We previously observed that the activation energies of the secondary contributions for the M = 3-6 samples are lower than what is normally observed for 'standard' *beta* relaxations. The secondary relaxation of toluene, however, shows the expected behaviour. Thus, we can hypothesize that the 'hidden' secondary relaxation that we have found evidence might be of the same origin as the secondary relaxation observed for toluene and that its activation energies would conform to $K = 24 \pm 3$. To test this idea, τ_β values were generated using the empirically based relationship (Equation 4.14) between the activation energy of the β process, E_A, and T_g [15, 61]. For the purposes of this test, the constant of proportionality, K, in this equation was set to 24 as is often observed for molecular glass formers [15]. The values of τ_β were generated by substituting the determined activation energy into the Arrhenius equation. The values of τ_0 were chosen so that the crossing of the secondary relaxation and the *alpha* relaxation took place at the temperature for which a peak in its amplitude was observed for each sample. The peak amplitude temperatures are marked in Figure 4.33 with vertical dashed red lines. The resulting τ_β values are plotted as blue dashed lines in Figure 4.33.

An Arrhenius plot, showing the timescales of the observed α and secondary relaxations and also the 'expected' values of τ_β obtained through the empirical

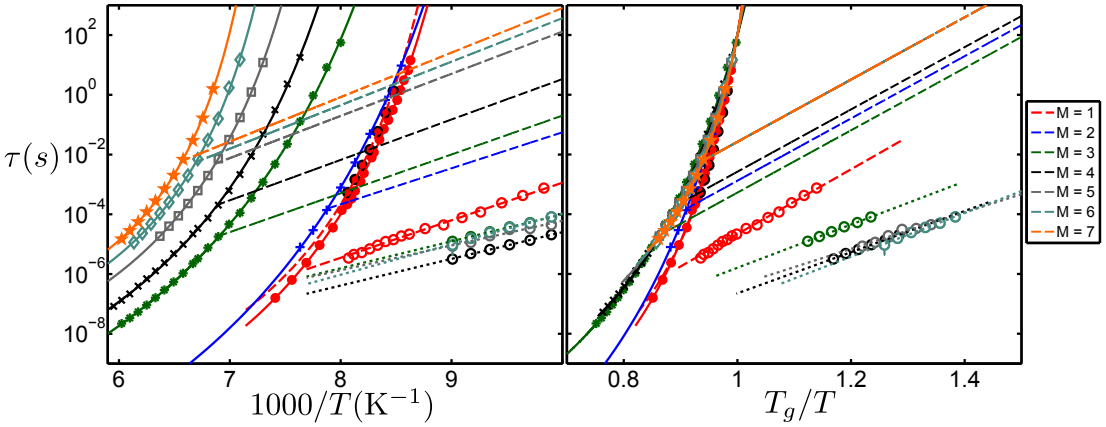

Figure 4.34: a) τ_α, 'expected' values of τ_β (dashed lines) and τ_γ values (open circles) for the alkylbenzene series. b) Data rescaled by T_g. The figures include data for the $M = 1$ sample (both τ_α and τ_β) from the literature [33, 55]. Arrhenius fits of the τ_γ data are denoted by dotted lines and VFT fits of the τ_α data are represented as solid lines.

relationship between the activation energy of the β process and T_g (Equation 4.14), is presented in Figure 4.34a. For the purposes of the following discussion, the faster directly observed secondary relaxation will now be termed the γ relaxation.

There is a definitive trend in the expected τ_β values which appear to approach, with decreasing alkyl tail-length, the behaviour of the τ_β data for the observed secondary process in the the $M = 1$ sample. This provides further evidence for an underlying secondary mode in the $M =$ 2-7 samples which is likely to be connected to the secondary mode observed for the $M = 1$ sample. The timescale, $\tau_{\alpha\beta}$ at which the expected values of τ_β cross the τ_α data also appears to follow a systematic trend, increasing with increasing tail-length across the range of samples. We note that the observed behaviour suggests that the α and β relaxations become increasingly separated with increasing molecular weight, which could explain both the clear secondary relaxation peak observed for the $M = 1$ sample and the clear excess wing observed for the $M = 2$ sample. In this representation, we observed no clear trend in the τ_γ data; the data for the $M = 3$, 5 and 6 samples appear to occur at similar timescales but the relaxation process appears faster for the $M = 4$ sample.

The behaviour of τ_β that slow down with increasing chain-length is fully consistent with the observations of an oligomeric chain-length series of propylene glycol dimethyl ethers [69, 193]. Also a chain length series of mono-methyl ethers demonstrate the same trend [18]. In the following chapters, we will further demonstrate a remarkable similarity between the behaviour observed for alkyl benzenes and the behaviour observed in two different oligomeric chain-length series.

A T_g rescaled Arrhenius plot of the data is shown in Figure 4.34b. This figure reiterates the scenario discussed in Section 4.3.6, in which we speculated that there might be a trend for the τ_γ data in a T_g scaled representation. We noted that if one used a rough extrapolation based on this trend to predict the relaxation timescales for the $M = 2$ sample, they would overlap with the γ relaxation timescales of the $M = 3, 5, 6$ and 7 samples. Given that the β relaxations appear to speed up with decreasing molecular weight, whereas the γ relaxations appear to be relatively fixed the apparent absence of these in the spectra for the $M = 1$ and $M = 2$ samples might just be due to the fact that their contributions are submerged under the more significant β relaxation contributions.

In order to further investigate the hypothesis of a 'hidden' β relaxation for the higher molecular weight samples, β relaxation spectra for the $M = 3$ sample and $M = 4$ sample were analysed at temperatures below their respective glass transitions in order to detect any hints of an underlying secondary relaxation. This analysis is shown in Figures 4.35a and b for the $M = 3$ and $M = 4$ samples respectively. We observe that there are indeed indications of a weak excess wing in both cases, as characterised by the variation of the exponent of the high frequency powerlaw flank of the α relaxation. The characteristic timescale expected for the β relaxations at the investigated temperature, based on the estimate above are marked with a vertical dashed blue line in each case. This further suggests that there is an additional secondary contribution to the spectra for all investigated samples. This contribution could not be resolved in the spectra above T_g and it would thus not made sense to attempt to perform the fitting described above using an extra functional contribution.

The implication of this analysis is thus that in addition to the γ relaxation observed at the shortest times, there appears to be one additional underlying secondary process which is difficult to resolve in the dielectric spectra and that

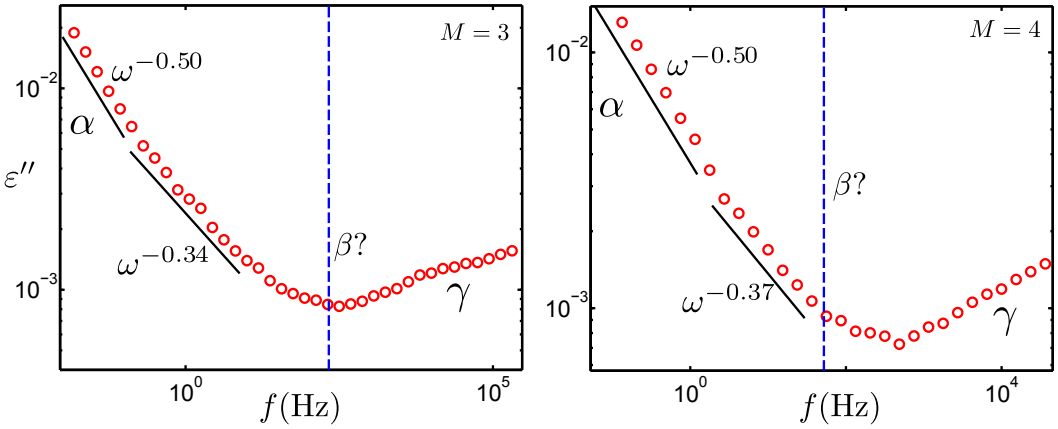

Figure 4.35: Dielectric spectra for the a) $M = 3$ and b) $M = 4$ samples taken at 123 K and 129 K respectively. The vertical dashed blue line indicates the 'expected' position of the β relaxation based on the analysis described in the text.

merges with the α relaxation for all samples except for toluene. There are several examples of other molecular glass formers that exhibit three relaxation processes, termed α, β and γ. Several relaxation processes have also been observed for polystyrene [200–204] which will be discussed in Chapter 6. Three relaxations have also been observed for *iso*-propylbenzene which is chemically similar to the $M = 3$ sample [205]. In summary, it appears that the nomenclature used to describe the observed relaxation processes for the alkyl benzenes should more appropriately be termed β relaxations for the largely 'hidden' secondary relaxation and γ relaxation for the observed secondary relaxation process for the $M = 3$, 4, 5 and 6 samples; following the standard of naming relaxations based on the order in which they occur in the spectra.

4.3.8 The excess-wing behaviour of the $M = 2$ sample.

Unlike the $M = 3$ to 6 samples, the $M = 2$ sample demonstrated a clear excess wing in the α relaxation peak also above T_g. As discussed above, one could make the assumption that the excess wing observed in the dielectric spectra is a manifestation of the merging of the α relaxation and a secondary β relaxation [69]. It is not clear what exactly determines when an α and β relaxation that approach

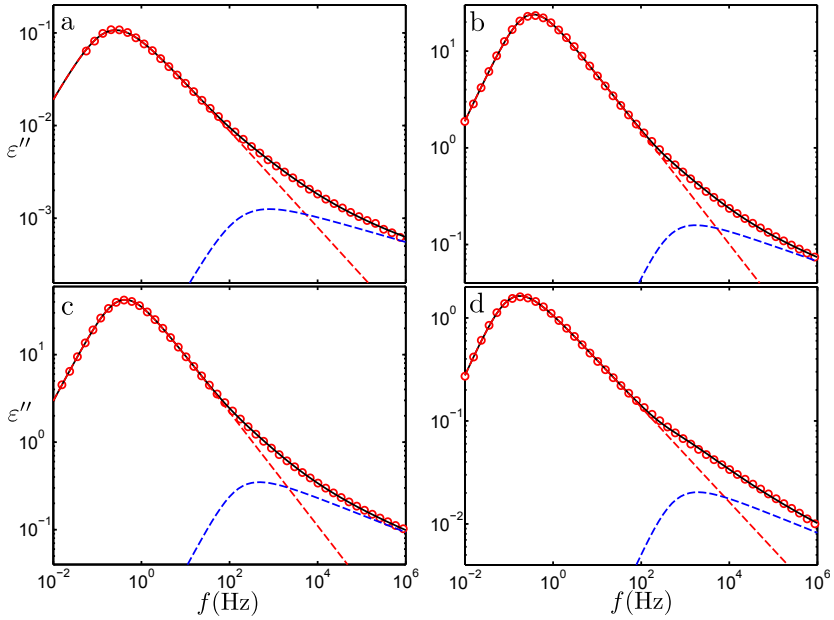

Figure 4.36: Comparison of the dielectric spectra of several different type A glass formers: a) ethylbenzene ($M = 2$) at 119 K) glycerol at 199K c)propylene carbonate at 162K d) salol at 225K. The dielectric spectra were fit using a combination of two HN functions in order to compare the strength of the α relaxation to the strength of the wing/β relaxation.

eachother in frequency will be observed as separate relaxations or as one relaxation with an excess wing. However, it makes sense that the distance in frequency between them and their relative dielectric strength must be of direct importance. To investigate this in some more detail, dielectric spectra were analysed for both the $M = 2$ sample and for three other so-called type A glass formers which also exhibit an excess-wing: glycerol, propylene carbonate and salol. The spectra are shown in Figure 4.36 and were fitted using an additive combination of two HN functions. These separate contributions are shown as dashed red (α) and blue (β) in the figure.

Through spectral analysis of these samples, the dielectric strengths of the α and β processes ($\Delta\varepsilon_\alpha$ and $\Delta\varepsilon_\beta$) were directly obtained. Values of $\Delta\varepsilon_\alpha$ and $\Delta\varepsilon_\beta$ were described using a linear fit in order to determine the dielectric strengths of the α and submerged β relaxation at T_g through extrapolation. The ratios between these dielectric strengths were then calculated and compared to the

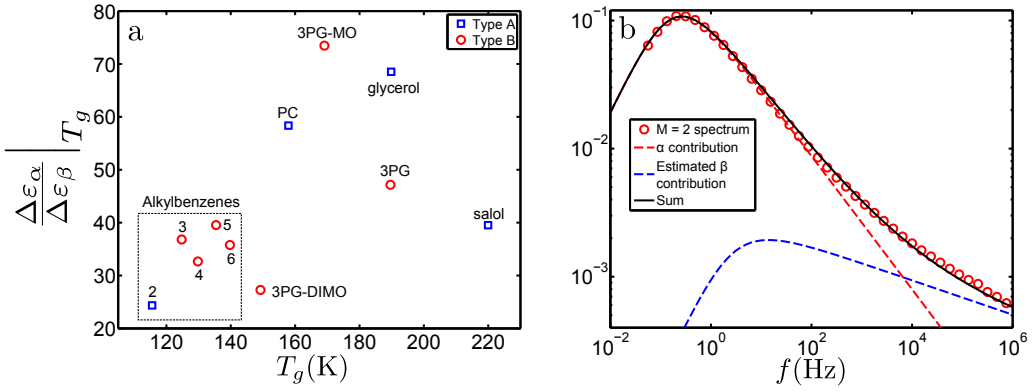

Figure 4.37: a) The ratio between the dielectric strengths for the α and β relaxations for several type A ($M = 2$ sample, glycerol, propylene carbonate (PC) and salol) and type B ($M = 3$ to 6 samples, tri-propylene glycol (3PG), tri-propylene glycol mono-methyl ether (3PG-MO) and tri-propylene glycol di-methyl ether (3PG-DIMO)) glass formers. b) Further analysis of the $M = 2$ sample as described in the text.

ratio obtained for so-called type B glass formers which demonstrate a clear (non-merged) secondary relaxation including the $M = 3$, 4, 5 and 6 samples from this series, tri-propylene glycol (3PG), tri-propylene glycol mono-methyl ether (3PG-MO) and tri-propylene glycol di-methyl ether (3PG-DIMO). The values of this ratio for the type A and type B glass formers are shown in Figure 4.37a.

The first conclusion we draw from Figure 4.37a is that the ratio appears to increase for the glass formers which exhibit higher T_g values. We also observe that the ratio for the $M = 2$ sample is similar to that of the other samples in the alkyl benzene series. In general there appears to be no quantifiable difference in the ratio for the type A or type B glass-formers which means that it is difficult, based on ratios between the α and β dielectric strengths, to predict whether an excess wing should be observed or not.

A further investigation of the behaviour of the $M = 2$ sample is shown in Figure 4.37b. Here, the dielectric spectrum at 119 K is shown. The α loss contribution is shown (dashed red line) together with an 'estimated' β loss contribution (dashed blue line). The estimated β contribution was obtained by parametrising the HN function (Equation 4.2) with estimated values of $\Delta\varepsilon$, α, β and the characteristic timescale τ_{HN}. The value of the exponent of the low frequency flank of

the relaxation, α, was taken to be the same as that of the α loss peak in order to mimic the frequency convolution of the two contributions. The value of τ_{HN} was calculated using Equation 4.6 with a peak timescale, τ^{p}_{HN} determined from the analysis shown in Section 4.3.6. The $\Delta\varepsilon$ and β values were varied such that the best description of the spectral data could be achieved. The sum of the α and estimated β contributions is shown as the solid black line in Figure 4.37b. This sum provides a good description of the data. A value of $\Delta\varepsilon = 14 \times 10^{-3}$ was used and this is in reasonable agreement with the trend in the dielectric strength for the observed γ relaxations for the $M = 3$ to 6 samples as shown in Figure 4.25a. It was also found that a value of $\beta = 0.16$ provided the best description of the data and this value is in good agreement with those obtained through both fits of the $M = 2$ spectra with the modified RB expression (Equation 4.3) and through the sum of two HN expressions. The analyses presented in this section thus further imply that the excess-wing observed for the $M = 2$ sample is likely due to a submerged secondary relaxation with similar characteristics to those observed for the observable secondary relaxation of the $M = 3$ samples.

4.4 Differential scanning calorimetry

Differential scanning calorimetry (DSC) measurements were performed on the samples in the alkylbenzene series in order to complement the data taken using dielectric spectroscopy. The samples were first supercooled to the lowest temperature attainable by the DSC and then scans at 10 K/min were performed, cycling above and below their expected glass transition temperatures. This rate of heating/cooling was chosen as it can be shown to be related to a structural relaxation timescale of 100s [138–141] corresponding to the timescale at which T_g was defined for dielectric measurements. Other authors have stated that a rate of 10K/min could also relate to a timescale of 1s rather than 100 [206]. This variation in the relation between DSC rate and τ_α could explain the difference between T_g values obtained from DSC and those obtained through analysis of dielectric data: if the probed timescale of the DSC at a rate of 10K/min is in fact related to a shorter timescale than 100s then this would lead to a higher T_g as shown in Figure 4.17a. However, for the purposes of this section it will be

assumed that the glass transition observed with DSC is related to a timescale of 100s.

4.4.1 Traces of the heat capacity

The DSC traces during heating were used to extract thermal information about the glass formers. Figure 4.38 shows the traces obtained during heating scans of the samples in the alkylbenzene series. The traces show the same systematic increase in the relevant temperature range of the glass transition shown for the τ_α data (Figure 4.16). The $M = 3$ to 7 samples show a very systematic increase in the onset temperature of the characteristic step in C_p relating to the glass transition. As observed (to a certain extent) in the τ_α data, the glass transition step for the $M = 1$ sample appears to occur at a slightly higher temperature than the $M = 2$ sample. The samples have a very similar absolute value for C_p within the glass (i.e. before the step) and demonstrate enthalpy relaxation peaks of similar size.

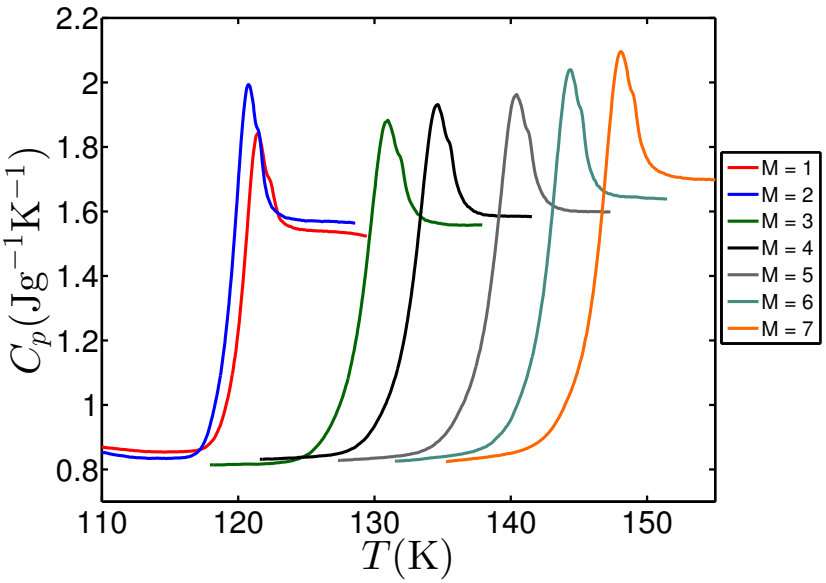

Figure 4.38: DSC traces for the alkylbenzene series. The traces shown are of increasing temperature at a rate of 10 K/min.

4.4.2 The 'step height' of the glass transition

The values quantifying the step height, ΔC_p, increase with increasing molecular weight in a systematic fashion except for the $M = 2$ sample which shows a higher value, as shown in Figure 4.39a. As the step in C_p at the glass transition is related to the release of degrees of freedom [120] it follows that a larger ΔC_p relates to a larger increase of entropy at the glass transition [207].

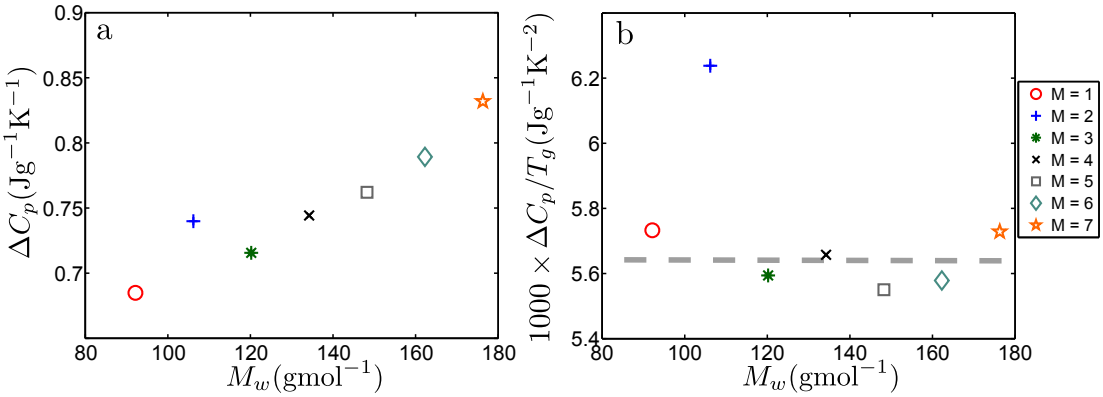

Figure 4.39: a)ΔC_p calculated from the DSC traces shown in Figure 4.38 and b) rescaled by T_g.

The isobaric heat capacity is related to the entropy through the relation,

$$C_p = T \left(\frac{\partial S}{\partial T} \right) \Big|_p \tag{4.15}$$

The difference in the heat capacities at T_g is given by ΔC_p as shown in Figure 4.39a. We can therefore reformulate Equation 4.15 in order to define ΔC_p as a function of T_g and the rate of change of entropy in both the liquid and glass [208] as follows:

$$\Delta C_p = T_g \left[\left(\frac{\partial S^{liquid}}{\partial T} \right) \Big|_{T_g} - \left(\frac{\partial S^{glass}}{\partial T} \right) \Big|_{T_g} \right]_p . \tag{4.16}$$

The difference in the temperature dependence of entropy in the liquid and glass can be analysed by rescaling ΔC_p by T_g. Such a rescaling is shown in Figure 4.39b. Rescaling the values in this fashion removes the trend and normalizes the ΔC_p values to a reasonably fixed value for the $M = 1$, 3, 4, 5, 6 and 7

samples, as indicated by the dashed guide to the eye in Figure 4.39b. This implies that the difference in temperature dependence of the entropies in the glassy and liquid states is relatively fixed for these samples. Interestingly, the value for the $M = 2$ sample does not rescale in this manner suggesting that the difference in the temperature dependence of the entropy is higher in this sample in comparison to the others.

Another indication from this analysis is that the trend shown in Figure 4.39a could be related to the linear increase of T_g shown in Figure 4.17a. Furthermore, as T_g is related to the dynamic fragility parameter m, the observed trend in Figure 4.39 could be related to the fragility. The difference in the glassy and crystalline heat capacities was defined to be a measure of the so-called thermodynamic fragility by Angell [91]. This idea was formulated based on the premise that fragile glass formers should show large changes in their response at T_g and that strong glass formers would show relatively small changes [122]. It can be shown that the so-called excess heat capacity, ΔC_p can be related to the kinetic fragility parameter, m [121]. It has also been suggested that one would expect a strong correlation between the thermodynamic and kinetic descriptions of fragility for molecular glass formers [122]. Indeed, we see a strong positive correlation of ΔC_p with increasing molecular weight for the $M = 3$ to 7 samples and similar correlations were observed for the m parameters and also the S parameters obtained through linearisation of the τ_α data. We also observed that the $M = 2$ sample does not follow this trend as was observed in the variation of the m and S parameters. However, the $M = 1$ sample does seem to follow the observed linear trend in ΔC_p, contrary to what was observed in the dynamic definitions of the fragility.

4.4.3 The width of the glass transition step

The width of the glass transition region, ΔT, is defined in this work as the difference between the onset and offset of the characteristic step in C_p. This definition of the width has also been attributed to the fragility of the material in question [209–211] although the validity of this relation has been questioned previously [212]. It has been assumed that the onset temperature of the glass transition

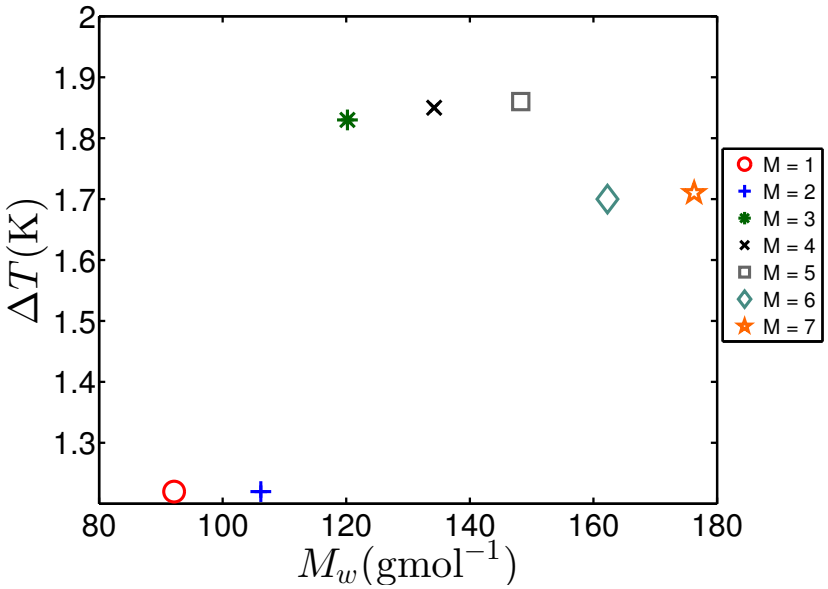

Figure 4.40: ΔT calculated from the DSC traces shown in Figure 4.38

step is related to a relaxation timescale of around 100s and that the offset temperature is related to a timescale of around 1s and therefore the difference in these temperatures could be related to the definition of the fragility parameter, m. Within the confines of these assumptions, the implication is that the more fragile a glass forming liquid is, the smaller ΔT would be.

Values of ΔT obtained through analysis of the DSC traces for this series of samples are shown in Figure 4.40.

It is clear from this figure that the widths are significantly smaller for the $M = 1$ and $M = 2$ samples. If the link between fragility and the width of the glass transition presented in the literature is correct then these results correspond reasonably well with the larger values of the dynamic fragility parameters observed for these two samples. The ΔT values observed for the other samples in the series are less conclusive but it could be said that there is a slight negative correlation with increasing molecular weight indicating that the fragility for these samples increases with increasing molecular weight: a conclusion also drawn from the corresponding m parameters.

4.4.4 Excess entropy

We will now consider the entropy for the samples in the alkylbenzene series. Microwave studies of the $M = 2$, 3 and 4 samples conducted by Maté *et. al.* have shown that the number of stable molecular conformers for these samples increase with increasing molecular weight: the determined number of stable conformers were 1, 2 and 4 respectively [213] in this study. These results correspond well to theoretical predictions for the number of conformers for the studied samples [214–216]. The implication of these results is that if the number of conformers increases with increasing tail length, it is likely that also the total liquid configurational entropy should increase. Moreover, since configurational entropy is a key element in many theoretical descriptions of supercooled liquids [217], it is very interesting to determine how the entropy varies in the alkylbenzene series as the glass transition is approached.

In order to achieve this for the alkylbenzene series, an integration of the DSC traces of C_p was performed. The difference between the entropies at two different temperatures can be determined from the heat capacity using the following equation [130]:

$$S(T) - S(T_0) = \int_{T_0}^{T} \frac{C_p}{T}\, dT \tag{4.17}$$

Therefore, in order to determine the entropy at a certain temperature, $S(T)$, one has to know the entropy at the reference temperature, T_0. A well established method of calculating $S(T)$ in the past has been to choose a reference temperature of 0 K and then assume, based on the third law of thermodynamics, that the entropy at 0 K must also be zero [123]. Although this reasoning is sound, the method requires some knowledge of the variation of C_p to very low temperatures in order to make appropriate extrapolations; such examples are available in the literature for a selection of low molecular weight alkylbenzenes measured with low temperature calorimetry [123, 160, 161], but not for the longer alkyl tail-length samples. Also, due to the temperature restrictions of the calorimeter used in this study, this method is not appropriate as we can not determine C_p sufficently far below T_g in order to make a constructive extrapolation of the glassy behaviour to 0 K.

Rather than using a reference temperature of absolute zero, a similar analysis of the entropy can be performed by choosing the melting point or temperature of fusion, T_{fus}, instead [78]. The entropy of fusion can be calculated if the enthalpy of fusion, ΔH_{fus}, is known:

$$\Delta S_{fus} = \frac{\Delta H_{fus}}{T_{fus}} \tag{4.18}$$

In most cases, the enthalpy of fusion, ΔH_{fus}, could not be determined from the DSC traces either due to the proximity between the melting peak and a crystallisation peak, observed after heating the samples above the glass transition, or due to the absence of a melting peak altogether. Also, to determine a proper value of the enthalpy of fusion either one needs to know that one creates a fully crystalline sample or alternatively quantiatively determine the degree of crystallinity. Thus, in order to make the most constructive comparison, values for ΔH_{fus} and the melting point, T_{fus}, were taken from the literature. The values obtained are shown in Table 4.5.

The excess entropy S_x is usually defined as the difference between the entropies in the liquid and crystalline states: $S_x = S^{liquid} - S^{cryst}$ and the total entropy S_{tot} in the liquid can be thought of as the combination of the vibrational and configurational entropies [2]. It has been assumed in the past that when a supercooled liquid forms a glass, the configurational component of the entropy is 'lost' and therefore the total entropy in the glassy state is purely vibrational [228, 229]. If the assumption that the vibrational contributions to the entropy in the crystalline and supercooled liquid states are the same [2] then one can say that S_x is equivalent to the configurational entropy, S_c which is lost (or gained) through the glass transition. However, this conjecture is now widely assumed to be incorrect [2, 57, 230] since the vibration contributions of the crystal can not be easily extrapoltated into the liquid state. However, the excess entropy is still largely a probe of the configurational part of the entropy even though we here, for the purposes of the following analysis, will consider the excess entropy as a separate entity to the configurational entropy. S_x can be determined through integration of the difference between the heat capacities in the liquid state and

Sample	ΔH_{fus} (J/g)	T_{fus} (K)	Reference
Toluene	72.02	178.17	[218]
	72.02	178.15	[161]
	71.84	177.95	[219]
	71.07	178.00	[220]
	71.85	178.00	[221]
Ethylbenzene	86.56	178.17	[218]
	86.33	178.08	[78]
	86.52	178.15	[222]
	86.30	178.17	[223]
	86.28	178.20	[221]
	86.30	178.00	[224]
Propylbenzene	77.16	173.65	[218]
	77.11	171.60	[160]
	77.28	173.60	[225]
Butylbenzene	83.66	185.18	[218]
	83.89	185.14	[160]
	83.59	185.31	[221]
	81.80	184.61	[226]
Pentylbenzene	102.90	194.90	[218]
Hexylbenzene	113.50	206.15	[218]
Heptylbenzene	123.60	225.10	[227]

Table 4.5: Table showing values for ΔH_{fus} and T_{fus} obtained from the literature for the alkylbenzene series.

the crystalline state: $\Delta C_p^x = C_p^{liquid} - C_p^{cryst}$ [75]. Equation 4.17 then becomes:

$$S_x = \int_{T_0}^{T} \frac{\Delta C_p^x}{T}\, dT \tag{4.19}$$

A similar calculation can be performed in order to determine the difference in entropy between the glassy and crystalline states. This can be achieved by using the difference in heat capacities of the glass and crystalline states in a similar fashion to Equation 4.19 [75]. This entropy could be approximated to be the difference in vibrational entropies of the glass and crystal states [78] although one would still expect a glass former to have some configurational contribution to its entropy below T_g due to the fact that the constituent molecules are still able to rearrange in the glassy state [231].

The change in the excess entropy of the samples in the alkylbenzene series in the temperature range probed with the DSC experiments was determined using the entropy of fusion as a reference point in the same way as presented by Yamamuro *et. al.* [78] (it should be noted that in their original calculation, the authors assume that the excess entropy was equivalent to the configurational entropy.):

$$S_x(T) = \Delta S_{fus} - \int_{T}^{T_{fus}} \frac{C_p^{lq}(T) - C_p^{gl}(T)}{T}\, dT - \int_{0}^{T_{fus}} \frac{C_p^{gl}(T) - C_p^{cr}(T)}{T}\, dT \tag{4.20}$$

The third term in Equation 4.20 is a correction due to the difference in vibrational entropy between the glass and the crystal states. As stated previously, the heat capacity of the samples could not be determined down to 0 K and although data exists in the literature for lower temperatures than were measured here the glassy states formed in these experiments are not the same as the states formed within our measurements [194]. Indeed, due to the amorphous nature of glasses our samples might thus show different heat capacities compared to those in the literature. Thus, there is no real justification for using literature data to extend the data taken within the experiments presented here. However, the difference between the entropies in the crystalline and glassy states is generally very small ($< 5\%$) compared with the entropy determined through the difference between

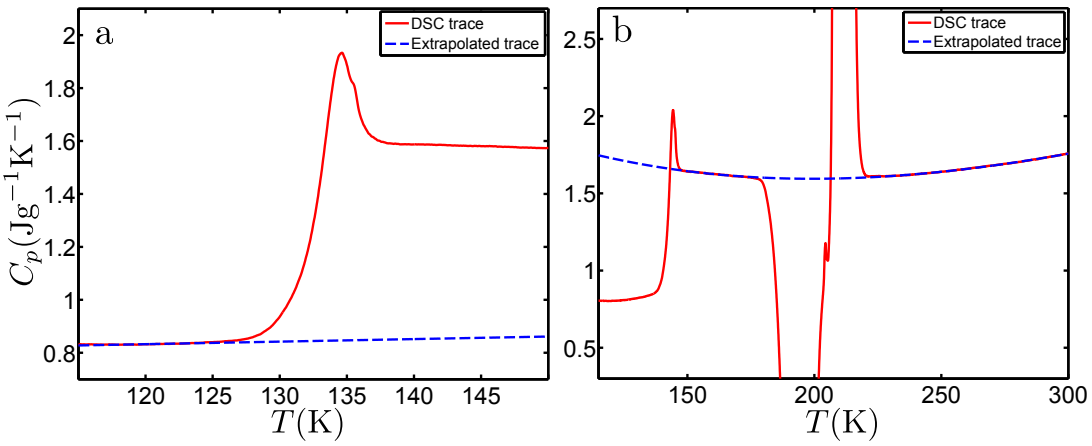

Figure 4.41: Figure showing the extrapolated a) glass behaviour for the $M = 4$ sample and b) liquid behaviour for the $M = 6$ sample.

the heat capacities of the liquid and glassy states and and has therefore been neglected in this calculation [78].

In order to calculate the second term in Equation 4.20, the glassy and liquid behaviours of the samples were extrapolated to cover the relevant temperature ranges. The extrapolation of the glassy behaviour to the melting point, T_{fus}, was approximated with a linear fit to the low temperature (below T_g) C_p data. An example of this extrapolation is shown in Figure 4.41a for the $M = 4$ sample, where the blue dashed line indicates the extension of the glassy behaviour to higher temperatures. Yamamuro *et. al.* [78] present a more detailed approach to this extrapolation by fitting their low temperature heat capacity data to a function containing contributions for the translational lattice vibration, rotational vibration, methyl-group rotation, intramolecular vibration and a correction between the heat capacities of constant pressure and constant volume.

The liquid behaviours of the samples were extrapolated based on a polynomial fit to a combination the liquid data obtained for the samples just above T_g (before a melting/crystallisation peak) and above T_{fus}. This extrapolation is similar to an example in the literature where the extension of data was necessary due to crystallisation [2, 232] of the sample at temperatures just above T_g [123]. An example of such an extrapolaton is shown in Figure 4.41b for the $M = 6$ sample.

The determined excess entropies as a function of temperature determined us-

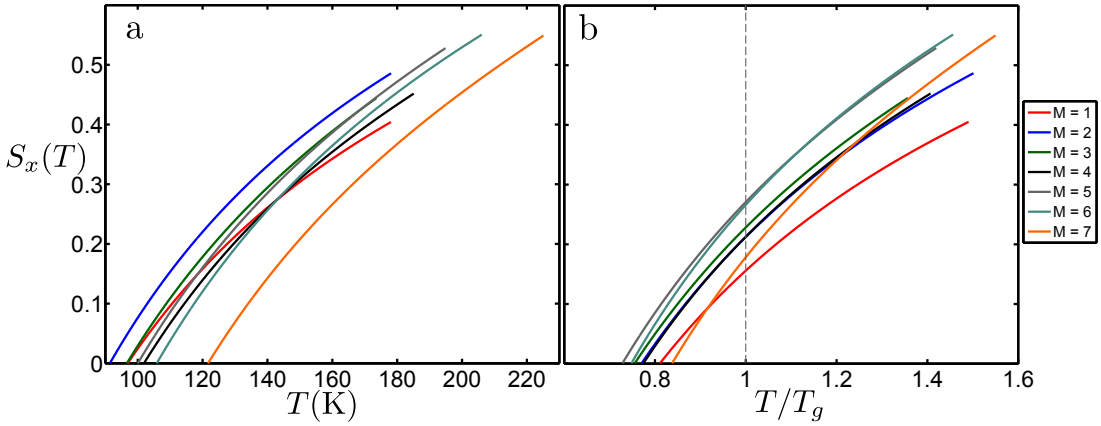

Figure 4.42: Figure showing the entropy values as calculated from Equation 4.20 plotted against a)T and b) T/T_g.

ing Equation 4.20 for the alkylbenzene samples are shown in Figure 4.42. S_x decreases in a similar manner for all samples with decreasing temperature, leading to an extrapolated value of zero at a certain temperature. The fact that the configurational entropy decreases to zero indicates an 'entropy crisis' as predicted by Kauzmann [16], whereby the entropy of a supercooled liquid decreases at a faster rate than what would be expected for the equivalent crystal (in which the entropy tends to zero as the temperature tends to zero). Therefore the temperature at which S_x reaches zero in Figure 4.42 is equivalent to the Kauzmann temperature, T_K at which an ideal thermodynamic glass transition have sometimed been speculated to exist [17], as postulated by Gibbs and DiMarzio [217]. We find that the determined T_K values increase with increasing molecular weight. If the conjecture that $S_x \cong S_c$ is correct, then the Adam-Gibbs model implies that T_K is equivalent to the temperature at which the structural relaxation timescale, τ_α, tends to infinity, T_0 in the VFT equation (Equation 4.7) [2, 233]. Values for both T_K (obtained from Figure 4.42a) and T_0 (from fits of the VFT equation to the τ_α data obtained from dielectric spectroscopy) are compared in Table 4.6.

There is reasonable agreement between values of T_K and T_0 for the lowest tail-length (samples $M = 1$ to 4) but this correlation breaks down for longer tail-length samples. Tanaka also observed this breakdown for a selection of glass forming liquids [77]. It was observed that the ratio T_K/T_0 increases from a value of unity (indicating perfect correlation) with decreasing fragility (characterised in

M	T_K(K)	T_0(K)
1	91.5	96.6 ± 0.6 [33]
		101.2 ± 0.6 [55]
2	91.5	90 ±0.1
3	96.7	95.6 ±0.7
4	102.0	104.3 ±0.6
5	100.1	113.9 ±0.2
6	105.9	121.2 ±0.9
7	121.7	127.0 ±0.6

Table 4.6: Table showing the comparison between the values of the Kauzmann temperature, T_K as obtained from Figure 4.42a and values of T_0 obtained through fitting of the VFT equation to the τ_α data obtained through dielectric spectroscopy.

this case by the strength parameter, D, from the VFT equation). We have already seen that the fragility (defined in both the kinetic and thermodynamic senses) appears to increase with increasing molecular weight and it is clear that T_K/T_0 decreases with increasing molecular weight, therefore confirming the results seen by Tanaka.

In order to aid further comparison between the samples, the S_x data obtained were rescaled by T_g, the result of which is shown in Figure 4.42b. S_{T_g} for the alkylbenzene samples were obtained by making a cut in Figure 4.42b, denoted by the dashed line. These values are shown in Figure 4.43. The S_{T_g} values for the $M = 1$ to 6 samples show a systematic growth with molecular weight and could be interpolated with a linear fit as denoted by the black dashed line in the figure. The trend indicates that this measure of the entropy of the alkylbenzene series increases with increasing molecular weight. Interestingly, a linear trend of the total entropy, S, with molecular weight for the alkylbenzenes in the gas phase has also been observed [234] and the entropy values for the series at 293 K are shown in the inset of Figure 4.43 for comparison. It is unclear why the $M = 7$ sample does not follow the same trend as the other samples. Of course, the determination of the absolute value of S_x relies on the values of ΔH_{fus} which are obtained from the literature. We were unable to fully crystallise any of the samples in this series and so the values of ΔH_{fus} could not be confirmed. One possible reason for the discrepancy is therefore that the literature value of ΔH_{fus}

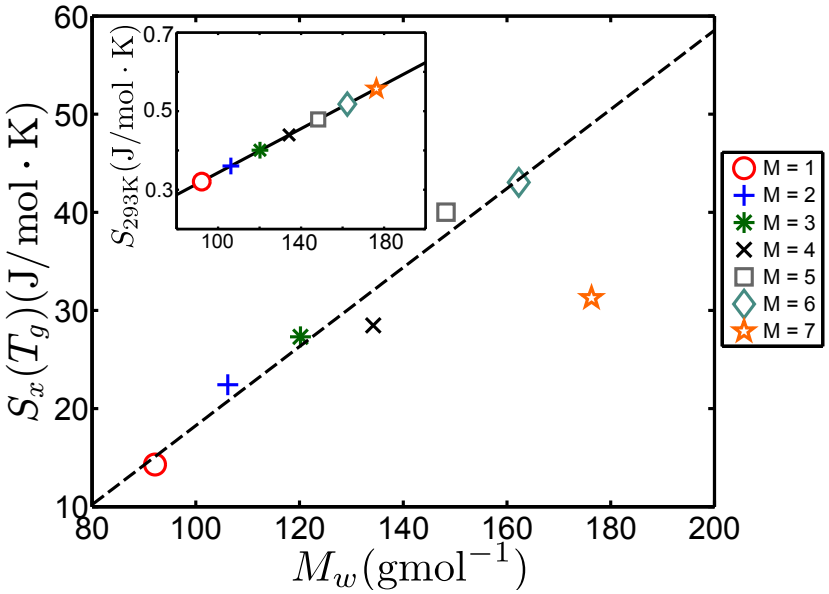

Figure 4.43: Figure showing the entropy values for the alkylbenzene series at T_g. The dashed black line is a linear fit to the M = 1-6 data.

is not accurate. However, we note that we expect any systematic behaviour observed for short alkyl chains to break down for long enough chains since at some point the alkyl-chains will stop acting essentially as a modification of phenyl ring and start dominating the behaviour which inevitably will lead to new behaviour.

It can be shown that through drawing an analogy between the Adam-Gibbs and VFT descriptions of the development of the structural relaxation timescale with temperature, the dynamic fragility parameter, m, could be related to ΔC_p and thus the excess entropy, S_x at T_g [121, 235]. Therefore, the systematic increase of S_x can be linked to the similar increase in the dynamic fragility of the glass formers in this series, quantifying that these separate measures of the fragility are, to a certain extent, equivalent descriptions of the change in dynamics as the glass transition is approached.

4.4.5 Testing the validity of the Adam-Gibbs expression.

One explanation of the drastically increased structural relaxation timescales as the glass transition is approached is the theory presented by Adam and Gibbs

[76] introduced in Chapter 1. This theory attributes the increase of τ_α to 'cooperatively rearranging regions' (CRRs), the size of which increases such that the number of configurations available to a system in order to relax decreases, thus the configurational entropy is closely related to the properties of a CRR. The theory predicts the behaviour of τ_α in the following fashion:

$$\tau_\alpha = \tau_0 e^{\frac{A}{TS_c(T)}} \tag{4.21}$$

It has already been stated that one condition of the Adam-Gibbs entropy based theory is that $S_x \cong S_c$ and that this implies that the thermodynamic and kinetic definitions of the 'critical' temperatures, T_0 and T_K should be equivalent.

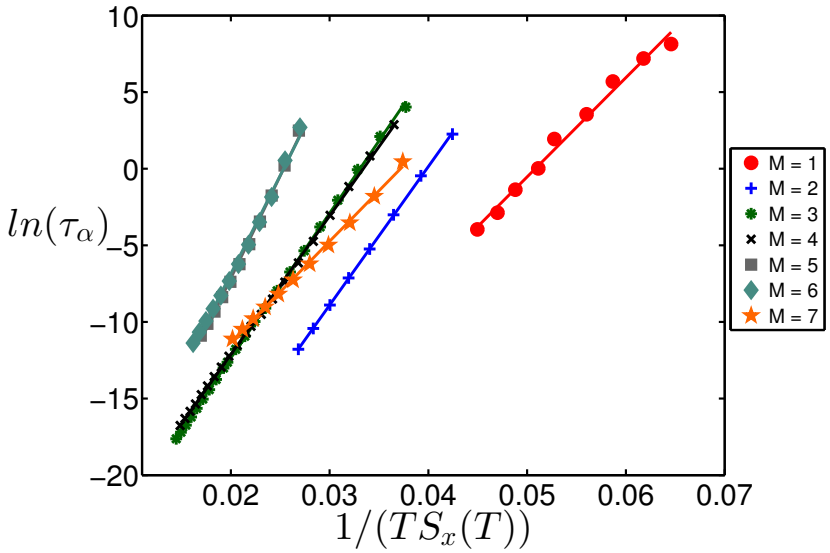

Figure 4.44: Plot of τ_α against $1/TS_x$ in order to test the Adam-Gibbs equation. If the relationship holds, the resulting plot should be a straight line with a positive gradient, A.

We have observed that the T_0 and T_K values correspond well to each other for the shorter tail-length samples in this series but this equivalence breaks down for the higher molecular weight samples, suggesting that perhaps the Adam-Gibbs equation would not be a good description of the development of the structural relaxation timescale with decreasing temperature. In order to test the theory, Equation 4.21 was fit to the τ_α data obtained from dielectric spectroscopy for all

the samples in the series. The configurational entropy component in the equation was assumed to be analogous to the excess entropy, as is required in order for the theory to be valid [2]. If we take the natural logarithm of Equation 4.21 then the τ_α should follow a linear behaviour with a positive correlation when plotted against $1/(TS_x(T))$. Figure 4.44 shows the result of the plotting of the data in this manner and interestingly we see that the τ_α values follow this expected linear trend and that the data are well described by Equation 4.21 suggesting that the entropy is an important property in a fundamental description of glass-formation.

4.5 Conclusions

In this chapter, results from the measurement of a series of alkylbenzenes using both Broadband Dielectric Spectroscopy and Differential Scanning Calorimetry have been presented. In a qualitative sense, there are two different scenarios that we could expect from increasing the length of an alkyl tail. On one hand we might expect that as the length of the tail increases, the tail could act to plasticise the bulk material, leading to a decrease of the glass transition temperature with increasing tail length. This effect has been observed series of polymers for which the length of a side chain is increased, for example the poly(n-alkyl methacrylates)[51]. On the other hand, the increase of the tail length could simply mean that the effective size of the molecules is bigger meaning that the glass transition increases proportionally to the length of the alkyl tail. We find a range of evidence, presented in this chapter, which suggest that the second scenario is the most likely.

We observe that values for the glass transition temperature, T_g, obtained through analysis of the structural relaxation timescales, τ_α and the DSC traces show an increase with increasing alkyl tail-length for the $M = 3$ to 7 samples. This suggests that the tails themselves do nothing to plasticise the bulk material. Furthermore, previous research has suggested that the T_g of simple molecular glass formers in related to the effective hard sphere radius, σ_0, of the constituent molecules [146, 150]. We can infer that σ_0 increases with increasing chain length for the $M > 2$ samples. This suggests that the alkyl tails are reasonably 'stiff' in this series of samples, as the effective volume of the molecules appears to be

systematically increasing with the length of the tail. In terms of glass formation, this means that as the alkyl tail-length increases, the molecules become more susceptible to dynamic arrest and therefore T_g is higher. The lowest tail-length samples, $M \leq 2$, appear to have similar values of T_g. The implication of this is that the effective size of the $M = 0$, 1 and 2 samples are similar and that the alkyl tail has no effect on the structural relaxation of the $M = 1$ and 2 samples.

Although we cannot state precisely what the dynamic processes involved in the α relaxation are, we can imagine that bulk structural relaxation of the glass formers in this series are likely to be largely dependent on the rearrangement of benzene rings because they are the bulkiest part of the molecules. For the $M = 1$ and 2 samples, it is possible that the alkyl tail is too short to effect the rearrangement of the benzene rings and therefore T_g is unaffected. However, for tail lengths longer than 2 units we might begin to see an effect on the dynamics of the benzene rings.

Systematic variations as a function of tail-length were also observed in the parameters describing the glass forming fragility of the samples in this series. The kinetic fragility and the thermodynamic fragility of the samples in this series were both calculated in several different ways. The kinetic fragility was determined through use of the strength parameter in the VFT expression, D, the m parameter relating to the gradient of the VFT fits of the τ_α data at T_g and the S parameter, obtained through linearisation of the τ_α data [31]. The thermodynamic fragility was inferred from the trends seen in the difference in specific heat capacity between the glassy and liquid states, ΔC_p, and the width of the step in C_p, ΔT. It was also inferred from the increase in excess entropy as determined through integration of the C_p traces. These separate measures of fragility all show similar trends for the $M = 3$ to 7 samples, increasing with increasing tail-length. In terms of glass formation, this means that not only does the glass transition occur at higher temperatures for samples with a longer tail but that the structural relaxation timescale increases at a faster rate with decreasing temperature. This again suggests that longer alkyl tails significantly hinder the structural relaxation process. The thermodynamic and dynamic definitions of fragility differ for the lowest tail-length samples, again suggesting a change in behaviour for these samples.

The nature of the frequency response of the structural α relaxation as a function of temperature was captured with BDS. Interestingly, although systematic variations with alkyl tail-length were observed for T_g and fragility, the overall variation of shape of the α loss peak was similar, regardless of tail length. We observe that, in general, there is a narrowing of the loss peak with increasing temperature. If we accept the connection between the shape of the response peak and dynamic heterogeneity [44], this suggests that the distribution of timescales of the structural relaxation also narrows.

Indications of secondary relaxation processes were also found. Secondary relaxations, persisting at $T < T_g$, were clearly observed in the dielectric spectra for the M = 3-6 samples and a secondary relaxation has also been observed for the $M = 1$ sample previously [55, 61]. The $M = 2$ sample demonstrated an excess-wing behaviour of the α loss peak. Through further analysis it was determined that the excess-wing was likely due to the manifestation of an underlying secondary process with similar shape parameters and timescales of the secondary process observed for the M = 3-6 samples. The timescales of this observed process for the M = 3-6 samples were very similar. This suggests that this relaxation process is relatively unaffected by alkyl tail-length. However, the timescales of this process for the $M = 1$ and $M = 2$ samples are slower than those of the other samples. This could be indicative of the physical mechanism responsible for this relaxation process. For example, we could suggest that the this mechanism is due to a characteristic motion of the ends of the alkyl-tails. For the $M = 1$ and 2 samples, the motion of a tail end would clearly be more hindered by the benzene ring and thus the relaxation timescale is slower. For the longer tail-length samples (M = 3-7), motion of the tail ends is no longer hindered by the benzene rings, meaning that the relaxation timescale is faster. The fact that the timescales are similar for the M = 3-7 sample could indicate a limiting timescale for the tail ends.

A peak was observed in the amplitudes of the α relaxation process for the samples which was thought to suggest the merging of an underlying secondary relaxation with the α relaxation. Acting on this assumption, 'expected' τ_β parameters were calculated using the relationship between the activation energy, E_A, and T_g suggested by Kudlik [55]. It was found that the dielectric spectra for

the $M = 3$ and $M = 4$ samples at low temperatures $T < T_g$ show indications of an excess-wing. The expected values of τ_β for these samples correspond with the frequency at which this wing is manifested, suggesting that it was a manifestation of an underlying β process.

The expected values of τ_β increase (at a fixed temperature) with increasing chain length. This suggests that the α and β relaxations become less separated with increasing molecular weight, which could explain the clear secondary relaxation peak observed for the $M = 1$ sample and provide another explanation for the excess-wing observed for the $M = 2$ sample. In polystyrene, the observed β relaxation has been attributed to characteristic motions of the benzene ring [200–202]. We could imagine a similar scenario occurring in the alkylbenzene series: as the length of the alkyl tail increases, it becomes more difficult for the benzene ring to move and therefore the timescale for the β relaxation increases.

4. RESULTS I: RELAXATION DYNAMICS IN A SYSTEMATIC SERIES OF SIMPLE MOLECULAR GLASS FORMERS

Chapter 5

Polymer dynamics and the influence of chain-length

In Chapters 6 and 7, results will be presented relating to two different series of glass formers characterised by the polymerisation of styrene and $\alpha-$methylstyrene, respectively. In order to describe the physics and dynamics of these systems correctly, it is first necessary to introduce the typical nomenclature used for polymeric systems. This nomenclature will be introduced together with a discussion on polymer dynamics and some key coarse-grained approaches used to describe polymer behaviour. Following this, the variation of various properties (such as T_g and various definitions of fragility) associated with the glass transition of polymers with varying chain-length will be discussed.

5.1 What is a polymer?

The word *polymer* is constructed from the Greek words *poly*, meaning many, and *mer*, meaning part [236]. The 'parts' of a polymer are repeating units termed 'monomers' and the process which covalently binds these monomers together to create polymers is termed polymerisation. Molecules consisting of a 'few' monomer units bound together are termed 'oligomers'.

Different forms of polymerisation can lead to variations in the steric order of the resulting polymer. For example, in PS the benzene ring could be placed either side of the backbone of the polymer. This variation in the steric order is

termed the 'tacticity' of the polymer [237]. Polymers in which the sustitutents attached to the backbone are all situated on the same side are called *isotactic*, those with substituents alternating between the two sides are called *syndiotactic* and polymers with no steric order are said to be *atactic*. The steric configuration of polymers does not change after synthesis unless the covalent bonds of the polymer are broken [18, 236].

The polymerisation process does not usually lead to monodisperse polymers with a unique degree of polymerisation [237] and thus a polymeric sample will display a certain level of polydispersity characterised by a distribution of molecular weights, $p(M)$, where M is the weight of a single polymer chain. The nature of $p(M)$ can be obtained through size exclusion chromatography [236]. A polymeric sample can be described by either the *number*, M_n, or *weight*, M_w, averages of the distribution, $p(M)$ [18, 236, 237]:

$$M_n = \sum_M p(M)M \tag{5.1a}$$

$$M_w = \frac{1}{M_n}\sum_M p(M)M^2 \tag{5.1b}$$

The width of the distribution of molecular weights can be described using the so called polydispersity index: $d = M_w/M_n$. Chain type polymerisations, such as anionic polymerisation, yield particularly narrow distributions and thus the degree of polymerisation can be reasonably well defined [237].

5.2 The Coarse-Grained Polymer Chain

When discussing the dynamics of a simple series of molecular glass formers, such as the alkylbenzene series which were presented in Chapter 4, the length-scale variation across the series is relatively small. However, for polymeric chain length series of the type demonstrated in Chapters 6 and 7, the relevant length-scales range from those similar to the alkylbenzenes to those with a much higher molecular weight. Generally, above a certain length scale, the dynamic and structural properties of polymers can be discussed at an effectively lower resolution and

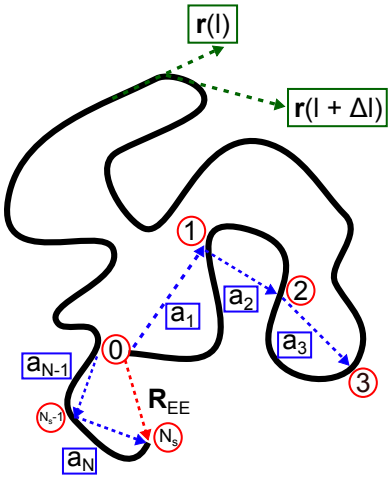

Figure 5.1: Diagram showing the coarse graining of a polymer. Details of the description of this worm-like chain are in the text.

thus the microscopic chemical nature (for example the bonds between constituent atoms and the angles between these bonds) can be omitted [237]. This is a useful approximation to make as such an analysis does not depend on the material specifics of the polymer and therefore a more general description of the behaviour of polymer chains can be achieved. The point at which the 'length scale of interest' for the polymeric samples changes will be discussed in detail in the results pertaining to those series.

Figure 5.1 depicts a polymer chain as a coarse-grained worm-like chain. The variation of the local chain direction can be described by the unit vectors $\mathbf{r}(l)$ (represented by the green arrows in Figure 5.1), where l is a curvilinear coordinate running along the length of the chain [237]. Firstly, we can consider the smallest length scale in such a coarse-graining of the polymer chain, namely the internal chain flexibility. The bond length between carbon atoms, l_b, in a hydrocarbon based polymer remains fixed at all times to 0.154 nm with an angle of 70.53° between successive bonds [238]. Although the angles between bonds are fixed, there is a certain freedom of rotation of the carbon atoms (and any side-chains attached to them) termed the *internal rotation* of the polymer chain. This allows the carbon atoms and any attached atoms to rotate about the chain axis between positions with local energy minima. The reference position, to which the rotation angle ϕ is defined, is termed the *trans* position, which is in the plane specified

by the preceding three carbon atoms [238]. For simple symmetric polymers, two energy minima exist for $\phi = \pm 120°$, and these are termed *gauche* positions. Different conformations of the polymer defined by these rotational states are termed *rotational isomers*. The energy difference between the trans and gauche positions is related to the flexibility of the chain and the average length of a sequence of trans or gauche carbon atoms is defined as the persistence length, l_p. This is related to the energy barrier between the rotational states, ΔE [238]:

$$l_p = l_b e^{\frac{\Delta E}{k_B T}} \tag{5.2}$$

We can also consider the so-called 'orientational correlation function', K_{or} which describes the correlation between two different chain directions separated by a distance, Δl. This correlation function can be constructed as an ensemble average of all possible chain conformations and their statistical weights [237]:

$$K_{or}(\Delta l) = \langle \mathbf{r}(l)\mathbf{r}(l + \Delta l) \rangle \tag{5.3}$$

As the chain has a finite flexibility, K_{or} decays to 0 over large length scales. One can also define the persistence length as the point at which the correlation function has decayed to $1/e$ [18] or the integral width of K_{or} [237]. In this definition of the persistence length is the length scale over which 'memory' of the orientation of a bond does not exist for future bonds. This value of l_p for a melt of PS ($M_w = 117000$) was determined by Brûlet *et. al.* [239] to be 9.2Å.

To further coarse-grain the worm-like chain, which represents a polymer, in order to describe the properties of the chain as a whole, the chain can be split into N_s uniformly spaced sub-chains described by the sequence of vectors $(a_1, a_2, a_3, \ldots, a_{N-1}, a_N)$ (represented by the blue arrows in Figure 5.1) connected by nodes $(1, 2, 3, \ldots, N-1, N)$ (represented by the red circles in Figure 5.1). The length of the sub-chains must be larger than the persistence length, l_p, such that there are no orientational correlations between successive sub-chains. In such a manner, the polymer chain can be thought of as a Gaussian random walk, with a mean segment length or step size a_s [238]. The distance between nodes i and

j, $\mathbf{d}_{ij}$ is defined as [237]:

$$\mathbf{d_{ij}} = \sum_{k=i+1}^{j} a_k \tag{5.4}$$

The end-to-end distance, R_{EE}, or the distance between nodes 0 and N as depicted in 5.1 can also be defined:

$$\mathbf{R_{EE}} = \sum_{k=1}^{N_s} a_k \tag{5.5}$$

The distribution function of R_{EE} is Gaussian in nature and is isotropic, thus only depending on the absolute magnitude of R_{EE} [237]. We can now relate the mean squared end-to-end distance, $\langle R^2 \rangle$, to the mean segment length, a_s and the number of segments, N_s. $\langle R^2 \rangle$ is a measured of the size of the ideal polymer chain [18, 237, 238].

$$\langle R^2 \rangle = N_s a_s^2 \tag{5.6}$$

The choice of nodes and vectors a used to describe the polymer chain is somewhat arbitrary, meaning that many different combinations of the positions of the nodes and the mean segment length can be made. The only caveat to the choice of N_s or a_s is that they must yield the same value of the root-mean-squared end-to-end distance, $\sqrt{\langle R^2 \rangle}$. The arbitrary nature of the choice of N_s and a_s can be removed by imposing the second condition that the length of the fully extended chain R_{max} must be related to N_s and a_s in the following manner [237]:

$$R_{max} = N_s a_s \tag{5.7}$$

This means that the 'real' chain agrees in both size (as implied by Equation 5.6) and contour length. We can now substitute a_s in both Equations 5.6 and 5.7 for the so-called Kuhn length, a_K which is a unique value for the length of a segment of the polymer chain. The persistence length characterises the 'stiffness' of the chain at a more local length scale whereas the Kuhn length characterises the stiffness of the entire chain: stiffer chains have a higher value of a_K [237].

Another related quantity is the characteristic ratio, C_∞ which was introduced by Flory.

$$C_\infty = \frac{\langle R^2 \rangle}{N a_b^2} \tag{5.8}$$

Here, a_b^2 is the sum of the squares of the lengths of the backbone bonds contained in one monomer unit and N is the degree of polymerisation. C_∞ scales with the degree of polymerisation for lower values of N but tends to an asymptotic value at large N. If the chain were made up of freely jointed backbone bonds then C_∞ would equal unity. However, this value becomes different for 'real' polymers due to fixed angles between successive bonds and hindered rotational freedom [237]. The C_∞ values for bulk atactic PS has been estimated to be 9.6 [240] through small angle neutron scattering (SANS) experiments. Through the combination of Equations 5.7 and 5.8 we can obtain the Kuhn length in terms of C_∞. Values of a_K have been determined to be 20Å for PS. However, it has been observed in some instances that polymers with similar values of C_∞ have a different value for the length of a Kuhn segment as determined from probe molecule analysis for poly(dimethylsiloxane) and poly(isobutylene) [241]. Indeed, although the theoretical value for a_K for PS has been estimated to be 20Å, corresponding to $N = 8$ to 10, experimental determinations of the length of the Kuhn segment have yielded a value closer to 50Å, corresponding to $N \approx 50$ monomers [242]. This discrepancy is thought to be due to the assumption that the chain is fully extended inside a Kuhn segment, which is clearly not the case for 'real' polymer chains.

5.3 Rouse Model

The coarse-graining of the shape of a polymer chain allows for a model description of the dynamics of polymer chains without having to consider the intricacies of their chemical structure. One such description of the general dynamic properties of polymers on this low resolution scaling is the Rouse model [243], which is particularly applicable to polymers short enough that entanglement effects can be ignored. If two node positions, as depicted in Figure 5.1 are held in a fixed

position, a tensile force arises due to the net moment transfer onto the nodes [237]. If the distance, $\Delta\mathbf{r}$, between the nodes is large enough such that Gaussian statistics of the chain can be assumed then this tensile force, $\mathbf{f}$ can be defined in terms of the mean squared node-to-node distance, $\langle\Delta\mathbf{r}^2\rangle$:

$$\mathbf{f} = \frac{3k_BT}{\{\Delta\mathbf{r}^2\}}\Delta\mathbf{r} = b_R\Delta\mathbf{r} \tag{5.9}$$

This equation suggests that the connection between the nodes can be approximated as a spring, with spring-constant b_R, as shown in Figure 5.2a. The Gaussian random walk description of the polymer chain can thus be extended under the assumption that the nodes are connected by springs. The polymer chain also 'feels' a force due to the surrounding polymer chains in the melt. This *viscous force* is related to the velocity of a node, $\mathbf{u}_N$ [237]:

$$\mathbf{f} = \zeta_R\mathbf{u}_N \tag{5.10}$$

Where ζ_R is the friction coefficient. Through these definitions of the forces acting on the nodes, the equation of motion for a single node at position, $\mathbf{r}_l$ can be constructed:

$$\zeta_R\frac{\mathrm{d}\mathbf{r}_l}{\mathrm{d}t} = b_R(\mathbf{r}_{l+1} - \mathbf{r}_l) + b_R(\mathbf{r}_l - 1 - \mathbf{r}_l) \tag{5.11}$$

The left hand side of Equation 5.11 relates to the viscous force acting on the node and the right hand side is related to the elastic forces between adjacent nodes [237]. The Rouse model only considers local interactions of the nodes and therefore ignores non-local interactions such as excluded-volume or hydrodynamic forces between 'distant' nodes but these interactions are expected to be effectively screened in a polymer melt [244]. We thus have a set of differential equations relating to the motion of each node describing the polymer chain. The motion of each node in all spacial directions decouple and are equivalent. Through appropriate choices of boundary conditions for the motion of the nodes, the equations of motion for all nodes can be solved yielding N_s independent solutions, termed the 'Rouse modes' of the polymer chain. For the Rouse mode with the lowest

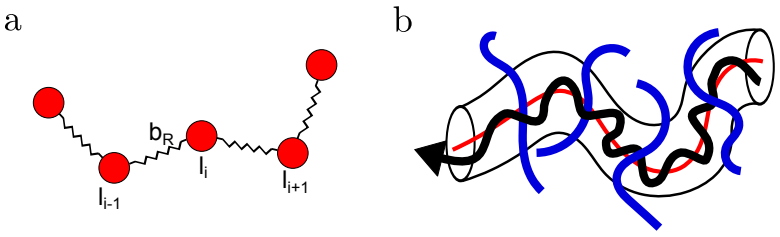

Figure 5.2: Pictorial representations of the a) Rouse and b) reptation models.

order, the characteristic timescale τ_R is proportional to the square of the number of nodes:

$$\tau_R = \frac{\zeta_R}{b_R}\frac{(N_s - 1)^2}{\pi^2} \tag{5.12}$$

5.4 Reptation

Beyond a certain degree of polymerisation, the polymer chains in a melt can become entangled. We can define the entanglement molecular weight, M_e, as molecular weight between entanglement points [245]. The interpenetration of the polymer chains and the fact that these chains cannot pass through each other means that the motion of an individual chain becomes constrained. It could be said that the main restriction of the polymer chains occurs in the direction perpendicular to the backbone of the polymer [237], a so-called topological constraint [238]. It was suggested by de Gennes [246] and Edwards [247] that the dynamics of an entangled polymer chain could be described as contained within a 'tube' defined by adjacent polymer chains as shown in Figure 5.2b. As depicted earlier (Figure 5.1), the polymer chain can be thought of as a number of nodes separated by the Kuhn length, a_K. We can further coarse-grain this approach by assuming that a high molecular weight polymer can be described as a series of 'blobs', each containing a number of Kuhn segments [248] which occur between entanglements. The motion of the chain within a blob, described as a rapid local 'wiggling' [237], can be described by the Rouse model. The average of this local wiggling gives the mean positions of the monomers constituting the chain and thus the so-called

'primitive path' of the polymer, which is the shortest end-to-end distance of the entire chain. This is represented by the red line in Figure 5.2b.

There are two possibilities of motion of the blobs describing the polymer chain within the tube. If there is a local fluctuation in the concentration then a blob can diffuse into the local environment in order to restore the concentration back to the mean value [238]. The other possibility is that the blob can move along the tube described by the surrounding polymer chains. The movement of the polymer along the tube through the movement of its constituent blobs is known as reptation [246]. Reptation of the polymer, and thus translation of the primitive path, is a form of curvilinear diffusion and can be derived from the Einstein relation [237]:

$$\hat{D} = \frac{k_B T}{\zeta_t} \tag{5.13}$$

Where $\hat{D}$ is the curvilinear diffusion coefficient and ζ_t is the fiction coefficient of the entire chain, formed as the sum of the friction coefficients of all nodes: $\zeta_t = N_s \zeta_R$. The reptation of the chain leads to its continuous disentanglement from the polymer chains describing the tube. The characteristic timescale, τ_d, for disentanglement is the time needed for the chain to reptate over a length equal to the length of its primitive path. This timescale is proportional to the number of repeating units in the following manner [237]:

$$\tau_d \propto N_s^3 \tag{5.14}$$

This equation also implies a power-law dependence of τ_d with the molecular weight: $\tau_d \propto M_w^\nu$. The experimental value of the exponent ν has been found to be between 2.9 and 3.6 [237, 249–251] and is therefore in good agreement with Equation 5.14.

5.5 Variations of the glass forming properties of polymeric chain-length series

In Chapters 6 and 7, the results of measurements performed on two different glass-forming series based on the polymerisation of styrene and $\alpha-$methylstyrene will be presented. Firstly, the variation of glass forming properties with increasing molecular weight will be discussed in general. Note that this represents a small sample of parameters which are dependent on chain length. More detailed discussions will be given in parallel to the discussion of the data obtained for the two chain-length series.

5.5.1 The glass transition temperature

There is a significant molecular weight dependence of the glass transition temperature, T_g for polymers. The chain-ends of a polymer have a higher mobility than any of the repeat units within the chain as they are only bound on one 'side'. As the degree of polymerisation increases, it follows that the density of these chain-ends must decrease and the average mobility of the polymer chain must decrease [252, 253]. If a free-volume is associated with the chain-ends then a polymers with lower molecular weights will have a greater free-volume at a specific temperature due to the higher density of chain-ends. Free-volume models such as presented by Cohen and Turnbull [79] (see Chapter 1) suggest that the increase of the structural relaxation time is related to the decrease of the free-volume in a glass forming system. It follows that a decrease of the density of chain-ends would then lead to an increase of T_g. One can also formulate a similar argument for the increase of T_g based on the configurational entropy instead through models such as the Gibbs-DiMarzio theory [254]. The first quantitative description of the development of T_g as a function of M_w for polymeric samples was made by Fox and Flory [255]:

$$T_g = T_g^{\infty} - \frac{A}{M_w} \tag{5.15}$$

In this empirically derived equation, A is a constant and T_g^{∞} refers to a saturation glass transition temperature: above a certain molecular weight, T_g remains

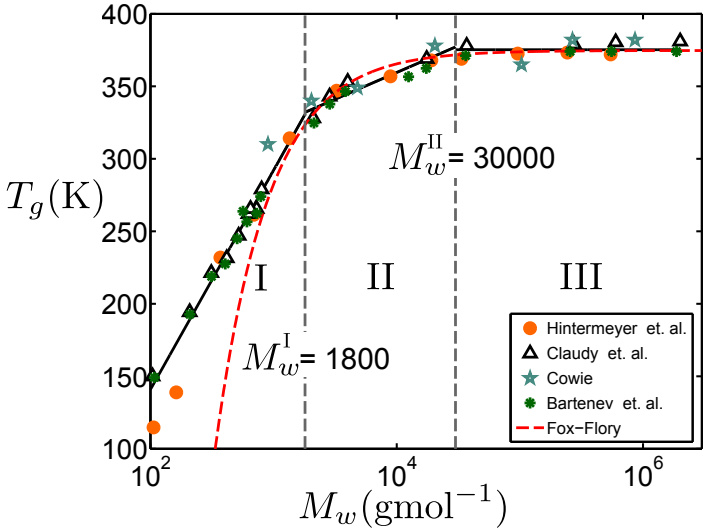

Figure 5.3: T_g values obtained from several sources of data for PS from the literature [258–261]. The red dashed line indicates a fit of the Fox-Flory equation (Equation 5.15). The black lines indicate fits to the data in the three distinct molecular weight regions, marked by the vertical dashed grey lines. The definition of the molecular weights marking the transition points were taken from Hintermeyer *et. al.* [258].

constant with further increasing molecular weight. Although this function describes the behaviour of T_g well for high molecular weight polymers, it fails to describe the variation of T_g for oligomeric glass formers below a certain molecular weight threshold [253]. Some extensions to Equation 5.15 have been made [256, 257] in order to describe the observed behaviour of T_g over a greater molecular weight range but these extensions are still based under the assumption that the variation of T_g can be described by a single functional shape over the whole range.

In contrast to this, several measurements of polymeric chain-length series have yielded three distinct regions in the molecular weight dependence of T_g. Data from a selection of these measurements for chain-length series of oligostyrenes [258–261] are shown in Figure 5.3. It is clear from this figure that the glass transition temperatures for these measurements seem to fall into three distinct molecular weight regions and the full behaviour cannot be described with the traditionally used Fox-Flory equation. In 1975, Cowie proposed that one could describe the

variation of T_g as discontinuous [259]. Region I indicates that there is a linear dependence of T_g with $log_{10}(M_w)$ for the short-chain oligomers of PS, similar to the dependence seen in the alkylbenzene series. Region II indicates another linear dependence with a slightly lower gradient and Region III indicates the point at which T_g becomes saturated for further increases of M_w The boundaries between the regions were taken from those described by Hintermeyer *et. al.* [258]. The authors attribute the distinctions between the three different regions to the changes in the dynamics of the polymer chain as it becomes longer (with larger molecular weight). The transition point between Regions I and II, M_w^I, is thought to be equivalent to the size of a Rouse unit as described in Section 5.3. The molecular weight they attribute to this point is equivalent to around 16 monomer units and therefore this could be related to the Kuhn length of PS, although definitions of the Kuhn length vary for polystyrene as explained previously [242]. The authors also attribute the transition point between Regions II and III, M_w^{II}, as the entanglement molecular weight, M_e, and thus this point could represent the onset of reptation behaviour of the polymer chain. They quantify this description of M_w^{II} by finding good agreement between its value and values of M_e for PS obtained from the literature. However this conjecture was countered by Agapov *et al.* [262] who demonstrated that although the M_e for PS and polydimethylsiloxane (PDMS) are relatively similar, the values for the saturation glass transition temperature, T_g^∞ differ by a factor of 2. Whether or not M_w^{II} is related to M_e, it is still clear from Figure 5.3 that the molecular weight dependence of T_g may not be completely described by a continuous function, such as Equation 5.15, and that it may be better to describe the variation using the discontinuous description presented by Cowie [259].

5.5.2 Dynamic fragility

We saw for the alkylbenzene series that several definitions of the fragility of these glass formers show a dependence on the alkyl-tail length. Hintermeyer *et. al.* also show similar dependencies of the fragility parameter m for PS, PDMS and PB. Interestingly, rather than falling into three separate regions in the same manner as the T_g values, the m parameter appears to increase monotonically with molecular

weight until a molecular weight equivalent to M_w^{II} is reached at which point m becomes invariant with further increasing chain-length. In other measurements of polystyrene by Santangelo *et. al.* [26] it was noticed that the response peak of the α relaxation in the imaginary part of the shear modulus, G'' was completely rescalable for a chain-length series of PS varying from chains with a degree of polymerisation of 6 to those consisting of $\approx$ 36000 monomer units. The KWW stretching exponent, β, has been linked to the so-called coupling parameter, n, in Ngai's coupling model [62, 83] (see Chapter 1), where $\beta = 1 - n$. It has been shown that for many systems n is correlated to the dynamic fragility parameter, m. The fact that the shape of the dispersion of a range of oligo(styrenes) was largely invariant also suggests a point at which m is no longer affected by changing the chain-length.

5.5.3 Thermodynamic fragility

In the alkylbenzene series we also observed a correlation between the variation of dynamic fragility parameters, such as m and D, with definitions of the thermodynamic fragility, quantified by the difference in the heat capacities in the liquid and the glass at T_g, ΔC_p, the width of the characteristic step in C_p, ΔT, and the excess entropy, S_x. However, for polymeric systems this correlation appears to break down. As discussed, metrics of the dynamic fragility tend to increase with increasing chain-length whereas thermodynamic metrics appear to follow the opposite trend or indeed no trend at all [122, 263]. This lack of correlation between thermodynamic and dynamic definitions of fragility will be discussed further in Chapter 6 by introducing the concept of vibrational anharmocity [264].

5.5.4 Bifurcation temperature of the α and β relaxations

The bifurcation temperature, $T_{\alpha\beta}$, relates to the decoupling of the α and β relaxation mechanisms. It has been observed that $T_{\alpha\beta}$ varies systematically with increasing chain length for systems based on monomethyl ethers, dimethyl ethers, glycols, polyalchohols and in certain polymeric gel systems [18, 166, 193, 265]. This behaviour was also observed for the alkylbenzene series suggesting a generality of the behaviour for systems which show systematic variations of size and

structure and thus makes for an interesting avenue of research. The bifurcation scenario as a function of chain-length will be fully discussed in Chapters 6 and 7 in relation to the samples studied in this research.

5.6 Summary

In this chapter, the typical nomenclature used to describe the size and dynamics of polymers has been introduced. Also a brief introduction was given into the variation of parameters associated with the glass transition with variation of chain-length. We now have the required tools in order to describe the results presented in Chapters 6 and 7.

Chapter 6

Results II: An oligomeric series of styrene

6.1 Introduction

In Chapter 4 results on the dynamics and glass-formation of a series of alkylbenzenes were presented. This series featured samples with an increase of the molecular weight characterised by the systematic addition of methylene groups to a carbon tail connected to a benzene ring. In this chapter in contrast, a chain-lengths series resulting from the polymerisation of styrene will be considered.

Atactic Polystyrene (PS) is particularly applicable in a study of this type as it does not crystallise readily upon cooling and is therefore ideal for the study of glass forming properties. PS has been widely studied in the literature [204, 258, 266–275](some results are discussed in Chapter 6) and thus allows for rigorous comparisons. Interesting variations of T_g with increasing molecular weight have also been reported for polystyrene [258–261] which imply that the Fox-Flory equation, commonly used to describe the molecular weight dependence of T_g for polymers, may not hold for all polymeric glass forming systems. Furthermore, the moiety of PS is relatively simple, consisting of a carbon backbone with a benzene ring bonded to alternate carbon atoms in the backbone chain. Although several relaxation mechanisms have been observed for PS [204, 258, 266–275] there is still no consensus regarding exactly what they are and not even what relaxations do exist. Moreover, there is a lack of systematic measurements of the

Degree of Polymerisation (N)	M_w g/mol	PDI	Measurement Techniques	Manufacturer
1	162	1	BDS and DSC	PSS
2	266	1	BDS and DSC	PSS
3	370	1	BDS and DSC	PSS
4	545	1.16	BDS and DSC	PSS
5	580 (M_p)	1.15	DSC	PL
6	725	1.09	BDS and DSC	PSS
16	1700 (M_p)	1.06	DSC	PL
18	1920	1.08	BDS and DSC	PSS
28	2960 (M_p)	1.04	DSC	PL
1160	120586	1.04	BDS and DSC	PS

Table 6.1: Table showing relevant information for the samples used in this series. This includes the degree of polymerisation, N; the weight averaged molecular weight, M_w (in some cases, only the 'peak' molecular weight M_p was quoted by the manufacturer as indicated in the table); the polydispersity index, $PDI = M_w/M_n$; the experimental techniques used in their measurement (either Broadband Dielectric Spectroscopy (BDS) or Differential Scanning Calorimetry (DSC)) and the manufacturer (PSS: Polymer Standards Service, PL: Polymer Laboratories, PS: Polymer Source) from which they were obtained.

observed secondary relaxation mechanisms for shorter chain oligomeric styrenes, thus prompting the need for further study. To reach a better understanding of the relaxation dynamics for polystyrene could thus help explain a wide variety of previously observed but not well understood phenomena. Examples of such include the dramatic change of glass-transition behaviour observed for thin polystyrene films either supported on a surface or free-standing [276–279].

The specific parameters for the samples used, including their degree of polymerisation, molecular weight and polydispersity index, are given in Table 6.1 together with the manufacturer of each sample. The samples will be referred to by their degree of polymerisation N for the remainder of this chapter. Also shown in table 6.1 are the techniques used for measurement. The majority of the samples were measured using both broadband dielectric spectroscopy (BDS) and differential scanning calorimetry (DSC). However, due to limited sample amounts, the $N = 5$, 16 and 28 samples were only measured using DSC.

The samples, obtained from Polymer Standards Service and Polymer Source,

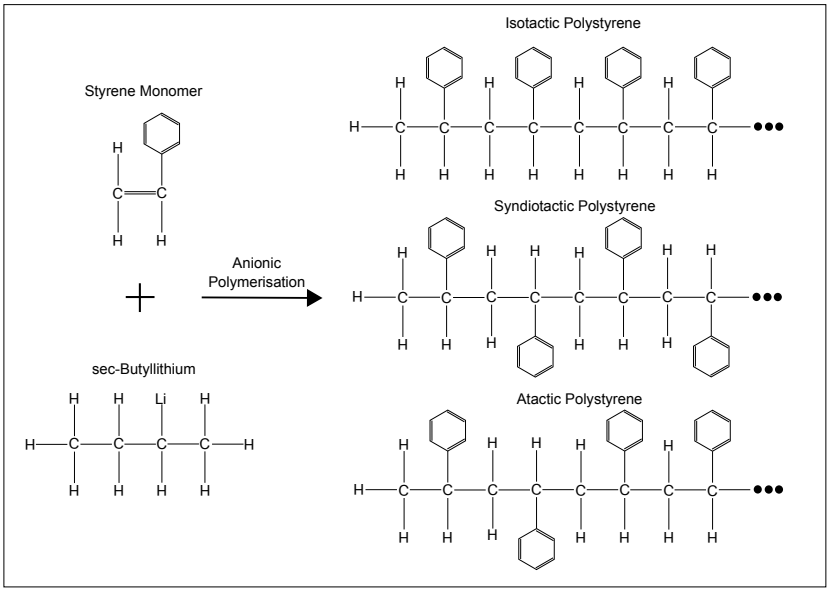

Figure 6.1: Diagram showing the anionic polymerisation of styrene including different representations of the tacticity of polystyrene.

used in this work were prepared using so-called anionic polymerisation. An example of this polymerisation of styrene is shown in Figure 6.1. Anionic polymerisation is an example of chain-growth polymerisation. The reaction is initiated by degradation of an initiator, in this case *sec*-butyllithium. Lithium free radicals are then created which break the unsaturated carbon-carbon bond of the styrene and the radical centre joins the end of the chain. Propagation of the chain, through consumption of monomeric species in the solution, then occurs. This form of polymerisation is a form of 'living' polymerisation which means that the propagation of the chains increases until all monomeric units have been consumed (whereas other forms of polymerisation require chemical termination of the process) [236]. Different forms of polymerisation can lead to variations in the steric order of the resulting polymer. For example, in PS the benzene ring could be placed in different positions as indicated in Figure 6.1. This variation in the steric order is termed the 'tacticity' of the polymer [237]. In this series of samples, the polymers are atactic and have no prefered steric order. As a result of this lack of order, these polymers cannot form regular crystalline structures and form amorphous glassy structures upon cooling from the melt.

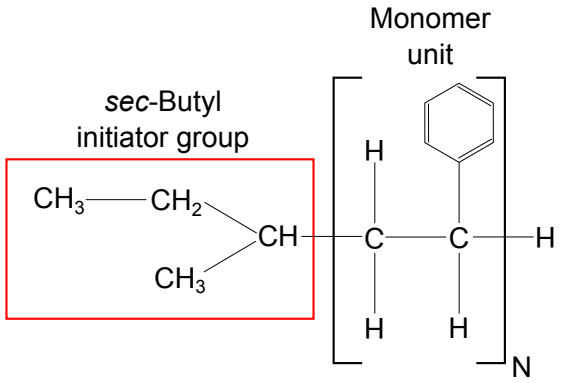

Figure 6.2: Diagram showing the position of the initiator group and the repeat monomer unit for the samples in the styrene series.

As a result of the polymerisation process, the samples have an initiator group attached to the polymer chain as shown in Figure 6.2. For the $N = 2$, 3, 4, 6, 18 and 1160 samples the initiator group is a sec-butyl group with a molecular weight of 58 g/mol and the degree of polymerisation for these samples is determined by substituting this value from the quoted values of M_w and dividing by the molecular weight of styrene, 104 g/mol. The $N = 1$ sample has an attached n-butyl group in order to saturate the double bond of the styrene monomer. This sample is therefore chemically identical to hexylbenzene, the $M = 6$ sample from the alkylbenzene series. We found that for the $N = 1$ sample from Polymer Source, there were significant repeatability issues between different batches in the dielectric measurements, which no other samples showed. This was possibly due to its degree of purity, to contamination or to water-uptake by the sample. Further measurements are required in order to determine the reason for this. Instead the $M = 6$ sample from the alkylbenzene series, which should be chemically identical and showed excellent repeatability, was used instead and will hereby be referred to as the $N = 1$ sample. Information regarding the polymerisation process could not be obtained for the samples obtained from Polymer Laboratories ($N = 5$, 16 and 28) shown in Table 6.1. It was thus assumed that these samples have similar attached initiator groups and the degree of polymerisation was calculated accordingly.

6.2 Dielectric spectroscopy: α relaxation

Dielectric measurements were performed at both the University of Leeds and Chalmers Institute of Technology, Gothenburg using the slightly different dielectric set-ups explained in Chapter 2. The lower molecular weight samples in this series had reasonably low viscosities at room temperature and were thus measured using the dielectric liquid cell. In this set-up, the sample was contained between two 20mm electodes kept at a fixed separation by silicon spacers of 100µm diameter. On the other hand, the $N = 6$, 18 and 1160 samples were measured using the two-electrode method in which the samples were sandwiched between a 20mm electrode and a 40mm electrode kept at a fixed separation of 50µm. In order to remove charged species from the $N = 6$, 18 and 1160 samples, and thus suppress the ionic conductivity contribution to the imaginary part of the permittivity, ε'', methanol precipitation was performed. The samples were then redissolved in toluene and solution cast to the 40mm electrode. The samples were dried for 24 hours prior to measurement at 473 K. The sample preparation methods are described in detail in Chapter 2. After cleaning and solution casting, the samples were heated on a hot-plate to lower their viscosity so that silicon spacers could be added. The top 20mm electrode was then placed on top of the sample/spacers and pressure was applied to ensure an even sample volume. For the $N = 1160$ sample, silicon spacers could not be added due to the high viscosity of the sample even at elevated temperatures. This led to an uncertainty in the absolute sample thickness and thus that the amplitude of the α relaxation loss peak, ε''_p, and the dielectric strength $\Delta\varepsilon$ could not be determined accurately as these parameters are dependent on the sample thickness. This sample does not 'flow' readily at the temperatures measured and therefore the change in thickness of the sample was assumed to be slight. It was also assumed that the majority of the change in the thickness would have occurred at the highest measured temperatures and that the sample would have had a relatively consistent thickness at lower temperatures. For the purposes of comparison with the other samples in this series, the spectra for the bulk polystyrene were rescaled in ε'' such that the amplitude of the α loss peaks were comparable to dielectric measurements of a similar sample ($N \approx 1000$) in the literature [258].

In order to obtain dielectric spectra in the α relaxation temperature regime, the $N = 2$ to 1160 samples were heated (or cooled, depending on whether the expected T_g was above or below room temperature) to a temperature such that the α relaxation loss peak in ε'' was just visible in the high frequency range (e.g. when the peak frequency of the loss peak was 10^6Hz). The samples were then cooled in steps of 2K to a temperature below the expected glass transition temperature and spectra were obtained at each of these steps. On the other hand, for the $N = 1$ sample, measurements were conducted by first cooling the sample at the maximum cooling rate ($\sim$ 20K/min) to a temperature just below the expected T_g. This was done to suppress crystallisation in the sample. Measurements were then obtained on heating the sample in steps of 2K. Furthermore, the frequency range was also restricted in order to reduced the measurement duration at each temperature and thus further hinder crystallisation.

6.2.1 Dielectric spectra

The dielectric loss ε'' spectra obtained for the samples in the styrene series ($N = 1$, 2, 3, 4, 6, 18 and 1160) are shown in Figures 6.3a-g. Firstly, let us consider the spectra for the $N = 1$ sample shown in Figure 6.3a. There are three resolvable contributions, which are also observed for the $N = 2$ - 18 samples. The most prominent of these is the loss peak relating to the α relaxation as marked in the figure. A high frequency power-law contribution is also visible, designated HF in the figure. Finally there is an intermediate contribution between the α loss peak and the high frequency contribution. This contribution was also observed for the alkylbenzene series (Chapter 4) and was likely due to an additional secondary relaxation, and the evidence for this assignment will be outlined in the following throughout the chapter. Thus, this secondary relaxation has been designated β in the figure. The $N = 1160$ spectra do not exhibit resolvable intermediate or high frequency contributions. However, a significant DC-conductivity contribution was observed at low frequencies, manifested as a power-law flank. The lines through the data in Figures 6.3a-h represent fits which were made by assuming an additive combination of functional descriptions for the observed features. This will be explained in detail in Section 6.2.3. The loss peaks of the $N = 1$ sample show a

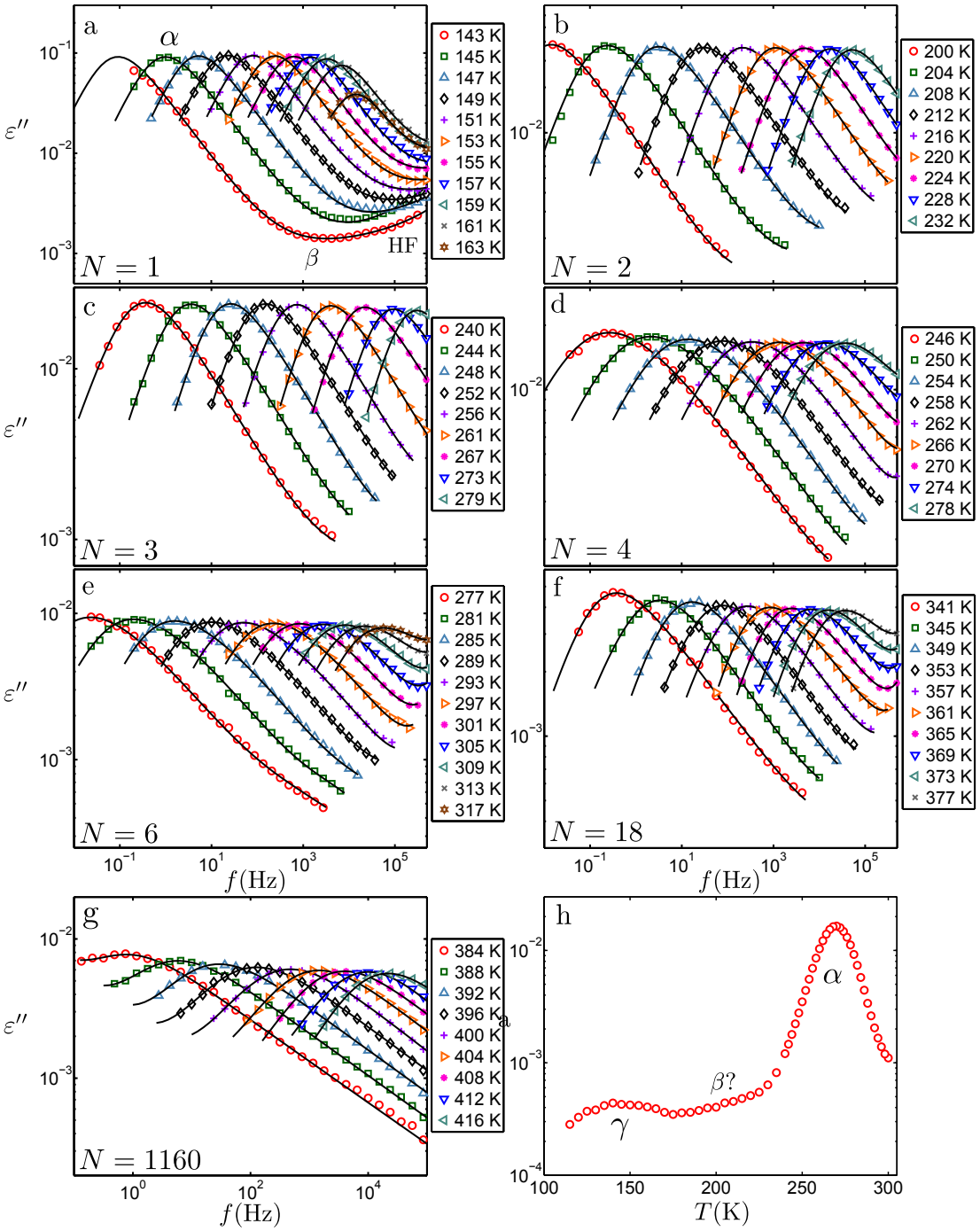

Figure 6.3: Dielectric spectra for a) N = 1 b) N = 2, c) N = 3, d) N = 4, e) N = 6, f) N = 18 and g) N = 1160 samples in the α relaxation regime. The lines through the data denote fits which will be described in Section 6.2.3 h) Fixed frequency spectra for the N = 4 sample.

decrease in the peak amplitude at high temperatures, which we interprete as due to crystallization. In support of this, Hintermeyer *et. al.* observed crystallisation of the same sample in a similar temperature regime in their measurements [258]. The spectra have been cut in frequency for samples $N = 2$, 3, 4, 6, 18(Figures 6.3b-h) in order to clarify the behaviour of the α loss peak. Similarly, the $N = 1160$ spectra have been cut in order to remove the conductivity flank at low frequencies.

The loss peaks all follow the expected behaviour with decreasing temperature: a decrease in the peak frequency indicating a slowing down of the structural relaxation timescale, τ_α. In the temperature/frequency range shown for these samples, the α relaxation loss peaks appear to have a relatively straightforward functional shape and no clear signature of an excess-wing is observed. The spectra presented in Figures 6.3a-g were thus fit without the assumption of an excess-wing (see Section 6.2.3) but the lowest temperature data for some of the samples (particularly the higher molecular weight ones) do indicate a slight change in the exponent of the high frequency flank of the α relaxation. This will be fully discussed in Section 6.4, where we demonstrate that we do indeed find evidence supporting the existence of an excess wing and thus implying the existence of a 'hidden' secondary contribution. The observation of an excess wing in the dielectric spectra is consistent with data for the oligo-styrenes presented by Hintermeyer *et. al.* [258] also appear to demonstrate a change in the power law exponent of the high frequency flank of the α relaxation, suggesting excess-wing like behaviour. However, we do not find it productive to introduce more fitting parameters to account for this weak excess wing since we can describe the data well in the presented dynamic range without introducing this extra complexity. In the interpretation of the analysis we will, however, keep in mind the likely existence of an underyling secondary relaxation and we will later investigate this further in the low-temperature range, as described in Section 6.2.4 and shown in Figure 6.30.

In order to gain a qualitative measure of the relaxation contributions within the samples, ε'' at a fixed frequency of 4.2×10^3Hz was analysed as a function of temperature. An example of this analysis is shown in Figure 6.3h for the $N = 4$ sample. Two relaxation processes are clearly defined in this description of ε'' which have been attributed to the structural α relaxation and a secondary

γ relaxation. In between the α and γ relaxations, there is also an indication of a possible additional secondary contribution (β relaxation) and we will see later that this can be confirmed in a detailed investigation. Given these observations, we thus follow the standard nomenclature and name the relaxation based on the order in which the appear, as α, β and γ. As discussed further below, the similarities in timescale and activation energy of the observed γ relaxation and the relaxation obtained from mechanical spectroscopy on PS and normally denoted γ [204] (see Section 6.3.4) further supports this assignment.

6.2.2 Rescaled spectra

The functional shapes of the α loss peaks were compared by rescaling the dielectric spectra. Spectra rescaled by the peak frequency, f_p as shown in Figure 6.4a and by both f_p and the amplitude, ε''_p, as shown in Figure 6.4b. The dashed grey line indicates the spectral fit of the bulk sample with the conductivity contribution removed.

It is clear from Figure 6.4a) that the amplitudes of the α loss peaks for the series decrease systematically with increasing degree of polymerisation for the $N = 1$, 2, 3, 4, 6 and 18 samples. The amplitude of the loss peak for the $N = 1160$ sample occurs between those of the $N = 6$ and 18 samples. The spectral shape of the loss peak for the $N = 4$ appears to be broader than those of the other samples in the series. From Figure 6.4b it could be said that the breadth of the α loss peak increases with increasing chain-length for the $N = 1$-4 samples. The breadth then decreases and remains fixed for the $N = 6$, 18 and 1160 samples. The very similar nature of the α relaxation peak for higher chain-length PS ($N \approx 6$ to ≈ 36000) was also observed by Santangelo *et. al.* in the imaginary part of the shear modulus, G'', through rheological experiments [26] and also in ε'' through dielectric measurements [269].

In a study of an oligomeric chain series of propylene glycol based dimethyl ethers in research published by Mattsson *et. al.* [69] it was observed that the spectra for the highest molecular weight sample yielded an α relaxation loss peak and a clearly separated β loss peak. The timescales of the α and β relaxations however approached each other as the chain-length was decreased. For the lowest

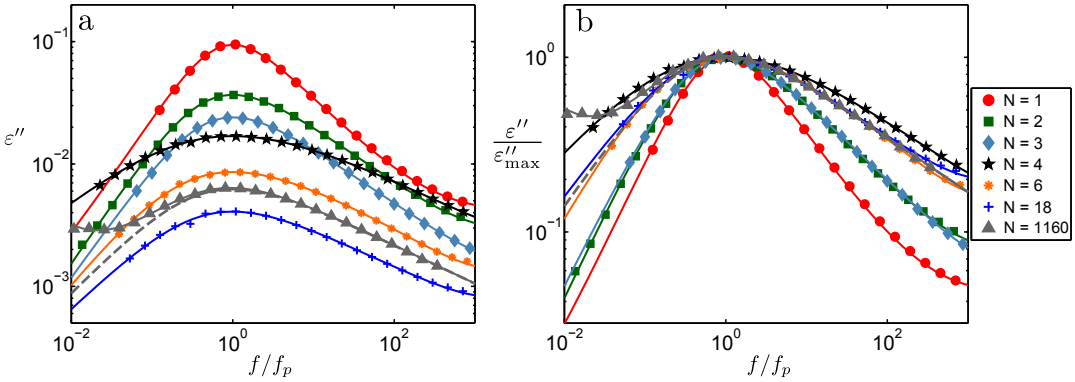

Figure 6.4: Dielectric spectra for the styrene series with a peak frequency, f_p, of around 100Hz rescaled by a) f/f_p and b) both f/f_p and ε''_p.

molecular weight samples, this has the effect that the β loss peak is no longer discernible as a separate process, and an excess wing is observed on the high frequency flank of the α loss peak. In analogy to these results, the broadening shown in Figure 6.4 could be indicative of the increasingly marked appearance of a secondary relaxation process for the higher chain-length samples. This will be discussed further in Section 6.4.

6.2.3 Fitting procedure

The dielectric spectra obtained in the α relaxation temperature regime for this series contain three clear features (as shown for the $N = 1$ sample shown in Figure 6.3a: an asymmetric loss peak relating to the α relaxation, an intermediate contribution corresponding to a secondary γ relaxation and a high frequency contribution manifested as a power law contribution. The fitting procedure for this series was similar to that of the alkylbenzene series (Chapter 4). More details about the fitted functions can be found in Chapters 2 and 4. The α relaxation loss peaks were described in two separate fits using the Rikard Bergman (RB) [104] and Havriliak-Negami (HN) [110] functions.

The intermediate contributions to the spectra were fitted using the Cole-Cole (CC) [176] expression which is often used to describe secondary relaxations in dielectric spectra [33, 61, 67, 94, 96, 116, 117]. The CC expression is obtained by

setting the β parameter to 1 in the HN expression. The high frequency contributions were fit with a power law flank of the form $\varepsilon'' = A\omega^k$. The full spectra were described using an additive combination of these functions. In some cases (most notably in the $N = 1160$ sample) it was also necessary to include a low frequency power law flank due to the contribution of ionic conductivity. Conductivity of charged species leads to a linear increase of ε'' with decreasing frequency which can be describe using the following relation [94]:

$$\varepsilon_{cond}(\omega) = -i\frac{\sigma_0}{\varepsilon_0\omega} \tag{6.1}$$

Where σ_0 is the ohmic or DC conductivity of the material. This relation implies that the exponent of the conductivity power law flank in ε'' should be 1. However, the observed low-frequency flank was best described using an exponent less than 1 in most cases, which has previously been observed for similar samples [258] and the behaviour had to be generalised. In order to fit the data, an exponent parameter was thus included, k' such that $\varepsilon''_{cond} \propto \omega^{k'}$. In the following sections, detailed analysis of the fitting parameters will be presented.

6.2.4 Fit parameters

The following sections will detail the development of the fitting parameters from the two functional descriptions of the α loss peak constructed using the RB and HN functions.

Bluntness of the Loss Peak

Firstly, the parametrisation of the bluntness of the α loss peak in ε'' will be addressed. The bluntness is characterised by the C parameter in the RB function. The C parameters for the styrene series are shown in Figure 6.5a. It was observed that this parameter did not have a significant temperature dependence and that the spectra for each sample could be fully described with a fixed value of C across the measured temperature range. Thus, each of the empirical response functions (RB or HN) used to describe the α relaxation had the same number of free parameters.

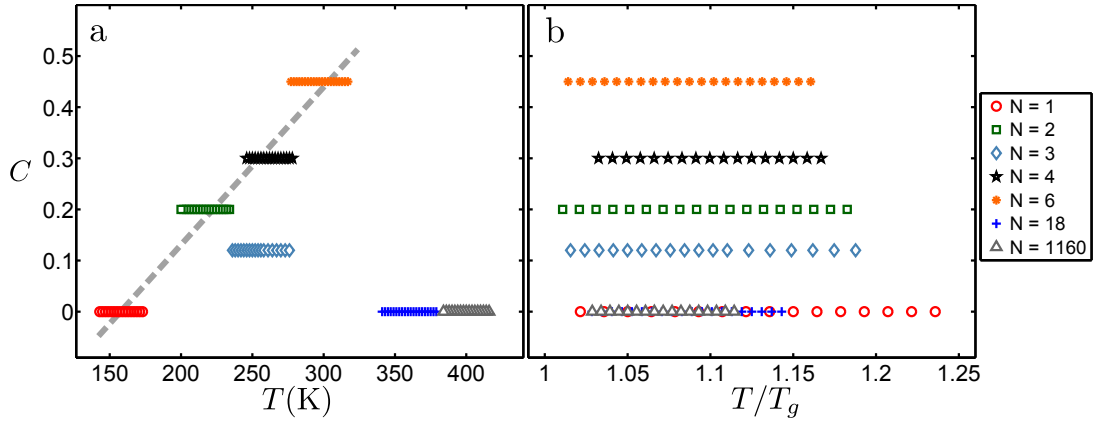

Figure 6.5: Bluntness, C, parameters obtained from fits of the RB function to the dielectric spectra plotted against a) T and b) T/T_g.

The $N = 1$, 2, 4 and 6 samples in this series show a systematic increase of the C parameter with increasing degree of polymerisation as shown clearly in the T_g rescaling of the parameters shown in Figure 6.5b and indicated by the dashed guide to the eye in Figure 6.5a. However, the C parameter for the $N = 3$ sample does not follow this trend. Also, the trend does not apply to the $N = 18$ and 1160 samples. The spectra for these samples could be fully described by setting $C = 0$.

A systematic variation of the C parameter has also been observed for oligomeric series of di-methyl ethers and glycols [18] although the physical explanation for this trend could not be determined. It was suggested that the origin might at least for higher molecular weights be related to an increasing breadth of the molecular weight distribution.

The HN function does not contain a parameter relating to the bluntness of the peak. Thus, as discussed in the following sections, particularly for the samples where C is non-zero, some differences are observed both for the low and high frequency exponents between the results obtained from the HN and RB functions, respectively.

Low frequency flank

In this section the parameters that describe the exponent of the low-frequency power-law flank of the α relaxation loss peak will be discussed. Many of the functional descriptions of the α loss peak including the CD function [109], the G_{GG} distribution [98], the KWW function and the circuit model [168] are all based on the assumption that the low frequency flank of the α relaxation loss peak should have an ω^1 dependence. It is clear, in a qualitative sense from Figure 6.4, that this behaviour cannot be universal for all glass forming systems as the gradient of the low frequency flank is not scalable for the styrene series and appears to decrease with increasing degree of polymerisation. This observation is also verified quantitatively by the variation of the a parameter, used to parametrise the gradient of the low frequency flank in the RB function as shown in Figure 6.6a). The behaviour of the low frequency flank is clearly different from the behaviour seen in the alkylbenzene series, where the a parameter could be set to 1 for all samples.

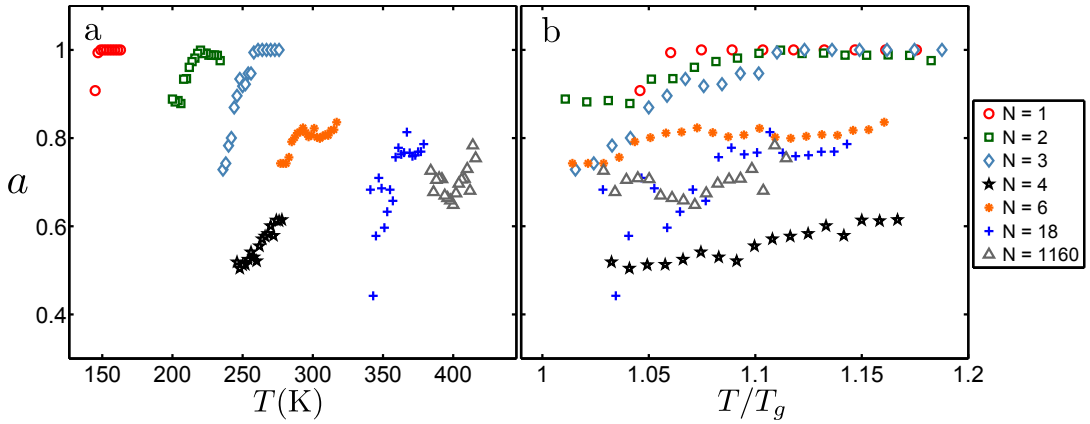

Figure 6.6: Low frequency power-law exponents, a, obtained from fits of the RB function to the dielectric spectra plotted against a) T and b) T/T_g.

The a parameters for the lowest molecular weight samples ($N = 1$, 2, and 3) show an increase with increasing temperature until they reach a value of 1. The samples with a higher degree of polymerisation show a similar increase of the a parameter with increasing temperature but the gradient of the low frequency flank remains at a value significantly less than 1 at even the highest measured

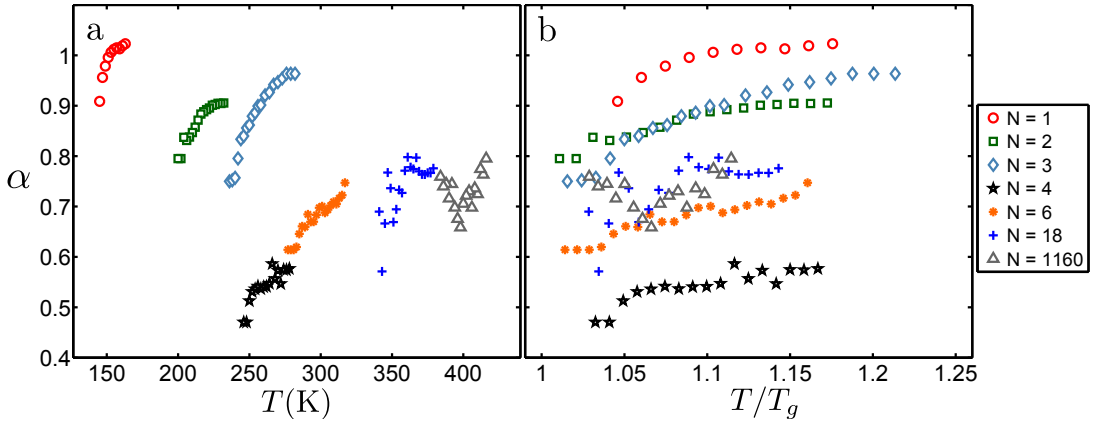

Figure 6.7: Low frequency power-law exponents, α, parameters obtained from fits of the HN function to the dielectric spectra plotted against a) T and b) T/T_g.

temperatures. A rescaling of the a parameters by T_g is shown in Figure 6.6b. This figure shows that the variation of the exponent of the low frequency power law flank has a similar temperature dependence throughout the series. The absolute values of the a parameter are similar for the lowest chain length samples ($N = 1$ to 3). The parameters decrease with increasing chain-length for the other samples in the series with the exception of the $N = 4$ sample which requires a lower value of this parameter in order to fully describe the loss peak.

The analogous parameter to a in the HN function is the α parameter which corresponds to the exponent of the low frequency power-law flank of the loss peak in ε''. These parameters are shown in Figure 6.7a). The values for this parameter show a similar trend to the a parameter, but for the $N = 2$, 3, 4 and 6 samples, $\alpha < a$. The reason for this is likely due to the fact that the HN function does not contain a parameter to describe the bluntness of the peak and thus the bluntness has to be approximated using appropriate combinations of the α and β parameters. Indeed, the parameters describing the bluntness in the RB function, C, for the $N = 2$, 3, 4 and 6 samples were non-zero indicating a greater bluntness for these samples. The α parameters rescaled by T_g are shown in Figure 6.7b) and show similar temperature dependence to the corresponding a parameters.

A similar broadening of the low-frequency power law flank of the α loss peak in ε'' has been observed for polyisoprene (PI) and polyisobutylene (PIB) in dielectric measurements by Paluch *et. al.* [280]. Paluch *et. al.* state that the reduction of

the exponent of the low frequency power law of the α loss peak for PI and PIB was attributed to the manifestation of so called sub-Rouse modes [281]; relaxations which occur at a length scale less than that of the Kuhn length but consisting of several monomeric units. These sub-Rouse modes have also been observed in mechanical measurements and photo-correlation spectroscopy of PIB [282, 283]. Importantly, the dielectric spectra for both PI and PIB also show a so called normal-mode relaxation process manifested as a loss peak which occurs at lower frequencies than the α relaxation loss peak. This normal-mode peak is attributed to the Rouse modes that relax the chain on length scales between the size of a Rouse unit or the Kuhn length [281] and the length of the full chain; it is thus due to fluctuations of the end-to-end distance of the polymer chain [96]. The reason that this normal-mode peak is visible in the dielectric spectra for polymers such as PI and PIB is that they have a component of the dipole moment parallel to the chain direction [280]. This leads to an effective dipole moment along the backbone chain of the polymer. This means that fluctuations of the end-to-end distance are resolvable in the dielectric loss. However, polystyrene does not have a component of the dipole moment in the direction of the backbone chain and so the Rouse modes can not be resolved in ε''. Also, the authors also show dielectric spectra for both oligomeric ($N \approx 5$) and polymeric ($N \approx 2000$) PS but these samples both show a low frequency power law exponent of $\sim$1 for the α loss peak. This exponent is also consistent with dielectric measurements conducted by Matsumiya *et. al.* on polymeric and oligomeric PS [106]. Thus, it seems unlikely that the decrease in the a and α parameters observed for this series is due to the manifestation of sub-Rouse modes. Another possible explanation for the decrease in the exponent of the low frequency flank power laws for the higher chain-length samples (N = 4,6, 18 and bulk) is that these samples show a degree of polydispersity. Indeed, the $N = 4$ sample had the highest polydispersity of all the samples and also has the lowest value of the a and α parameters. However the PS samples studied by Paluch *et. al.* also have a comparable degree of polydispersity and yet show α loss peaks with a low frequency power law exponent of 1. Therefore, it is not clear why the a and α parameters decrease for longer chain lengths. However, we note that the behaviour might be related to our observation of a non-ideal conductivity contribution which had to be effectively accounted for by a use of a

powerlaw expression with a generalised powerlaw exponent and Hintermeyer *et. al.* also observe significant low frequency contributions for a range of oligomeric styrenes from the same manufacturer as those measured here.

High frequency flank

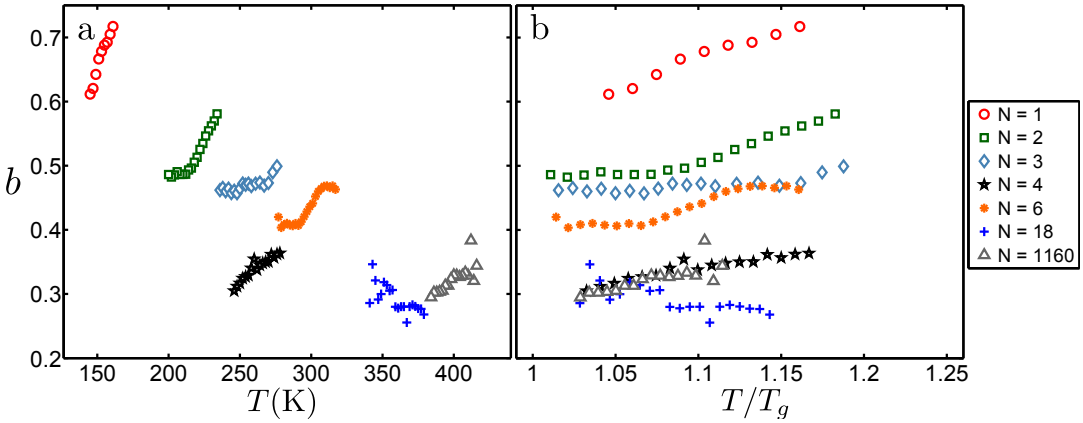

Figure 6.8: High frequency power-law exponent, b, parameters obtained from fits of the RB function to the dielectric spectra plotted against a) T and b) T/T_g.

In this section, the development of the high frequency flank with increasing chain-length will be addressed. The b parameter values, which describe the power law exponent of the high frequency flank of the α loss peak the RB function, are shown in Figure 6.8 a). Although these parameters show a slight increase with increasing temperature, this trend is less pronounced than it was for the alkylbenzene series. In some cases, for example the $N = 3$ and 18 samples, the trend is so slight that one could be tempted to say that the b parameter is essentially invariant with temperature for these samples. Another key feature of the variation of the b parameters is shown clearly in the T_g rescaling of Figure 6.8b). If we were to take the value of b at a specific value of T/T_g (a certain relaxation time) for each sample we observe a relatively systematic decrease of the parameter with increasing degree of polymerisation. This is another indication that the overall breadth of the loss peak increases with increasing molecular weight.

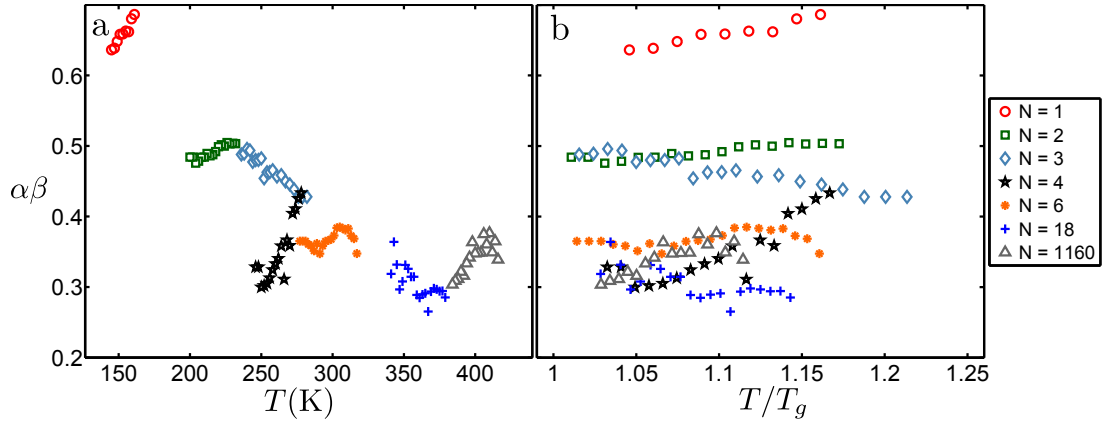

Figure 6.9: High frequency power-law exponent, β, parameters obtained from fits of the HN function to the dielectric spectra plotted against a) T and b) T/T_g.

The corresponding parameter for the exponent of the high frequency flank in the HN equation can be obtained by multiplying the anti-symmetric and symmetric stretching parameters: $\alpha\beta$. These parameters are shown in Figure 6.9a). In general, the overall trend of the $\alpha\beta$ parameters is very similar to that of the corresponding b parameters but there is a slight difference in the temperature dependence of $\alpha\beta$ for the $N = 2$, 3, 4 and 6 samples. In the HN function, the α and β parameters are correlated. The difference in the temperature dependence is therefore an indication of a compensation due to the bluntness. The T_g rescaled $\alpha\beta$ parameters are shown in Figure 6.9b) and demonstrate the same decrease with increasing chain length as observed for the b parameter and highlight the differences between the two descriptions of the high frequency flank.

The stretching exponent in the KWW function, describing the α relaxation phenomena in the time-domain (see Chapter 2) has been linked to the dynamic fragility of glass formers via the coupling model [62, 83]. It has also be shown that the breadth of the α relaxation loss peak in the frequency domain is related to the fragility of polymeric glass formers, whereby a broader dispersion implies a higher fragility [11, 26, 190]. A broader dispersion will have a lower value of the exponent of the high frequency power-law flank. Therefore based on the observed trends in the b and $\alpha\beta$ parameters with increasing chain length, the implication is that fragility increases with chain length. We do indeed find some evidence for such a trend in the dynamic fragility parameter, m, in Section 6.2.7. This result

is also in good correspondence with fragilities determined for chain length series of PS in the literature, in which a similar increase of the dynamic fragility with increasing molecular weight was observed [26, 258]. However, the opposite trend is observed for estimations of the thermodynamic fragility as will be addressed in Sections 6.5.2 and 6.5.3.

If we make the assumption that the departure from Debye-like relaxational behaviour in glass forming systems is a consequence of dynamic heterogeneity [44, 284], then the decrease in the b and $\alpha\beta$ parameters further implies that the degree of dynamic heterogeneity might increase with increasing chain length. Dynamic heterogeneity in polymers can be attributed to the ability of some sections of the polymer chain being more able to explore different structural conformations than other parts of the chain [285]. Furthermore, Ngai suggests a correlation between the stretching parameter and cooperative motions involved in the structural relaxation [62, 83]. The general decrease in the b and $\alpha\beta$ parameters for the lower molecular weight samples could imply that the degree of cooperativity increases as a function of chain-length. Given the similar absolute values of these parameters for the longer chain-length samples, this also suggests that above a certain chain-length, the degree of cooperativity is similar.

Cavaille *et. al.* note through mechanical experiments that time-temperature superposition does not hold for polystyrene [270]. On the other hand, TTS has been assumed for a number of polymeric systems in the past [170–173]. The temperature dependence of the b and $\alpha\beta$ parameters (and also the a and α parameters) for this series is, however, relatively small near the glass transition, most notably the $N = 3$ and $N = 18$ samples and for these samples at least TTS holds reasonably well.

Dielectric strength

We will now consider the dielectric strength, $\Delta\varepsilon$. Firstly, values of $\Delta\varepsilon$ were determined by numerical integration of the fits of the RB function to the dielectric spectra. This integral is given in Chapter 4. The results of this numerical integration are shown in Figure 6.10a. The Onsager equation (introduced in Chapter 2) predicts a $1/T$ dependence of $\Delta\varepsilon$ given that the dipole density is temperature

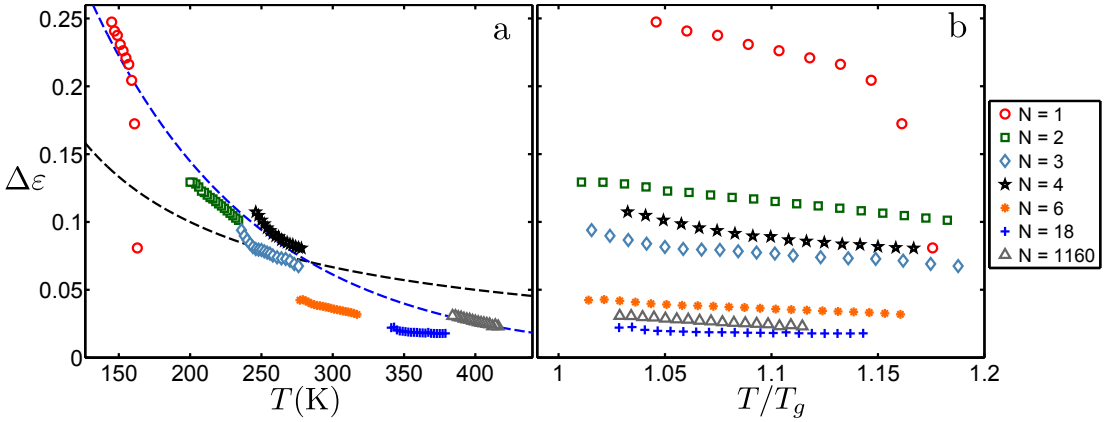

Figure 6.10: $\Delta\varepsilon$ parameters obtained through numerical integration of the fits of the RB function to the dielectric spectra plotted against a) T and b) T/T_g. The blue and black dashed lines in panel a) are examples of exponential and $1/T$ behaviour respectively.

independent, which is of course not realistic. However, as a rough check on the functional shape of the temperature dependence for the data sets we include a simple $1/T$ dependence as shown by the black dashed line in Figure 6.10a. We find that a $1/T$ behaviour does not describe the composite data set over the full temperature range, but it is clear that a $1/T$ dependence might reasonably well describe individual data sets. In contrast an exponential dependence gives a better description for the data over the full temperature range, as shown in the blue dashed line. For the $N = 1$ sample (Figure 6.3a) we observe that the α loss peak decreases strongly in amplitude at higher temperatures, which is an indication of crystallisation. The overall behaviour demonstrates that $\Delta\varepsilon$ decreases with increasing chain length. This trend is further highlighted in the T_g rescaled plot shown in Figure 6.10b. The trend is most pronounced for the lower chain length samples in the series. The higher chain length samples on the other hand appear to have similar values of $\Delta\varepsilon$. This is consistent with previous measurements of PS which indicate an almost identical shape (i.e. peak area) of the α loss for samples ranging from $N \approx 6$ to 36000 in mechanical [26] and dielectric measurements [269].

Values of $\Delta\varepsilon$ were also obtained from fits of the HN function to the α loss peaks. These parameters are shown in Figures 6.11a and b. The values are

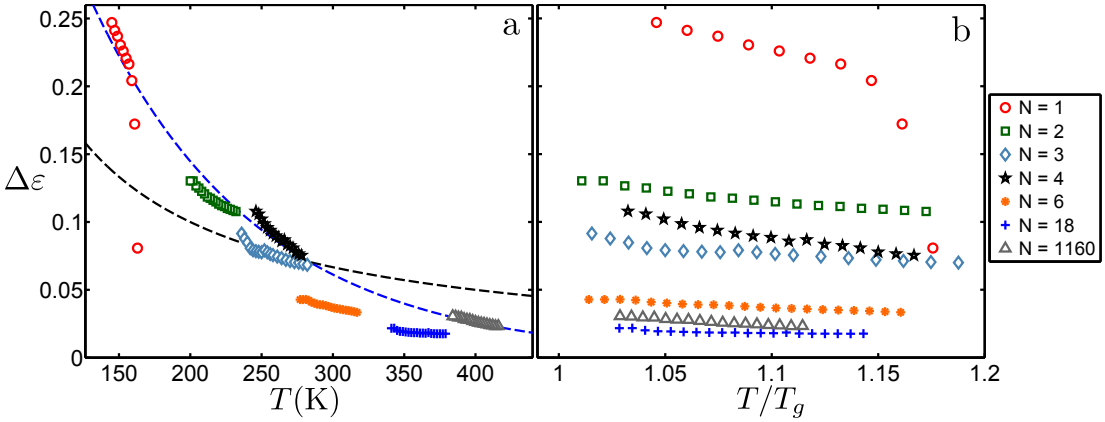

Figure 6.11: Dielectric strength, $\Delta\varepsilon$, parameters obtained from fits of the HN equation to the dielectric spectra plotted against a) T and b) T/T_g. The blue and black dashed lines in panel a) are examples of exponential and $1/T$ behaviour respectively.

very similar to those obtained through numerical integration of the fits of the RB function suggesting that both functions provide a similar description of the overall shape of the α loss peaks. Again, a simple $1/T$ and exponential dependence, respectively, are shown in Figure 6.11a in order to highlight the decrease of $\Delta\varepsilon$ with increasing temperature.

In order to further analyse the temperature dependence of the $\Delta\varepsilon$ values, the Kirkwood-Frölich generalisation of the Onsager equation was parametrised for the $N = 1$ sample in a similar manner to the analysis shown in Chapter 4 for the $M = 2$ sample. The equation is restated here to aid the following discussion[94, 96, 100–103]:

$$\Delta\varepsilon = \frac{\varepsilon_s(\varepsilon_\infty + 2)^2}{(2\varepsilon_s + \varepsilon_\infty)} \frac{n}{9k_BT\varepsilon_0} g_K\mu^2. \tag{6.2}$$

Where ε_s and ε_∞ are the limits of $\Delta\varepsilon$ at low and high frequencies respectively, ε_0 is the permittivity of free space, μ is the dipole moment and n, is the number density of dipoles within a material, where $n = \rho N_A/M_w$. The correlation factor, g_K, introduced by Kirkwood and Frölich [102, 103] is a measure of the alignment of the dipoles due to orientational correlations between molecules [94]. Values of $g_K < 1$ indicate that the dipoles have anti-parallel alignment and parallel alignment is indicated by values of $g_K > 1$.

It should be noted that accurate calculations of $\Delta\varepsilon$ using Equation 6.2 are difficult for polymer melts, since it is not generally clear how to model the correlations between a dipole in a repeat unit and those in neighbouring repeat units in the same chain or in other nearby chains [96, 286]. Successful calculations have thus only been obtained for isolated polymer chains via statistical mechanics and the rotational isomeric state model [96, 287]. Such calculations are beyond the scope of this thesis, however a test of Equation 6.2 was made for the $N = 1$ sample in the following manner:

1. In order to estimate the number density of dipoles, n, it was assumed that the temperature dependence of the density of the $N = 1$ sample would be the same as that of polystyrene. The density ρ in the measured temperature range was determined using an empirical expression given by Höcker *et. al.* [288].

2. The dipole moment of the styrene monomer unit was taken to be 0.6 D from measurements of the dielectric constant of atactic polystyrene by Krigbaum *et. al.* [289].

3. Values for ε_s and ε_∞, the limits of the dielectric permittivity at low and high frequencies respectively, were obtained from the real part of the dielectric permittivity, ε' (a figure depicting how these values can be obtained from ε' has been shown in Chapter 2).

4. The correlation factor, g_K, was varied such that the resulting $\Delta\varepsilon$ values fell into the same region as those obtained through integration of the fits of the RB function to the dielectric spectra.

Figure 6.12a shows the result of this analysis with the dashed black line indicating the expected behaviour of $\Delta\varepsilon$ calculated using Equation 6.2. In order to scale these values, a value of $g_K = 0.38$ was used. This implies anti-parallel alignment of the dipoles within the sample. It is clear from this figure that the values obtained through numerical integration have a stronger temperature dependence than those predicted by Equation 6.2. However, the predicted values were calculated under the assumption that the density dependence of the $N = 1$ sample

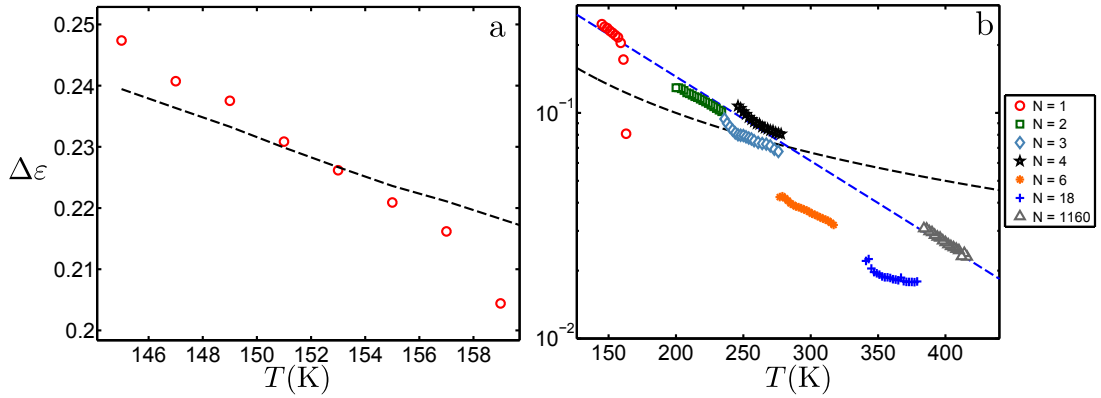

Figure 6.12: a) $\Delta\varepsilon$ parameters for the $N = 1$ sample obtained through integration of the fits of the RB function to the dielectric spectra. The dashed black line indicates an example of the expected Onsager behaviour for $\Delta\varepsilon$. b) $\Delta\varepsilon$ values for the series plotted on a log-scaled y-axis. The dashed black line indicates a simple $1/T$ behaviour and the dashed blue line indicates a guide to the eye, hinting at an exponential dependence of $\Delta\varepsilon$ with temperature.

should be the same as that obtained for polystyrene and this is not necessarily the case. Furthermore, it was assumed that g_K is independent of temperature.

To empirically investigate the development of $\Delta\varepsilon$ across the molecular weight range of this series, a plot of $\log_{10}(\Delta\varepsilon)$ against T was constructed and this is shown in Figure 6.12. The dashed black line indicates the simple $1/T$ behaviour as shown in Figures 6.10 and 6.11. In this scaling, the values for each sample appear to have an almost linear dependence with temperature. Furthermore, if we were to take values of $\Delta\varepsilon$ at a certain temperature for each sample, the values would follow this linear dependence across the temperature range, with the exception of the $N = 6$ and $N = 18$ samples. This trend is highlighted by the dashed blue guide to the eye in the figure. This implies that the $\Delta\varepsilon$ values relatively well follow a exponential dependence with temperature. The implication of this behaviour would be that the dielectric strength is solely set by the temperature and the molecular weight only controls the temperature range that is probed and thus by changing the molecular weight, one can access different part of the exponential master curve. Presently, we do not know the exact origin of such a possible exponential behaviour. It is, however, interesting that a similar behaviour has been observed for a chain-length series of polypropylene glycol dimethyl ethers

[18] and as will be shown in the next chapter, the same behaviour is observed for poly(α-methylstyrenes).

Loss peak amplitude

Although one normally characterises the 'size' of the α loss peaks using the dielectric strength, we can also consider the amplitude of the peaks, ε''_p. This is a very direct method of quantifying the size of the peak as the parameters can be read-off from the dielectric spectra. Values for the amplitude parameter are shown in a log-scaling in Figure 6.13. In such a scaling, the parameters show a decrease with increasing degree of polymerisation, in a similar manner to that observed for the $\Delta\varepsilon$ data. Signs of crystallisation of the $N = 1$ sample are indicated by the dramatic decrease of the amplitude for the highest measured temperatures. It appears that, in general, the amplitude of the α loss peak decreases with increasing temperature for the samples in this series highlighted in the T_g rescaling shown in Figure 6.4b. However, there is no signature of a peak in these values as observed for the alkylbenzene series.

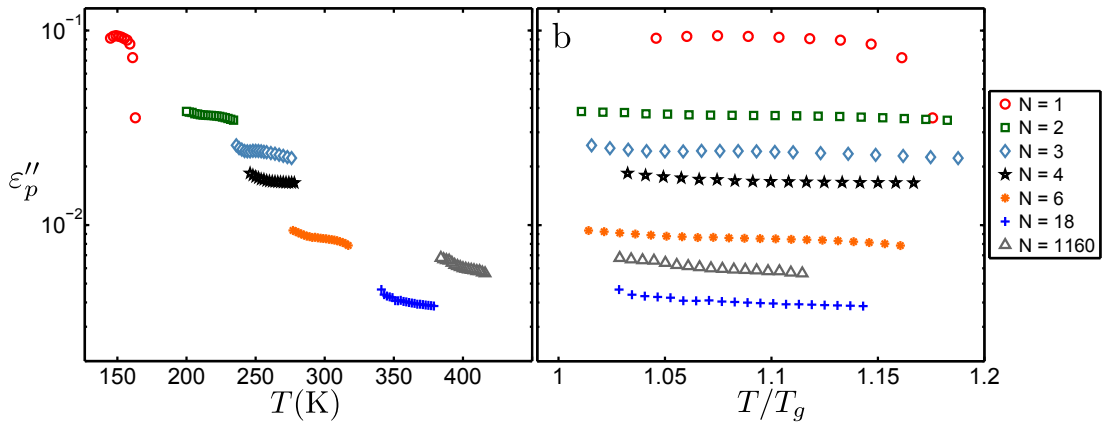

Figure 6.13: ε''_p parameters obtained through fits of the RB function to the dielectric spectra plotted against a) T and b) T_g/T.

6.2.5 Relaxation timescales

In this section, the characteristic timescales, τ_α, of the α relaxations for the styrene series will be discussed. The data were determined from the peak fre-

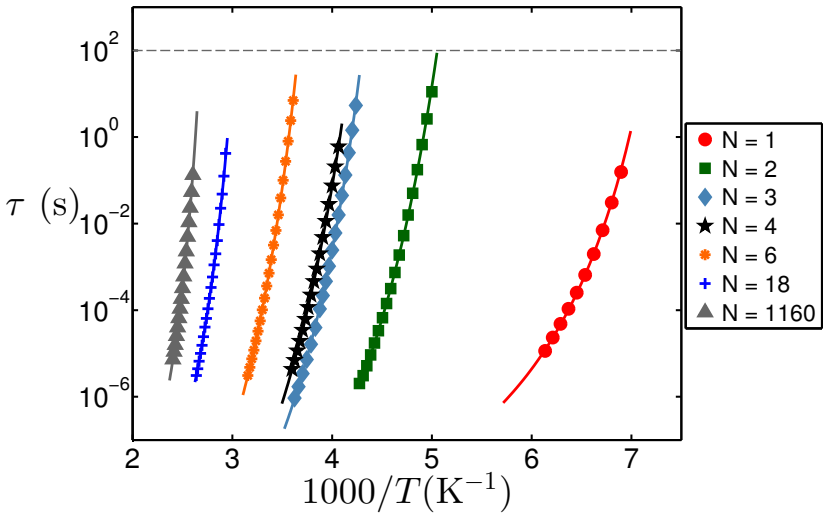

Figure 6.14: τ_α data for the styrene series. The black dotted line indicates $\tau =$ 100s. The solid lines are fits of the VFT equation to the data.

quencies obtained through the fitting of the α loss peak with the RB function as $\tau_\alpha = 1/\omega_p$. It was shown in the previous chapter that timescales obtained through fitting of both the RB and HN functions show no significant differences in values of τ_α and the same was true for this series. The data are shown in Figure 6.14 and show the expected trend with increasing chain-length: a shift in the τ_α values to higher temperatures for the longer chain-length samples [69, 146, 258]. This shift is largest between the values for the $N = 1$ and $N = 2$ samples and becomes less pronounced as the sample chain length increases.

The relaxation time values are all well described by fits of the Vogel-Fulcher-Tammann equation [27–29] and the fit parameters are shown in Table 6.2. The values of T_0 increase systematically with increasing molecular weight and the values for τ_0 adhere to values close to typical microscopic timescales at high temperatures [2, 24–26] and show no systematic variation with degree of polymerisation. The other parameters in Table 6.2 (D, m and T_g) will be discussed in full in the following sections.

N	$log_{10}\tau_0$(s)	D	T_0(K)	T_g(K)	m
1	-(10.4 ± 0.5)	4.4 ± 0.3	121.2 ± 0.9	139.7	93.7
2	-(-14.4 ± 0.2)	9.5 ±0.4	158 ± 1	197.9	81.2
3	-(14.3 ± 0.2)	9.0 ± 0.3	187.5 ± 0.9	232.4	84.6
4	-(15.1 ± 0.3)	11.1 ± 0.6	186 ± 2	238.3	77.8
6	-(14.7 ± 0.2)	9.4 ± 0.4	220 ± 1	273.1	85.1
18	-(13.1 ± 0.2)	5.9 ± 0.3	283 ± 2	331.6	104.1
1160	-(12.6 ± 0.2)	4.5 ± 0.2	329 ± 0.2	373.3	122.5

Table 6.2: Table showing the fitting parameters obtained through fits of the VFT equation to the τ_α data. The table also includes T_g and the fragility parameter m for each sample. The reported errors were obtained from a least mean squares fit of the VFT function to the τ_α data.

6.2.6 Glass transition temperature

Values for the glass transition temperature, T_g were obtained by extrapolating the fitted VFT descriptions of the τ_α data to a timescale of 100s. This timescale is denoted by the horizontal dashed line in Figure 6.14. A plot of T_g as a function of molecular weight is shown in Figure 6.15a including values obtained from the onset of the characteristic step in C_p (see Section 6.5). In this linear scaling of M_w the data for the N = 16, 18 and 28 samples are well described by the often used Fox-Flory equation (introduced in Chapter 5) as denoted by the green dashed line. Note that this figure does not show data for the N = 1160 sample in order to highlight the development of T_g for the lower chain-length samples but this data was also used in order to test the Fox-Flory equation. However, the T_g values are not well described by such a fit for the lower molecular weight samples.

A similar plot of the T_g data is shown in Figure 6.15b, with a logarithmic scaling of the x-axis. It is also clear from this scaling that the Fox-Flory behaviour does not scale as well for the low molecular weight samples.

In order to further analyse the molecular weight dependence of T_g data, the obtained values for T_g were compared with those obtained from several sources in the literature [258–261]. The T_g data obtained in this series are clearly consistent with those in the literature. It was shown in Chapter 5 that the behaviour of T_g as a function of molecular weight can often be split into three distinct regions as first introduced by Cowie [259] and these regions are denoted by the

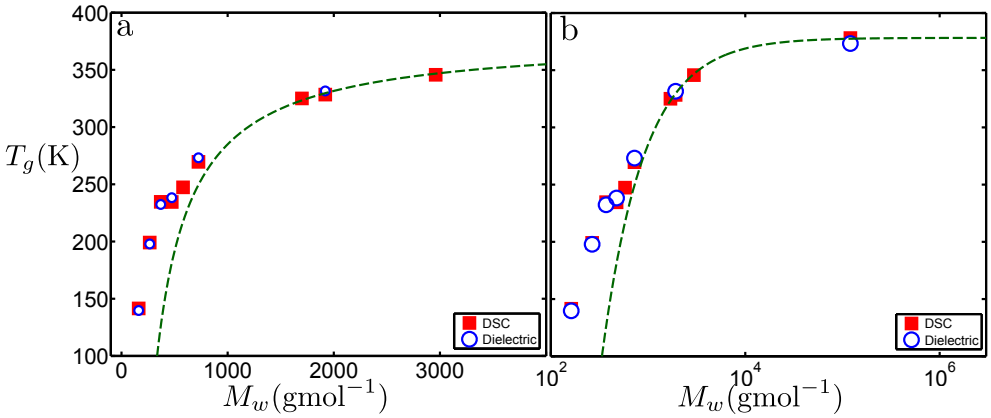

Figure 6.15: a) T_g data obtained through analysis of the DSC traces (taken at 10K/min) of the styrene series in comparison to those obtained through analysis of the dielectric spectra plotted against M_w. The range of M_w has been cut to highlight the development of T_g for the shorter chain-length samples. b) T_g versus $\log_{10}(M_w)$. The green dashed lines in both figures indicate fits of the Fox-Flory equation.

vertical dashed lines in Figure 6.16. The transition molecular weights between the different regions, M_w^I and M_w^{II}, were obtained from the paper by Hintermeyer *et. al.* [258]. The data within each region are well described with a linear fit, shown by the black solid lines through the data in Figure 6.16. However, we note that the T_g value for the monomer is not so clearly well described by the fit of the Region I data. This implies that there might be a change in the behaviour between the monomer and the dimer.

In order to provide a simpler comparison between the different regions, the data were colour designated depending on the region in which they fell as shown in Figure 6.16b. Region I refers to low molecular weight oligomers and shows a linear dependence of T_g with increasing M_w. Region II also shows a similar but weaker dependence of T_g with M_w. Region III refers to the high molecular weight polymers for which the T_g values are no longer molecular weight dependent. Hintermeyer *et. al.* suggested that the transition point between Region I and Region II, M_w^I could be related to the molecular weight of a Rouse unit or Kuhn unit [290] and would thereby mark the point at which more coarse grained polymer chain dynamics come into effect [258]. The authors also state that the transition point between Regions II and III is similar to the molecular weight

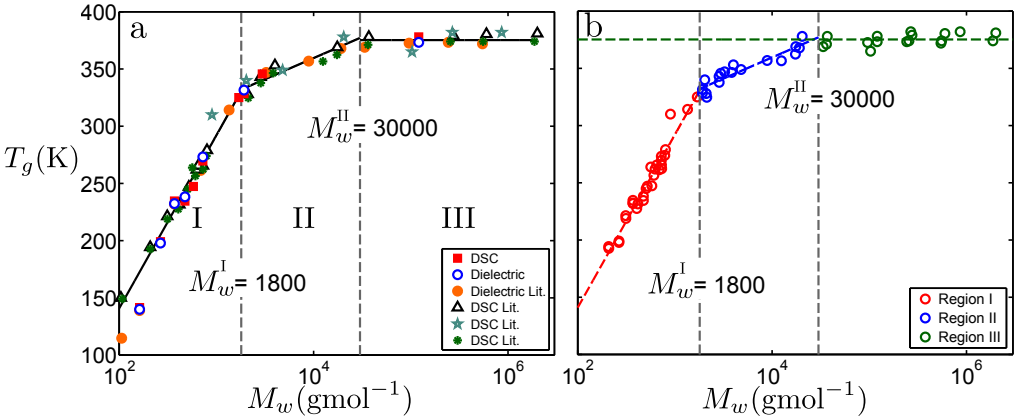

Figure 6.16: a) T_g data obtained through analysis of the DSC traces of the styrene series in comparison to those obtained through analysis of the dielectric spectra and also to examples from the literature (Hintermeyer *et. al.* [258]: orange circles, Cowie [259]: light blue stars , Claudy *et. al.* [261]: black triangles, Bartenev *et. al.* [260]: green asterisks). Vertical lines indicate the separation of regimes of T_g dependence with molecular weight and solid lines are linear fits to the data in these regimes. b) T_g values clearly separated into three regions.

of entanglements, M_e, and could thus be an indication of the onset of reptation dynamics of the polymer chains. However, this idea has was contested in further analysis of the data [262] as explained in Chapter 5.

The number of monomer units associated with M_w^I and M_w^{II} are 16 and 288, respectively. One could hypothesize that the dynamic behaviour of the polymer chain changes at M_w^I from that associated with the number of monomers in a chain to that in which the dynamics of a different coarse-grained unit, with a size on the order of a Rouse unit, sets the value of T_g for the polymer melt. There is no consensus as to the Kuhn length, or size of a Rouse unit, for PS. The theoretical value has been estimated to be 20Å, corresponding to 8 - 10 monomer units but experimental determinations have yielded a value closer to 50Å, corresponding to $\approx$ 50 monomer units [242]. Still, it makes sense that the transition from Region I to Region II is associated with the onset of course-graining and the emergence of a new characteristic length-scale, which can be estimated by the M_w^I and thus corresponds 16 monomer units; we will in the following discussion call this the Rouse unit. We can express M_w^I and M_w^{II} in terms of the Rouse units as corresponding to 1 and $\approx$ 17 units respectively. The

width of Region II ($M_w^{II} - M_w^I$) is then equivalent to 16 units. Thus, interestingly the width of Regions I and II are equivalent in terms of the monomer unit and the Rouse unit, respectively. Therefore, it could be said that the increase of the number of 'fundamental units (monomers in Region I, Rouse units in Region II) in a polymer chain causes a systematic increase in T_g until a certain number of Rouse units are reached, at which the dynamics become independent of molecular weight. It might be reasonable to hypothesize that Region III is entered as the chains are long enough to be well described using Gaussian statistics. It should be reiterated, however, that these arguments are based on a number of obvious caveats. Firstly, we have assumed that the size of a Rouse unit corresponds to 16 monomer units whereas in reality, this size could be quite different. Secondly, the statistical descriptions of very short oligomeric chains in Region I and longer course-grained ones in Region II should show significant differences.

The point at which polymer chains are long enough to be described as a Gaussian random walk is an interesting topic of discussion in itself [242, 291–293]. The polymer chain is in the Gaussian regime when fluctuations of its end-to-end distance can be described with Gaussian statistics. However it is difficult to quantify the transition between dynamic regimes purely based on experimental data. Gainaru *et. al.* [291] studied the dielectric normal mode and structural relaxation mechanisms of polypropylene glycol in order to address this issue. Specifically they looked at the ratio between the dielectric strengths of these two mechanisms and observed that over a certain number of monomer units ($N = 30$) the ratio remained fixed with respect to further increase of monomer units. The authors state that this ratio should be independent of molecular weight within the Gaussian regime and therefore state that $N = 30$ corresponds to the onset of this regime. This particular polymer however has hydroxyl end-groups and is known to form larger 'effective' chains mediated by hydrogen bonding so this exact number would only provide a lower bound to any estimate for non-associating systems such as PS. Unfortunately, the same type of analysis described above can not be performed for PS. The normal mode relaxation is not resolvable in dielectric spectra as PS does not have a component of its dipole aligned along the backbone chain. Ding *et. al.* provide an analysis for PS by plotting T_g against M_w/m_R, where m_R is the molecular weight of a Rouse unit [292]. They state that

the m_R for PS should be $\sim$ 50 monomer units. This is significantly larger than the traditionally defined Kuhn segement size which is found to be between 8 - 10 monomer units (see Chapter 5) but the authors have previously shown that this estimation of m_R provides a better description of experimental data from small angle neutron scattering and neutron spin-echo experiments [242]. In plots of T_g versus M_w/m_R the authors show that at a certain point T_g becomes invariant of this ratio. They attribute this behaviour to the onset of Gaussian chain dynamics and state that this occurs at a molecular weight of 10 - 20 Rouse units, equivalent to a molecular weight of 50000 - 100000 g/mol, which is quite similar to where we observe the start of Region III for PS. Furthermore, Kreer *et. al.*[294] found that there were no well defined boundaries for either Rouse dynamics or reptation dynamics in Monte-Carlo simulations of model polymers ranging from $N = 16$ to 512. The transitions between different dynamic regimes were much smoother than implied by the variation of T_g shown here. Therefore it is unclear whether the onset of Region III can be explained by the appearance of Gaussian statistics or not. However, there is clearly a difference in the T_g dependence which occurs at a molecular weight lower than that predicted for the size of a Rouse unit by Ding *et. al.* [242].

6.2.7 Dynamic fragility

The fragility parameter, m, was obtained using the method described in Chapters 1 and 4, using the τ_α data obtained through fits of the dielectric spectra. These values are shown in Figure 6.17 in comparison with m values obtained by Hintermeyer *et. al*[258]. The two sets of data are in reasonable agreement with each other. It was noticed for the alkylbenzene series that the fragility parameter showed a systematic increase with increasing molecular weight. However, this trend does not seem to hold for the lower molecular weight samples in this series as the lower molecular weight samples have similar values of m. The values for the $N = 18$ and 1160 samples have a much higher m value than the lower molecular weight samples. We saw in the previous section that the temperature dependence of T_g changes at a certain molecular weight which has previously been attributed to the size of a Rouse unit [258]. Thus, a possible implication

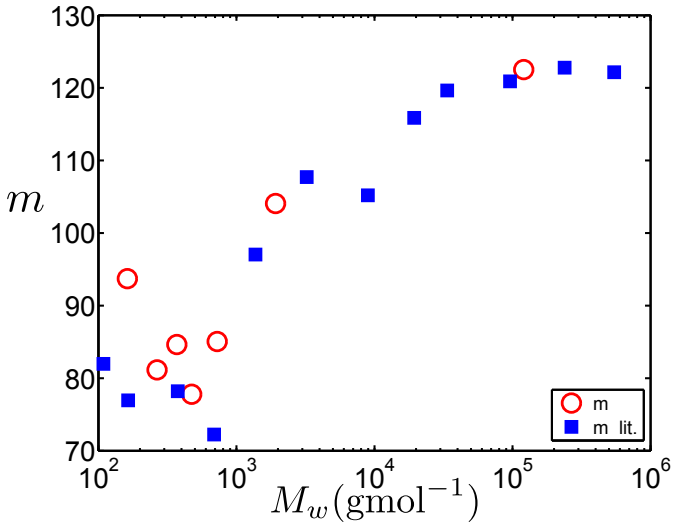

Figure 6.17: Values for the fragility parameter m for the styrene series in comparison with values obtained from the literature [258].

of these results is that higher dynamic fragility is introduced as the nature of the dynamics of the polymer chain changes. The m parameters also indicate a systematic increase with M_w beyond the molecular weight corresponding to the Kuhn length (as defined by Hintermeyer *et. al.* $\approx$ 1800 g/mol) before a constant m observed for the highest molecular weight samples. A further implication is that the dynamic fragility is only variable in Region II, whereas it is relatively fixed in Region I and III.

Strong glass-formers, have low m values and an m value of 16 corresponds to 'strong' Arrhenius-like behaviour [2, 11] (if τ_0 is assumed to be 10^{-14}s). The m values presented for this series indicate a dramatic departure from Arrhenius like behaviour of the τ_α values. Particularly high fragilities have been observed for several bulk polymeric samples including polymethylmethacrylate (PMMA), polypropelene (PP), polyvinylchloride) (PVC) and polycarbonate (PC) [11, 116, 190, 295]. This suggests that a high fragility is a common property of polymers.

6.2.8 Linearisation of relaxation timescales

In order to further analyse the temperature dependence of τ_α, the timescale values were linearised by performing the analysis presented by Stickel *et. al.* [31] as

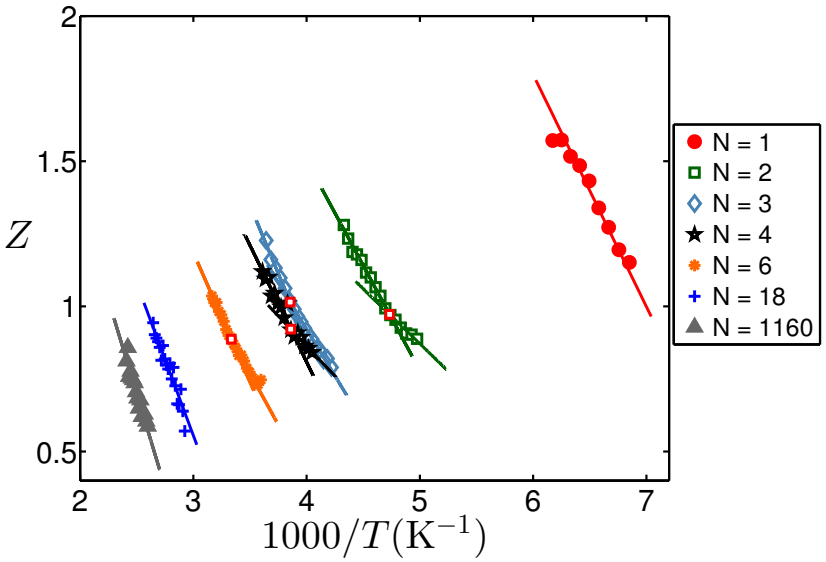

Figure 6.18: Stickel analysis of the τ_α data. The red squares indicate the crossover point for different regimes of Z, obtained through analysis as shown in Figure 6.19.

explained in Chapters 1 and 4. This was done as such an analysis can yield subtle differences in the behaviour of τ_α which are not necessarily obvious in an Arrhenius plot. The results of this linearisation are shown in Figure 6.18. The Z parameters obtained for the $N = 1$, 18 and 1160 samples demonstrate dynamic behaviours which are well described by the linearised VFT fits of the τ_α values. The fits through the Z data for these samples have a gradient, S, formulated from the VFT parameters:

$$S = \left(\frac{T_0}{log e^1 D} \right)^{-\frac{1}{2}} \tag{6.3}$$

The $N = 2$, 3, 4 and 6 samples show a 'kink' in the Z parameter indicating a change in the temperature dependency of τ_α and therefore these samples could not be described by the corresponding linearised VFT fits over the whole temperature range. To investigate this behaviour in more detail, the crossover points between the two different temperature dependencies of Z for these samples were determined by fitting the low and high temperature regimes with linear fits and calculating the point at which the two linear descriptions of the data crossed.

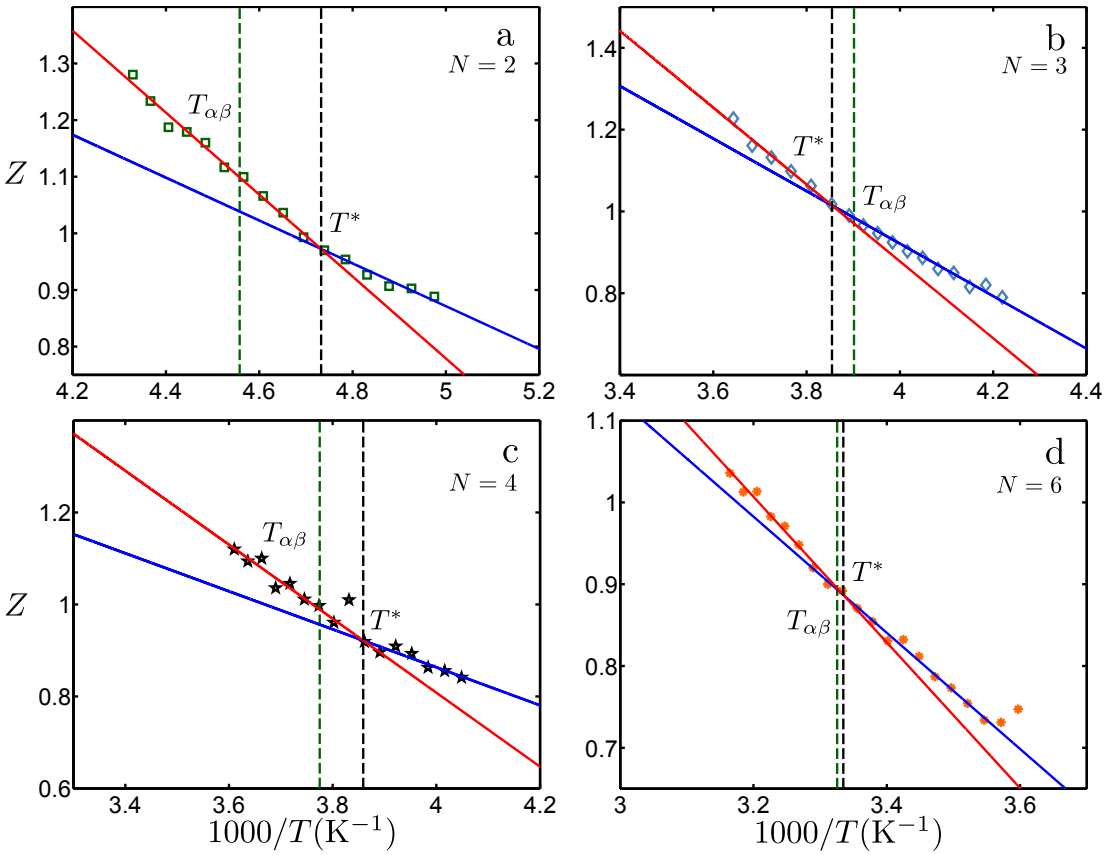

Figure 6.19: Stickel parameters for the a) N = 2, b) N = 3, c) N = 4, and d) N = 6 samples showing possible changes in gradient of the Z parameter. Vertical dashed lines indicate the crossover point T^* defined in this case as the crossover between the two gradient regimes. Also shown are vertical dashed green lines indicating the position of $T_{\alpha\beta}$ determined through calculation of expected τ_β values using 'Procedure 1' as described in Section 6.4.1

This analysis is shown in Figure 6.19 and the determined crossover points are indicated by the red squares in Figure 6.18. We observed that the crossover occurs at a similar Z value for the $N = 2$, 3, 4 and 6 samples. It should be noted that the temperature ranges used in the determination of the point at which the temperature dependency of Z changed were chosen somewhat arbitrarily. For instance, Figures 6.19b and d show the linearised τ_α data for the $N = 3$ and 6 samples and the difference between the two fitted regions in each case is slight. Error analysis of this procedure has not been completed but the determined crossover points give a reasonable indication of the temperature *range* of the dynamic crossover. As a means of comparison, $T_{\alpha\beta}$ values are shown as vertical dashed green lines. These indicate the temperature at which a crossover was observed between the τ_α data and expected values of τ_β as will be explained in Section 6.4.1. We observe that values of $T_{\alpha\beta}$ are in the same temperature range as determined values of T^* for the $N = 3$, 4 and 6 samples, validating the method for determining T^*. However there is a discrepancy between these values for the $N = 2$ sample.

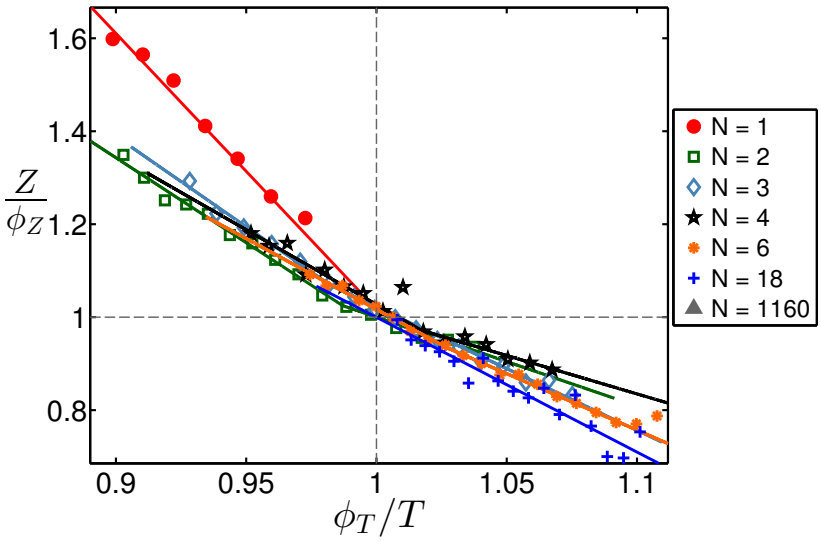

Figure 6.20: Stickel parameters rescaled by both ϕ_T and ϕ_Z in order to collapse the Stickel data for all samples.

To facilitate a comparison of the Z parameters obtained for the samples, the data were rescaled in both T and Z by the values corresponding to the crossover

point for the samples where a kink was observed. Since very similar values of Z^* were observed, see Figure 6.18, for the N = 1, 18 and 1160 samples where a kink could not be observed we used a Z^* taken as an average of the four determined values. For the samples where a kink was not observed, T^* values were determined that correspond to the calculated average Z^*. This rescaling is shown in Figure 6.20. One finds that the samples, except for N=1, follow a similar temperature dependence in high temperature range $T/T^* > 1$ although there is a non-systematic variation of the behaviour with molecular weight in the low temperature range $T/T^* < 1$.

6.3 Dielectric spectroscopy: γ relaxation

In this section, the analysis of the secondary relaxation mechanism manifested as a symmetrically stretched loss peak in ε'' observed for the N = 1,2 3, and 4 samples will be discussed. This relaxation will be termed the γ relaxation in this chapter due to the similarities of the activation energy and timescales of the observed relaxations with the so-called γ relaxation observed through mechanical measurements of bulk polystyrene [204] (this similarity will be shown in Section 6.3.4).

6.3.1 Spectra

The observed γ relaxation loss peaks have relatively low dielectric strength in comparison to the α loss peaks and were therefore more difficult to distinguish in the dielectric spectra. In order to address the repeatability of the observed γ relaxation, two different runs (where each 'run' involves a separate sample preparation) of the $N = 3$ sample were performed. The samples were cooled at the maximum rate of the cooling system ($\sim$ 20K/min) to a temperature just below the glass transition temperature. Measurements were obtained upon further cooling of the sample in steps of 5K. A comparison of the spectra obtained for the different runs of the $N = 3$ sample at 140 K are shown in Figure 6.21. It is clear from this figure that the γ relaxation is clearly observed in both instances, although

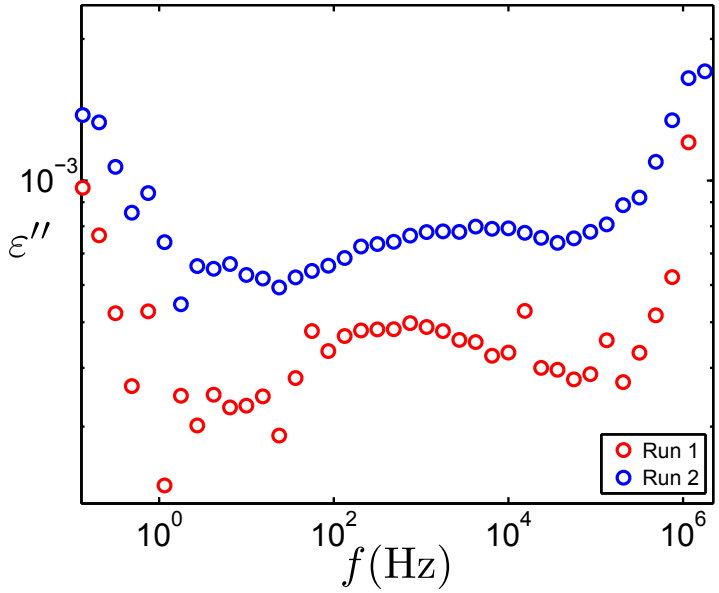

Figure 6.21: Dielectric spectra taken at 140K for the $N = 3$ sample showing two separate runs taken using two different spectrometers.

the dielectric strength appears to be different. This was also seen in similar 're-peatability' experiments for the secondary process observed for the alkylbenzene series. The reason for the difference in $\Delta\varepsilon$ is likely to be a consequence of the fact that cooling a glass-forming material into the glassy state does not necessarily yield the same amorphous structure [51, 194]. This has been fully discussed in Chapter 4.

It is also clear from this figure that contributions to the spectra at both low and high frequencies must be described in order to analyse the behaviour of the γ loss peak in ε''. The low frequency contribution is due to the high frequency power-law flank of the α loss peak. The physical origins of the high frequency contribution are unclear but it has similar characteristics to the high frequency contribution observed in the α relaxation temperature regime, as discussed in Section 6.2.

6.3.2 Rescaled spectra

In order to gain a qualitative estimate of the variation of the shape and frequency position of the γ loss peak for the samples, the loss peaks were rescaled in both

frequency and ε'' in order to create master curves of the spectra. This rescaling is shown in Figure 6.22. The spectra were scaled using the parameters ϕ_f and $\phi_{\varepsilon''}$. These parameters were determined by rescaling the peaks onto the loss peak obtained at the lowest measured temperature. This rescaling demonstrates that the overall shape of γ loss peak appears to be preserved throughout the measured temperature range. We note that the $N = 2$, 3 and 4 samples have a significant high frequency power-law contribution to the dielectric loss. At the highest temperatures, the γ process became significantly merged with this high frequency contribution. This made the rescaling of the spectra difficult as the shape of the peak became more obscured at these temperatures. At the other end of the temperature range, the spectra for the $N = 2$ sample became quite scattered at low frequencies. This again made the rescaling process difficult.

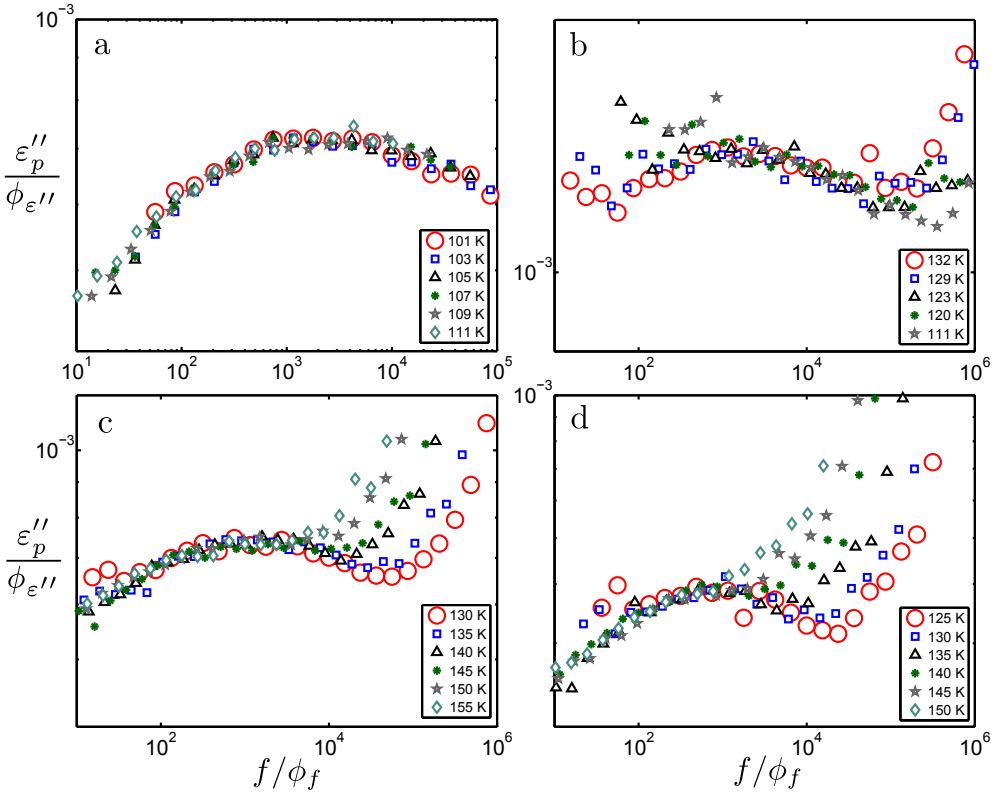

Figure 6.22: Dielectric spectra in the β relaxation regime for a) N = 1, b) N = 2, c) N = 3 and d) N = 4 samples rescaled in both frequency and ε''.

6.3.3 Fitting procedure

The γ loss peaks could be well described with the Cole-Cole (CC) expression. The high frequency contribution observed in Figure 6.22 was fit using a power law, with the exponent kept reasonably fixed and allowing for small variations of the amplitude. Figure 6.21 indicates another low frequency contribution, most likely due to the proximity of the α relaxation. It was found that this low frequency contribution did not have a significant effect on the shape of the γ relaxation for the $N = 1$ sample. Thus, the low frequency range was restricted such that the low frequency contributions could be neglected. For the other samples, the low frequency contribution was described with a power-law of the form $\varepsilon'' = A\omega^{-k}$. The results of this fitting procedure are shown in Figure 6.23 and the fit lines interpolate the spectral data well.

The parameters relating to the dielectric strength, $\Delta\varepsilon$, and the symmetric stretching, α, parameters from fitting of the CC function are shown in Figure 6.24. These parameters demonstrate quantitatively that there was little variation in the strength or the shape of the γ loss peak with increasing temperature. The values for $\Delta\varepsilon$ shown in Figure 6.24a) show a difference between the samples but the variation is not systematic with chain-length. Likewise, the α parameters show that the symmetric stretching of the loss peaks is independent of chain length.

In order to confirm the behaviour of the $\Delta\varepsilon$ parameters obtained from fits of the CC function, the values were compared to the amplitude scale factors, $\phi_{\varepsilon''}$, used to rescale the spectra as shown in Figure 6.22. The method for determining $\Delta\varepsilon$ from the rescaling parameters is fully described in Chapter 4. Firstly, the amplitude of the γ loss peak at the lowest measured temperature was obtained. This was subsequently multiplied by the rescaling parameters in order to determine the temperature dependence of the amplitude. Finally, the corresponding $\Delta\varepsilon$ values were calculated. The comparison between the two determinations of the $\Delta\varepsilon$ parameters is displayed in Figure 6.25. The values from both fits of the CC function and rescaling of the spectra show good agreement for the $N = 1$, 2 and 4 samples. However, for the $N = 3$ sample, it appears that $\Delta\varepsilon$ obtained through fitting of the spectra have larger absolute values.

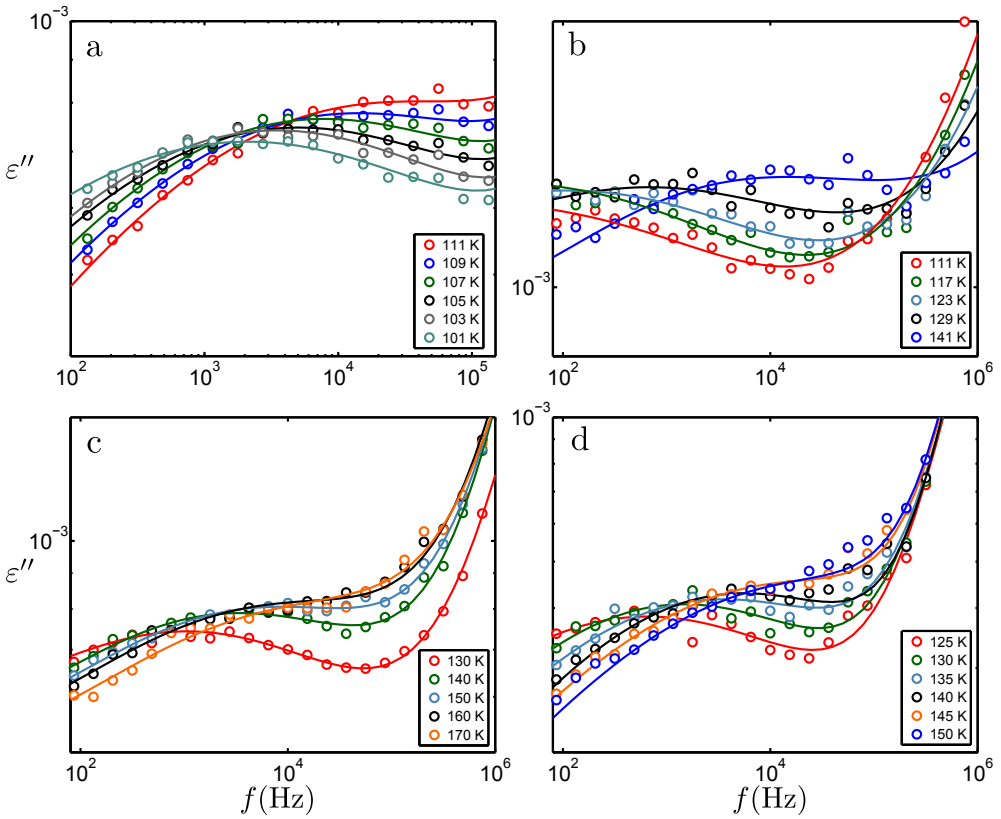

Figure 6.23: Dielectric spectra in the β relaxation regime for a) N = 1, b) N = 2, c) N = 3 and d) N = 4 samples. These spectra were fit using an additive combination of the Cole-Cole equation with a high frequency power law and, where appropriate, the RB function to take account of low frequency contributions due to the proximity of the α relaxation.

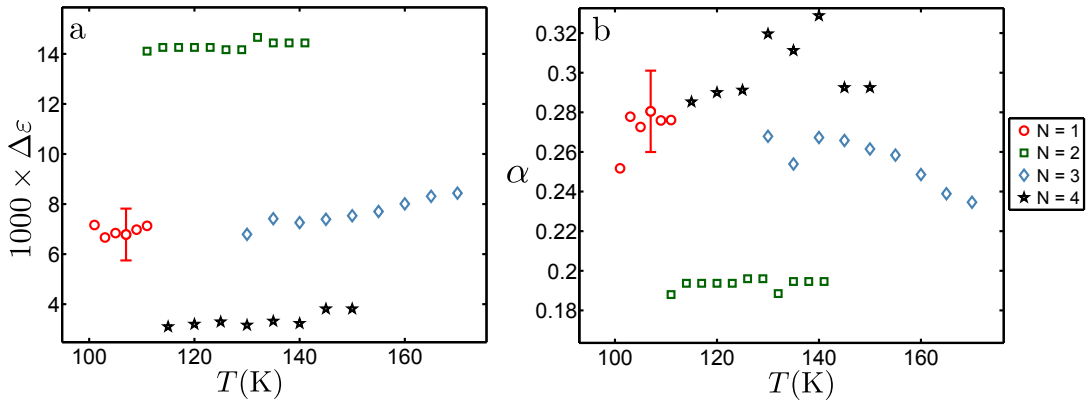

Figure 6.24: a) $\Delta\varepsilon$ and b) α parameters for the N = 1,2,3 and 4 samples obtained through fits of the γ relaxation process. Errors for the values obtained for the $N = 1$ sample are the standard deviation between different measurements.

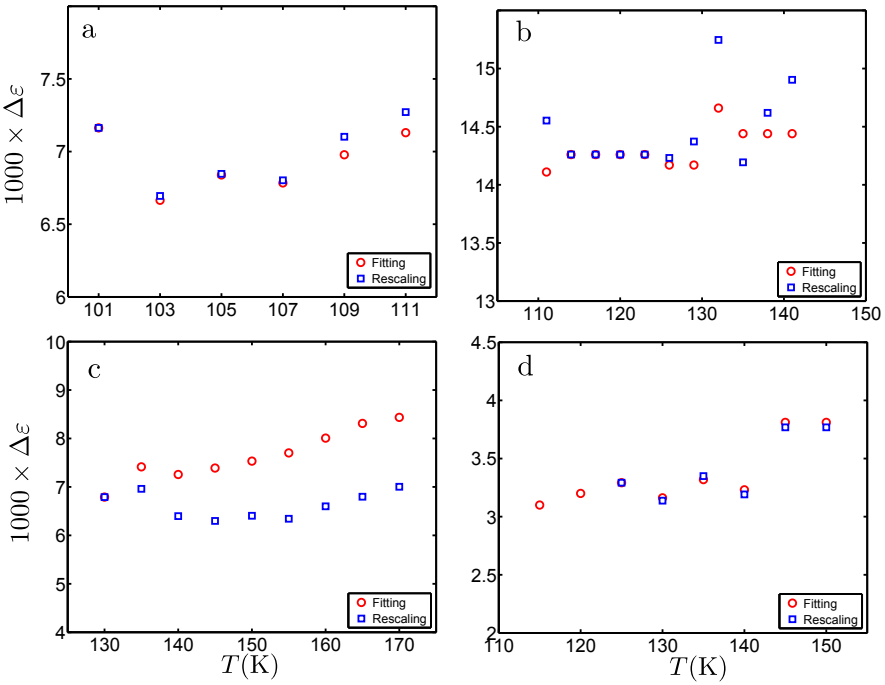

Figure 6.25: $\Delta\varepsilon$ values for a) N = 1, b) N = 2, c) N = 3 and d) N = 4 from both fitting and rescaling.

6.3.4 Relaxation timescales

In this section, the characteristic timescales corresponding to the observed secondary relaxation for the $N = 1$, 2, 3 and 4 samples will be discussed. Timescales corresponding to the frequency of the loss maximum for this relaxation, τ_γ, were obtained directly from the fitted Cole-Cole (CC) descriptions of the dielectric spectra as the characteristic timescale in the CC function corresponds to the peak timescale: $\tau_{CC} = \tau_p$. In order to confirm the values obtained through fitting of the spectra, τ_γ values were also obtained using the rescaling parameters, ϕ_f required to rescale the secondary loss peaks as shown in Figure 6.22. Values of ϕ_f across the measured temperature range were multiplied by values of τ_γ obtained through fitting of the CC function to the secondary loss peak at the lowest temperature for all samples. This allowed for an estimation of the temperature dependence of the timescale values obtained from the rescaling procedure. The comparisons between τ_γ values from fitting and rescaling are shown in Figure 6.26. The timescales show the same behaviour in both methods of determination, thereby confirming the results of the fitting procedure.

An Arrhenius plot showing the timescales for the α relaxation, τ_α, and the observed secondary relaxation, τ_γ, is shown in Figure 6.27a. Also shown are dashed grey lines indicating the behaviour of the timescales of the γ relaxation observed through mechanical measurements of PS performed by Yano *et. al.* [204] and the β relaxation observed through dielectric measurements of PS performed by Lupaşcu et. al. [268] (these timescales have also been confirmed in mechanical measurements by Cavaille *et. al.* [270]). The values of τ_γ obtained in this research are very similar to those of the so-called γ relaxation as obtained in literature and these are therefore likely to be indicative of the same relaxation mechanism.

In the T_g rescaling of this data as shown in Figure 6.27b the τ_γ values of the $N = 1$, 2, 4 and polymer samples appear to have a similar dependence; however, the $N = 3$ sample shows a slightly different temperature dependence. From the T_g scaled plot we see that the γ relaxation in this representation appears to become slower with increasing molecular weight. Interestingly, a similar trend was observed for the γ relaxation observed for the alkylbenzene series. The τ_γ

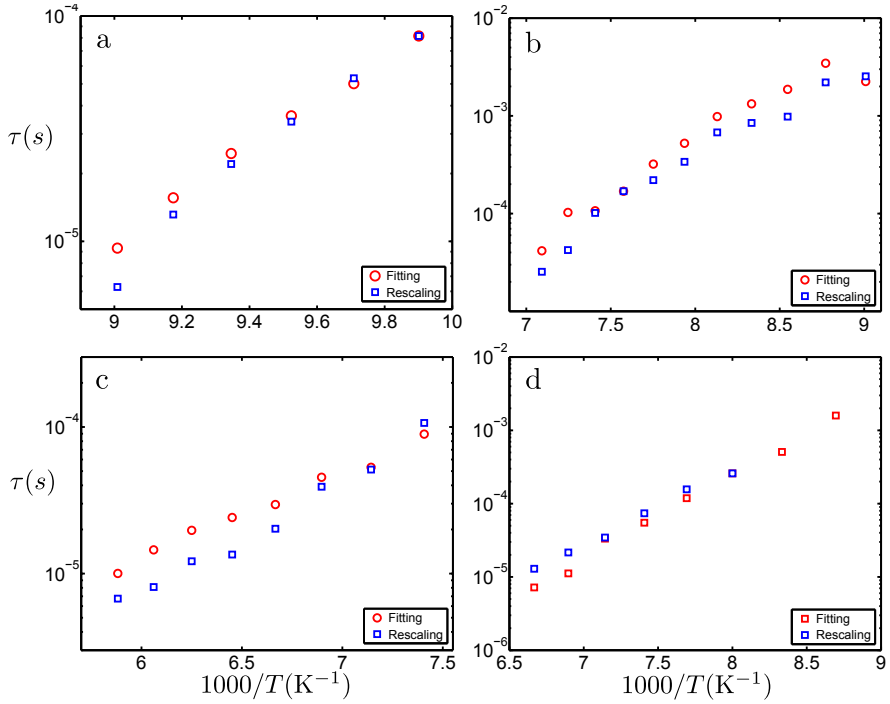

Figure 6.26: τ_β values for a) N = 1, b) N = 2, c) N = 3 and d) N = 4 from both fitting and rescaling.

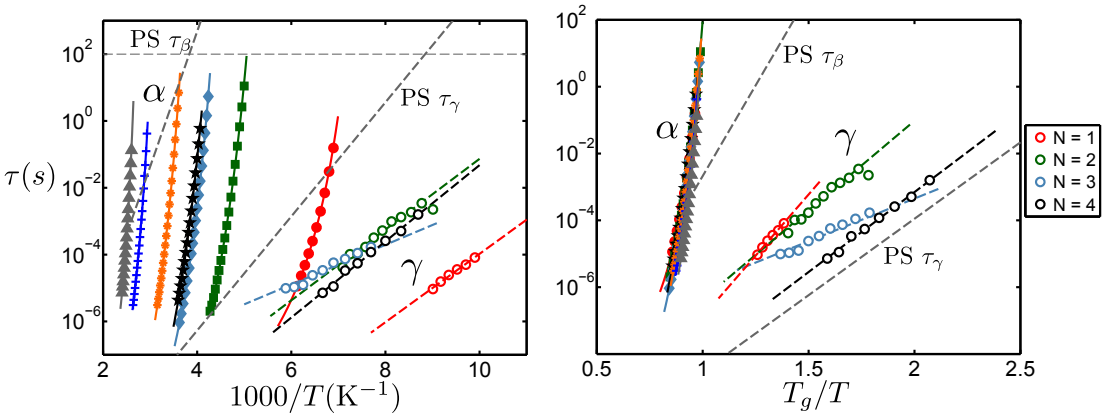

Figure 6.27: τ_α and τ_γ data for the styrene series plotted against a) $1000/T$ and b) rescaled by T_g. Solid lines indicate fits of the VFT equation to the τ_α data and dashed lines indicate fits of the τ_γ data with the Arrhenius equation.

Sample	E_A kJ/mol	$\log_{10}\tau_0$ (s)	K $\frac{E_A}{RT_g}$	Reference
$N = 1$	19.6 ± 0.8	-14.2 ± 0.4	16.9 ± 0.7	
$N = 2$	20.2 ± 0.9	-11.7 ± 0.4	12.3 ± 0.6	
$N = 3$	11.3 ± 0.4	-8.5 ± 0.1	5.9 ± 0.2	
$N = 4$	21.8 ± 0.7	-12.7 ± 0.3	11.0 ± 0.3	
$N \approx 3570$ (β)	77 ± 1	-13.5 ± 0.2	24.9 ± 0.4	[268]
$N \approx 2300$ (γ)	32 ± 3	-13 ± 1	10 ± 1	[204]

Table 6.3: Table showing the parameters obtained through fitting of the Arrhenius equation to the τ_γ data. Also shown are values obtained through fitting of the timescale data for the observed β [268] and γ [204] relaxations. Errors in the values were determined from least mean squares fitting of the data.

values are well described by the Arrhenius equation (as described in Chapters 1 and 4) denoted by the fitted dashed lines in Figure 6.27:

$$\tau = \tau_0 e^{\frac{E_A}{k_B T}} \tag{6.4}$$

Where τ_0 is the limiting timescale of the relaxation at high temperatures and E_A is the activation energy of the relaxation mechanism. The values of E_A and τ_0 are shown in Table 6.3. Also shown are values of the constant of proportionality, K between E_A and T_g as determined using the equation postulated by Kudlik *et. al.*[15, 55, 61]

$$E_A = KRT_g \tag{6.5}$$

Where R is the universal gas constant.

The values of E_A shown in Table 6.3 for the $N = 1$,2 and 4 show reasonable agreement with the determined activation energy of the so called γ relaxation observed in mechanical measurements of bulk PS [204] and are clearly very different from the activation energy of the β process as observed in both dielectric and mechanical data [268, 270]. This further solidifies the postulation that the observed secondary relaxation for low molecular weight samples in this series is similar in nature to the previously observed γ relaxation. The E_A values for the $N = 3$ sample is lower than the values obtained for the other samples but it should also be noted that it also has an unusually high value of τ_0 whereas the τ_0

values obtained for the other samples shown in the table agree with the expected typical microscopic timescales of 10^{-12} to 10^{-14} [2, 24–26].

The γ relaxation has also been observed in nuclear magnetic resonance (NMR) measurements [200–202] and in molecular dynamics (MD) simulations [203] and the timescales obtained agree well with those obtained from dielectric and mechanical measurements. However, the physical nature of the mechanism itself is not clear. Lyulin *et. al.* [203] attributed the observed relaxation with the translation of the phenyl-rings and the main chain whereas Schaefer *et. al.* and Kulik *et. al.* [200, 201] suggest that the mechanism involves 180° flipping of the phenyl-ring as has been observed for other polymeric systems such as polycarbonate [296], polysulphone [297] and phenoxy [298] using quasielastic neutron scattering (QENS). Another interpretation, by Zhao *et. al.* [272], is that the relaxation is due to oscillations of the phenyl-rings rather than flipping. This notion was confirmed to a certain degree by QENS measurements of PS performed by Arrese-Igor *et. al.* [299] whose results suggest phenyl-ring oscillation with a mean activation energy of 19.3 kJ/mol. The activation energies obtained through fits of the τ_γ data correspond well to the value obtained by Arrese-Igor *et. al.* suggesting that the observed γ relaxations are of a similar physical origin: an oscillation of phenyl-rings.

6.4 Hidden β relaxation

In the linearisation of the τ_α data obtained for this series shown in Section 6.2.8, it was observed that the $N = 2$, 3, 4 and 6 samples showed a change in the temperature dependence of τ_α at a certain temperature, termed the crossover temperature T^*. For some glass forming systems, the crossover temperature is also indicative of the decoupling or bifurcation of the α and β relaxations [30]. If this were true for the styrene series, one could postulate that the crossover in temperature dependencies of τ_α obtained for the $N = 2$, 3, 4 and 6 samples are indicative of another secondary relaxation process which could not be resolved separately to the α relaxation loss peak in the dielectric spectra. In order to further test this hypothesis, estimates of the location of the expected τ_β relaxation for the series were made based on the Arrhenius equation.

Firstly, an assumption was made that the empirical equation relating the activation energy E_A and T_g (Equation 6.5 [15, 61]) should hold for all samples across the series and that the constant of proportionality, K, should remain fixed with changes in the molecular weight. This assumption is validated to a certain extent because the K values obtained for the secondary relaxations observed in the alkylbenzene series remain reasonably similar with increasing molecular weight. The K value in this instance was determined through fitting of τ_β data obtained from the literature for PS ($N = 3570$) [268] using the Arrhenius equation in order to determine the activation energy. It was found, through substitution of E_A into Equation 6.5 that $K = 24.9 \pm 0.4$. Interestingly, this value is consistent with the value of 24 ± 3 obtained empirically for several molecular glasses [61], through calculations based on the coupling model [15] and also consistent with a value of 26 ± 2 obtained for metallic glasses [9]. Through knowledge of K, Equation 6.5 could then be used in order to determine what the activation energy of the β relaxations should have been for the other samples, had they been observed. The expected values of τ_β were then determined using two different procedures either based on a fixed τ_0 for all samples, or a variable τ_0 determined so that the α and β relaxations cross at the crossover temperature determined from the kink in the Stickel linearisation; only the samples which showed a kink in the linearised Stickel representation were included in this procedure.

6.4.1 Determination of τ_β values with fixed τ_0: Procedure 1

In the first procedure, it was assumed that τ_0 is fixed for the samples in the styrene series. This determination will be referred to as 'Procedure 1'. Values of τ_0 were set to the fitted value obtained from analysis of the $N = 3570$ τ_β data obtained from the literature [268]. A fixed constant of proportionality, K, between the activation energy, E_A and T_g was assumed. Values for the 'expected' τ_β were then determined using the Arrhenius equation. The obtained values from this analysis are shown in Figure 6.28a. Also shown are the τ_α values obtained through fits of the dielectric spectra and the τ_β values obtained from the literature [268]. Values of the obtained activation energy, E_a, and the crossover timescale,

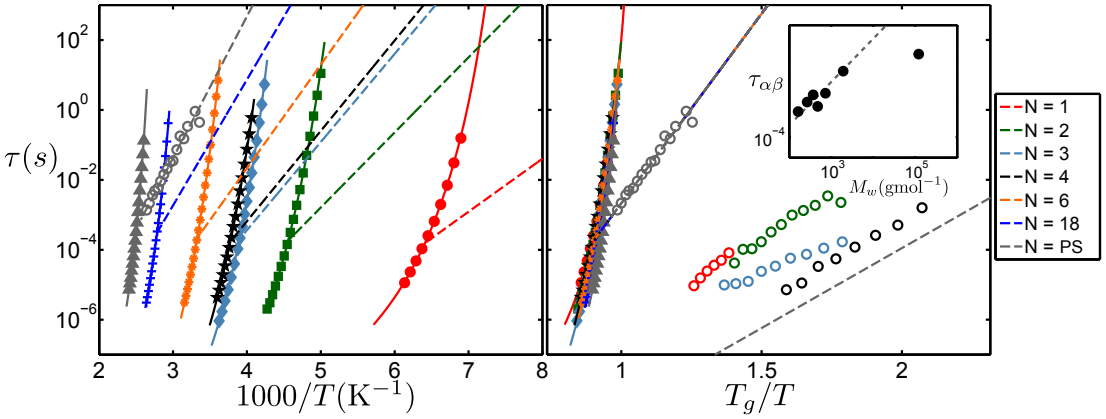

Figure 6.28: a) τ_α and theoretically determined τ_β data for the styrene series, determined using Procedure 1 as described in the text. Data were for τ_β for the bulk sample were taken from Ref. [268]. b) The same data rescaled by T_g including τ_γ data for the samples in which this secondary relaxation was observed. The inset in panel b shows values for the timescale corresponding to the crossing of the theoretically determined τ_β values and the τ_α data.

$\tau_{\alpha\beta}$ determined from the crossing of the τ_β data and the VFT fits of the τ_α data are tabulated in Table 6.4.

The expected τ_β values obtained using Procedure 1 demonstrate a systematic behaviour with a slowing down of the β relaxations as the molecular weight increases. By definition E_A shows an increase with increasing chain-length since it is proportional to T_g. In the next chapter we find an almost identical trend in the τ_β values for the PAMS chain-length series (Chapter 7) and a similar behaviour has already been shown for the alkylbenzenes. Similar trends have also been observed for PMMA for which the β relaxations can be directly observed since they are strongly dielectrically active (although we do not show the data here since the analysis of these data are still tentative). For the PMMA series we also find that the scaling between the β relaxation activation energy and T_g holds, which gives further support to our present analysis. A speeding up of the β relaxations with decreasing molecular weight are also observed in chain-length series of mono- and dimethyl ethers [18]. This is important as it suggests that this behaviour is highly general and not necessarily dependent on chemical structure. Furthermore, since the trend is also observed for the alkylbenzenes, the general behaviour does not appear to be limited to polymers.

N	$\log(\tau_0)$(s)	$\log(\tau_{\alpha\beta})$(s)	E_A(kJ/mol)	Reference
1	-13.5 $\pm$0.1	-3.81 ± 0.01	28.8 ± 0.5	
2	-13.5 $\pm$0.1	-3.73 ± 0.01	41.1 ± 0.7	
3	-13.5 $\pm$0.1	-3.68 ± 0.01	48.3 ± 0.8	
4	-13.5 $\pm$0.1	-3.77 ± 0.01	49.5 ± 0.8	
6	-13.5 $\pm$0.1	-3.67 ± 0.01	56.7 ± 0.9	
18	-13.5 $\pm$0.1	-3.50 ± 0.01	69 ± 1	
3570(PS)	-13.5 $\pm$0.1	-3.40 ± 0.01	77 ± 1	[268]

Table 6.4: Table showing values of $\tau_{\alpha\beta}$, τ_0 and the activation energy, E_A, obtained through determination of potential τ_β values using Procedure 1. Errors in the values for the $N = 3570$ sample reflect least-mean squares fitting of the τ_β data obtained from Ref. [268].

A T_g rescaled Arrhenius plot is shown in Figure 6.28b. In this scaling, the expected values of τ_β collapse onto the behaviour of the $N = 1160$ sample. This is expected as we have assumed the same τ_0 for each sample, based on the τ_0 obtained through Arrhenius fits of the $N = 1160$ data. The τ_γ values are also shown in order to highlight the point that the hidden β relaxations show different behaviour. The inset in Figure 6.28 shows the development of the bifurcation timescale, $\tau_{\alpha\beta}$. We observe an increase in $\tau_{\alpha\beta}$ with increasing chain-length.

In order to confirm the nature of the expected τ_β values, the bifurcation temperature, $T_{\alpha\beta}$ was determined from the crossing of the estimated τ_β and the τ_α data. These values were then compared with the linearised τ_α data shown in Figure 6.19. The linearised τ_α data show a kink at a certain temperature. We observe that for the $N = 3$ and 6 samples, $T_{\alpha\beta}$ are very similar to the fitted crossover temperature T^*. The values agree less for the $N = 2$ and 4 samples but are still in the same temperature region. This analysis therefore provides support for the idea that T^* could be related to the bifurcation of the α and β relaxations.

6.4.2 Determination of τ_β values with variable τ_0: Procedure 2

In this determination, it was assumed that τ_0 could vary for the samples in the styrene series. This determination will be referred to as 'Procedure 2'. This determination uses the obtained crossover temperature T^* obtained through analysis

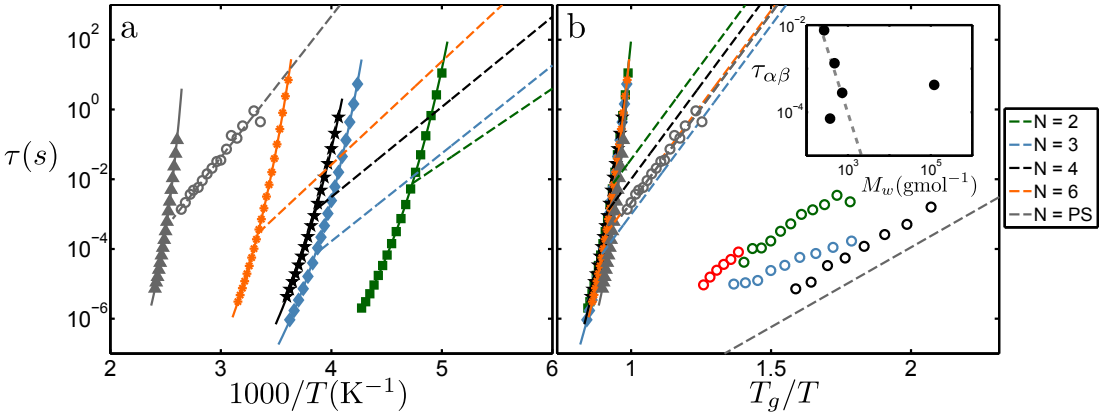

Figure 6.29: a) τ_α and theoretically determined τ_β data for the styrene series using Procedure 2 as described in the text. Data were for τ_β for PS ($N = 3570$) were taken from Ref. [268]. b) The same data rescaled by T_g including τ_γ data for the samples in which this secondary relaxation was observed. The inset in panel b shows values for the timescale corresponding to the crossing of the theoretically determined τ_β values and the τ_α data.

of the linearised τ_α data. As such, only data relating to samples which demonstrated crossover behaviour (N = 2-6) and the $N = 1160$ sample will be shown as it is too speculative to assume the crossover temperatures for the other samples.

As we have assumed that T^* is the temperature at which the α and β relaxations merge, it makes sense to first approximation to assume that at $T = T^*$, the timescales of the two relaxation processes should be the same and can be quantified by the timescale, $\tau_{\alpha\beta}$. Therefore, by determination of $\tau_{\alpha\beta}$ and substitution of this value into the Arrhenius equation, the limiting high temperature timescale, τ_0, could be calculated. Finally, once τ_0 and E_A values had been determined, the 'expected' values of τ_β could be produced through the Arrhenius equation. The values obtained through this analysis are shown in Figure 6.29a, denoted by the dashed lines. Also shown are the τ_α values obtained through fits of the dielectric spectra and the τ_β values for PS ($N = 3570$) obtained from the literature [268]. The behaviour of the expected τ_β values calculated using Procedure 2 is similar to those calculated using Procedure 1. Values of τ_0, $\tau_{\alpha\beta}$ and E_A obtained through this analysis are also shown in Table 6.5.

In order to characterise the behaviour of these expected values of τ_β further, the temperature was rescaled by T_g as shown in Figure 6.29b. Again, the τ_γ

N	$\log(\tau_0)$(s)	$\log(\tau_{\alpha\beta})$(s)	E_A(kJ/mol)	Reference
2	-12 ± 1	-2.1 ± 0.1	41.1 ± 0.7	
3	-14 ± 1	-4.1 ± 0.1	48.3 ± 0.8	
4	-13 ± 2	-2.9 ± 0.1	49.5 ± 0.8	
6	-13 ± 1	-3.6 ± 0.1	56.7 ± 0.9	
3570(PS)	-13.5 $\pm$0.1	-3.4 ± 0.1	77 ± 1	[268]

Table 6.5: Table showing values of $\tau_{\alpha\beta}$, τ_0 and the activation energy, E_A, obtained through determination of potential τ_β values. Errors in the values for the $N = 3570$ sample reflect least-mean squares fitting of the τ_β data obtained from Ref. [268].

values obtained for several samples are also shown here to highlight the difference between the timescales for this observed relaxation and the timescales of the expected β values. In this scaling the expected values of τ_β do not collapse in the manner observed from the values calculated using Procedure 1 and this is a reflection of the variation of τ_0. The inset in Figure 6.29b shows values of $\tau_{\alpha\beta}$ plotted as a function of molecular weight. There appears to be no observed trend in these values, contrary to what was observed for the values calculated using Procedure 1. The τ_0 values shown in Table 6.5 do not show a dependence on chain-length and show very little variation.

6.4.3 The excess wing

The α relaxation loss peak often exhibits a change in the power law exponent describing the high frequency flank and a so called excess-wing is observed. This excess-wing is often thought to be the result of a secondary relaxation which is significantly merged with the α relaxation [12]. In a study of an oligomeric chain series of propylene glycol based dimethyl ethers in research published by Mattsson *et. al.* [69] a clear β relaxation was observed for the highest molecular weight sample and became increasingly merged with the α relaxation for the lower molecular weight samples. For the shortest chain length samples, the β relaxation was manifested as an excess-wing on the high frequency flank of the α relaxation. Similar observations for a series of polyalcohols [166] and for an oligomeric series of propylene glycol [167] have been shown. The dielectric spectra in the α relaxation regime for this series of measurements were able to be fully

described without the assumption of an excess-wing on the high frequency flank of the α relaxation loss peak. However it should be noted that in a similar study of styrene and its oligomers, Hintermeyer *et. al.* assumed that all the α relaxation loss peaks showed an excess wing and the spectra were fit using an extension of the generalised Gaussian (G_{GG}) distribution as described in Chapter 2 in order to take the wing into account.

In order to check for signatures of the expected β relaxation, dielectric spectra for the $N = 2$, 3, 4 and 6 samples (samples which all show a clear change in the temperature dependence of τ_α) were examined at temperatures just below T_g. At these temperatures, the peak of the α loss was out of the frequency window, but the high frequency flank of the relaxation was still resolvable. These spectra are shown in Figures 6.30a - d. The high frequency flank of the α loss peak in the spectrum for the $N = 2$ sample has a fairly constant gradient in a log-log scaling whereas the $N = 3$ and 4 samples show slight deviations of this gradient at higher frequencies indicating excess-wing like behaviour not observed at higher temperatures. The $N = 6$ spectra shown in Figure 6.30d has the most pronounced change in the exponent of the high frequency flank, varying by almost a factor of 2. The expected peak positions of the β relaxations for these samples are denoted by the red and blue vertical dashed lines in Figure 6.30, referring to values obtained from Procedure 1 (Section 6.4.1) and Procedure 2 (Section 6.4.2) respectively. We observe that the expected peak positions coincide with frequencies inside the high frequency flank of the α loss peak for the $N = 3$, 4 and 6 samples indicating that the observed excess wing behaviour is likely due to a submerged β relaxation. We also observe that the wing-behaviour becomes more pronounced with increasing molecular weight, similar to previously published results [69, 166, 167]. Furthermore, in the $N = 2$ sample there are less obvious signs of an excess-wing.

The overall conclusion is that the two tests performed using Procedure 1 and 2, give very similar behaviour regarding the general behaviour of the β relaxations and both are consistent with the data. Given the assumptions involved, it is not possible to confirm the exact behaviour of more subtle trends such as the molecular weight dependence of the crossing between the α and β relaxations.

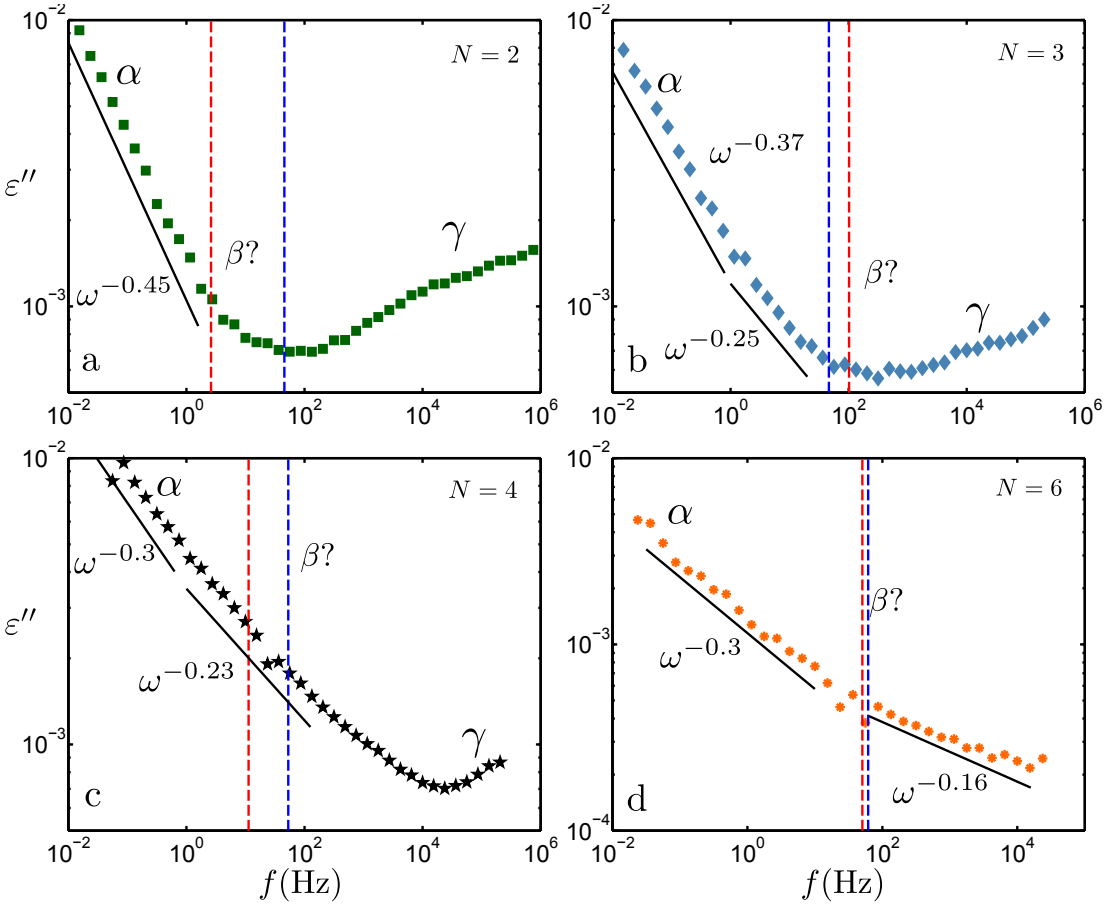

Figure 6.30: Dielectric spectra in ε'' for the a) $N = 2$, b) $N = 3$, c) $N = 4$ and d) $N = 6$ samples showing the expected peak positions of the β relaxation loss peak based on the analysis describe in the text and the expected τ_β values shown in Figure 6.29. Here the blue and red dashed indicate values calculated using Procedure 1 and Procedure 2 respectively.

A secondary β relaxation has been observed for PS in several techniques including dielectric spectroscopy [268], mechanical measurements [270] and NMR measurements [271, 272]. Figure 6.31 shows the dielectric spectrum for the $N = 1160$ sample at 386K (just above T_g) including the positions of the β relaxation obtained from fits of these literature data to the Arrhenius equation. It is clear from the figure that the broad nature of the α relaxation loss peak in ε'' could be the result of an underlying β relaxation which cannot be resolved separately to the α loss peak.

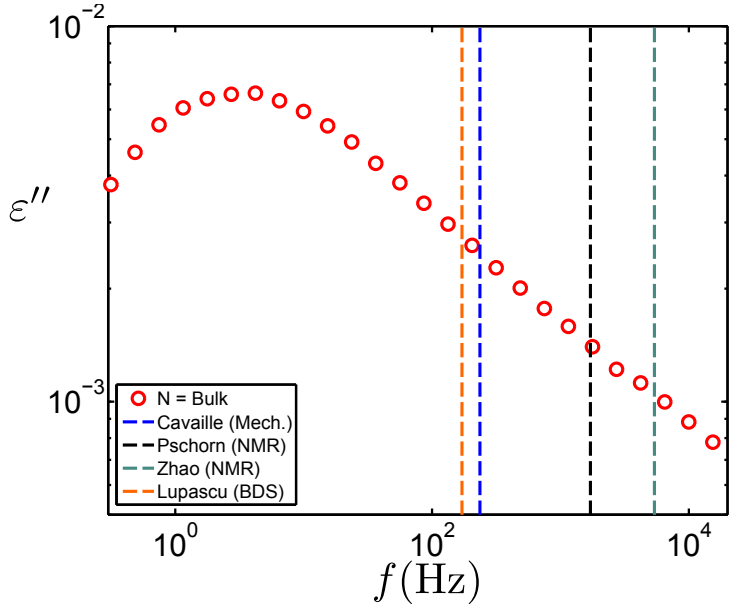

Figure 6.31: Dielectric spectra for bulk polystyrene showing the supposed positions of the β relaxation determined from Arrhenius fits of the τ_β data obtained from literature [268, 270–272]. The conductivity contribution has been subtracted from the spectra for clarity.

The physical nature of the observed β relaxation for bulk PS is still not resolved. The observed relaxation mechanism has been attributed to 180° flipping of the benzene rings about the chain axis [201], small angular rotations of the benzene rings [202] or a combination of both of these processes [200]. In general, it is thought that the β relaxations in polymers relate to some small-scale motion of the repeat units within the polymer chain [51]. Secondary β relaxations have been observed in a huge variety of different glass formers including molecular, polymeric, colloidal, inorganic and metallic systems [9, 51, 300]. Due to the correlation between the activation energy of this secondary process, E_A and T_g [15, 55, 61], the β relaxation has been thought to be a precursor to the α relaxation and could be intrinsically linked to the glass properties of materials [15]. The energy barrier associated with this process also appears to increase with chain-length if the relationship between E_A and T_g holds, suggesting that the process becomes more hindered as the chain-length increases in the same manner as the α relaxation. The broadening of the frequency dispersion of the

α relaxation has also been linked to the separation between the timescale of the α relaxation, τ_α and the timescale of the β relaxation, τ_β, through the coupling model [15, 84]. In the fitting of the α loss spectra for this series we observed a broadening of the dispersion with increasing chain-length and this indicates a greater separation between τ_α and τ_β giving further evidence for the suggested behaviour of the hidden β relaxation.

6.5 Differential scanning calorimetry

In order to complement the data obtained from the dielectric measurements, the samples were analysed using Differential Scanning Calorimetry (DSC). DSC measurements were performed using the TA Instruments Q2000 calorimeter, the details of which are given in Chapter 3. The samples were run by heating/cooling the samples in a cyclic manner around their expected T_g values at a rate of 10K/min. This rate was chosen as it can be shown to correspond to a relaxation timescale of 100s [138–141], thus facilitating comparison between DSC and dielectric measurements. Due to the relatively simple sample preparation and the small amount of material required to perform DSC, measurements were performed on a slightly wider range of samples than were performed using dielectric spectroscopy.

6.5.1 Traces of the heat capacity

The obtained DSC data for the series of styrene samples are shown in Figure 6.32. The steps in C_p, correspond to the glass transition and shift to higher temperatures with increasing molecular weight, demonstrating the increasing T_g values. The absolute values of the specific heat capacity seem to vary without a consistent trend between the samples although there is a slight indication that the absolute values of the specific heat capacity in the glassy state (in the temperature region lower than the step in C_p) increases with increasing molecular weight, although this clearly is not the case for the polymer sample. The DSC traces were analysed in the manner described in Chapter 3, with T_g determined from the onset of the characteristic step in C_p associated with the glass transition.

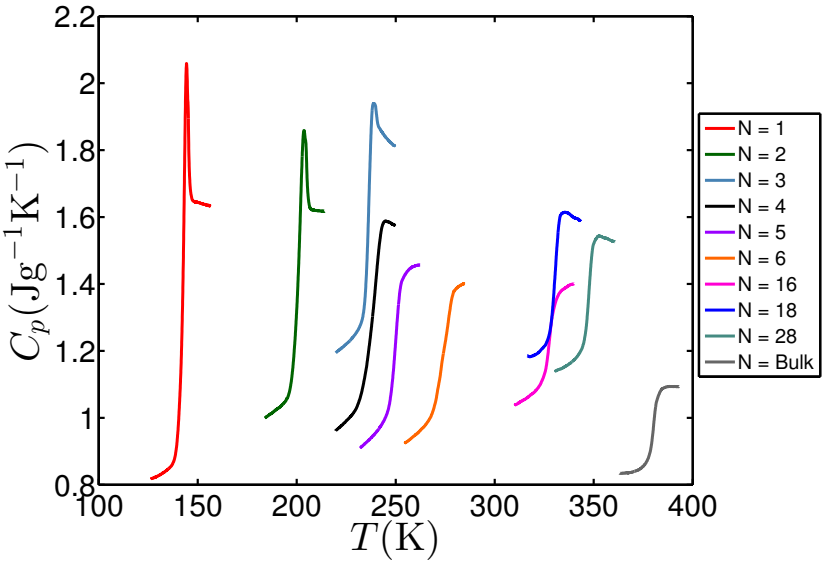

Figure 6.32: DSC traces for the styrene series. The traces shown are of increasing temperature at a rate of 10 K/min.

These values were shown in Section 6.2.6 and follow the same behaviour of the values obtained through dielectric spectroscopy and also the selection of data obtained from the literature.

6.5.2 The 'step height' of the glass transition

In order to characterise the observed glass transition steps in C_p, the difference between C_p in the glassy and liquid states, ΔC_p was determined and these values are shown in Figure 6.33a. The ΔC_p values decrease with increasing molecular weight and appear to move towards a molecular weight independent value for the highest M_w. A similar trend was also observed in DSC measurements on PS conducted by Santangelo *et. al* [26] and the authors note that the molecular weight at which ΔC_p becomes invariant is equivalent to the molecular weight at which the glass transition temperature saturates. The same conclusions could be drawn for the data shown here, although the study would require further measurements of higher molecular weight samples in order to be sure.

In the previous chapter (Chapter 4) the relationship between ΔC_p and the

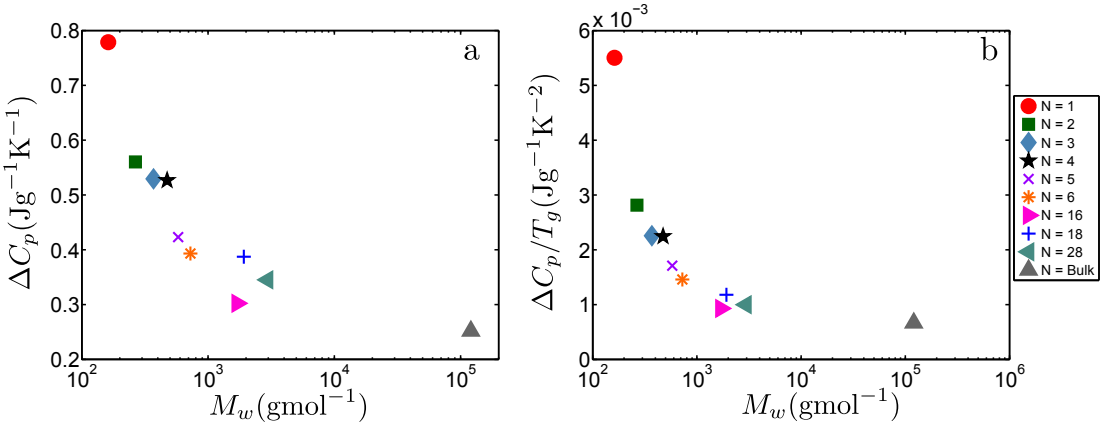

Figure 6.33: a) ΔC_p for the styrene series obtained through analysis of the DSC traces shown in Figure 6.32 and b) $\Delta C_p/T_g$.

sensitivity of the entropy to a temperature change at T_g,

$$\Delta C_p = T_g \left[\left(\frac{\partial S^{liquid}}{\partial T} \right)\Big|_{T_g} - \left(\frac{\partial S^{glass}}{\partial T} \right)\Big|_{T_g} \right]_p . \tag{6.6}$$

In order to analyse the difference in the temperature dependence of the entropy at T_g with increasing chain length, the ΔC_p values were rescaled by T_g. The results of this rescaling are shown in Figure 6.33b. The observed trend in the values still persists in this rescaling, showing a strong decrease with increasing molecular weight suggesting that the change in ΔC_p is most dependent on the change in the temperature dependence of the entropy at T_g.

The difference in the glassy and crystalline heat capacities has been defined to be a measure of the so-called thermodynamic fragility [91, 122]. It can be shown that the so-called excess heat capacity, ΔC_p can be related to the kinetic fragility parameter, m [121] and we observed a correlation between m and ΔC_p for the alkylbenzene series. The behaviour of this polymeric series appears to break this correlation as it was observed that m increases with increasing molecular weight whereas the inverse is true for the ΔC_p values. The inverse correlation between the thermodynamic definition of fragility provided by ΔC_p and the dynamic definition provided by the m parameter has been observed for a series of 17 polymeric systems analysed by Roland *et. al.* [263]. The same conclusions were drawn

by Huang *et. al.* [122] in a study of 23 bulk polymeric glass forming systems. This suggests that the mismatch between these two definitions is characteristic of polymeric glass formers. Huang *et. al.* go one step further and suggest that polymers can be grouped into those with strong and weak inverse proportionality between m and ΔC_p. PS falls into the 'middle' of this range.

Angell provides a tentative explanation for this by considering the vibrational anharmonicity in the glassy state [264]. One can say that C_p in the glass is largely vibrational in nature as the majority of the configurational component of C_p is lost through the glass transition. In pressure studies of 3-methyl pentane conducted by Takara *et. al.* [301] it was observed that the heat capacity in the glassy state increased with increasing pressure as did the glass transition temperature. Similar observations were also made for polyvinylacetate (PVAc) by Sandberg *et. al.* [302] indicating that the increase of C_p with increasing pressure in the glassy state is applicable to polymeric glass forming systems. Angell states that the reason for this increase of C_p in the glass is that vibrational frequencies are increased which render the vibrational modes more harmonic [264]. This leads to an increase in T_g as it can be shown to be related to anharmonicity [303]. He also states that an increased degree of polymerisation will have a similar effect on the vibrational anharmonicity in the glassy state. This means that the heat capacity of the polymeric glassy state can attain higher values before the glass transition whilst the heat capacity in the liquid state after the transition is relatively unaffected. This therefore leads to a decrease in ΔC_p with increasing chain length and the glass transition is 'postponed' until the excitation of a higher vibrational heat capacity [122, 264].

6.5.3 The width of the glass transition step

Further analysis of the DSC traces were performed by determining the width of the glass transition step, where ΔT is defined as the different between the onset and offset temperatures. Values of ΔT are shown in Figure 6.34. The width of the step appears to increase with increasing molecular weight before becoming relatively fixed for the highest chain length samples. The width of the $N = 4$ sample appears to be particularly large. Interestingly, a similar trend was

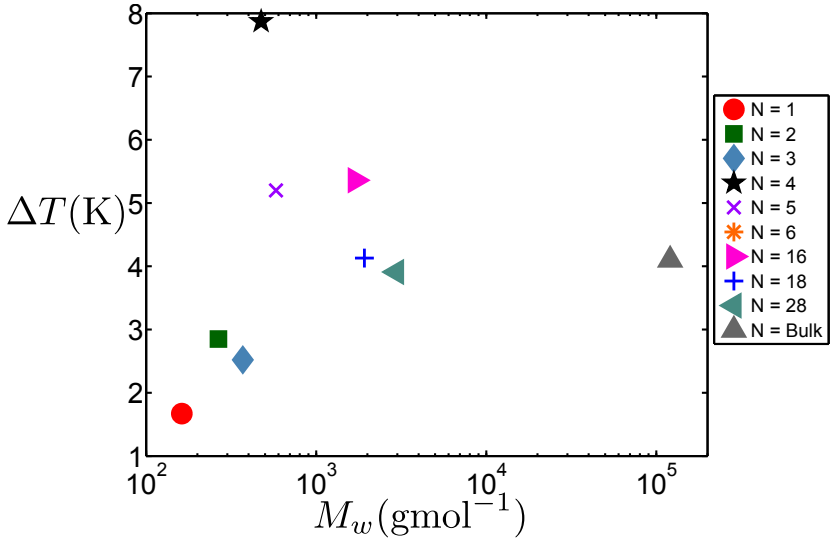

Figure 6.34: ΔT values obtained through analysis of the DSC traces shown in Figure 6.32

observed in the exponent of the high frequency power law of the α relaxation as determined through fitting of the dielectric spectra, shown in Section 6.2.4. One can tentatively suggest that, as DSC scans were performed at 10K/min, that the ΔT values indicate the stretching of the α relaxation with a timescale of 100s. Furthermore, as the coupling model indicates a correlation between the stretching parameter and the dynamic fragility parameter, m [62], this implies an increase in the dynamic fragility with increasing chain length. Indeed, a similar increase of the m parameter was observed for those samples studied using dielectric spectroscopy.

6.5.4 Excess entropy

In this section the excess entropy, S_x, obtained for the styrene series will be discussed. Values of S_x as a function of temperature could be determined using the method described in detail in Chapter 4. The excess entropy was determined from the difference in extrapolated glassy, C_p^{glass} and liquid, C_p^{liq}, heat capacity

behaviours and S_x was calculated as:

$$S_x(T) = S_x(T_m) - \int_T^{T_m} \frac{C_p^{liq} - C_p^{glass}}{T} \, \mathrm{d}T \tag{6.7}$$

This expression requires knowledge of the excess entropy at the melting poing, T_m, and thus in order to determine absolute values of S_x, the enthalpy of fusion, ΔH_{fus}, must be known in order to calculate the reference entropy of fusion, ΔS_{fus}, as $\Delta S_{fus} = \frac{\Delta H_{fus}}{T_m}$. For the alkylbenzene series, values of T_m and ΔH_{fus}, were obtained from the literature but this was not possible for the styrene series as no such data is available due to the atactic nature of the polymer. Instead, T_m was calculated using the T_g values obtained for this series as it can be shown in a number of instances that $T_g = \frac{2}{3}T_m$ (a collation of the T_g/T_m for 132 different polymers was published by Lee *et. al.* [149]). Since we do not know $S_x(T_m)$ here we instead focus on the $\Delta S_x(T) = S_x(T) - S_x(T_m)$, which is representative of the change of the excess entropy from that at the melting point. Values of ΔS_x determined for the samples in this series are shown in Figure 6.35. The y-axis in this case was set to $1 - \Delta S_x$ and the x-axis was rescaled by the calculated values of T_m in order to mimic the so called Kauzmann plot [16, 211] which shows the excess entropy at each temperature normalised by the value at the melting point. It is clear from the plot that $1 - \Delta S_x$ decreases at a far faster rate for the $N = 1$ sample than the other samples and that this rate of decrease appears to decrease with increasing molecular weight, indicating that the thermodynamic fragility becomes less with increasing chain length as seen from the variation in ΔC_p. In order to better quantify this trend a cut was made at T_g and the values obtained from this cut are shown in the inset of Figure 6.35. These values indicate that the the excess entropy at T_g increases with increasing molecular weight in a similar manner to what was observed for the alkylbenzene series. However, note again that we have here set $S_x(T_m) = 0$ for all samples whereas this of course in reality has a finite value that would vary between the samples and affect the absolute value of the determined excess entropies.

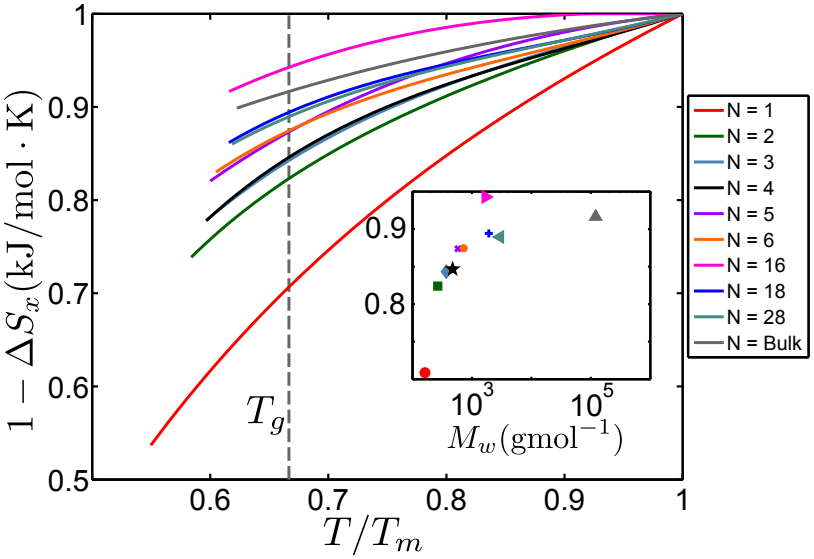

Figure 6.35: ΔS_x values obtained through analysis of the DSC traces shown in Figure 6.32, where ΔS_x is the difference between the extrapolated glassy and liquid heat capacities, plotted against T/T_m.

6.6 Conclusions

In this chapter, measurements of a series involving the polymerisation of styrene were performed using Broadband Dielectric Spectroscopy (BDS) and Differential Scanning Calorimetry (DSC). These measurements spanned a range of samples with three orders of magnitude difference in molecular weight. In this series, the relaxation dynamics for the lower molecular weight samples are likely to be significantly different to those of the polymeric samples. For example, the structural relaxation of a glass former containing small molecules is related to cooperative translation of the molecules, allowing the bulk sample to relax. Clearly this is not the case for a high molecular weight polymeric sample. Instead, here it is more likely that the structural relaxation is related to the cooperative motion of smaller segments of the chain but it is difficult to quantify the exact size of these relaxing regimes.

Quantification of the difference in dynamics between the short chain oligomeric and polymeric samples in this series was obtained through analysis of values of T_g, obtained from analysis of BDS and DSC data and from the literature. It

was observed that the molecular weight dependence of T_g could be separated into three distinct regions, as originally introduced by Cowie [259]. Values of T_g for low degree of polymerisation, N, samples (Region I) increased systematically with increasing molecular weight in a similar manner to the alkylbenzene series. For intermediate N (Region II), T_g also increased in a similar manner but with a weaker dependence on M_w than in Region I. At a certain point T_g values became fixed with further increases of M_w (Region III). This behaviour is indicative of the changing nature of the dynamics as N increases. In Regions I and II, the structural relaxation timescale is strongly dependent on N, suggesting that the relaxation mechanism is strongly affected by the length of the chain. In Region III, the structural relaxation timescale is clearly no longer dependent on the length of the polymer but cooperative relaxation of sections of chains with sections of neighbouring chains. It was also noticed that if one expresses Regions I and II in terms of a suggested primitive unit, a monomer and a Rouse bead respectively, the the 'width' of the Regions is equivalent to the same number of units, determined to be on the order of 16. This suggests that the dynamics of a polymeric glass former change when the 'size' of the polymer reaches a certain number of primitive units.

We also saw evidence of a three region behaviour in the dynamic fragility parameter, m. It was observed that values of m was relatively invariant for the lowest chain-length samples in Region I. The values then show a systematic increase with M_w beyond the molecular weight corresponding to the Kuhn length in Region II (as defined by Hintermeyer *et. al.* ≈ 1800 g/mol) before a constant m observed for the highest molecular weight samples in Region III. It was suggested that the dynamic fragility is only variable in Region II, whereas it is relatively fixed in Region I and III. Given the behaviour of T_g we should perhaps expect the m parameter to behave in this manner. As stated, in Region III, the α relaxation is likely to be unaffected by the total length of the polymer chains and therefore we can expect the same fragility. Likewise, in Region II we should expect that the fragility should increase with chain length as we saw an increase in T_g in the same region. However, it is unclear why the fragility should be approximately invariant in Region I. More measurements on a greater number of samples in this region should be performed in order to ascertain the reason.

We find evidence for three relaxation modes, α, β and γ in this series in a similar manner to those found in the alkylbenzene series. The α relaxation loss peak in ε'' is clearly observed for all samples measured using BDS. This loss peak appears to become increasingly stretched with increasing molecular weight. The stretching of the α loss peak has been previously linked to the dynamic fragility of glass-formers [11, 26, 190] suggesting that this measure of fragility increases with increasing molecular weight for this series. Furthermore, one would expect a longer chain to have a larger molecular weight distribution and therefore a larger distribution of relaxation timescales. The broad nature of the response for the higher N samples is a reflection of this.

The γ relaxation was directly observed for the N = 1-4 samples. The timescales of this relaxation mechanism correspond well to those obtained for PS [204]. This suggests that the relaxation mechanism is of similar origins across the series and implies that whatever physical process is responsible is largely unaffected by chain length. Indeed, previous studies in the literature have attributed this relaxation process to translation [203], 180° flipping [200, 201] or oscillations [272] of the phenyl-rings. It is unlikely that small motions of the phenyl-rings are strongly affected by the length of the main chain itself and therefore the similarity of the relaxation timescales of the γ relaxation for different samples is expected. The activation energies obtained for this relaxation process also correspond well to those observed for the γ relaxation in the alkylbenzene series. This suggests the relaxation mechanisms are of a similar nature in both series. This is further evidence that the γ relaxation involves the motion of phenyl-rings.

Data for the timescale of the β relaxation for PS was obtained from the literature [268]. These data were used to construct 'expected' values of τ_β for the other samples in the series through use of the relationship between activation energy, E_A, and T_g [55] and the Arrhenius equation. Two procedures were outlined based on setting τ_0 to the same value for all samples (Procedure 1) or determining τ_0 explicitly for each sample (Procedure 2). The observed β relaxation mechanism for PS has been attributed to 180° flipping of the phenyl rings about the chain axis [201], small angular rotations of the phenyl rings [202] or a combination of both of these processes [200]. However we observe that the timescale for the β relaxations increase significantly with increasing chain length. This suggests that

the relaxation mechanism is strongly dependent on the length of the chain and therefore it seems unlikely that it should be simply a result of phenyl ring motion and perhaps it is the result of correlated dynamics of larger sections of the chain [51]. Values of τ_β obtained through both of these procedures show similar trends to those observed for the alkylbenzene series. This suggests that the physical nature of the β relaxation is a general property of molecular glass formers and directly related to some measure of the 'size' of a constituent molecule rather than dependent on sample chemistry.

Chapter 7

Results III: An oligomeric chain-length series of α-methylstyrene

7.1 Introduction

In this Chapter, results from measurements of a chain-length series based on the polymerisation of α-methylstyrene is presented. Results from both Broadband Dielectric Spectroscopy (BDS) and Differential Scanning Calorimetry (DSC) measurements are presented. To our knowledge, the only systematic data on a chain-length series of α-methylstyrenes was T_g data that were published by Cowie *et. al.* [259, 304] using Differential Thermal Analysis (DTA). These literature data will be specifically discussed and compared with our new results. Other examples of the use of poly(α-methylstyrene) (PAMS) include a DSC study of the effects of mixtures of poly(α-methylstyrene) with a lower chain length oligomer of α-methylstyrene [305]. This will be discussed in the relevant sections in the chapter.

Technical specifications for the samples used in the PAMS series are shown in Table 7.1. The samples will be referred to by their degree of polymerisation, N_α, as shown in the table. Values of N_α were determined by dividing the weight averaged molecular weight, M_w, by the M_w of the α-methylstyrene monomer (118.18 g/mol). The lowest molecular weight samples in the series ($N_\alpha = 2$ and 3)

N_α	M_w (g/mol)	PDI	Manufacturer
2	236.36	1	Sigma-Aldrich
3	354	1	Polymer Source
5	590.9	1.16	Polymer Source
15	1740.2	1.13	Polymer Source
19	2200	1.12	Polymer Standards Service
31	3660	1.09	Polymer Standards Service
61	7260	1.06	Polymer Standards Service
135	15900	1.12	Polymer Standards Service
239	28200	1.02	Polymer Standards Service
320	37800	1.04	Polymer Standards Service
353	41700	1.02	Polymer Standards Service
502	59300	1.02	Polymer Standards Service
603	71300	1.02	Polymer Standards Service
914	108000	1.02	Polymer Standards Service
1972	233000	1.03	Polymer Standards Service

Table 7.1: Technical specifications of the PAMS series including the degree of polymerisation, N_α, weight averaged molecular weight, M_w, polydispersity index (PDI) and the manufacturer.

had a stated polydispersity index (PDI) of 1, implying that the number average and weight averaged molecular weights were equivalent. The higher molecular weight samples have varying degrees of polydispersity as shown in the table. The samples were all run using BDS and DSC with the exception of the $N_\alpha = 2$ sample which was only run using BDS.

The chemical structures differ slightly between samples obtained from Polymer Source/Sigma Aldrich (low N_α) and those obtained from Polymer Standards Service (PSS; high N_α). The differences in structure are shown in Figure 7.1. All samples were produced through anionic living polymerisation in the same manner as the samples in the styrene series. The difference in the chemical structure of the samples results from the difference in the initiators used in this process. The low molecular weight samples obtained from Sigma-Aldrich and Polymer Source were produced using cumyl-potassium as an initiator and the resulting polymers are capped on one end with a cumyl-group. This is effectively equivalent to having a PAMS chain with each end capped with a proton as indicated in the figure. The higher molecular weight samples obtained from PSS are manufactured with sec-

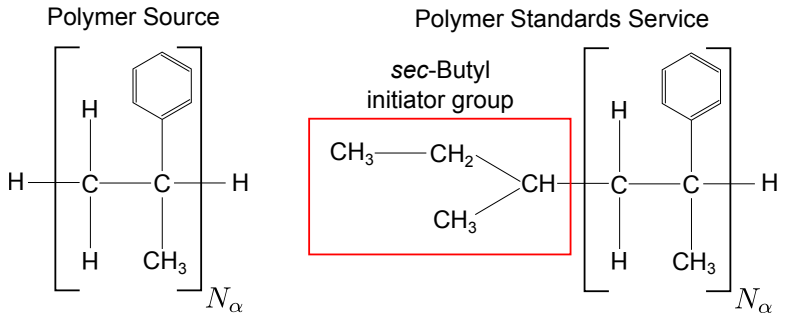

Figure 7.1: Schematic of the chemical structure for the PAMS series.

butyllithium as an initiator and the resulting polymers have a sec-butyl initiator group attached in a similar manner to the samples in the styrenes series.

7.2 Dielectric Spectroscopy - α relaxation

BDS measurements were performed both the University of Leeds and Chalmers Institute of Technology, Gothenburg, using the slightly different dielectric set-ups described in Chapter 2. The higher molecular weight samples in this series demonstrated significant DC-conductivity contributions to the dielectric spectra due to the presence of charged impurities. In order to attempt to remove these contributions, the samples were 'cleaned' using the methanol precipitation technique described in Chapter 2. An example of the effect of this cleaning procedure on the dielectric spectra of the $N_\alpha = 1972$ sample is shown in Figure 7.2a. After methanol precipitation the conductivity contribution is lowered by around a decade in ε'', thus obscuring the α loss peak less at low frequencies. However, despite this cleaning procedure the conductivity contribution was still present in the dielectric spectra. Further cleaning, involving multiple precipitation steps would have to be performed in order to remove all the charged species from within the samples.

The lowest chain length samples in this series ($N_\alpha = 2$ and 3) had a relatively low viscosity at room temperature and were thus run using the dielectric liquid cell (Novocontrol, BDS 1308). The other samples in the series were run using the two electrode set-up. Detailed descriptions of these two sample geometries can be found in Chapter2. In both cases, the separation between the electrodes

was 50μm, maintained through the use of silicon spacers. The longer chain-length samples were first dissolved in toluene, solution-cast to a 40mm diameter electrode and dried under vacuum at 473 K for 24 hours prior to measurement. The 40mm electrodes were then heated on a hot-plate in order to decrease the viscosity of the samples so that silicon spacers could be added. Finally, a 20mm electrode was placed onto the sample/spacers and pressure was applied in order to ensure a constant measurement volume.

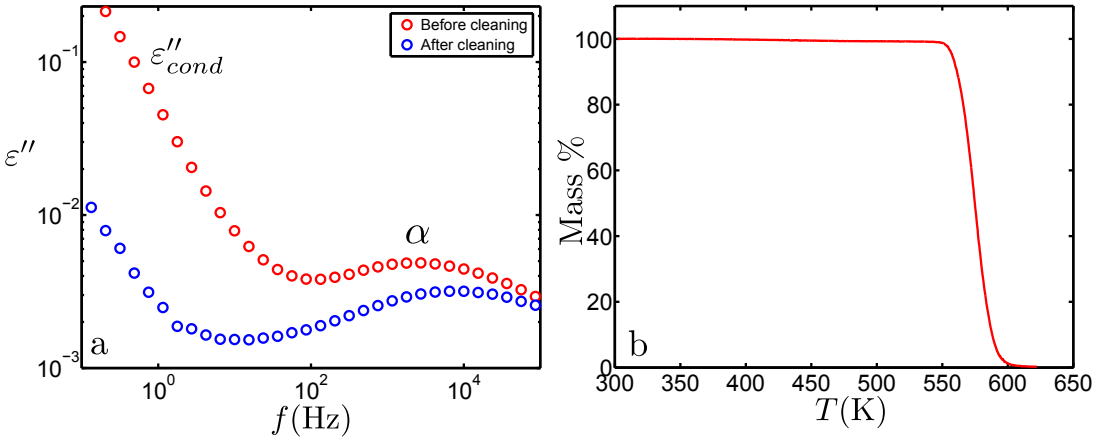

Figure 7.2: a) Dielectric spectra for the $N_\alpha = 1972$ sample before and after methanol precipitation. b) Mass percentage as a function of temperature obtained from Thermogravimetric Analysis (TGA) for the $N_\alpha = 239$

The viscosity of these samples remains relatively high even at temperatures $\sim$ 50K above T_g. At a certain temperature, polymeric samples experience thermal degradation in which the backbone bonds are broken. In order to avoid degradation of the samples during sample preparation, the degradation temperature, T_D, was determined by measurement of the samples using Thermogravimetric Analsis (TGA), as described in Chapter 3. TGA measurements involve heating a sample and observation of the variation of its percentage mass, where 100% percentage mass denotes the mass of the sample at the beginning of a measurement. An example of the mass trace obtained for the $N_\alpha = 239$ sample is shown in Figure 7.2b. For the lower temperatures in the measured range, the mass percentage remains at 100%. However, at a certain temperature, T_D, the sample degrades and the mass rapidly decreases. Analysis of this kind provided an upper-bound

of the temperature for the sample preparation process. In the case of $N_\alpha = 239$, $T_D \approx 550$K.

The samples were run by first heating (or cooling, depending on the expected value of T_g) the dielectric sample cell to a temperature such that the loss peak corresponding to the α relaxation was just visible in the experimental frequency window (for example, when the peak frequency, f_p, was $\sim 10^6$Hz). The samples were then cooled in steps of 2K from this starting temperature and spectra were obtained at each step.

7.2.1 Dielectric Spectra

The spectra obtained for a selection of the samples ($N_\alpha = 2$, 3, 5, 13, 19, 31, 353 and 1972) in the PAMS series in the α relaxation temperature regime are shown in Figures 7.3a-h. Spectral data are only shown for temperatures at which the α relaxation loss peak could be fully resolved. The lines through the points in the spectra correspond to fits to the data. The fitting procedure is outlined in detail in Section 7.2.2. All samples show a clear loss peak corresponding to the α relaxation with the peak position moving to lower frequencies as a result of decreasing temperature. Despite the cleaning of these samples to remove charged species, a significant conductivity contribution, manifested as a power-law flank in ε'', was observed at frequencies lower than the peak frequency of the α loss peak. This contribution has been removed (the low frequency range where this dominated was cut in the plot) in the displayed spectra so that the α loss peaks are clearly visible. For many of the samples, this contribution significantly obscured the α loss peak in the low frequency range. This was particularly apparent for the samples with higher chain-length and for these samples the frequency position of the α loss peak could not be determined across the entire frequency range. At the highest frequencies, a power law contribution was observed as was also observed for the alkylbenzene (Chapter 4) and styrene (Chapter 6) series. This contribution has also been removed in the displayed spectra (the highest frequencies where this affected the data was cut in the plot) so that the development of the α loss peaks are clearly visible at all temperatures.

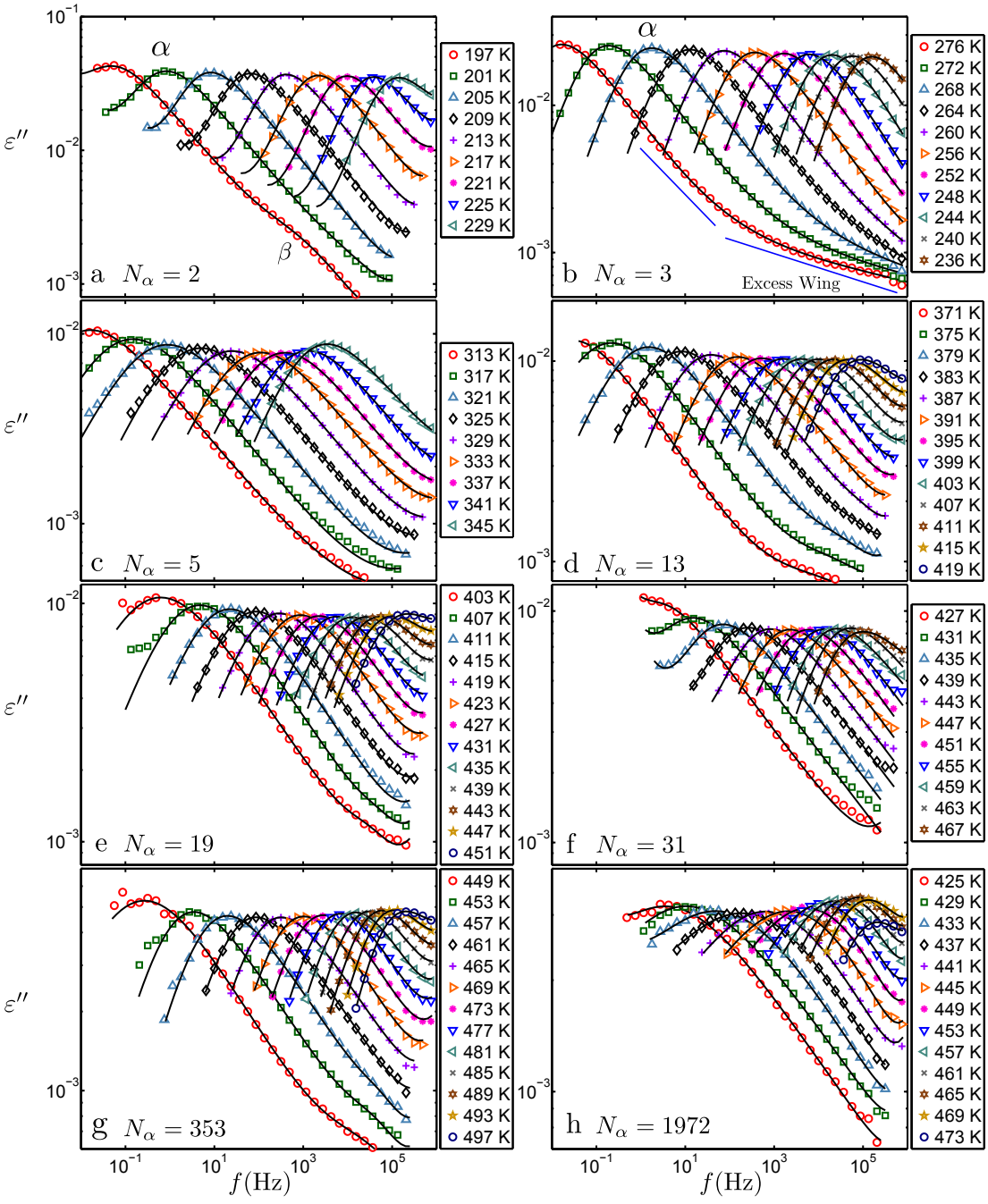

Figure 7.3: Dielectric spectra in the α relaxation temperature regime for the N_α = a) 2, b) 3, c) 5, d) 13, e) 19, f) 31, g) 353 and h) 1972 samples. The excess-wing behaviour of the $N_\alpha = 3$ sample is denoted by the blue lines in b)

For some of the samples, other contributions to ε'' were also visible. For example, the spectra for the $N_\alpha = 2$ sample shown in Figure 7.3a has a clear secondary relaxation peak. This demonstrates the presence of a secondary relaxation process the nature of which will be discussed in Section 7.7. Furthermore, the loss peaks for the α relaxation of the $N_\alpha = 3$ sample shown in Figure 7.3b show a change in the power law exponent of the high frequency flank and thus show a so-called 'excess-wing' behaviour as described in previous chapters. The change in the exponent of the high frequency power-law is indicated by the solid blue lines in Figure 7.3b. This again is indicative of a secondary relaxation process but this process could not be resolved separately to the α relaxation. Note that indications of excess wings can be observed also for several of the other samples, as observed in Figure 7.3 indicating the presence of secondary relaxations.

7.2.2 Fitting Procedure

In Section 7.2.1 it was shown that the dielectric spectra for the samples in the PAMS series show three contributions: a loss peak corresponding to the α relaxation, a low frequency contribution as a result of DC-conductivity and a high frequency powerlaw contribution. The dielectric spectra were fit using a similar procedure to that of the alkylbenzene and styrene series as described in Chapters 4 and 6.

The α loss peaks were fit using the Rikard Bergman (RB) function [104] (a full explanation of the parameters in this function can be found in Chapters 2 and 4). It was found that the parameter corresponding to the bluntness of the loss peak, C, could be fixed for all temperatures for each sample. This parameter was set to a value of 0 for all samples with the exception of the $N_\alpha = 3$ sample for which the spectra were best described by setting $C = 0.37$. The other parameters were left 'free' and thus the α loss peak could be well described using a four parameter expression. In Chapters 4 and 6 it was shown that there is a good agreement between fits of the RB and Havriliak-Negami (HN) [110] functions to the α loss peak and thus it was determined that a full account of the spectral shape of this loss peak could be attained through use of the RB function. The spectra for

the $N_\alpha = 3$ sample shows a clear excess-wing and were fitted using the modified version of the RB function as described in Chapters 4 and 2.

The DC-conductivity contribution to the dielectric loss was fit using the following function [94]:

$$\varepsilon_{cond}(\omega) = -i\frac{\sigma_0}{\varepsilon_0\omega} \tag{7.1}$$

Where σ_0 is the ohmic or DC conductivity of the material. This relation implies that the exponent of the conductivity power law flank in ε'' should be 1. In most cases it was required to lower the value of this exponent in order to fit the data correctly by including an exponent parameter, k such that $\varepsilon''_{cond} \propto \omega^k$. The high frequency contribution was fit using a power-law of the form $\varepsilon'' = A\omega^B$.

The spectra for the $N_\alpha = 2$ sample show the emergence of a secondary loss peak in the high frequency flank of the α loss. Secondary relaxations are often manifested as symmetrically stretched loss peaks [33, 61, 67, 94, 96, 116, 117] and therefore this contribution was fitted using the Cole-Cole [176] function as described in Chapter 2.

The spectra for some of the other samples in the series also contained a weak contribution at frequencies between the α loss peak and the high frequency contribution. In order to provide a full description of the spectra, it was assumed that this contribution was the manifestation of a weak secondary process and was thus fit using the CC expression.

A full description of the dielectric spectra in each case was obtained through an additive combination of the functions used in order to fit the separate contributions to ε''.

7.2.3 Fitting parameters for the α relaxation loss peak.

The parameters corresponding to the decription of the α loss peaks obtained through fits using the RB function (and modified RB function for the $N_\alpha = 3$ sample) are shown in Figures 7.4a-d. Although time-temperature superposition (TTS) has been shown to be applicable for some polymeric systems [170–173] it appears that it does not hold for this series. The parameters will be addressed individually in the following sections. The dashed lines in Figure 7.4c denote

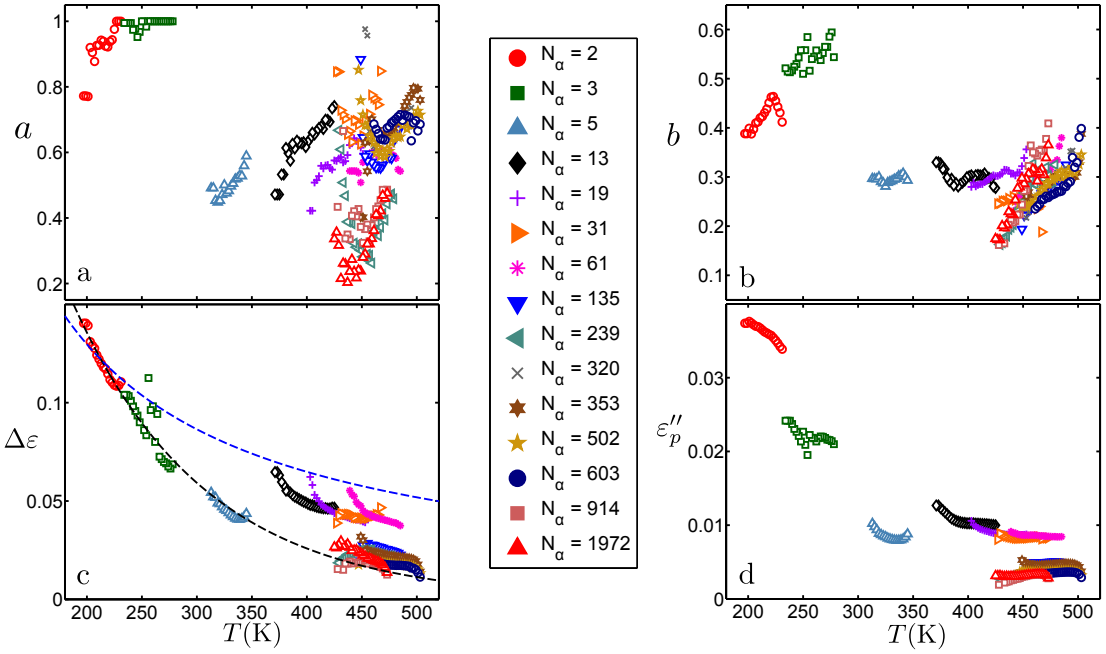

Figure 7.4: Parameters obtained through fits of the RB function to the dielectric spectra. Parameters shown are a) the exponent of the low frequency power law, a, b) the exponent of the high frequency power law, b, c) the dielectric strength, $\Delta\varepsilon$, d) the amplitude, ε''_p

fits of the $\Delta\varepsilon$ values for the $N_\alpha = 2$ sample with a simple $1/T$ dependence (blue dashed line) and an exponential dependence (dashed black line). The exponential dependence appears to provide a better description of the data of the data over the full temperature range, which is fully consistent with the behaviour observed for the oligo(styrenes). This will be discussed further in Section 7.2.3.

Low frequency flank

The fitted exponents, a, of the low frequency power-law flank of the α loss peak are shown in Figure 7.4a. The values increase with increasing temperature across the range of samples, indicating a narrowing of the low frequency portion of the peak. For the lowest chain-length sample, $N_\alpha = 2$, the values increase towards a value of unity with increasing temperature. The a parameter values for the $N_\alpha = 3$ sample seem to have an almost temperature invariant behaviour and the spectra could be well described with a set to values approaching unity across

the measured temperature range. We observe that, for the higher chain-length samples, values of a increase with increasing temperature and the temperature dependence of the values is similar. The values for the higher chain-length samples are lower than those of the $N_\alpha = 2$ and 3 samples.

Many authors state that the low frequency power-law flank of the α loss peak should have an ω^1 dependence and many of the functional descriptions of dielectric loss peaks assume this dependence [55, 98, 109, 168]. Although the $N_\alpha = 3$ sample conforms to this expected behaviour, the other samples in the series clearly do not. In Chapter 6 a similar behaviour was observed for the styrene series and a possible reasoning for this behaviour was discussed and we refer to the previous discussion.

High frequency flank

The parameters corresponding to the exponent of the high frequency power-law flank, b, are shown in Figure 7.4b. In general, these parameters also show an increase with increasing temperature as observed for the styrene series. There does not, however, appear to be an obvious trend with molecular weight. The lowest chain-length samples ($N_\alpha = 2$ and 3) show a similar temperature dependence to the highest chain-length samples and it appears that, in general, the higher chain-length samples have lower values of the b parameter. Interestingly, the $N_\alpha = 5$, 15 and 19 show a relatively temperature independent behaviour.

In general, through the exponents of the low and high frequency flanks (a and b) we observe that the α loss peak is broader for the higher molecular weight samples. This was also observed for the styrene series. We also observe that the higher molecular weight samples have very similar values of these exponents indicating that the shape of the α loss peak is effectively independent of molecular weight for polymers in this series past a certain chain-length. Similar behaviour has also been observed for oligomeric series of styrene (see Chapter 6 and Refs. [26, 269]). Furthermore, the breadth of the α loss has been attributed to the fragility, with more fragile glass-formers exhibiting a broader relaxation dispersion [11, 26, 190] and similar conclusions have been drawn for the behaviour of the KWW stretching parameter (which is related, in some respect, to the b parameter)

[62, 83]. This implies that the fragility increases with increasing molecular weight until a certain point at which the fragility no longer exhibits a molecular weight dependence. This will be confirmed, to a certain extent, by the determined values of the fragility parameter m in Section 7.5 and also through analysis of the width of the DSC traces in C_p in Section 7.8.1. Furthermore, it could be said that the breadth of the α loss peak could be related to the degree of cooperativity in glass-formers [62, 83]. This implies that the degree of cooperativity increases as a function of chain-length. This might be expected as systems with longer chains are likely to have more complex intramolecular interactions [193].

Dielectric strength

Values of the dielectric strength, $\Delta\varepsilon$ of the α loss peaks for the samples were obtained by numerical integration of the fits of the RB function to the dielectric spectra (the integral is given in Chapters 2 and 4). These values are shown in Figure 7.4c. To aid further discussion, the values have been plotted on a logarithmic y-axis as shown in Figure 7.5. The dielectric strength decreases with increasing molecular weight. This trend is indicated by the dashed grey guide to the eye in Figure 7.5 and a similar trend is observed also for the amplitude of the α loss peaks.

In general values of $\Delta\varepsilon$ show a $1/T$ dependence as predicted by the Onsager equation [94] which has been fully discussed in Chapters 4, 6 and 2. In order to highlight this trend, the data for the $N_\alpha = 2$ sample were fit using an equation of the form $\Delta\varepsilon = \frac{A}{T}$. This fit is denoted by the blue line in Figure 7.5. In general, the temperature dependence of $\Delta\varepsilon$ appears to be stronger than a simple $1/T$ behaviour for the lowest molecular weight samples (N_α = 2, 3 and 5) although it could be a reasonable description of the data for the higher molecular weight samples.

As a further test, the $N_\alpha = 2$ samples data were fit with an exponential of the form $\Delta\varepsilon = Ae^{BT}$. This is denoted by the black dashed line and appears to be a better description of the data. Interestingly this fit encompasses the low temperature data for the $N_\alpha = 3$ sample and almost predicts the behaviour of $\Delta\varepsilon$ across the range of samples with the obvious exception of the $N_\alpha = 15, 19, 31$

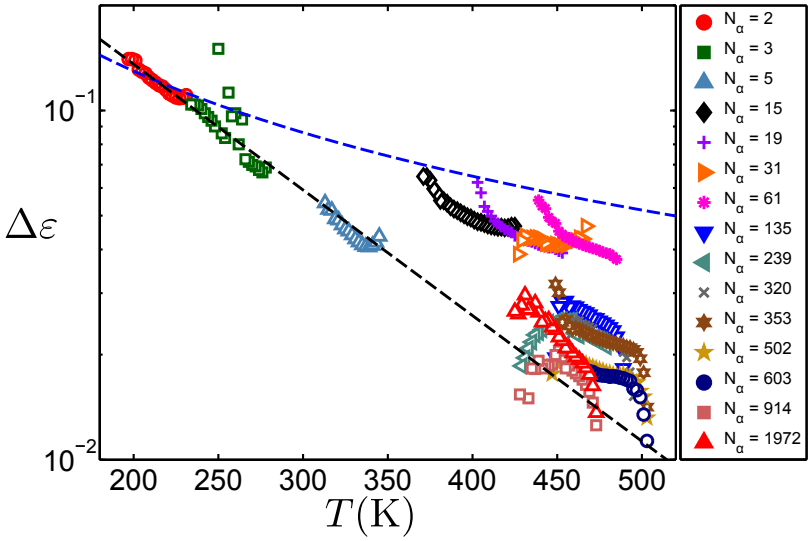

Figure 7.5: Values of $\Delta\varepsilon$ obtained through fitting of the dielectric spectra plotted on a log axis against $1000/T$. The blue dashed line corresponds to a fit of the form $\Delta\varepsilon = A/T$ and the black dashed fit line in panel corresponds to a fit of the form $\Delta\varepsilon = Ae^{BT}$. Both fits were conducted on the $N_\alpha = 2$ sample.

and 61 samples. This could indicate a more general behaviour of $\Delta\varepsilon$ as a function of chain-length and is consistent with the observations for the oligo(styrenes).

7.3 Relaxation timescales

In this section, the relaxation timescales obtained through fits of the RB function to the dielectric data will be considered. The data are shown in an Arrhenius plot in Figure 7.6a. The figure also includes data for isopropylbenzene (IPB) obtained from the literature [162]. IPB is chemically similar to the monomer unit of PAMS, the only difference being that the α-methylstyrene monomer has a double bond between a methyl group and a carbon atom and thus has 1 less hydrogen atom than IPB. The τ_α data shows a shift to higher temperatures with increasing chain-length indicating an increase in T_g, which is consistent with the general trend observed for both the styrene and alkyl benzene series. The dashed horizontal line indicates a timescale of 100s, at which T_g is often defined [189].

Figure 7.6b shows the τ_α data rescaled by T_g. The behaviour of the data in this scaling indicates qualitatively that the longer chain-length samples in

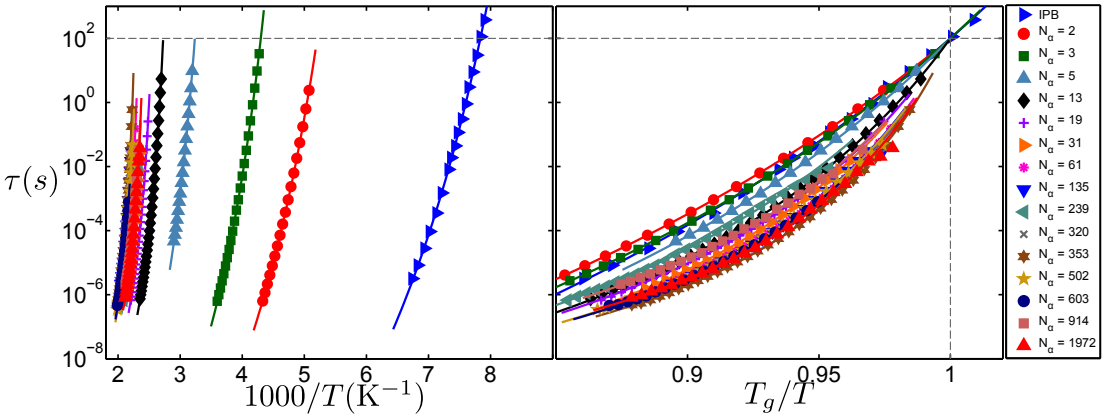

Figure 7.6: a) Relaxation timescales of the α relaxation, τ_α, for the PAMS series. b) τ_α values plotted against T_g/T. The plots include data for isopropylbenzene (IPB) obtained from Ref.[162], which is chemically similar to the α-methylstyrene monomer.

this series are more fragile than the shorter chain-length samples [91]. In other words, close to T_g, the longer chain-length samples exhibit a greater change in the timescale of the α relaxation with decreasing temperature. This appears to vary systematically for the N_α = 2, 3 and 5 samples but it it difficult to say whether the longer chain-length samples also show a systematic dependence of the fragility. The observed behaviour of the τ_α data will be quantified by further analyis of the data in Section 7.5.

The data are well described by fits of the VFT equation (see Chapters 1, 4 and 6) [27–29] as denoted by the solid lines through the data. The fit parameters τ_0, D and T_0 are shown in Table 7.2. Also shown are values of T_g (defined at τ_α = 100s) and the fragility parameter, m.

In general, values of τ_0 decrease with increasing chain-length. For the N_α = 13, 19, 31 and 239 samples these values fall within the range expected for typical microscopic timescales (10^{-12} - 10^{-14}s) [2, 24–26]. However, the values for the other samples do not fall within this region. Values for T_0 also show an increase with increasing molecular weight as expected, given the shift of the τ_α data to higher temperatures with increasing chain-length. The other parameters in Table 7.2 will be addressed in full in the following sections.

N_α	$\log_{10}(\tau_0)$(s)	D	T_0 (K)	T_g	m	Reference
1 (IPB)	-19.5 ± 0.8	21 ± 3	89 ± 2	127.6	72.0	[162]
2	-18.2 ± 0.1	19.8 ± 0.2	134.7 ± 0.3	192.0	67.8	
3	-17.0 ± 0.2	14.9 ± 0.4	173.5 ± 0.9	232.6	74.5	
5	-16.2 ± 0.5	12 ± 1	242 ± 3	309	84	
13	-13.0 ± 0.1	5.2 ± 0.2	318 ± 1	367	113	
19	-12.1 ± 0.1	4.1 ± 0.1	349 ± 1	393	126	
31	-12.3 ± 0.1	4.0 ± 0.2	368 ± 1	413	131	
61	-10.9 ± 0.2	2.6 ± 0.1	394 ± 1	429	156	
135	-11.7 ± 0.2	3.2 ± 0.2	397 ± 2	437	148	
239	-13.3 ± 0.4	6.1 ± 0.6	349 ± 5	409	104	
320	-11.3 ± 0.1	2.8 ± 0.1	405 ± 1	442	159	
353	-10.7 ± 0.1	2.3 ± 0.1	410 ± 1	442	177	
502	-11.4 ± 0.1	3.0 ± 0.1	397 ± 1	435	151	
603	-11.2 ± 0.1	2.8 ± 0.1	401 ± 1	438	157	
914	-11.4 ± 0.3	3.6 ± 0.3	370 ± 3	414	127	
1972	-10.4 ± 0.2	2.3 ± 0.1	385 ± 2	416	170	

Table 7.2: Table showing the fitting parameters obtained through fits of the VFT equation to the τ_α data. The table also includes T_g and the fragility parameter m for each sample. The reported errors were obtained from a least mean squares fit of the VFT function to the τ_α data.

7.4 Glass transition temperature

In this section, the T_g values obtained through extrapolation of the VFT fits to the τ_α data will be discussed. Figure 7.7a shows these data for a selection of the lower chain-length samples plotted against molecular weight on a linear scale. Values of T_g for the same selection of samples, obtained from analysis of the DSC data, (see Section 7.8.1) are shown for comparison. Also shown is the T_g value determined for IPB from VFT fits of the τ_α data obtained from the literature [162]. There is reasonable agreement between T_g values obtained from analysis of τ_α and those obtained from analysis of the DSC data with the exception of the $N_\alpha = 13$ and 19 samples (as marked in Figure 7.7a) for which the DSC values appear to be lower. The dashed black line in Figure 7.7a indicates a fit of the Fox-Flory equation to the whole data set. In this scaling, the Fox-Flory relationship describes the variation of T_g reasonably well with the exception of the $N_\alpha = 13$ and 19 samples and the value for IPB. The T_g data for all the samples in the series is shown in Figure 7.7b, this time plotted with a logarithmic scaling of M_w. Again we see that the Fox-Flory relationship described the high M_w data well but this does not extend to the T_g values for IPB and the $N_\alpha = 2$ sample.

It should be noted that the T_g values obtained through VFT analysis of the τ_α data are lower than expected for the $N_\alpha = 239$, 914 and 1972 samples, plotted as grey circles in Figure 7.8a. The differ significantly to the DSC T_g data for the same samples. These samples show a particularly strong conductivity contribution and therefore timescales could not be obtained from the α loss peaks across the whole frequency range (see for example the spectra for the $N_\alpha = 1972$ sample in Figure 7.3h). This could mean that the VFT fits of the data may not be an accurate representation of the peak timescales of the α loss peak at low frequencies (longer timescales) and because of this the extrapolation of the VFT fits to $\tau = 100$s may not have given an accurate indication of T_g. In order to test this, T_g values were also obtained at $\tau = 1$s instead as this required no extrapolation of the VFT fits. These values are denoted by the green circles in Figure 7.7a. However, we see that that these values of T_g are still lower than expected for the $N_\alpha = 239$, 914 and 1972 samples. The most probable origin of the lower values for the dielectric data for these three samples is that some level of degradation occurred in these

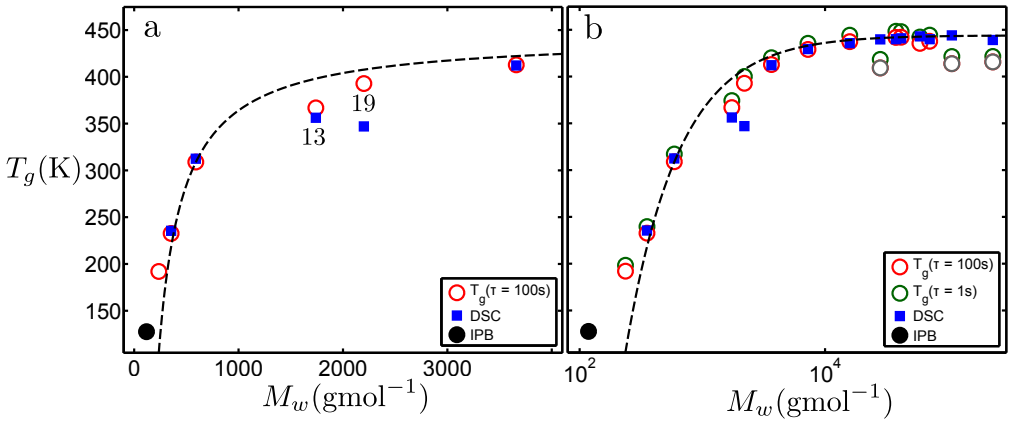

Figure 7.7: Values for the glass transition temperature, T_g, obtained through analysis of τ_α, where T_g has been defined at 1s (green circles) and 100s (red circles). These are plotted on a linear (panel a) and a logarithmic (panel b) x-axis. Also shown are values obtained from analysis of the DSC traces in C_p. The grey circles indicate the T_g values of the N_α = 239, 914 and 1972 samples. The black dashed line indicates a fit of the Fox-Flory equation.

samples during the sample preparation. This is supported by the fact that the DSC results for the same three samples are consistent with the behaviour of the other samples.

We saw for the styrene series that the T_g data were well described by assigning three distinct molecular weight regions based on plotting the data in a semilogarithmic plot. Indeed, Cowie [259] saw that the three-region behaviour was also present for T_g values of a similar chain-length series of PAMS, measured using Differential Thermal Analysis (DTA) [259, 304]. In Figure 7.8 we present a comparison of the T_g values obtained for this series (Figure 7.8a) with those obtained by Cowie (Figure 7.8b).

The dashed guides to the eye in Figure 7.8a indicate a suggested linear increase of T_g for the low molecular weight samples (red line) and the value at which T_g becomes invariant with increasing molecular weight (grey line). We have not attempted to fit the intermediate regime (II) or determine the borders between the three regimes. The vertical dashed lines are here the same as those used by Cowie and shown in Figure 7.8b. Qualitatively, it appears that we observe a similar behaviour to Cowie et al. However, for higher molecular weights, our

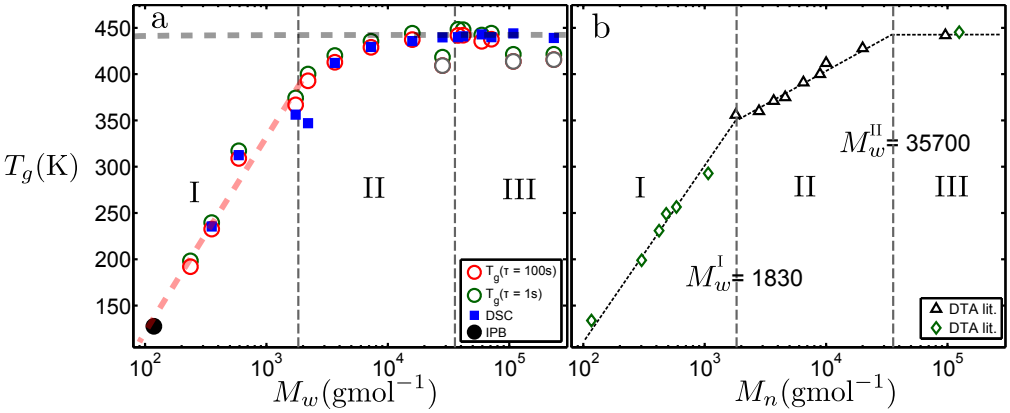

Figure 7.8: a) Values for the glass transition temperature, T_g, obtained through analysis of the dielectric and DSC data, including data for IPB [162]. b) Values of T_g obtained from the literature [259, 304]. The vertical dashed lines in each figure denote the molecular weight regions defined by Cowie [259]

data is less clear than the DTA data obtained from the literature which shows a behaviour which is strongly suggestive of a three-region behaviour of T_g rather than a smooth function of M_w. The values of molecular weight that separate the three different regions (as determined by Cowie [259]), M_w^I and M_w^{II} are shown in Figure 7.7b, corresponding to $N_\alpha \approx 15$ and $N_\alpha \approx 300$. These values are similar to those observed for chain-length series of styrenes as shown in Chapter 6. Hintermeyer *et. al.* associated M_w^I with the molecular weight of a Rouse unit or Kuhn segment [258]. The Kuhn-length of poly(α-methylstyrene) has been quoted as 1.7nm [306]. If we assume that the carbon-carbon bond to be 1.544Å [307] then the size of a Kuhn segment is equivalent to ~ 11 monomer units. This is smaller than the number of monomer units associated with M_w^I for chain length series of poly($\alpha-$methyl styrene) (15 units). However, the definition of M_w^I is somewhat arbitrary so one could still imagine M_w^I to be equivalent to the molecular weight of a Kuhn segment. This again suggests, as it did for the styrenes, that the onset of Rouse dynamics could affect the molecular weight dependence of T_g.

Our T_g values, particularly for the molecular weights in Region II, are higher than those in the literature[259, 304]. The reason for this might be a difference with regards to the initiator group or it might be due to a difference in tacticity. We note that the samples in the styrene series also have an initiator group but

the values were in very good agreement with those obtained from the literature [258–261]. There is unfortunately no information available regarding the initiator used in the synthesis of the samples in the literature [259, 304]. However, even with these differences present, the overall behaviour suggesting an initial regime (I) with a linear behaviour in a semi-logarithmic plot and a final high molecular weight regime which lacks molecular weight dependence are the same. Our data might also be best described within an intermediate regime (II) using the same functional shape as in Region I, but the small range and few data points within this regime makes it impossible to know for sure.

7.5 Dynamic Fragility

We will now consider the dynamic fragility of the samples in this series. It was observed, through rescaling of the τ_α data by T_g (Figure 7.6b), that the fragility of the samples increased as a function of molecular weight. In order to parametrise this trend, the dynamic fragility parameters, m, were calculated (as defined in Chapters 1 and 4). Values of m are shown in Figure 7.9a. Those samples which had unexpected values of T_g are represented as grey points.

The values show a similar trend to that observed for the oligostyrene series: an increase with increasing molecular weight for the lower chain-length samples before reaching a limiting value for the longer chain-length samples. This occurs at a similar molecular weight as the point at which T_g becomes invariant with molecular weight. Similar trends in the fragility parameter have also been observed for other polymeric chain length series (for example: polydimethylsiloxane (PDMS) and polybutadiene (PB) [258]) and also for the styrene series shown in Chapter 6.

The implication of this is that fragility is only molecular weight dependent in a certain dynamic regime before reaching a constant value for polymers for which descriptions of their dynamics are effectively independent of molecular weight. A similar trend of fragility is implied by the variation of values of the strength parameter, D, shown in Figure 7.9b as obtained from the VFT fits of the τ_α data. Interestingly, the values of D appear to reach a limiting value of D at a

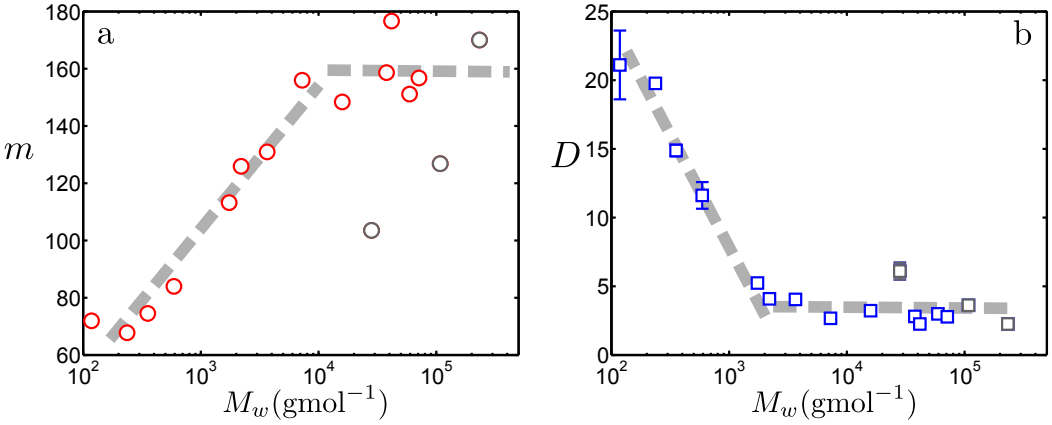

Figure 7.9: Values for a) the dynamic fragility parameter, m, and b) the strength parameter, D, obtained through fits of the VFT function to the τ_α data. The values for the samples which demonstrated unexpected values of T_g (N_α = 239, 914 and 1972) are shown in grey in both cases.

lower molecular weight than the corresponding m parameters or T_g although it is difficult to say for sure.

7.6 Linearisation of timescale data

Further analysis of the temperature dependence of the τ_α data was done by performing a so-called Stickel analysis of the data [31]. This involved taking the derivative of the logarithm of the τ_α data as described in Chapters 1 and 4. This derivative is quantified by the Z parameter. The linearised τ_α values are shown in Figure 7.10a. The lines through the data indicate the linearised VFT fits of the τ_α data as shown in Figure 7.6. We observe that the temperature dependence of Z appears to increase with increasing molecular weight. This again implies an increase in fragility as strong Arrhenius-like behaviour would be represented with a temperature independent Z parameter. The increase in dynamic fragility is parametrised by the $-S$ parameter as shown in Figure 7.10b. We observe an increase of $-S$ with increasing molecular weight for the shorter chain-length samples before $-S$ becomes invariant with molecular weight for longer chain-length samples in a similar manner to the m and D parameters.

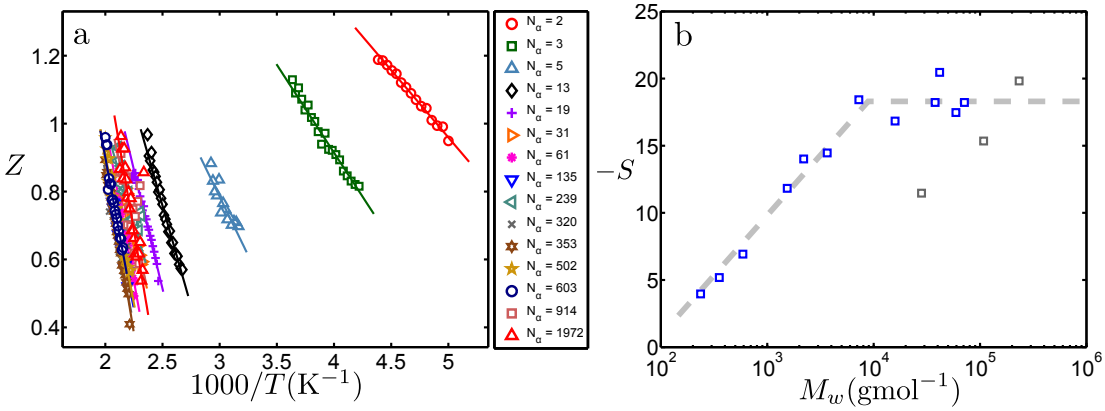

Figure 7.10: a) Linearised τ_α data for the PAMS series. Solid lines through the data are linearised fits of the τ_α data with the VFT equation. b) Values of the Stickel gradient parameter, $-S$.

Closer analyses of the linearised τ_α data for the $N_\alpha = 2$, 3, 5 and 13 samples are shown in Figures 7.11a-d. Linearising the τ_α data in this manner can sometimes yield subtle differences in the temperature dependence of the data that can not be resolved in Arrhenius plots of τ_α versus $1/T$. Also, it is often observed that a kink in a Stickel plot indicating the change from one VFT-like behaviour to another coincides with the merging or bifurcation of a secondary relaxation [193]. The vertical dashed black lines show the temperatures $T_{\alpha\beta}$. For the $N_\alpha = 2$ sample, its value was obtained by determining the crossover between the Arrhenius description of the τ_β data and the fits of the VFT equation to the τ_α data. For the other samples, values of $T_{\alpha\beta}$ were obtained by calculating 'expected' values of τ_β. This will be fully explained in Section 7.7.2. The dashed red-lines in the figures show linear fits to the low temperature linearised data ($T < T_{\alpha\beta}$).

We observe that, for the $N_\alpha = 2$ sample (Figure 7.11a) there is no clear indication of a change of temperature dependence of Z at $T_{\alpha\beta}$ and the data are well described across the whole temperature range by a fit of the low temperature data. However, the other samples do appear to exhibit a slight change in the temperature dependence of Z and this occurs in a similar temperature range to that of $T_{\alpha\beta}$. This change is emphasised by the fits of the low temperature data which do not provide an adequate description of the data over the whole temperature range. This is more obvious for the $N_\alpha = 3$ and 13 samples but more

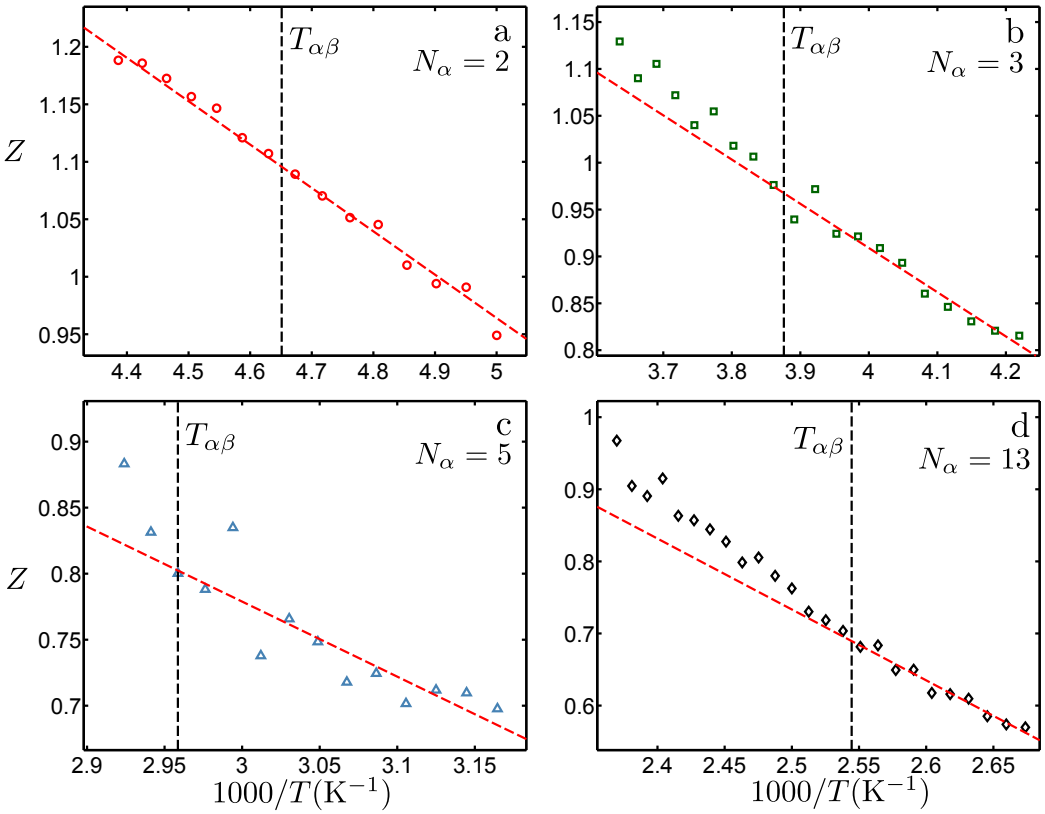

Figure 7.11: Linearised τ_α data for the a) $N_\alpha = 2$, b) $N_\alpha = 3$, c) $N_\alpha = 5$ and d) $N_\alpha = 13$ samples. The vertical black dashed lines indicate the crossing point, $T_{\alpha\beta}$ of the τ_α and τ_β values in an Arrhenius plot. For the $N_\alpha = 3$, 5 and 13 samples this was obtained from the expected timescales of the β relaxation as explained in the text. The red dashed line indicates a linear fit to the low temperature data ($T < T_{\alpha\beta}$)

data would be required at high temperatures (shorter timescales) to confirm this behaviour for the $N_\alpha = 5$ sample.

7.7 Secondary Relaxation

The only sample in which a secondary, β relaxation loss peak could be fully resolved in the dielectric spectra was the $N_\alpha = 2$ sample. At higher temperatures the peak was manifested as a 'shoulder' on the high frequency power-law flank of the α loss peak as shown in Figure 7.3a.

7.7.1 Fitting procedure

In order to analyse this relaxation process, spectra were analysed at temperatures close to T_g. A selection of loss spectra are shown in Figure 7.12a. The lines represent fits of the data. The β relaxation is often observed as a symmetrically stretched loss peak in the dielectric loss, ε'' [33, 61, 67, 94, 96, 116, 117]. . Therefore it was assumed that the secondary relaxation observed for the $N_\alpha = 2$ sample had a similar shape and was fit using the Cole-Cole (CC) expression [176]. The low frequency flank of the β relaxation loss peak was, at most temperatures, significantly obscured by the high frequency flank of the α loss peak. A power-law of the form $\varepsilon'' = A\omega^{-k}$ was used in order to take account of the high frequency flank of the α loss peak.

The spectra were fit using an additive combination of the functional descriptions of the β loss peak and the high frequency flank of the α loss peak. The two fit contributions are shown clearly in Figure 7.12b at a temperature of 193 K. It is clear from this figure that the combination of these two functions provides a good interpolation of the data. It should be noted that frequency range was restricted such as to remove high frequency contributions to the spectra.

It was obviously difficult to describe the shape of the β loss peak precisely due to the proximity of the α relaxation loss peak. It was found that the symmetric stretching parameter, α, in the CC expression could be fixed for all temperatures to a value of 0.43. The dielectric strength, $\Delta\varepsilon$ showed little variation with

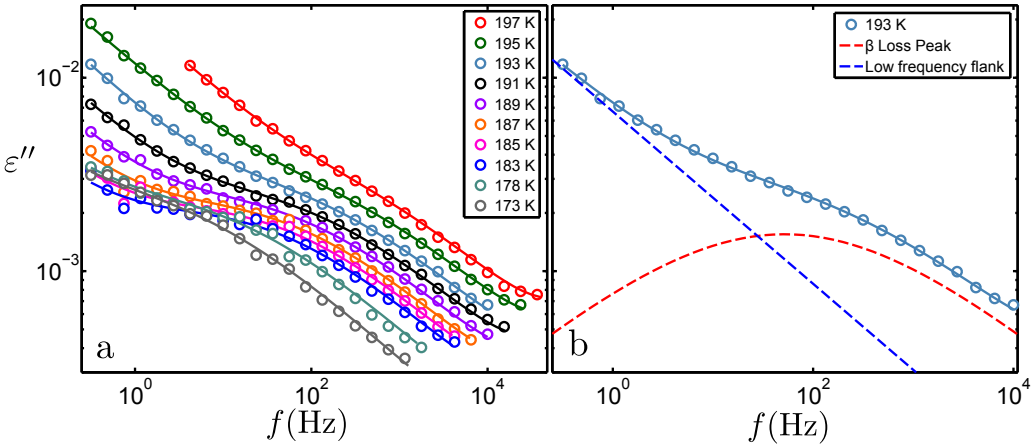

Figure 7.12: a) Dielectric spectra for the $N_\alpha = 2$ sample in the β relaxation regime. b) Dielectric spectrum at 193 K showing the different fit contributions.

temperature, and had an average value of $\sim 8 \times 10^{-3}$. The temperature dependence and absolute value of $\Delta\varepsilon$ are similar to those of the secondary relaxations observed for the alkylbenzene and styrene series (Chapters 4 and 6).

7.7.2 Relaxation timescales

In this section, the timescales of the observed β relaxation will be compared to those of the α relaxation. Again, IPB has been included for comparison as it is chemically similar to $\alpha-$methylstyrene. For the $N_\alpha = 3$, 5, and 13 samples, predictions of the expected values of τ_β were calculated. A similar analysis was performed for samples in the styrene series (Procedure 1), as shown in Chapter 6. This involved calculating expected values of τ_β using the Arrhenius equation. In order to do this, values of the activation energy, E_A, and the limiting timescale at high temperatures, τ_0, needed to be determined.

Firstly, the activation energies, E_A were determined using using the relationship between T_g and E_A suggested by Kudlik *et. al.* [61]($E_A = KRT_g$) and assuming that the constant of proportionality, K was the same across the series. A value of $K = 29$ was calculated using values of τ_β for the $N_\alpha = 2$ sample which is similar to typical values of K observed for molecular glass formers (24 ± 3) [15] and metallic glasses (26 ± 2) [9]. The variation of τ_0 determined through Arrhenius fits of the τ_β data for the IPB [52] and $N_\alpha = 2$ samples is very small

N_α	$\log_{10}(\tau_0)$(s)	$\log_{10}(\tau_{\alpha\beta})$	E_A(kJ/mol)	K	T_g	Reference
1 (IPB)	-15.2 ± 0.2	-6.2 ± 0.1	26.3 ± 0.4	24.8 ± 0.4	127.6	[52]
2	-15.1 ± 0.3	-3.8 ± 0.1	46 ± 1	29.0 ±0.8	192.0	
3	-	-3.7 ± 0.1	56 ± 1	-	232.6	
5	-	-3.5 ± 0.1	75 ± 2	-	309	
13	-	-3.2 ± 0.1	89 ± 2	-	367	

Table 7.3: Table showing parameters obtained through the Arrhenius fits of the τ_β data for the IPB (obtained from Ref.[52]) and $N_\alpha = 2$ samples: the limiting timescale at high temperatures, τ_0 and the activation energy, E_A. Also shown are the activation energies for the $N_\alpha = 3$, 5 and 13 samples obtained using the method described in the text. The constant of proportionality, K, between E_A and T_g is also given as well as the glass transition temperature, T_g, and the bifurcation timescale, $\tau_\alpha\beta$. Note that values of τ_0 and K for the $N_\alpha = 3$, 5 and 13 samples are the same as those given for the $N_\alpha = 2$ sample.

as shown in Table 7.3. Therefore the assumption was made that this value of τ_0 should hold for the other samples as well.

Finally, 'expected' values of τ_β for the samples in the series were calculated using the Arrhenius equation. Some samples in the styrenes series exhibited an excess-wing behaviour of the α loss peak at temperatures below T_g. It was observed, by looking at spectra at specific temperatures, that the expected values of τ_β corresponded to the frequency regime in which the high frequency power-law exponent of the α loss peak changed, thus providing support for the method (Procedure 1 in Chapter 6) in which expected τ_β values were calculated.

Timescales for both the α and β (both expected and observed) relaxations for the $N_\alpha = 2$, 3, 5 and 13 samples are shown in Figure 7.13a. The τ_β values for IPB were obtained from dielectric measurements conducted by Johari *et. al.* [52]. The τ_β data for IPB and the $N_\alpha = 2$ sample were well described by fits of the Arrhenius equation as denoted by the dashed fit lines through the data. The parameters, τ_0 and E_A obtained from these fits and for the expected values of τ_β are shown in Table 7.3. The τ_β data show a very similar variation to those of the styrene series and appear to increase systematically (at a certain temperature) with increasing chain-length. This behaviour also extends to IPB. The variation of the activation energy (which sets the gradient of the data in an Arrhenius plot) is also evident in Figure 7.13 which increases systematically

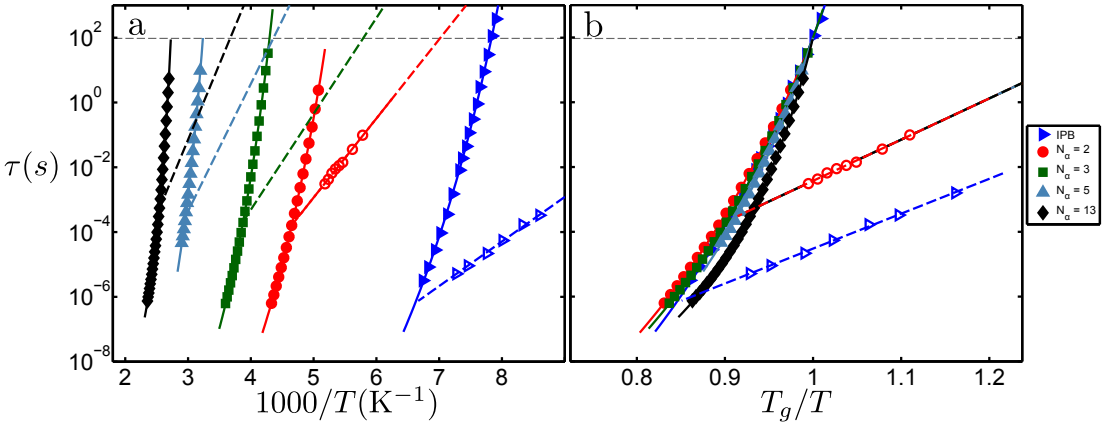

Figure 7.13: Values of τ_α and τ_β plotted against a) $1000/T$ and b) T_g/T. The figure also includes data from the literature for IPB (Ref.[162] for τ_α and Ref.[52] for τ_β.). The dashed lines through the τ_β data for IPB and $N_\alpha = 2$ indicate fits of the Arrhenius equation. The dashed lines for the other samples ($N_\alpha = 3$, 5 and 13) indicated expected values of τ_β determined as described in the text.

with increasing temperature by necessity as E_A was calculated using values of T_g which also increase systematically with chain-length for these samples. The implication of the data is that, as the T_g values reach a limiting value at high M_w (see Figure 7.7) the timescales of the β relaxation for the higher molecular weight samples should follow a similar behaviour [69, 193]. Similar observations have been made for the samples in the styrene and alkylbenzene series and also for a series of PMMAs (which are not discussed in this thesis). Chain-length series of monomethyl ethers and glycols also show similar behaviour [18]. This could indicate that the observed behaviour of the τ_β could be a general phenomena of glass-forming systems.

A T_g rescaled Arrhenius plot is shown in Figure 7.13b. In this scaling, the expected τ_β values collapse onto the behaviour of the τ_β values for the $N_\alpha = 2$ sample. This is expected as E_a was calculated for the N_α = 3,5, 13 samples assuming the same constant, K, as and limiting timescale, τ_0, as determined from the Arrhenius fits of the τ_β values of the observed secondary relaxation of the $N_\alpha = 2$ sample. Again, it should be reiterated that this is a valid choice as similar values of K are observed for many different glass forming systems [9, 15]. However the τ_β data for IPB do not collapse in the same way.

A confirmation of the nature of the obtained τ_β values for this series can be obtained by referring back to the linearised τ_α data shown in Section 7.6. These values show a slight kink indicating a change in the dynamic behaviour of τ_α for the N_α = 2, 3, 5 and 13 samples. The temperature range at which a change in the dynamics of τ_α is observed is often called the crossover regime and can sometimes be associated with the temperature, $T_{\alpha\beta}$ at which bifurcation of the α and β relaxations occurs [30]. Values of $T_{\alpha\beta}$ were obtained by determining the point at which the expected values of τ_β (dashed lines in Figure 7.13) cross the VFT fits of the τ_α data (solid lines in Figure 7.13). These values are shown as dashed black lines in the plots of the linearised τ_α data and correspond well to the temperature at which the 'kink' is observed suggesting that the determined values of τ_β are indicative of a real, underlying β relaxation which could not be observed in the dielectric spectra.

Values of $\tau_{\alpha\beta}$ were also calculated (see Table 7.3). Interestingly, these values show an increase with increasing chain-length rather similar to that suggested for the styrene series using a similar approach to estimate the β timescales, for the, alkylbenzene series, for a chain length series of PMMA. The coupling model suggests a connection between the fragility parameter m and the coupling parameter, n, which is another measure of the cooperativity [83]. We observe an increase of m with increasing molecular weight implying that the cooperativity also increases with chain-length and thus strengthens the conclusions drawn from the τ_β data.

7.8 Differential Scanning Calorimetry

The samples, with the exception of the N_α = 2 sample were also measured using Differential Scanning Calorimetry (DSC). DSC measurements were performed using the TA Instruments Q2000 calorimeter, the details of which are given in Chapter 3. The samples were run by heating/cooling the samples in a cyclic manner around their expected T_g values at a rate of 10K/min. This rate was chosen as it can be shown to correspond to a relaxation timescale of 100s [138–141], meaning that DSC and dielectric measurements could be compared constructively.

7.8.1 Traces of the heat capacity

The DSC data obtained through this series of measurements are shown in Figure 7.14. The steps in C_p, denoting the glass transition, shift to higher temperatures with increasing molecular weight, indicating increasing T_g values. The DSC traces were analysed in the manner described in Chapter 3, with T_g determined from the onset of the characteristic step in C_p associated with the glass transition. It has already been shown (Figure 7.7) that the T_g values obtained from DSC and dielectric experiments are in good agreement. Interestingly, the absolute values of C_p below T_g appear to fall on the same temperature dependence as denoted by the dashed guide to the eye.

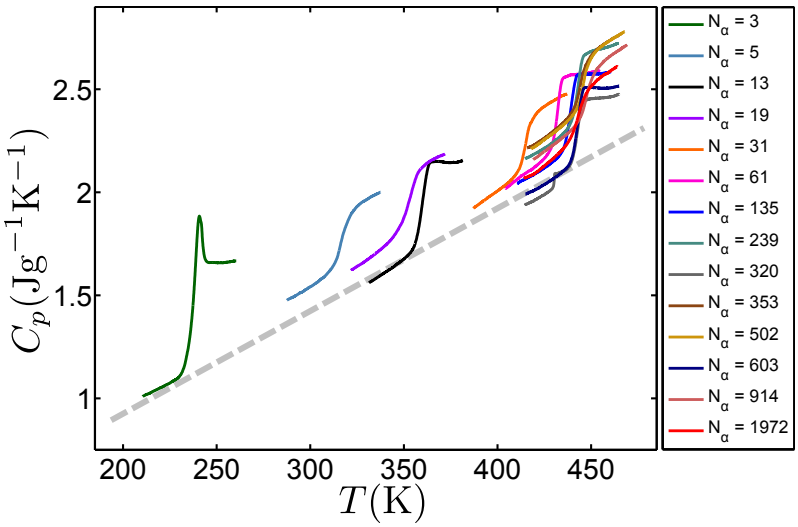

Figure 7.14: Figure showing the C_p traces obtained through DSC measurements of the PAMS series.

Measurements of mixtures of $N_\alpha = 5$ and $N_\alpha = 915$ samples of performed by Huang *et. al.* [305] yield similar results. The glass transition was observed to increase with higher concentrations of the $N_\alpha = 915$ polymeric sample but the C_p traces fall onto the same glass and liquid specific heat capacity behaviour. In Chapter 4, similarities were seen between measurements of the alkylbenzene series and measurements of different mixtures of polystyrene and toluene. It appears that one may be able to draw similar conclusions here, that in terms of the specific

heat, an increasing degree of polymerisation is analogous to increasing the long-chain polymer component in a mixture with the same but shorter chain polymer. The glassy base-line indicated using a dashed grey line in Figure 7.14 appears to be very similar throughout the temperature range demonstrating that the properties of the glass are similar independent of molecular weight even though the glass-transition temperature is strongly affected by the molecular size.

Huang *et. al.* [305] also compare the C_p data for IPB and the α-methylstyrene dimer with that of $N_\alpha = 5$ and $N_\alpha = 13$ and conclude that the specific heat capacities in the liquid and glass are only molecular weight dependent up to $N_\alpha = 5$. The results presented here seem to suggest that this behaviour actually extends to the $N_\alpha = 3$ sample. The authors attribute the observed behaviour to the suppression of rotational and translational contributions to the heat capacity with increasing polymerisation beyond $N_\alpha = 5$, as previously suggested by Wunderlich [308].

7.8.2 The 'step height' of the glass transition

In order to characterise the observed glass transition steps in C_p, the difference between C_p in the glassy and liquid states, ΔC_p was determined and these values are shown in Figure 7.15a. The values of C_p show no obvious trend with increasing degree of polymerisation but appear to be similar for most of the samples in the series with the exception of the $N_\alpha = 3$ sample which has a far greater step size. Again the behaviour of these values could also been explained by Wunderlich's hypothesis [308].

In Chapters 4 and 6 it was shown that one can analyse the difference in the temperature dependence of the entropy at the glass transition by rescaling values of ΔC_p by T_g. This analysis is shown in Figure 7.15. In this scaling, the values show a very systematic decrease with increasing molecular weight as highlighted by the dashed guide to the eye. This indicates the difference in the temperature dependence of the entropy at T_g decreases with increasing degree of polymerisation. This difference is far larger for the $N_\alpha = 3$ sample.

As stated in previous chapters, the difference in the glassy and crystalline heat capacities has been defined to be a measure of the so-called thermodynamic

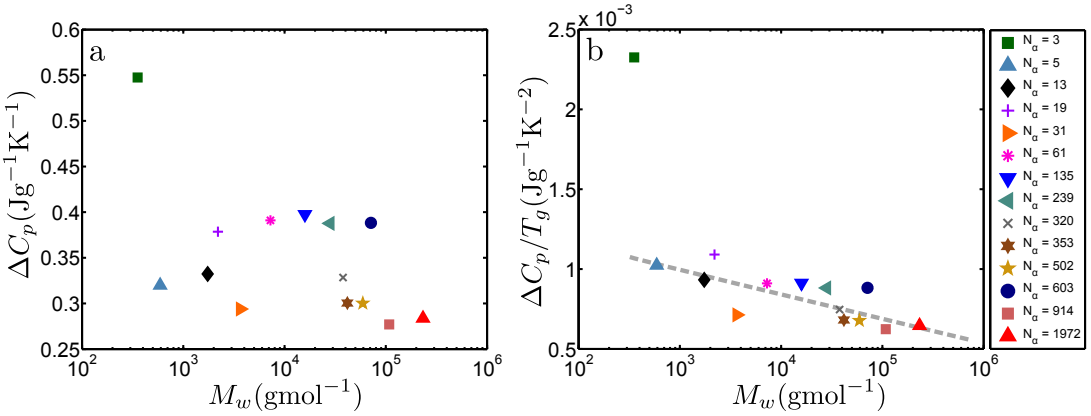

Figure 7.15: a) Values for ΔC_p obtained through analysis of the DSC traces shown in Figure 7.14. b) The same values rescaled by T_g

fragility [91, 122]. It can also be shown that, for simple molecular glass formers (such as the alkylbenzene series), ΔC_p can be related to the kinetic fragility parameter, m [121]. However, for this series of samples we can show no such correlation. The ΔC_p values show very little variation with molecular weight whereas measures of the dynamic fragility (the m, D and $-S$ parameters) show a strong molecular weight dependence.

An inverse correlation between the thermodynamic definition of fragility provided by ΔC_p and the dynamic definition provided by the m parameter was observed for the styrene series and has been observed for a range polymeric systems [122, 263]. There is no such correlation for the values obtained in the analysis presented here. Huang *et. al.* suggest that polymers can be grouped into those with strong and weak inverse proportionality between m and ΔC_p. PAMS clearly falls into the 'weak' category. A possible explanation for the difference in the two definitions of fragility was given in Chapter 6 with reference to an argument presented by Angell in which he attributes the difference to the increase in vibrational anharmocity in the glassy state [264].

7.8.3 The width of the glass transition step

The difference between the onset and offset temperatures of the glass transition step in C_p, ΔT has also been attributed to the fragility of glass formers [209–

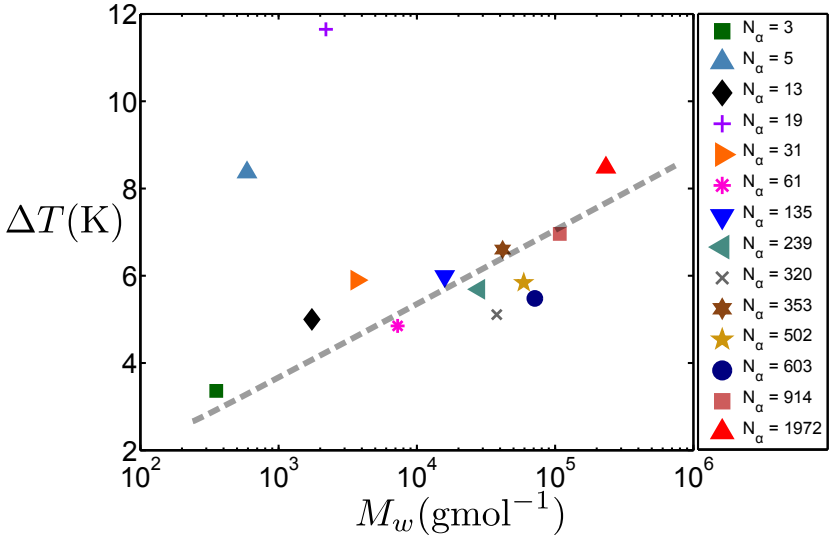

Figure 7.16: a) Values for ΔT obtained through analysis of the DSC traces shown in Figure 7.14.

211]. Values of ΔT are shown in Figure 7.16 and show a systematic increase with increasing temperature for the majority of samples as indicated by the dashed guide to the eye. Notable exceptions to this trend are the $N_\alpha = 5$ and 19 samples which have higher values of ΔT

We have discussed previously [211] that the onset temperature of the glass transition step is related to a relaxation timescale of around 100s and that the offset temperature is related to a timescale of around 1s and therefore the difference in these temperatures could be related to the definition of the fragility parameter, m. Indeed we see a similar increase in the m parameter with increasing molecular weight. However, we observed that m became independent of molecular weight for the longer chain samples whereas ΔT seems to increase at the same rate across the molecular weight range.

7.9 Conclusions

In this chapter the measurements of another oligo-/polymeric series have been presented. This series was characterised by the polymerisation of α-methyl styrene and is the first example (to our knowledge) of a systematic chain-length study of

this range of samples using dielectric spectroscopy.

This series of samples is chemically similar to the styrene series and therefore we might expect similar glass forming behaviour. Indeed, it was observed that the molecular weight dependence of T_g showed very similar behaviour to the styrene series and, in the low molecular weight range, the alkylbenzene series. Values of T_g increased with increasing chain-length up to a certain point at which they become invariant. The data could also be said to follow the three-region behaviour observed for a number of polymeric systems including PS [258–261]. We also note that the molecular weight boundary between Regions I and II, M_w^I is consistent with the size of a Kuhn segment. Furthermore, the parameters describing the dynamic fragility (m, D, and $-S$) of the glass formers in this series all indicate an increase of the fragility with increasing chain-length. The data implies that the glass forming properties of the systems presented in this thesis follow similar behaviour independent of their specific chemistry.

Direct evidence for two different relaxation modes, α and β, were observed. In addition, a third γ relaxation has also been observed for IPB, which is equivalent to the monomer in this series [52]. This suggests that there may be an underlying γ relaxation for the other samples in the PAMS series. Furthermore, the presence of three relaxation mechanisms may be a more general feature of molecular glass formers as similar behaviour was observed for the alkylbenzene and styrene series.

The α relaxation loss peak in ε'' is clearly observed for all samples measured using BDS. This loss peak becomes increasingly broad with increasing chain length. This broadening with degree of polymerisation is very similar to that observed for the styrene series and we can make the same argument to explain it: as the length of a polymer increases, we expect the distribution of relaxation times to become broader and thus this is reflected in the observed loss peak.

A secondary relaxation mechanism was observed for the $N_\alpha = 2$ sample in the dielectric spectra. Analysis of the timescales of this relaxation process allowed for the determination of 'expected' values of τ_β for the $N_\alpha = 3$, 5 and 13 samples. Validation of the obtained values was gained through determination of values of $T_{\alpha\beta}$, the point at which bifurcation of the α and β relaxations occurs and it was shown that this corresponds to the 'kink' in the linearised τ_α data for these samples. The expected τ_β data (at a fixed temperature) appear to increase with

increasing chain-length and are characterised by an increasing activation energy which scales with the glass transition temperature. Similar observations have been made for the alkylbenzene and styrene series as well as chain-length series of PMMA, monomethyl ethers and glycols. This suggests that the behaviour of τ_β, and thus the nature of the β relaxation, may be a more general property of glass formers rather than dependent on microscopic chemistries. It was also observed that the $\tau_{\alpha\beta}$ values increased with increasing chain-length. This was argued [193] to be indicative of the increasing cooperativity as a function of chain length.

We have observed striking similarities between the PAMS and the styrene series in terms of their glass forming behaviour. However, one significant question remains: why is the glass transition $\sim$ 40K higher for PAMS than it is for PS? Clearly this must have something to do with the differing chemistries between the two series. PAMS has an extra methyl group in each monomer unit and perhaps this methyl group serves to further hinder relaxation of the polymer chain meaning that the temperature at which dynamic arrest occurs is higher than that of PS. Despite the differences in T_g, we have observed that different glass forming systems have similar relaxation behaviour and thus it could be that the difference in their chemistries simply changes the temperature regime in which the different relaxation processes occur.

Chapter 8

Conclusions

8.1 Overall Conclusions

Glasses are amorphous materials which exhibit solid-like properties on certain timescales but do not contain the long range order and periodicity found in crystalline solids. The work presented in this thesis is aimed at understanding the dynamics of glass-forming systems through the analysis of three systematic series of molecular glass formers. These series were characterised by the systematic variation of chemical structure: an alkylbenzene series (Chapter 4) involving the systematic variation of the length of an alkyl tail attached to a phenyl-ring and two series involving the successive oligomerisation of styrene (Chapter 6) and α-methylstyrene (Chapter 7), respectively. The thesis systems were chosen as they show similarities in their chemistry, facilitating a consistent investigation of how structural modification affects relaxation behaviour in supercooled liquids and polymers. Throughout the course of this thesis, several trends have been observed which suggest a generality of relaxation behaviour in both polymeric and molecular glass forming systems. This chapter serves as a summary of the overall conclusions found. System specific conclusions are available at the end of the relevant results chapters.

An important implication of the results is that the glass transition, T_g, is strongly dependent on the 'size' of the constituent molecules in the glass forming systems studied. For the polymeric chain-length series, the often used Fox-Flory relation [255] provides a reasonable description of T_g over a range of molecular

weights but fails to capture the behaviour for the shortest chain-length samples. It was found that the T_g values are more consistent with a T_g versus $\log(M_w)$ behaviour, separated into three distinct molecular weight regions as suggested by Cowie [259]. This behaviour has been shown to apply for a range of polymeric systems such as the systematic chain-length studies of polystyrene, polydimethylsiloxane and polybutadiene performed by Hintermeyer *et. al.* [258]. We are not aware of a theoretical explanation for this behaviour and thus further research is required in order to confirm the observed behaviour of T_g with molecular weight. A similar $log(M_w)$ dependence could also describe the alkylbenzene series, consistent with observations of other molecular liquids [37, 150], suggesting that a relationship between T_g and $log(M_w)$ may be a more general property of glass forming systems.

Values of T_g obtained for the samples in the alkylbenzene series (red squares) and those of the lower molecular weight samples in the styrene (green triangles) and PAMS series (black diamonds) are shown in Figure 8.1. For comparison these are shown with those obtained for a series of molecular liquids analysed by Larsen *et. al.* [150] (blue circles). The latter glass-formers are specifically chosen as they span a wide T_g range, yet are considered rigid as they all contain alkane chains that are shorter than three carbons. Thus, these provide a good baseline for the detailed behaviour for rigid molecules. As shown in Figure 8.1, the T_g values can be well described as a simple linear relationship with $\log(M_w)$. In fact this functional dependence is the same for our three investigated series even though the slope in this type of plot is clearly different for different types of system. We find that the polystyrenes and the poly(alpha methyl styrenes) that are structurally very similar show a very similar behaviour. However, the alkyl benzenes show a singificantly lower slope. For both the two polymer series and the alkyl benzenes, we see, however, that as the molecules becomes short or 'rigid' they conform to the behaviour showed in the blue circles for 'rigid' glass-formers.

Figure 8.1 raises an interesting question: can the behaviour of different systems be mapped onto a single master curve? Clearly size is important, but to achieve this one also needs to build in the notion of shape. Thus, further studies involving computer simulations and/or direct shape determination using neutron diffraction to determine how the shape and size develops in a systematically

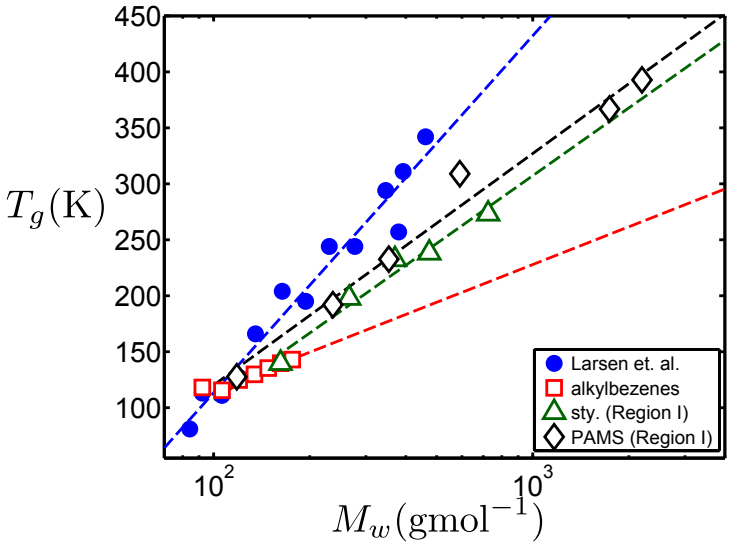

Figure 8.1: a) Values for T_g obtained for the alkylbenzene, styrene and PAMS series in comparison with those obtained for a range of molecular liquids analysed by Larsen *et. al.* [150].

structurally modified chain-series might be highly revealing. Moreover, we have found a significant degree of generality in the relaxation behaviour of three investigated systems. The alkylbenzene and oligostyrene series appear to exhibit three relaxation modes, designated α, β and γ. We have established that the molecular weight dependence of these three relaxations were very similar between the systems when they could be observed. In work not included here (due to the unfinished state of the analysis) for a chain-series of polymethyl methacrylates, we have also found both β and γ relaxations. Importantly, for the methacrylates the relaxation strengths are significant enough to directly follow both relaxations across the series. The results for this series confirm the results presented here for existence and development of the β relaxation, both for the styrene and PAMS series.

We found support for the notion that the activation energy of the β relaxations in all three systems follow a relationship with T_g, which has been previously suggested. A further implication of the relationship between E_A and T_g is that the activation energy of the β relaxation could set the glass forming behaviour of molecular glass formers. The fact that this relationship has also been shown to

apply for metallic glasses with a similar value of the constant of proportionality, $K = 26 \pm 3$ [9], to that found for a range of molecular glass formers: $K = 24 \pm 3$ [15, 55], further suggests that the connection between the β relaxation and T_g could be a general property for glass formers. If this is true then perhaps one avenue of approach to explain the trends in T_g shown in Figure 8.1 could be to analyse the activation energy of the β relaxation and its molecular weight dependence.

The α relaxations could be observed directly in the dielectric spectra for all samples. The breadths of the loss peaks relating to this process were observed to increase monotonically with temperature for most samples. It was also observed that the breadths of the oligomeric and polymeric samples were chain-length dependent, with longer chain-length samples exhibiting broader relaxation dispersions. This implied a greater fragility with increasing chain-length [62, 83], which was observed. Moreover, it was observed that the shape of the peak becames invariant at a certain chain-length, corresponding to previous observations of polystyrene [26, 269] suggesting that the fragility also increases but becomes invariant at a certain chain-length.

This behaviour was quantified by the metrics used to describe the dynamic fragility. Values of the fragility parameter, m and the gradient of the linearised τ_α data $-S$ all show a molecular weight dependence. For the polymeric systems, metrics of the dynamic fragility show a similar molecular weight dependence to T_g: increasing with increasing chain-length for shorter chain samples before becoming invariant at higher molecular weights. This implies a connection between T_g and the fragility of glass forming systems. Furthermore, as a similar dependence of the dynamic fragility was also observed for the alkylbenzene series, this implies that the size dependence of fragility may be a general feature of glass forming systems. We observed a correlation between dynamic and thermodynamic definitions of the fragility for the alkylbenzene series. However, discrepancies were found between these two definitions for the polymeric systems. These observations serve to confirm the behaviour observed for a range of simple molecular and polymeric glass formers [122].

Analysis of the DSC traces for the alkylbenzene and styrene samples led to a determination of the so-called excess entropy, S_x, at T_g. For these systems, S_x was

shown to increase with molecular weight. By assuming that S_x was equivalent to the configurational entropy, S_c, validation of the Adam-Gibbs model [76] was obtained for the alkylbenzene series.

8.2 Outlook

The results of the research presented in this thesis have provided several conclusions as to the generality of the relaxation behaviour of glass forming systems. In order to confirm the conclusions obtained, further research will need to be conducted into the relationship between the size of the constituent molecules of a glass former and its glass forming properties. For example, preliminary analysis of a chain-length series of PMMA has been completed and this appears to be an ideal system to further confirm the generality of the results presented here.

The impact of the fundamental work in this thesis could also have important applications in areas such as the cryopreservation of biological matter, which is often performed by the use of sugar based glasses. One example of such a sugar, trehalose, has been shown to be very effective in the preservation of cells and proteins [309, 310]. The sugar glass is here used to stabilise proteins and/or preserve proteins for instance in biotechnology or medical applications. It has been shown that the stability of these proteins is directly linked to the properties of a secondary β relaxation [14]. Thus, an understanding of the behaviour of such sugar based glass formers is key to the development of this process. We have initiated work to study mixtures of trehalose and other glass-formers with the aim of controlling the relaxation behaviour. This might be a highly important avenue for more applied work in the future which links strongly to the fundamental work of this thesis.

Finally, the importance of the idea of investigating how systematic structural modifications affect glass-formation is not unique to molecular systems. Suspensions of colloidal particles form glasses as a function of increasing colloid volume fraction. In parallel to the work presented here we have synthesized and characterised soft microgel colloids where the single particle properties can be tuned by variation of the microgel network cross-link properties. We have thus studied the glass-forming properties of colloidal suspensions consisting of

poly(N-isopropylacrylamide) (pNIPAM) spheres in water. Colloids are an excellent system for investigating glass- formation as their size means that light can be used as a probe and their properties can be easily and systematically tuned. For example, it has previously been shown that colloids with different elasticities exhibit variable fragility [73]. There are very interesing links between the work presented in this thesis and the work on colloids.

References

[1] M. Ediger, C. Angell, and S. R. Nagel, "Supercooled liquids and glasses," *The journal of physical chemistry*, vol. 100, no. 31, pp. 13200–13212, 1996. 2, 5, 15, 17, 18, 19

[2] J. C. Dyre, "Colloquium: The glass transition and elastic models of glass-forming liquids," *Reviews of Modern Physics*, vol. 78, pp. 953–972, Jul.-Sep. 2006. 2, 5, 6, 7, 8, 9, 11, 15, 16, 17, 18, 60, 78, 84, 107, 108, 112, 113, 130, 133, 150, 153, 154, 158, 200, 206, 219, 251

[3] F. Petrie, "Glass found in egypt.," *Transactions of the Newcomen Society*, vol. 5, no. 1, pp. 72–76, 1924. 2

[4] A. Shortland and M. Tite, "Raw materials of glass from amarna and implications for the origins of egyptian glass*," *Archaeometry*, vol. 42, no. 1, pp. 141–151, 2000. 2

[5] L. A. B. Pilkington, "Review lecture. the float glass process," *Proceedings of the Royal Society of London. Series A, Mathematical and Physical Sciences*, pp. 1–25, 1969. 2

[6] M. L. Meste, D. Champion, G. Roudaut, G. Blond, and D. Simatos, "Glass transition and food technology: A critical appraisal," *Journal of Food Science*, vol. 67, no. 7, pp. 2444–2458, 2002. 2

[7] B. C. Hancock and G. Zografi, "The relationship between the glass transition temperature and the water content of amorphous pharmaceutical solids," *Pharmaceutical Research*, vol. 11, no. 4, pp. 471–477, 1994. 2

[8] P. G. Royall, D. Q. Craig, and C. Doherty, "Characterisation of the glass transition of an amorphous drug using modulated DSC," *Pharmaceutical research*, vol. 15, no. 7, pp. 1117–1121, 1998. 2

[9] H. B. Yu, W. H. Wang, H. Y. Bai, and K. Samwer, "The β-relaxation in metallic glasses," *National Science Review*, p. nwu018, 2014. 2, 3, 12, 14, 15, 130, 220, 227, 261, 263, 274

[10] G. Tammann and J. Davidson, *On Glasses as supercooled liquids*. 1925. 2

[11] R. Böhmer, K. Ngai, C. Angell, and D. Plazek, "Nonexponential relaxations in strong and fragile glass formers," *The Journal of chemical physics*, vol. 99, no. 5, pp. 4201–4209, 1993. xvii, 2, 15, 101, 112, 113, 193, 206, 236, 248

[12] K. Ngai, "Dynamic and thermodynamic properties of glass-forming substances," *Journal of Non-Crystalline Solids*, vol. 275, no. 1, pp. 7–51, 2000. 224

[13] C. A. Angell, K. L. Ngai, G. B. McKenna, P. F. McMillan, and S. W. Martin, "Relaxation in glassforming liquids and amorphous solids," *Journal of Applied Physics*, vol. 88, no. 6, pp. 3113–3157, 2000. 2, 16, 20, 21, 91, 100, 107, 112, 116

[14] M. T. Cicerone and J. F. Douglas, "β-relaxation governs protein stability in sugar-glass matrices," *Soft Matter*, vol. 8, no. 10, pp. 2983–2991, 2012. 3, 275

[15] K. Ngai and S. Capaccioli, "Relation between the activation energy of the Johari-Goldstein β relaxation and T_g of glass formers," *Physical Review E*, vol. 69, no. 3, p. 031501, 2004. 3, 13, 15, 130, 131, 133, 134, 138, 218, 220, 227, 228, 261, 263, 274

[16] W. Kauzmann, "The nature of the glassy state and the behavior of liquids at low temperatures.," *Chemical Reviews*, vol. 43, no. 2, pp. 219–256, 1948. xiii, 4, 5, 154, 233

[17] P. G. Debenedetti and F. H. Stillinger, "Supercooled liquids and the glass transition," *Nature*, vol. 410, no. 6825, pp. 259–267, 2001. 5, 6, 20, 21, 116, 154

[18] J. Mattsson, *Glass Transition Dynamics in Soft Condensed Matter*. PhD thesis, Chalmers University of Technology, Gothenburg, Sweden, 2002. 5, 6, 12, 17, 18, 19, 20, 25, 32, 34, 35, 36, 37, 53, 94, 96, 102, 116, 140, 164, 166, 167, 175, 188, 199, 221, 263

[19] R. J. Speedy, "Kauzmann's paradox and the glass transition," *Biophysical chemistry*, vol. 105, no. 2, pp. 411–420, 2003. 5

[20] F. Sausset, G. Biroli, and J. Kurchan, "Do solids flow?," *Journal of Statistical Physics*, vol. 140, no. 4, pp. 718–727, 2010. 6

[21] L. Berthier and G. Biroli, "Theoretical perspective on the glass transition and amorphous materials," *Reviews of Modern Physics*, vol. 83, no. 2, p. 587, 2011. 6, 100

[22] J. C. Maxwell, "On the dynamical theory of gases," *Philosophical transactions of the Royal Society of London*, pp. 49–88, 1867. 6

[23] L. Dagdug and L. Garcia-Colin, "Theoretical framework for the Arrhenius equation in strong glasses," *Journal of Physics - Condensed Matter*, vol. 11, pp. 2193–2198, Mar. 15 1999. 7

[24] U. Buchenau, "Mechanical relaxation in glasses and at the glass transition," *Physical Review B*, vol. 63, no. 10, p. 104203, 2001. 7, 9, 108, 130, 133, 200, 219, 251

[25] T. Hecksher, A. I. Nielsen, N. B. Olsen, and J. C. Dyre, "Little evidence for dynamic divergences in ultraviscous molecular liquids," *Nature Physics*, vol. 4, no. 9, pp. 737–741, 2008. 8, 79

[26] P. Santangelo and C. Roland, "Molecular weight dependence of fragility in polystyrene," *Macromolecules*, vol. 31, no. 14, pp. 4581–4585, 1998. 7, 9, 108, 130, 133, 175, 185, 193, 194, 195, 200, 219, 229, 236, 248, 251, 274

[27] H. Vogel, "The law of the relation between the viscosity of liquids and the temperature," *Phys. Z*, vol. 22, pp. 645–646, 1921. 7, 108, 200, 251

[28] G. S. Fulcher, "Analysis of recent measurements of the viscosity of glasses," *Journal of the American Ceramic Society*, vol. 8, no. 6, pp. 339–355, 1925.

[29] G. Tammann and W. Hesse, "Die abhängigkeit der viscosität von der temperatur bie unterkühlten flüssigkeiten," *Zeitschrift für anorganische und allgemeine Chemie*, vol. 156, no. 1, pp. 245–257, 1926. 7, 108, 200, 251

[30] J. Mattsson, R. Bergman, P. Jacobsson, and L. Borjesson, "Effects of hydrogen bonding on supercooled liquid dynamics and the implications for supercooled water," *Physical Review B*, vol. 79, May 2009. 7, 10, 115, 136, 219, 264

[31] F. Stickel, E. Fischer, and R. Richert, "Dynamics of glass-forming liquids. i. temperature-derivative analysis of dielectric relaxation data," *The Journal of chemical physics*, vol. 102, no. 15, pp. 6251–6257, 1995. 8, 9, 113, 136, 159, 206, 257

[32] C. Angell, "Formation of glasses from liquids and biopolymers," *Science*, vol. 267, pp. 1924–1935, Mar. 31 1995. 8, 9, 16, 61

[33] A. Döß, G. Hinze, B. Schiener, J. Hemberger, R. Böhmer, *et al.*, "Dielectric relaxation in the fragile viscous liquid state of toluene," *The Journal of chemical physics*, vol. 107, no. 6, pp. 1740–1743, 1997. xvi, xvii, xviii, xix, 9, 54, 82, 84, 92, 94, 98, 99, 100, 101, 107, 108, 109, 110, 121, 129, 139, 155, 186, 246, 260

[34] C. Hansen, F. Stickel, R. Richert, and E. Fischer, "Dynamics of glass-forming liquids. IV. True activated behavior above 2 GHz in the dielectric alpha-relaxation of organic liquids," *Journal of Chemical Physics*, vol. 108, pp. 6408–6415, Apr. 15 1998. xiii, xix, 10, 82, 116, 136, 137

[35] F. Mallamace, C. Branca, C. Corsaro, N. Leone, J. Spooren, S.-H. Chen, and H. E. Stanley, "Transport properties of glass-forming liquids suggest that dynamic crossover temperature is as important as the glass transition

temperature," *Proceedings of the National Academy of Sciences*, vol. 107, no. 52, pp. 22457–22462, 2010. 10, 115

[36] R. Casalini and C. Roland, "Scaling of the supercooled dynamics and its relation to the pressure dependences of the dynamic crossover and the fragility of glass formers," *Physical Review B*, vol. 71, no. 1, p. 014210, 2005. 10, 115

[37] V. Novikov and A. Sokolov, "Universality of the dynamic crossover in glass-forming liquids: A magic relaxation time," *Physical Review E*, vol. 67, no. 3, p. 031507, 2003. 10, 79, 115, 272

[38] E. Rössler, "Indications for a change of diffusion mechanism in supercooled liquids," *Physical review letters*, vol. 65, no. 13, p. 1595, 1990. 10, 115

[39] A. Schönhals, "Evidence for a universal crossover behaviour of the dynamic glass transition," *EPL (Europhysics Letters)*, vol. 56, no. 6, p. 815, 2001. 10, 115

[40] O. Mazurin, "Relaxation phenomena in glass," *Journal of Non Crystalline Solids*, vol. 25, pp. 129–169, 1977. 11

[41] R. Kohlrausch, "Theorie des elektrischen rückstandes in der leidener flasche," *Annalen der Physik*, vol. 167, no. 2, pp. 179–214, 1854. 11, 51, 95

[42] G. Williams and D. C. Watts, "Non-symmetrical dielectric relaxation behaviour arising from a simple empirical decay function," *Transactions of the Faraday Society*, vol. 66, pp. 80–85, 1970. 11, 51, 95

[43] R. Richert, "Heterogeneous dynamics in liquids: fluctuations in space and time," *Journal of Physics: Condensed Matter*, vol. 14, no. 23, p. R703, 2002. 11

[44] H. Sillescu, "Heterogeneity at the glass transition: a review," *Journal of Non-Crystalline Solids*, vol. 243, no. 2, pp. 81–108, 1999. 11, 16, 92, 100, 160, 194

[45] F. Fujara, B. Geil, H. Sillescu, and G. Fleischer, "Translational and rotational diffusion in supercooled orthoterphenyl close to the glass transition," *Zeitschrift für Physik B Condensed Matter*, vol. 88, no. 2, pp. 195–204, 1992. 11

[46] B. Schiener, R. Böhmer, A. Loidl, and R. Chamberlin, "Nonresonant spectral hole burning in the slow dielectric response of supercooled liquids," *Science*, vol. 274, no. 5288, pp. 752–754, 1996.

[47] R. Böhmer, R. Chamberlin, G. Diezemann, B. Geil, A. Heuer, G. Hinze, S. Kuebler, R. Richert, B. Schiener, H. Sillescu, *et al.*, "Nature of the non-exponential primary relaxation in structural glass-formers probed by dynamically selective experiments," *Journal of non-crystalline solids*, vol. 235, pp. 1–9, 1998. 11

[48] N. B. Olsen, T. Christensen, and J. C. Dyre, "β relaxation of nonpolymeric liquids close to the glass transition," *Physical Review E*, vol. 62, no. 3, p. 4435, 2000. 12

[49] N. McCrum, B. Read, and G. Williams, *Anelastic and Dielectric Effects in Polymeric Solids*. Dover Books on Engineering, Dover Publications, 1967. 12, 35

[50] J. Heijboer, "Molecular origin of relaxations in polymers," *Annals of the New York Academy of Sciences*, vol. 279, no. 1, pp. 104–116, 1976. 12

[51] K. Ngai and M. Paluch, "Classification of secondary relaxation in glass-formers based on dynamic properties," *The Journal of chemical physics*, vol. 120, no. 2, pp. 857–873, 2004. 12, 118, 119, 123, 130, 158, 211, 227, 237

[52] G. P. Johari and M. Goldstein, "Viscous liquids and the glass transition. ii. secondary relaxations in glasses of rigid molecules," *The Journal of Chemical Physics*, vol. 53, no. 6, pp. 2372–2388, 1970. xxvi, 12, 79, 261, 262, 263, 269

[53] G. P. Johari, "Intrinsic mobility of molecular glasses," *The Journal of Chemical Physics*, vol. 58, no. 4, pp. 1766–1770, 1973.

[54] G. Johari, "Glass transition phenomenon and molecular mobility in glasses-12. 1857 (1974)(1 977) in plastic deformation of amorphous and semicrystalline materials, b. escaig, cg sel1, ed., les editions de physique publisher 1982, p. 109," *Ann. NY Acad. Sci*, vol. 279, p. 102, 1976. 12

[55] A. Kudlik, S. Benkhof, T. Blochowicz, C. Tschirwitz, and E. Rössler, "The dielectric response of simple organic glass formers," *Journal of molecular structure*, vol. 479, no. 2, pp. 201–218, 1999. xiv, xvii, xviii, xix, 13, 14, 52, 82, 84, 94, 102, 107, 108, 109, 110, 129, 130, 133, 134, 139, 155, 160, 218, 227, 236, 248, 274

[56] L. Hu, C. Zhang, Y. Yue, and X. Bian, "A new threshold of uncovering the nature of glass transition: The slow ß relaxation in glassy states," *Chinese Science Bulletin*, vol. 55, no. 6, pp. 457–472, 2010. 12, 14

[57] G. Johari, "The entropy loss on supercooling a liquid and anharmonic contributions," *The Journal of chemical physics*, vol. 116, no. 5, pp. 2043–2046, 2002. 12, 150

[58] H. Tanaka, "Origin of the excess wing and slow β relaxation of glass formers: A unified picture of local orientational fluctuations," *Physical Review E*, vol. 69, no. 2, p. 021502, 2004. 12

[59] G. Williams and D. C. Watts, "Molecular motion in the glassy state. the effect of temperature and pressure on the dielectric β relaxation of polyvinyl chloride," *Transactions of the Faraday Society*, vol. 67, 1971. 13

[60] G. Williams, "Molecular aspects of multiple dielectric relaxation processes in solid polymers," in *Electric Phenomena in Polymer Science*, pp. 59–92, Springer, 1979. 13, 94

[61] A. Kudlik, C. Tschirwitz, S. Benkhof, T. Blochowicz, and E. Rössler, "Slow secondary relaxation process in supercooled liquids," *EPL (Europhysics*

Letters), vol. 40, no. 6, p. 649, 1997. xv, 13, 54, 82, 84, 89, 92, 121, 130, 134, 138, 160, 186, 218, 220, 227, 246, 260, 261

[62] K. Ngai, "Relation between some secondary relaxations and the α relaxations in glass-forming materials according to the coupling model," *The Journal of chemical physics*, vol. 109, no. 16, pp. 6982–6994, 1998. 14, 19, 175, 193, 194, 232, 249, 274

[63] P. Lunkenheimer, A. Pimenov, B. Schiener, R. Böhmer, and A. Loidl, "High-frequency dielectric spectroscopy on glycerol," *EPL (Europhysics Letters)*, vol. 33, no. 8, p. 611, 1996. 14

[64] U. Schneider, P. Lunkenheimer, R. Brand, and A. Loidl, "Broadband dielectric spectroscopy on glass-forming propylene carbonate," *Physical Review E*, vol. 59, no. 6, p. 6924, 1999. 14

[65] R. Casalini, M. Paluch, and C. Roland, "Dynamics of salol at elevated pressure," *The Journal of Physical Chemistry A*, vol. 107, no. 13, pp. 2369–2373, 2003. 14

[66] J. Wiedersich, T. Blochowicz, S. Benkhof, A. Kudlik, N. Surovtsev, C. Tschirwitz, V. Novikov, and E. Rössler, "Fast and slow relaxation processes in glasses," *Journal of Physics: Condensed Matter*, vol. 11, no. 10A, p. A147, 1999. 14

[67] K. Ngai, P. Lunkenheimer, C. Leon, U. Schneider, R. Brand, and A. Loidl, "Nature and properties of the Johari-Goldstein β-relaxation in the equilibrium liquid state of a class of glass-formers," *The Journal of Chemical Physics*, vol. 115, no. 3, pp. 1405–1413, 2001. 14, 121, 186, 246, 260

[68] P. K. Dixon, "Specific-heat spectroscopy and dielectric susceptibility measurements of salol at the glass transition," *Physical Review B*, vol. 42, no. 13, p. 8179, 1990. 14, 100

[69] J. Mattsson, R. Bergman, P. Jacobsson, and L. Börjesson, "Chain-length-dependent relaxation scenarios in an oligomeric glass-forming system: From

merged to well-separated α and β loss peaks," *Physical review letters*, vol. 90, no. 7, p. 075702, 2003. 14, 86, 140, 141, 185, 200, 224, 225, 263

[70] R. Casalini and C. M. Roland, "Pressure evolution of the excess wing in a type-b glass former," *Physical review letters*, vol. 91, no. 1, p. 015702, 2003. 15, 87

[71] U. Schneider, R. Brand, P. Lunkenheimer, and A. Loidl, "Excess wing in the dielectric loss of glass formers: A Johari-Goldstein beta relaxation?," *Physical Review Letters*, vol. 84, pp. 5560–5563, Jun. 12 2000. 15, 87

[72] R. Bergman, J. Mattsson, C. Svanberg, G. Schwartz, and J. Swenson, "Confinement effects on the excess wing in the dielectric loss of glass-formers," *EPL (Europhysics Letters)*, vol. 64, no. 5, p. 675, 2003. 15

[73] J. Mattsson, H. M. Wyss, A. Fernandez-Nieves, K. Miyazaki, Z. Hu, D. R. Reichman, and D. A. Weitz, "Soft colloids make strong glasses," *Nature*, vol. 462, no. 7269, pp. 83–86, 2009. 15, 276

[74] P. G. Debenedetti, *Metastable liquids: concepts and principles*. Princeton University Press, 1996. 16

[75] E.-J. Donth, *The glass transition: relaxation dynamics in liquids and disordered materials*, vol. 48. Springer, 2001. 16, 152

[76] G. Adam and J. H. Gibbs, "On the temperature dependence of cooperative relaxation properties in glass-forming liquids," *The journal of chemical physics*, vol. 43, no. 1, pp. 139–146, 1965. 16, 157, 275

[77] H. Tanaka, "Relation between thermodynamics and kinetics of glass-forming liquids," *Physical review letters*, vol. 90, no. 5, p. 055701, 2003. 17, 154

[78] O. Yamamuro, I. Tsukushi, A. Lindqvist, S. Takahara, M. Ishikawa, and T. Matsuo, "Calorimetric study of glassy and liquid toluene and ethylbenzene: Thermodynamic approach to spatial heterogeneity in glass-forming molecular liquids," *The Journal of Physical Chemistry B*, vol. 102, no. 9, pp. 1605–1609, 1998. 17, 82, 109, 150, 151, 152, 153

[79] M. H. Cohen and D. Turnbull, "Molecular transport in liquids and glasses," *The Journal of Chemical Physics*, vol. 31, no. 5, pp. 1164–1169, 1959. 17, 172

[80] G. S. Grest and M. H. Cohen, "Liquids, glasses, and the glass transition: A free-volume approach," *Adv. Chem. Phys*, vol. 48, pp. 455–525, 1981. 17

[81] C. Zhang and R. D. Priestley, "Fragility and glass transition temperature of polymer confined under isobaric and isochoric conditions," *Soft Matter*, vol. 9, no. 29, pp. 7076–7085, 2013. 18

[82] K. Ngai, "Coupling model explanation of salient dynamic properties of glass-forming substances," *Dielectrics and Electrical Insulation, IEEE Transactions on*, vol. 8, no. 3, pp. 329–344, 2001. 18, 19

[83] K. Ngai, "Short-time and long-time relaxation dynamics of glass-forming substances: a coupling model perspective," *Journal of Physics: Condensed Matter*, vol. 12, no. 29, p. 6437, 2000. 101, 175, 193, 194, 249, 264, 274

[84] K. Ngai, "An extended coupling model description of the evolution of dynamics with time in supercooled liquids and ionic conductors," *Journal of Physics: Condensed Matter*, vol. 15, no. 11, p. S1107, 2003. 18, 228

[85] W. Gotze, "The essentials of the mode-coupling theory for glassy dynamics," *Condens. Matter Phys*, vol. 4, pp. 873–904, 1998. 19, 91

[86] W. Gotze and L. Sjogren, "Relaxation processes in supercooled liquids," *Reports on Progress in Physics*, vol. 55, no. 3, p. 241, 1992. 19, 20

[87] U. Bengtzelius, W. Gotze, and A. Sjolander, "Dynamics of supercooled liquids and the glass transition," *Journal of Physics C: solid state Physics*, vol. 17, no. 33, p. 5915, 1984. 20

[88] D. Engberg, *Structural dynamics of glass-forming liquids*. PhD thesis, Chalmers University of Technology, Gothenburg, Sweden, 1997. 19

[89] M. Goldstein, "Viscous liquids and the glass transition: a potential energy barrier picture," *The Journal of Chemical Physics*, vol. 51, no. 9, pp. 3728–3739, 1969. 20, 116

[90] C. Angell, B. Richards, and V. Velikov, "Simple glass-forming liquids: their definition, fragilities, and landscape excitation profiles," *Journal of Physics: Condensed Matter*, vol. 11, no. 10A, p. A75, 1999. 20, 116

[91] C. Angell, "Relaxation in liquids, polymers and plastic crystalsstrong/fragile patterns and problems," *Journal of Non-Crystalline Solids*, vol. 131, pp. 13–31, 1991. 21, 59, 116, 147, 230, 251, 267

[92] C. Angell, "Perspective on the glass transition," *Journal of Physics and Chemistry of Solids*, vol. 49, no. 8, pp. 863–871, 1988. 21, 116

[93] P. Lunkenheimer, U. Schneider, R. Brand, and A. Loid, "Glassy dynamics," *Contemporary Physics*, vol. 41, no. 1, pp. 15–36, 2000. 23, 101

[94] F. Kremer and A. Schönhals, *Broadband Dielectric Spectroscopy*. Springer, 2003. 24, 25, 26, 27, 28, 29, 30, 32, 35, 36, 37, 38, 46, 47, 54, 92, 95, 98, 102, 103, 106, 121, 186, 187, 196, 246, 249, 260

[95] C. J. F. Bottcher, O. Belle, P. Bordewijk, and A. Rip, *Theory of electric polarisation*. Elsevier, 1973. 24, 25, 27, 28, 31, 32

[96] J. Runt and J. Fitzgerald, *Dielectric spectroscopy of polymeric materials: fundamentals and applications*. ACS professional reference book, American Chemical Society, 1997. 24, 26, 29, 36, 37, 46, 47, 54, 92, 96, 102, 103, 106, 119, 121, 186, 191, 196, 197, 246, 260

[97] C. P. Gainaru, *Dielectric Properties of Molecular Glass Formers; from the Liquid State to the Tunneling Regime*. PhD thesis, University of Bayreuth, 2008. 24, 25, 27, 29, 30, 31, 51, 52

[98] T. Blochowicz, *Broadband Dielectric Spectroscopy in Neat and Binary Molecular Glass Formers*. PhD thesis, University of Bayreuth, 2003. xvi, 24, 27, 28, 35, 51, 52, 82, 84, 92, 94, 95, 98, 99, 100, 189, 248

[99] J. Sjöström, *Relaxation dynamics of perturbed water and other H-bonding liquids*. PhD thesis, Chalmers University of Technology, Gothenburg, Sweden, 2010. 25, 26, 32

[100] L. Onsager, "Electric moments of molecules in liquids," *Journal of the American Chemical Society*, vol. 58, no. 8, pp. 1486–1493, 1936. 28, 29, 102, 196

[101] G. Katana, F. Kremer, E. Fischer, and R. Plaetschke, "Broadband dielectric study on binary blends of bisphenol-a and tetramethylbisphenol-a polycarbonate," *Macromolecules*, vol. 26, no. 12, pp. 3075–3080, 1993.

[102] J. G. Kirkwood, "The dielectric polarization of polar liquids," *The Journal of Chemical Physics*, vol. 7, no. 10, pp. 911–919, 1939. 196

[103] H. Fröhlich, "General theory of the static dielectric constant," *Transactions of the Faraday Society*, vol. 44, pp. 238–243, 1948. 29, 102, 196

[104] R. Bergman, "General susceptibility functions for relaxations in disordered systems," *Journal of Applied Physics*, vol. 88, no. 3, pp. 1356–1365, 2000. 34, 47, 48, 51, 92, 106, 124, 186, 245

[105] G. Schaumburg, "Dielectrics newsletter," *Novocontrol Issue*, pp. 4–6, 1999. 37

[106] Y. Matsumiya, A. Uno, H. Watanabe, T. Inoue, and O. Urakawa, "Dielectric and viscoelastic investigation of segmental dynamics of polystyrene above glass transition temperature: Cooperative sequence length and relaxation mode distribution," *Macromolecules*, vol. 44, no. 11, pp. 4355–4365, 2011. 41, 191

[107] Novocontrol Technologies, *WinDETA Owner's Manual*. Hundsangen, Germany, 8 ed., 2011. 42

[108] K. Cole and R. Cole, "Dispersion and absorption in dielectrics I. Alternating current characteristics," *Journal of Chemical Physics*, vol. 9, pp. 341–351, Apr. 1941. 45

[109] D. Davidson and R. Cole, "Dielectric relaxation in glycerol, propylene glycol, and n-propanol," *The Journal of Chemical Physics*, vol. 19, no. 12, pp. 1484–1490, 1951. 45, 95, 97, 189, 248

[110] S. Havriliak and S. Negami, "A complex plane representation of dielectric and mechanical relaxation processes in some polymers," *Polymer*, vol. 8, pp. 161–210, 1967. 46, 92, 94, 186, 245

[111] S. Havriliak Jr and S. Havriliak, "Results from an unbiased analysis of nearly 1000 sets of relaxation data," *Journal of non-crystalline solids*, vol. 172, pp. 297–310, 1994. 46, 98, 106

[112] J. G. Kirkwood and R. M. Fuoss, "Anomalous dispersion and dielectric loss in polar polymers," *The Journal of Chemical Physics*, vol. 9, no. 4, pp. 329–340, 1941. 47

[113] A. Jonscher, "A new model of dielectric loss in polymers," *Colloid and polymer Science*, vol. 253, no. 3, pp. 231–250, 1975. 47, 48

[114] G. Williams, D. C. Watts, S. Dev, and A. North, "Further considerations of non symmetrical dielectric relaxation behaviour arising from a simple empirical decay function," *Transactions of the faraday Society*, vol. 67, pp. 1323–1335, 1971. 51

[115] G. Williams, "Molecular motion in glass-forming systems," *Journal of Non-Crystalline Solids*, vol. 131, pp. 1–12, 1991. 51, 52, 93

[116] R. Bergman, F. Alvarez, A. Alegrıa, and J. Colmenero, "The merging of the dielectric α-and β-relaxations in poly-(methyl methacrylate)," *The Journal of chemical physics*, vol. 109, no. 17, pp. 7546–7555, 1998. 54, 92, 121, 186, 206, 246, 260

[117] A. Schönhals, F. Kremer, and E. Schlosser, "Scaling of the α relaxation in low-molecular-weight glass-forming liquids and polymers," *Physical review letters*, vol. 67, no. 8, p. 999, 1991. 54, 92, 121, 186, 246, 260

[118] Novocontrol Technologies, *WinFit Owner's Manual*. Hundsangen, Germany, 5 ed., 2011. 55

[119] MATLAB, *version 8.0.0.783 (R2012b)*. Natick, Massachusetts: The MathWorks Inc., 2012. 55

[120] B. Cassel and A. T. Riga, "Glass transition of a liquid crystal polymer," *ASTM Special Technical Publication*, vol. 1249, pp. 202–202, 1994. 59, 146

[121] D. Cangialosi, A. Alegría, and J. Colmenero, "A thermodynamic approach to the fragility of glass-forming polymers," *The Journal of chemical physics*, vol. 124, no. 2, p. 024906, 2006. 59, 147, 156, 230, 267

[122] D. Huang and G. B. McKenna, "New insights into the fragility dilemma in liquids," *The Journal of Chemical Physics*, vol. 114, no. 13, pp. 5621–5630, 2001. 59, 147, 175, 230, 231, 267, 274

[123] K. Kishimoto, H. Suga, and S. Seki, "Calorimetric study of the glassy state. viii. heat capacity and relaxational phenomena of isopropylbenzene," *Bull. Chem. Soc. Jpn*, vol. 46, pp. 3020–3031, 1973. 60, 149, 153

[124] H. Wiedemann, G. Widmann, and G. Bayer, "Glass transition in polymers: Comparison of results from DSC, TMA, and TOA measurements," *ASTM Special Technical Publication*, vol. 1249, pp. 174–174, 1994. 61

[125] B. Wunderlich, "The nature of the glass transition and its determination by thermal analysis," *ASTM Special Technical Publication*, vol. 1249, pp. 17–17, 1994. 61, 62

[126] C. T. Moynihan, "Phenomenology of the structural relaxation process and the glass transition," *ASTM Special Technical Publication*, vol. 1249, pp. 32–32, 1994. 61

[127] J. R. Saffell, "Analysis of dsc thermal curves for assigning a characteristic glass transition temperature, dependent on either the type or thermal history of the polymer," *ASTM Special Technical Publication*, vol. 1249, pp. 137–137, 1994. 61

[128] H. E. Bair, "Glass transition measurements by dsc," *ASTM Special Technical Publication*, vol. 1249, pp. 50–50, 1994. 61, 73

[129] M. Gupta, "Glass transition measurements on automotive coatings by DSC, DMA, and TMA," tech. rep., 1994. 61

[130] G. Höhne, W. Hemminger, and H.-J. Flammersheim, *Differential scanning calorimetry*. Springer, 2003. 62, 63, 64, 66, 68, 149

[131] S. Tanaka, "Theory of power-compensated dsc," *Thermochimica acta*, vol. 210, pp. 67–76, 1992. 62

[132] R. L. Danley, "New heat flux dsc measurement technique," *Thermochimica acta*, vol. 395, no. 1, pp. 201–208, 2002. 63, 64, 65, 66, 68, 71, 72

[133] T. Narasimhan, "Fourier's heat conduction equation: History, influence, and connections," *Reviews of Geophysics*, vol. 37, no. 1, pp. 151–172, 1999. 63

[134] R. B. Cassel, "How Tzero technology improves DSC performance, part ii: Peak shape and resolution," *TA Instruments Applications Brief TA298*. 66

[135] C. Gorse, D. Johnston, and M. Pritchard, *A Dictionary of Construction, Surveying, and Civil Engineering*. Oxford University Press, 2012. 69

[136] L. Waguespack and R. Blaine, "Design of a new DSC cell with Tzero technology," in *Proceedings of the 29th Conference of the North American Thermal Analysis Society*, pp. 721–727, 2001. 69

[137] R. B. Cassel, "Purity determination and DSC Tzero technology," *TA instruments internal publication TA295a*, 2002. 69

[138] A. Hensel and C. Schick, "Relation between freezing-in due to linear cooling and the dynamic glass transition temperature by temperature-modulated DSC," *Journal of non-crystalline solids*, vol. 235, pp. 510–516, 1998. 70, 144, 228, 264

[139] K. Fukao and Y. Miyamoto, "Slow dynamics near glass transitions in thin polymer films," *Physical Review E*, vol. 64, no. 1, p. 011803, 2001.

[140] R. Casalini and C. Roland, "Dynamic properties of polyvinylmethylether near the glass transition," *The Journal of chemical physics*, vol. 119, no. 7, pp. 4052–4059, 2003.

[141] Z. Fakhraai and J. A. Forrest, "Probing slow dynamics in supported thin polymer films," *Physical review letters*, vol. 95, no. 2, p. 025701, 2005. 70, 144, 228, 264

[142] G. Della Gatta, M. J. Richardson, S. M. Sarge, and S. Stølen, "Standards, calibration, and guidelines in microcalorimetry. part 2. calibration standards for differential scanning calorimetry*(iupac technical report)," *Pure and applied chemistry*, vol. 78, no. 7, pp. 1455–1476, 2006. 72

[143] B. Riechers, F. Wittbracht, A. Hütten, and T. Koop, "The homogeneous ice nucleation rate of water droplets produced in a microfluidic device and the role of temperature uncertainty," *Physical Chemistry Chemical Physics*, vol. 15, no. 16, pp. 5873–5887, 2013. 73

[144] P. Gabbott, *Principles and applications of thermal analysis*. John Wiley & Sons, 2008. 73

[145] P. J. Haines, *Principles of thermal analysis and calorimetry*, vol. 30. Royal society of chemistry, 2002. 73

[146] V. Novikov and E. Rssler, "Correlation between glass transition temperature and molecular mass in non-polymeric and polymer glass formers," *Polymer*, vol. 54, no. 26, pp. 6987 – 6991, 2013. xv, xvii, 77, 78, 79, 110, 111, 158, 200

[147] F. A. Lindemann, "Ueber die berechnung molekularer eigenfrequenzen," *Phys. Z*, vol. 11, pp. 609–612, 1910. 78

[148] N. Ashcroft and N. Mermin, "Solid state physicsholt-saunders," *New York*, p. 4, 1976. 78

[149] W. Lee and G. Knight, "Ratio of the glass transition temperature to the melting point in polymers," *British Polymer Journal*, vol. 2, no. 1, pp. 73–80, 1970. 78, 233

[150] R. J. Larsen and C. F. Zukoski, "Effect of particle size on the glass transition," *Physical Review E*, vol. 83, no. 5, p. 051504, 2011. xv, xxvii, 78, 79, 111, 158, 272, 273

[151] V. Privalko, "Excess entropies and related quantities in glass-forming liquids," *The Journal of Physical Chemistry*, vol. 84, no. 24, pp. 3307–3312, 1980. 78, 79

[152] G. P. Johari and M. Goldstein, "Viscous liquids and the glass transition. ii. secondary relaxations in glasses of rigid molecules," *The Journal of Chemical Physics*, vol. 53, no. 6, pp. 2372–2388, 1970.

[153] C. Gainaru, R. Kahlau, E. A. Rössler, and R. Böhmer, "Evolution of excess wing and β-process in simple glass formers," *The Journal of chemical physics*, vol. 131, no. 18, p. 184510, 2009.

[154] S. Corezzi, E. Campani, P. Rolla, S. Capaccioli, and D. Fioretto, "Changes in the dynamics of supercooled systems revealed by dielectric spectroscopy," *The Journal of chemical physics*, vol. 111, no. 20, pp. 9343–9351, 1999.

[155] F. Stickel, F. Kremer, and E. Fischer, "The scaling of the dielectric and electric relaxation in two low molecular weight glass forming liquids," *Physica A: Statistical Mechanics and its Applications*, vol. 201, no. 1, pp. 318–321, 1993.

[156] D. J. Plazek and J. H. Magill, "Physical properties of aromatic hydrocarbons. i. viscous and viscoelastic behavior of 1: 3: 5-tri-α-naphthyl benzene," *The Journal of Chemical Physics*, vol. 45, no. 8, pp. 3038–3050, 1966. 78

[157] D. Ben-Amotz and D. R. Herschbach, "Estimation of effective diameters for molecular fluids," *Journal of Physical Chemistry*, vol. 94, no. 3, pp. 1038–1047, 1990. 79

[158] G. L. Hunter and E. R. Weeks, "The physics of the colloidal glass transition," *Reports on Progress in Physics*, vol. 75, no. 6, p. 066501, 2012. 79

[159] A. K. Low, J. R. Meeks, and C. R. Mackerer, "Health effects of the alkylbenzenes. i. toluene," *Toxicology and industrial health*, vol. 4, no. 1, pp. 49–75, 1988. 80

[160] J. F. Messerly, S. S. Todd, and H. L. Finke, "Low-temperature thermodynamic properties of n-propyl-and n-butylbenzene," *The Journal of Physical Chemistry*, vol. 69, no. 12, pp. 4304–4311, 1965. 82, 149, 151

[161] D. Scott, G. Guthrie, J. Messerly, S. Todd, W. Berg, I. Hossenlopp, and J. McCullough, "Toluene: thermodynamic properties, molecular vibrations, and internal rotation," *The Journal of Physical Chemistry*, vol. 66, no. 5, pp. 911–914, 1962. 149, 151

[162] Z. Chen and R. Richert, "Dynamics of glass-forming liquids. XV. Dynamical features of molecular liquids that form ultra-stable glasses by vapor deposition," *Journal of Chemical Physics*, vol. 135, Sep. 28 2011. xxv, xxvi, 250, 251, 252, 253, 255, 263

[163] S. Murthy, J. Sobhanadri, *et al.*, "The origin of β relaxation in organic glasses," *The Journal of chemical physics*, vol. 100, no. 6, pp. 4601–4606, 1994. 123, 130

[164] T. G. Copeland and D. J. Denney, "Dielectric dispersion in n-propylbenzene," *The Journal of Physical Chemistry*, vol. 80, no. 2, pp. 210–212, 1976.

[165] M. S. Ahmed, J. Chao, J. Crossley, M. S. Hossain, and S. Walker, "Co-operative motion in some simple hydrocarbons," *Journal of the Chemical Society, Faraday Transactions 2: Molecular and Chemical Physics*, vol. 80, no. 9, pp. 1047–1054, 1984. 82, 130

[166] A. Döß, M. Paluch, H. Sillescu, and G. Hinze, "From strong to fragile glass formers: Secondary relaxation in polyalcohols," *Physical review letters*, vol. 88, no. 9, p. 095701, 2002. 86, 175, 224, 225

[167] C. Leon, K. Ngai, and C. Roland, "Relationship between the primary and secondary dielectric relaxation processes in propylene glycol and its oligomers," *The Journal of chemical physics*, vol. 110, no. 23, pp. 11585–11591, 1999. 86, 224, 225

[168] N. Sağlanmak, A. I. Nielsen, N. B. Olsen, J. C. Dyre, and K. Niss, "An electrical circuit model of the alpha-beta merging seen in dielectric relaxation of ultraviscous liquids," *Journal of Chemical Physics*, vol. 132, no. 2, p. 4503, 2010. 88, 189, 248

[169] W. Kob and H. C. Andersen, "Testing mode-coupling theory for a supercooled binary lennard-jones mixture i: The van hove correlation function," *Physical Review E*, vol. 51, no. 5, p. 4626, 1995. 91

[170] I. Morfin, P. Lindner, and F. Boue, "Temperature and shear rate dependence of small angle neutron scattering from semidilute polymer solutions," *Macromolecules*, vol. 32, no. 21, pp. 7208–7223, 1999. 91, 194, 246

[171] R. Li, "Time-temperature superposition method for glass transition temperature of plastic materials," *Materials Science and Engineering: A*, vol. 278, no. 1, pp. 36–45, 2000.

[172] M. McBrearty and S. Perusich, "Dielectric rheological measurements of molten polymers," *Polymer Engineering & Science*, vol. 40, no. 1, pp. 201–213, 2000.

[173] Y. Miyano, M. Nakada, H. Kudoh, and R. Muki, "Prediction of tensile fatigue life for unidirectional cfrp," *Journal of composite materials*, vol. 34, no. 7, pp. 538–550, 2000. 91, 194, 246

[174] N. B. Olsen, T. Christensen, and J. C. Dyre, "Time-temperature superposition in viscous liquids," *Physical review letters*, vol. 86, no. 7, p. 1271, 2001. 91, 101

[175] G. Meier, B. Gerharz, D. Boese, and E. Fischer, "Dynamical processes in organic glassforming van der waals liquids," *The Journal of chemical physics*, vol. 94, no. 4, pp. 3050–3059, 1991. 91

[176] K. S. Cole and R. H. Cole, "Dispersion and absorption in dielectrics i. alternating current characteristics," *The Journal of Chemical Physics*, vol. 9, no. 4, pp. 341–351, 1941. 93, 119, 186, 246, 260

[177] A. Schönhals, F. Kremer, A. Hofmann, E. W. Fischer, and E. Schlosser, "Anomalies in the scaling of the dielectric α-relaxation," *Physical review letters*, vol. 70, no. 22, p. 3459, 1993. 101

[178] L.-M. Wang and R. Richert, "Primary and secondary relaxation time dispersions in fragile supercooled liquids," *Physical Review B*, vol. 76, no. 6, p. 064201, 2007. 101

[179] P. K. Dixon, N. Menon, and S. R. Nagel, "Comment on light-scattering investigation of α and β relaxation near the liquid-glass transition of the molecular glass salol," *Physical Review E*, vol. 50, no. 2, p. 1717, 1994. 102

[180] L. D. Landau, J. Bell, M. Kearsley, L. Pitaevskii, E. Lifshitz, and J. Sykes, *Electrodynamics of continuous media*, vol. 8. Elsevier, 1984. 102

[181] L. Groves and J. Baker, "251. the determination of dipole moments in the vapour phase. part i. an improved apparatus. part ii. the moments of alkylbenzenes and alkylcyclohexanes," *J. Chem. Soc.*, pp. 1144–1150, 1939. 103

[182] V. Ben'kovskii, T. Bogoslovskaya, and M. K. Nauruzov, "Density, surface tension and refractive index of aromatic hydrocarbons at low temperatures," *Chemistry and Technology of Fuels and Oils*, vol. 2, no. 1, pp. 23–26, 1966. 103

[183] J. Dubochet, C. Alba, D. MacFarlane, C. Angell, R. Kadiyala, M. Adrian, and J. Teixeira, "Glass-forming microemulsions: vitrification of simple liquids and electron microscope probing of droplet-packing modes," *The Jour-*

nal of Physical Chemistry, vol. 88, no. 26, pp. 6727–6732, 1984. xvii, 107, 108, 109, 110

[184] C. Angell, J. Sare, and E. Sare, "Glass transition temperatures for simple molecular liquids and their binary solutions," *The Journal of Physical Chemistry*, vol. 82, no. 24, pp. 2622–2629, 1978. 109

[185] A. Lesikar, "Glass transitions of organic solvent mixtures," *Physics and Chemistry of Glasses*, vol. 16, no. 4, pp. 83–90, 1975. 109

[186] M. Carpenter, D. Davies, and A. Matheson, "Measurement of the glass-transition temperature of simple liquids," *The Journal of Chemical Physics*, vol. 46, no. 7, pp. 2451–2454, 1967. 109

[187] J. Gordon, G. Rouse, J. Gibbs, and W. M. Risen Jr, "The composition dependence of glass transition properties," *The Journal of Chemical Physics*, vol. 66, no. 11, pp. 4971–4976, 1977. 109

[188] L.-M. Wang and R. Richert, "Glass transition dynamics and boiling temperatures of molecular liquids and their isomers," *The Journal of Physical Chemistry B*, vol. 111, no. 12, pp. 3201–3207, 2007. 109

[189] H. C. Andersen, "Molecular dynamics studies of heterogeneous dynamics and dynamic crossover in supercooled atomic liquids," *Proceedings of the National Academy of Sciences of the United States of America*, vol. 102, no. 19, pp. 6686–6691, 2005. 110, 250

[190] D. J. Plazek and K. L. Ngai, "Correlation of polymer segmental chain dynamics with temperature-dependent time-scale shifts," *Macromolecules*, vol. 24, no. 5, pp. 1222–1224, 1991. 112, 193, 206, 236, 248

[191] R. Böhmer and C. A. Angell, "Correlations of the nonexponentiality and state dependence of mechanical relaxations with bond connectivity in ge-as-se supercooled liquids," *Physical Review B*, vol. 45, no. 17, p. 10091, 1992. 112

[192] G. Ruocco, F. Sciortino, F. Zamponi, C. De Michele, and T. Scopigno, "Landscapes and fragilities," *The Journal of chemical physics*, vol. 120, no. 22, pp. 10666–10680, 2004. 113

[193] J. Mattsson, R. Bergman, P. Jacobsson, and L. Börjesson, "Influence of chain length on the α-β bifurcation in oligomeric glass formers," *Physical review letters*, vol. 94, no. 16, p. 165701, 2005. 116, 140, 175, 249, 258, 263, 270

[194] R. J. Speedy, "Estimates of the configurational entropy of a liquid," *The Journal of Physical Chemistry B*, vol. 105, no. 47, pp. 11737–11742, 2001. 118, 152, 211

[195] H. Wagner and R. Richert, "Dielectric beta relaxations in the glassy state of salol?," *The Journal of chemical physics*, vol. 110, no. 23, pp. 11660–11663, 1999. 118

[196] T. Blochowicz and E. Rössler, "Beta relaxation versus high frequency wing in the dielectric spectra of a binary molecular glass former," *Physical review letters*, vol. 92, no. 22, p. 225701, 2004. 119, 123

[197] C. Svanberg, R. Bergman, and P. Jacobsson, "Secondary relaxation in confined and bulk propylene carbonate," *EPL (Europhysics Letters)*, vol. 64, no. 3, p. 358, 2003. 119

[198] G. Johari, G. Power, and J. Vij, "Localized relaxation's strength and its mimicry of glass-softening thermodynamics," *Journal of Chemical Physics*, vol. 116, pp. 5908–5909, 2002. 123

[199] A. Matic, J. Mattsson, and R. Bergman, "Dynamics around the sol-gel transition in thermoreversible atactic polystyrene gels," in *Slow Dynamics in Complex Systems: 3rd International Symposium on Slow Dynamics in Complex Systems*, vol. 708, pp. 72–75, AIP Publishing, 2004. 133, 134

[200] J. Schaefer, M. Sefcik, E. Stejskal, R. McKay, W. T. Dixon, and R. Cais, "Molecular motion in glassy polystyrenes," *Macromolecules*, vol. 17, no. 6, pp. 1107–1118, 1984. 141, 161, 219, 227, 236

[201] A. Kulik and K. Prins, "^{2}H NMR study of high pressure effects on the molecular dynamics in polystyrene: 2. Phenyl group motion," *Polymer*, vol. 34, no. 22, pp. 4635–4641, 1993. 219, 227, 236

[202] J. Zhao, Y. H. Chin, Y. Liu, A. A. Jones, P. T. Inglefield, R. P. Kambour, and D. M. White, "Deuterium nmr study of phenyl group motion in glassy polystyrene and a blend of polystyrene with polyphenylene oxide," *Macromolecules*, vol. 28, no. 11, pp. 3881–3889, 1995. 161, 219, 227, 236

[203] A. V. Lyulin, N. K. Balabaev, and M. Michels, "Correlated segmental dynamics in amorphous atactic polystyrene: A molecular dynamics simulation study," *Macromolecules*, vol. 35, no. 25, pp. 9595–9604, 2002. 219, 236

[204] O. Yano and Y. Wada, "Dynamic mechanical and dielectric relaxations of polystyrene below the glass temperature," *Journal of Polymer Science Part A-2: Polymer Physics*, vol. 9, no. 4, pp. 669–686, 1971. 141, 177, 185, 210, 216, 218, 236

[205] S. Murthy *et al.*, "Study of α-, β-, and γ-relaxation processes in some supercooled liquids and supercooled plastic crystals," *The Journal of Chemical Physics*, vol. 99, no. 12, pp. 9865–9873, 1993. 141

[206] Y. P. Koh and S. L. Simon, "Structural relaxation of stacked ultrathin polystyrene films," *Journal of Polymer Science Part B: Polymer Physics*, vol. 46, no. 24, pp. 2741–2753, 2008. 144

[207] C. A. Angell and W. Sichina, "Thermodynamics of the glass transition: Empirical aspects*," *Annals of the New York Academy of Sciences*, vol. 279, no. 1, pp. 53–67, 1976. 146

[208] J. Sjöström, J. Mattsson, R. Bergman, and J. Swenson, "Hydrogen bond induced nonmonotonic composition behavior of the glass transition in aqueous binary mixtures," *The Journal of Physical Chemistry B*, vol. 115, no. 33, pp. 10013–10017, 2011. 146

[209] M. J. Pikal, L. L. Chang, and X. C. Tang, "Evaluation of glassy-state dynamics from the width of the glass transition: Results from theoretical simulation of differential scanning calorimetry and comparisons with experiment," *Journal of pharmaceutical sciences*, vol. 93, no. 4, pp. 981–994, 2004. 147, 267

[210] G. Johari, M. Beiner, C. Macdonald, and J. Wang, "The glass-softening temperature range and non-arrhenius dynamics: the case of vitrified water," *Journal of non-crystalline solids*, vol. 278, no. 1, pp. 58–68, 2000.

[211] K. Ito, C. T. Moynihan, and C. A. Angell, "Thermodynamic determination of fragility in liquids and a fragile-to-strong liquid transition in water," *Nature*, vol. 398, no. 6727, pp. 492–495, 1999. 147, 233, 268

[212] K. Ngai and O. Yamamuro, "Thermodynamic fragility and kinetic fragility in supercooling liquids: A missing link in molecular liquids," *The Journal of Chemical Physics*, vol. 111, no. 23, pp. 10403–10406, 1999. 147

[213] B. Maté, R. D. Suenram, and C. Lugez, "Microwave studies of three alkylbenzenes: Ethyl, n-propyl, and n-butylbenzene," *The Journal of Chemical Physics*, vol. 113, no. 1, pp. 192–199, 2000. 149

[214] W. Caminati, D. Damiani, G. Corbelli, B. Velino, and C. Bock, "Microwave spectrum and ab initio calculations of ethylbenzene: potential energy surface of the ethyl group torsion," *Molecular Physics*, vol. 74, no. 4, pp. 885–895, 1991. 149

[215] S. Halbert, C. Clavaguéra, and G. Bouchoux, "The shape of gaseous n-butylbenzene: Assessment of computational methods and comparison with experiments," *Journal of computational chemistry*, vol. 32, no. 8, pp. 1550–1560, 2011.

[216] J. Dickinson, P. Joireman, R. Kroemer, E. Robertson, and J. Simons, "Conformationally induced transition moment rotations in the s 1 s 0 electronic spectra of n-propylbenzene and n-butylbenzene," *Journal of the Chemical Society, Faraday Transactions*, vol. 93, no. 8, pp. 1467–1472, 1997. 149

[217] J. H. Gibbs and E. A. DiMarzio, "Nature of the glass transition and the glassy state," *The Journal of Chemical Physics*, vol. 28, no. 3, pp. 373–383, 1958. 149, 154

[218] G. Leissmann, W. Schmidt, and S. Reiffarth, "Data compilation of the Saechsische Olefinwerke Boehlen,Germany," 1995. 151

[219] K. K. Kelley, "The heat capacity of toluene from 14 k. to 298 k. the entropy and the free energy of formation," *Journal of the American Chemical Society*, vol. 51, no. 9, pp. 2738–2741, 1929. 151

[220] W. T. Ziegler and D. Andrews, "The heat capacity of benzene-d61, 2," *Journal of the American Chemical Society*, vol. 64, no. 10, pp. 2482–2485, 1942. 151

[221] E. S. Domalski and E. D. Hearing, "Heat capacities and entropies of organic compounds in the condensed phase. volume iii," *Journal of physical and chemical reference data*, vol. 25, no. 1, pp. 1–525, 1996. 151

[222] R. B. Scott and F. G. Brickwedde, "Thermodynamic properties of solid and liquid ethylbenzene from 0 to 300 k," *J. Res. Natl. Bur. Stand*, vol. 35, pp. 501–512, 1945. 151

[223] G. B. Guthrie Jr, R. W. Spitzer, and H. M. Huffman, "Thermal data. xviii. the heat capacity, heat of fusion, entropy and free energy of ethylbenzene," *Journal of the American Chemical Society*, vol. 66, no. 12, pp. 2120–2121, 1944. 151

[224] H. M. Huffman, G. S. Parks, and A. C. Daniels, "Thermal data on organic compounds. vii. the heat capacities, entropies and free energies of twelve aromatic hydrocarbons1," *Journal of the American Chemical Society*, vol. 52, no. 4, pp. 1547–1558, 1930. 151

[225] W. E. Acree Jr, "Thermodynamic properties of organic compounds: enthalpy of fusion and melting point temperature compilation," *Thermochimica acta*, vol. 189, no. 1, pp. 37–56, 1991. 151

[226] H. M. Huffman, G. S. Parks, and M. Barmore, "Thermal data on organic compounds. x. further studies on the heat capacities, entropies and free energies of hydrocarbons," *Journal of the American Chemical Society*, vol. 53, no. 10, pp. 3876–3888, 1931. 151

[227] D. Hopfe, "Thermophysical data of pure substances. data compilation of fiz chemie, germany," 1990. 151

[228] M. Goldstein, "Viscous liquids and the glass transition. v. sources of the excess specific heat of the liquid," *The Journal of Chemical Physics*, vol. 64, no. 11, pp. 4767–4774, 1976. 150

[229] S. Sastry, "The relationship between fragility, configurational entropy and the potential energy landscape of glass-forming liquids," *Nature*, vol. 409, no. 6817, pp. 164–167, 2001. 150

[230] L.-M. Martinez and C. Angell, "Vibrational entropy, configurational entropy, and the fragility of glassforming liquids," *arXiv preprint cond-mat/0012248*, 2000. 150

[231] G. Johari, "On the excess entropy of disordered solids," *Philosophical Magazine B*, vol. 41, no. 1, pp. 41–47, 1980. 152

[232] K. Mortensen, W. Brown, and B. Nordén, "Inverse melting transition and evidence of three-dimensional cubatic structure in a block-copolymer micellar system," *Physical review letters*, vol. 68, no. 15, p. 2340, 1992. 153

[233] C. Angell, "Entropy and fragility in supercooling liquids," *National Institute of Standards and Technology, Journal of Research*, vol. 102, no. 2, pp. 171–185, 1997. 154

[234] D. R. Stull, E. F. Westrum, and G. C. Sinke, "The chemical thermodynamics of organic compounds," 1969. 155

[235] L.-M. Wang, C. A. Angell, and R. Richert, "Fragility and thermodynamics in nonpolymeric glass-forming liquids," *Journal of Chemical Physics*, vol. 125, no. 7, pp. 74505–74505, 2006. 156

[236] U. Gedde, *Polymer physics*. Springer, 1995. 163, 164, 179

[237] G. R. Strobl and G. R. Strobl, *The physics of polymers*, vol. 2. Springer, 1997. 164, 165, 166, 167, 168, 169, 170, 171, 179

[238] F. Tanaka, *Polymer Physics: Applications to Molecular Association and Thermoreversible Gelation*. Cambridge University Press, 2011. 165, 166, 167, 170, 171

[239] A. Brûlet, F. Boué, and J. Cotton, "About the experimental determination of the persistence length of wormlike chains of polystyrene," *Journal de Physique II*, vol. 6, no. 6, pp. 885–891, 1996. 166

[240] L. Fetters, D. Lohse, D. Richter, T. Witten, and A. Zirkel, "Connection between polymer molecular weight, density, chain dimensions, and melt viscoelastic properties," *Macromolecules*, vol. 27, no. 17, pp. 4639–4647, 1994. 168

[241] M. M. Somoza, M. I. Sluch, and M. A. Berg, "Torsional relaxation and friction on the nanometer length scale: Comparison of small-molecule rotation in poly (dimethylsiloxane) and poly (isobutylene)," *Macromolecules*, vol. 36, no. 8, pp. 2721–2732, 2003. 168

[242] Y. Ding and A. Sokolov, "Comment on the dynamic bead size and kuhn segment length in polymers: Example of polystyrene," *Journal of Polymer Science Part B: Polymer Physics*, vol. 42, no. 18, pp. 3505–3511, 2004. 168, 174, 203, 204, 205

[243] P. E. Rouse Jr, "A theory of the linear viscoelastic properties of dilute solutions of coiling polymers," *The Journal of Chemical Physics*, vol. 21, no. 7, pp. 1272–1280, 1953. 168

[244] H. Meyer, J. Wittmer, T. Kreer, P. Beckrich, A. Johner, J. Farago, and J. Baschnagel, "Static rouse modes and related quantities: Corrections to chain ideality in polymer melts," *The European Physical Journal E: Soft Matter and Biological Physics*, vol. 26, no. 1, pp. 25–33, 2008. 169

[245] Z. Dobkowski, "Determination of critical molecular weight for entangled macromolecules using the tensile strength data," *Rheologica acta*, vol. 34, no. 6, pp. 578–585, 1995. 170

[246] P.-G. de Gennes, "Reptation of a polymer chain in the presence of fixed obstacles," *The Journal of Chemical Physics*, vol. 55, no. 2, pp. 572–579, 1971. 170, 171

[247] M. Doi and S. d. Edwards, "Dynamics of concentrated polymer systems. part 1.brownian motion in the equilibrium state," *Journal of the Chemical Society, Faraday Transactions 2: Molecular and Chemical Physics*, vol. 74, pp. 1789–1801, 1978. 170

[248] N. Fatkullin, R. Kimmich, E. Fischer, C. Mattea, U. Beginn, and M. Kroutieva, "The confined-to-bulk dynamics transition of polymer melts in nanoscopic pores of solid matrices with varying pore diameter," *New Journal of Physics*, vol. 6, no. 1, p. 46, 2004. 170

[249] S. Gabriele, S. Sclavons, G. Reiter, and P. Damman, "Disentanglement time of polymers determines the onset of rim instabilities in dewetting," *Physical review letters*, vol. 96, no. 15, p. 156105, 2006. 171

[250] L. L. Berger and E. J. Kramer, "Chain disentanglement during high-temperature crazing of polystyrene," *Macromolecules*, vol. 20, no. 8, pp. 1980–1985, 1987.

[251] J. Padding and W. Briels, "Time and length scales of polymer melts studied by coarse-grained molecular dynamics simulations," *The Journal of chemical physics*, vol. 117, no. 2, pp. 925–943, 2002. 171

[252] J. E. Mark, *Physical properties of polymers handbook*, vol. 1076. Springer, 2007. 172

[253] P. C. Hiemenz, *Polymer chemistry: the basic concepts*. CRC press, 1984. 172, 173

[254] E. A. Di Marzio and A. J. Yang, "Configurational entropy approach to the kinetics of glasses," *Journal of Research of the National Institute of standards and Technology*, vol. 102, no. 2, pp. 135–157, 1997. 172

[255] T. G. Fox Jr and P. J. Flory, "Second-order transition temperatures and related properties of polystyrene. i. influence of molecular weight," *Journal of Applied Physics*, vol. 21, no. 6, pp. 581–591, 1950. 172, 271

[256] T. Ogawa, "Effects of molecular weight on mechanical properties of polypropylene," *Journal of applied polymer science*, vol. 44, no. 10, pp. 1869–1871, 1992. 173

[257] T. Fox and S. Loshaek, "Influence of molecular weight and degree of crosslinking on the specific volume and glass temperature of polymers," *Journal of Polymer Science*, vol. 15, no. 80, pp. 371–390, 1955. 173

[258] J. Hintermeyer, A. Herrmann, R. Kahlau, C. Goiceanu, and E. A. Roessler, "Molecular Weight Dependence of Glassy Dynamics in Linear Polymers Revisited," *Macromolecules*, vol. 41, pp. 9335–9344, Dec. 9 2008. xx, xxii, 173, 174, 177, 181, 184, 187, 194, 200, 201, 202, 203, 205, 206, 255, 256, 269, 272

[259] J. Cowie, "Some general features of tg-m relations for oligomers and amorphous polymers," *European Polymer Journal*, vol. 11, no. 4, pp. 297–300, 1975. xxii, xxvi, 174, 201, 203, 235, 239, 254, 255, 256, 272

[260] G. Bartenev and S. Y. Frenkel, "Polymer physics," *Khimiya, Leningrad*, 1990. xxii, 203

[261] P. Claudy, J. Letoffe, Y. Camberlain, and J. Pascault, "Glass transition of polystyrene versus molecular weight," *Polymer bulletin*, vol. 9, no. 4-5, pp. 208–215, 1983. xx, xxii, 173, 177, 201, 203, 256, 269

[262] A. L. Agapov and A. P. Sokolov, "Does the Molecular Weight Dependence of T-g Correlate to M-e?," *Macromolecules*, vol. 42, pp. 2877–2878, Apr. 14 2009. 174, 203

[263] C. Roland, P. Santangelo, and K. Ngai, "The application of the energy landscape model to polymers," *The Journal of chemical physics*, vol. 111, no. 12, pp. 5593–5598, 1999. 175, 230, 267

[264] C. Angell, "Entropy, landscapes, and fragility in liquids and polymers, and the δcp problem, chapter 3," in *ACS Symposium Series*, vol. 710, pp. 37–53. 175, 231, 267

[265] C. Levelut, Y. Scheyer, J. Pelous, O. Randl, F. Prochazka, and D. Durand, "β relaxation related to the glass transition temperature in polymeric gels," *Physics Letters A*, vol. 261, no. 3, pp. 205–211, 1999. 175

[266] B. Wunderlich, D. M. Bodily, and M. H. Kaplan, "Theory and measurements of the glass-transformation interval of polystyrene," *Journal of Applied Physics*, vol. 35, no. 1, pp. 95–102, 1964. 177

[267] G. Tammann, "The glassy state," *Leopold Voss, Leipzig*, p. 123, 1933.

[268] V. Lupaşcu, S. J. Picken, and M. Wbbenhorst, "Dynamics of t2g2 helices in atactic and syndiotactic polystyrene: new evidence from dielectric spectroscopy and ftir," *Macromolecules*, vol. 39, no. 15, pp. 5152–5158, 2006. xxiv, 216, 218, 220, 221, 222, 223, 224, 226, 227, 236

[269] C. Roland and R. Casalini, "Temperature dependence of local segmental motion in polystyrene and its variation with molecular weight," *The Journal of chemical physics*, vol. 119, no. 3, p. 1838, 2003. 185, 195, 248, 274

[270] J. Cavaille, C. Jourdan, J. Perez, L. Monnerie, and G. Johari, "Time-temperature superposition and dynamic mechanical behavior of atactic polystyrene," *Journal of Polymer Science Part B: Polymer Physics*, vol. 25, no. 6, pp. 1235–1251, 1987. xxiv, 194, 216, 218, 226, 227

[271] U. Pschorn, E. Rössler, H. Sillescu, S. Kaufmann, D. Schaefer, and H. Spiess, "Local and cooperative motions at the glass transition of polystyrene: information from one-and two-dimensional nmr as compared with other techniques," *Macromolecules*, vol. 24, no. 2, pp. 398–402, 1991. 226

[272] J. Zhao, Y. H. Chin, Y. Liu, A. A. Jones, P. T. Inglefield, R. P. Kambour, and D. M. White, "Deuterium nmr study of phenyl group motion in glassy polystyrene and a blend of polystyrene with polyphenylene oxide," *Macromolecules*, vol. 28, no. 11, pp. 3881–3889, 1995. xxiv, 219, 226, 227, 236

[273] G. Patterson, P. Carroll, and J. Stevens, "Photon correlation spectroscopy of polystyrene as a function of temperature and pressure," *Journal of Polymer Science: Polymer Physics Edition*, vol. 21, no. 4, pp. 605–611, 1983.

[274] H. Lee, A. Jamieson, and R. Simha, "Photon correlation spectroscopy of polystyrene in the glass transition region," *Macromolecules*, vol. 12, no. 2, pp. 329–332, 1979.

[275] A. Dhinojwala, G. K. Wong, and J. M. Torkelson, "Rotational reorientation dynamics of disperse red 1 in polystyrene: α-relaxation dynamics probed by second harmonic generation and dielectric relaxation," *The Journal of chemical physics*, vol. 100, no. 8, pp. 6046–6054, 1994. 177

[276] J. Mattsson, J. Forrest, and L. Börjesson, "Quantifying glass transition behavior in ultrathin free-standing polymer films," *Physical Review E*, vol. 62, no. 4, p. 5187, 2000. 178

[277] J. Sharp and J. Forrest, "Free surfaces cause reductions in the glass transition temperature of thin polystyrene films," *Physical review letters*, vol. 91, no. 23, p. 235701, 2003.

[278] J. Sharp, J. Teichroeb, and J. Forrest, "The properties of free polymer surfaces and their influence on the glass transition temperature of thin polystyrene films," *The European Physical Journal E: Soft Matter and Biological Physics*, vol. 15, no. 4, pp. 473–487, 2004.

[279] J.-H. Zhao, M. Kiene, C. Hu, and P. S. Ho, "Thermal stress and glass transition of ultrathin polystyrene films," *Applied Physics Letters*, vol. 77, no. 18, pp. 2843–2845, 2000. 178

[280] M. Paluch, S. Pawlus, A. P. Sokolov, and K. Ngai, "Sub-rouse modes in polymers observed by dielectric spectroscopy," *Macromolecules*, vol. 43, no. 6, pp. 3103–3106, 2010. 190, 191

[281] P. Santangelo, K. Ngai, and C. Roland, "Distinctive manifestations of segmental motion in amorphous poly (tetrahydrofuran) and polyisobutylene," *Macromolecules*, vol. 26, no. 11, pp. 2682–2687, 1993. 191

[282] D. Plazek, I.-C. Chay, K. Ngai, and C. Roland, "Viscoelastic properties of polymers. 4. thermorheological complexity of the softening dispersion in polyisobutylene," *Macromolecules*, vol. 28, no. 19, pp. 6432–6436, 1995. 191

[283] A. K. Rizos, K. L. Ngai, and D. J. Plazek, "Local segmental and sub-rouse modes in polyisobutylene by photon correlation spectroscopy," *Polymer*, vol. 38, no. 25, pp. 6103–6107, 1997. 191

[284] C.-Y. Wang and M. Ediger, "Lifetime of spatially heterogeneous dynamic domains in polystyrene melts," *The Journal of Chemical Physics*, vol. 112, no. 15, pp. 6933–6937, 2000. 194

[285] W. Jin and R. H. Boyd, "Time evolution of dynamic heterogeneity in a polymeric glass: a molecular dynamics simulation study," *Polymer*, vol. 43, no. 2, pp. 503–507, 2002. 194

[286] G. Williams, M. Cook, and P. Hains, "Molecular motion in amorphous polymers. consideration of the mechanism for α, β and $(\alpha\beta)$ dielectric relaxations," *Journal of the Chemical Society, Faraday Transactions 2: Molecular and Chemical Physics*, vol. 68, pp. 1045–1050, 1972. 197

[287] P. Debye and F. Bueche, "Distribution of segments in a coiling polymer molecule," *The Journal of Chemical Physics*, vol. 20, no. 8, pp. 1337–1338, 1952. 197

[288] H. Höcker, G. Blake, and P. Flory, "Equation-of-state parameters for polystyrene," *Transactions of the Faraday Society*, vol. 67, pp. 2251–2257, 1971. 197

[289] W. Krigbaum and A. Roig, "Dipole moments of atactic and isotactic polystyrene," *The Journal of Chemical Physics*, vol. 31, no. 2, pp. 544–545, 1959. 197

[290] V. Harmandaris, V. Mavrantzas, D. Theodorou, M. Kröger, J. Ramirez, H. Öttinger, and D. Vlassopoulos, "Crossover from the rouse to the entangled polymer melt regime: signals from long, detailed atomistic molecular dynamics simulations, supported by rheological experiments," *Macromolecules*, vol. 36, no. 4, pp. 1376–1387, 2003. 202

[291] C. Gainaru and R. Bohmer, "Oligomer-to-polymer transition of poly (propylene glycol) revealed by dielectric normal modes," *Macromolecules*, vol. 42, no. 20, pp. 7616–7618, 2009. 204

[292] Y. Ding, A. Kisliuk, and A. Sokolov, "When does a molecule become a polymer?," *Macromolecules*, vol. 37, no. 1, pp. 161–166, 2004. 204

[293] C. Gainaru, W. Hiller, and R. Bohmer, "A dielectric study of oligo-and poly (propylene glycol)," *Macromolecules*, vol. 43, no. 4, pp. 1907–1914, 2010. 204

[294] T. Kreer, J. Baschnagel, M. Müller, and K. Binder, "Monte carlo simulation of long chain polymer melts: Crossover from rouse to reptation dynamics," *Macromolecules*, vol. 34, no. 4, pp. 1105–1117, 2001. 205

[295] K. Ngai, J. Colmenero, A. Alegria, and A. Arbe, "Interpretation of anomalous momentum transfer dependences of local chain motion of polymers observed by quasielastic incoherent neutron scattering experiments," *Macromolecules*, vol. 25, no. 24, pp. 6727–6729, 1992. 206

[296] S. Arrese-Igor, A. Arbe, A. Alegría, J. Colmenero, and B. Frick, "Sub-tg dynamics in polycarbonate by neutron scattering and its relation with secondary γ relaxation," *The Journal of chemical physics*, vol. 123, no. 1, p. 014907, 2005. 219

[297] S. Arrese-Igor, A. Arbe, A. Alegrıa, J. Colmenero, and B. Frick, "Phenylene ring dynamics in bisphenol-a-polysulfone by neutron scattering," *The Journal of chemical physics*, vol. 120, no. 1, pp. 423–436, 2004. 219

[298] S. Arrese-Igor, A. Arbe, A. Alegría, J. Colmenero, and B. Frick, "Phenylene ring dynamics in phenoxy and the effect of intramolecular linkages on the dynamics of some engineering thermoplastics below the glass transition temperature," *Physical Review E*, vol. 75, no. 5, p. 051801, 2007. 219

[299] S. Arrese-Igor, A. Arbe, B. Frick, and J. Colmenero, "Glassy Dynamics of Polystyrene by Quasielastic Neutron Scattering," *Macromolecules*, vol. 44, pp. 3161–3168, Apr. 26 2011. 219

[300] S. Capaccioli, M. Paluch, D. Prevosto, L.-M. Wang, and K. Ngai, "Many-body nature of relaxation processes in glass-forming systems," *The Journal of Physical Chemistry Letters*, vol. 3, no. 6, pp. 735–743, 2012. 227

[301] S. Takahara, O. Yamamuro, and H. Suga, "Heat capacities and glass transitions of 1-propanol and 3-methylpentane under pressure. new evidence for the entropy theory," *Journal of non-crystalline solids*, vol. 171, no. 3, pp. 259–270, 1994. 231

[302] O. Sandberg and G. Bäckström, "Thermal conductivity and heat capacity of liquid and glassy poly (vinyl acetate) under pressure," *Journal of Polymer Science: Polymer Physics Edition*, vol. 18, no. 10, pp. 2123–2133, 1980. 231

[303] C. Angell, P. Poole, and J. Shao, "Glass-forming liquids, anomalous liquids, and polyamorphism in liquids and biopolymers," *Il Nuovo Cimento D*, vol. 16, no. 8, pp. 993–1025, 1994. 231

[304] J. Cowie and P. Toporowski, "The dependence of glass temperature on molecular weight for poly α-methyl styrene," *European Polymer Journal*, vol. 4, no. 5, pp. 621–625, 1968. xxvi, 239, 254, 255, 256

[305] D. Huang, S. L. Simon, and G. B. McKenna, "Equilibrium heat capacity of the glass-forming poly (α-methyl styrene) far below the kauzmann temperature: the case of the missing glass transition," *The Journal of chemical physics*, vol. 119, no. 7, pp. 3590–3593, 2003. 239, 265, 266

[306] W. Zheng and S. L. Simon, "The glass transition in athermal poly(alpha-methyl styrene)/oligomer blends," *Journal of Polymer Science Part B - Polymer Physics*, vol. 46, pp. 418–430, Feb. 15 2008. 255

[307] L. S. Bartell, "On the length of the carbon-carbon single bond1," *Journal of the American Chemical Society*, vol. 81, no. 14, pp. 3497–3498, 1959. 255

[308] K. Loufakis and B. Wunderlich, "Computation of heat capacity of liquid macromolecules based on a statistical mechanical approximation," *The Journal of Physical Chemistry*, vol. 92, no. 14, pp. 4205–4209, 1988. 266

[309] W. Q. Sun and P. Davidson, "Protein inactivation in amorphous sucrose and trehalose matrices: effects of phase separation and crystallization," *Biochimica et Biophysica Acta (BBA)-General Subjects*, vol. 1425, no. 1, pp. 235–244, 1998. 275

[310] P. Sundaramurthi and R. Suryanarayanan, "Trehalose crystallization during freeze-drying: implications on lyoprotection," *The Journal of Physical Chemistry Letters*, vol. 1, no. 2, pp. 510–514, 2009. 275